

**Topographic characterization of polymer materials at different
length scales and the mechanistic understanding of wetting
phenomena**

D I S S E R T A T I O N

Zur Erlangung des akademischen Grades

**Doctor rerum naturalium
(Dr. rer. nat.)**

vorgelegt

**der Fakultät Mathematik und Naturwissenschaften
der Technischen Universität Dresden**

von

M. Sc. Alfredo Calvimontes

geboren am 23. Januar 1965 in La Paz, Bolivien

Verteidigt am 10.12.2009

Die Dissertation wurde in der Zeit von 01.05.2007 bis 30.04.2009
im Leibniz-Institut für Polymerforschung Dresden e.V. angefertigt.

To my wife Mónica

Acknowledgement

I gratefully acknowledge Prof. Dr. Manfred Stamm, Dr. Karina Grundke and Dr. Victoria Dutschk for giving the opportunity to carry out this work and for scientific supervision.

I would like to acknowledge Prof. Dr. Gert Heinrich, Prof. Dr. Chokri Cherif, Dr. Burkhard Breitzke, Dr. Neil Lant and Mr. Stefan Werner for working ideas, friendship and helpful discussions.

I am very grateful all my colleagues from the Department of Polymer Interfaces for the warm working atmosphere and permanent support.

My special thanks address to my wife and sons.

This research is made possible through the financial support from German Ministry of Education and Research and Leibniz-Institut für Polymerforschung Dresden e.V.

Abstract

The present study suggests new insights into topographic characterisation of engineering polymer surfaces towards to physical-chemical and mechanistic understanding of wetting phenomena on rough surfaces.

Non-contact chromatic confocal imaging was chosen and justified as the optimal measuring method to study and correlate surface topography and surface properties of Sheet Moulding Compounds (SMC) as well as polyester and cotton fabrics. Before topographical characterisation, an adequate selection of optimal sampling conditions (cut-off length and resolution) were done by a systematic procedure proposed for periodic and non-periodic surfaces.

Topographical characterisation of the surfaces was realized by an innovative methodology, separately considering different length scales in dependence on the surface morphologies of the materials.

For SMC materials, the influence of moulding conditions (pressure, moulding time, metallic mold topography, metallic mold form, prepregs placement procedure, glass fibres content and orientation) on resulting macro-, meso- and micro-topography was studied. A model to conceptualize the influence of the most important moulding conditions on topographic characteristics and, as a consequence, on the quality of the resulting surface was presented. To quantify the effect of surface modification, a new parameter (Surface Relative Smooth) was suggested, developed and validated, which can be used for the characterisation of changes due to surface modifications for every solid material.

A very important and innovative part of the present study is the development of new concepts for topographic characterisation of textile materials using different length scales, that makes possible to consider and analyse separately their specific morphologies caused by weave, yarn and filament/fibres, and to investigate the influence of topography on wettability by modification processes, e.g. construction parameters, thermosetting, impregnation with Soil Release Polymers (SRP) and wash-dry cycles.

The present study showed, how construction parameters of polyester textiles, such as fineness of filaments and yarn, warp and weft densities as well as the type of weave, control the surface topography - characterised as meso-porosity (spaces between yarns) and micro-porosity (spaces between filaments) - and as a consequence strongly influence their capillarity. On the basis of experimental results, revealing differences in three basic types of woven fabrics – plain, twill and Panama – in respect to water penetration, the concept of an innovative novel wicking model was developed.

Additionally, the influence of thermosetting and impregnation of polyester fabrics with Soil Release Polymers on topography, wetting and cleanability of three woven plain polyester fabrics, having different wefts, were studied.

To characterise the soiling behaviour, an 'spot analysis method' was suggested, allowing wetting dynamics studies of liquids on fabrics with anisotropic surface properties. This method is applicable also to surfaces with anisotropic roughness characteristics and to porous media.

The effect of wash-dry cycles on topography, spreading, wetting and soiling of woven plain and knitted cotton fabrics was in addition investigated.

In all cases studied, the topographical characterisation and interpretation of results on different length scales contributed to a better understanding of wetting phenomena.

A mathematical model for a virtual construction of textile surfaces to predict effects resulting from topographic changes on the behaviour of polymer and textiles surfaces was developed. Woven plain textiles and SMC surfaces were mathematically synthesized by a combination of various harmonic waves, i.e. Fourier synthesis. Topographic and technical construction parameters were taken into account to build their virtual topographies. In the case of textile surfaces, the effect of wash-dry cycles for cotton fabrics and thermosetting of polyester fabrics on their meso- and micro-morphology was investigated on the basis of the real topography of a given textile surface. The model allows to predict changes in the porosity of resulting textile materials, their wettability and soiling behaviour. The method presented provides possibilities to simulate controlled changes in textile construction parameters and to study their effect on the resulting topography.

Kurzfassung

Die vorliegende Arbeit vermittelt neue Einblicke in die topographische Charakterisierung technisch relevanter Polymeroberflächen mit dem Ziel, die Mechanismen der Benetzungsphänomene auf rauen Oberflächen besser zu verstehen.

Eine 3D-Abbildung der Oberflächentopographie wurde mit einem konfokalen Mikroskop mit chromatischer Kodierung zwecks optimaler Charakterisierung duromerer Verbundwerkstoffsystemen (SMS: Sheet Moulding Compounds) sowie Polyester- und Baumwolltextilien berührungsfrei durchgeführt. Zur topographischen Oberflächencharakterisierung wurde eine systematische Prozedur vorgeschlagen, welche es erlaubt, eine entsprechende Auswahl von optimalen Messbedingungen, wie die Bewertungslänge (cut-off length) und Auflösung, für Oberflächen mit periodischer und nicht-periodischer Rauheit zu treffen.

Die topographische Charakterisierung von Oberflächen wurde methodologisch weiter entwickelt, indem die Oberflächen auf verschiedenen Längenskalen je nach Morphologie untersucht werden können.

Für duromere Verbundwerkstoffsysteme wurde der Einfluss von den Bedingungen des Formpressens (Druck, Zeit, Topographie und Form des metallischen Werkzeugs, Einbringen des Prepregs, Glasfasergehalt und -orientierung) auf die resultierende makro-, meso- und mikroskopische Topographie studiert. Eine modellmäßige Beschreibung des Einflusses der wichtigsten Charakteristiken des Herstellungsprozesses duromerer Verbundwerkstoffsysteme auf ihre topographische Charakteristiken und demzufolge auf die Qualität des Endproduktes wurde konzipiert.

Zur Quantifizierung des Effekts der Oberflächenmodifizierung wurde einen neuen Parameter – Surface Relative Smooth – vorgeschlagen und dessen Nutzung für jedes beliebige Feststoffkörpers verifiziert.

Das Hauptaugenmerk bei der Durchführung der Arbeit wurde auf die Entwicklung neuer Konzepte zur topographischen Charakterisierung textiler Materialien gelegt, welche die Nutzung mehrerer Längenskalen in Betracht ziehen. Dies ermöglicht die

spezifische Morphologien textiler Strukturen zu berücksichtigen und jede Struktur, welche durch die Gewebeat, die Art der Fasern und des Garns entstanden ist, gesondert bezüglich ihr Einflusses auf die Benetzbarkeit infolge der Modifizierung (Konstruktionsparameter, Thermofixierung, Imprägnierung mit Soil-Release-Polymeren, Waschen/Trocknen-Zyklen) zu analysieren.

In der vorliegenden Arbeit wird gezeigt, wie die Konstruktionsparameter von Polyestertextilien, wie z.B. die Filament- und Garnfeinheit, Kett- und Schussdichte sowie die Gewebbindung Einfluss auf die Oberflächentopographie und als Folge auf ihre Kapillarität nehmen, und zwar als Mesoporesität (Abstände zwischen Garnwindungen) und als Mikroporesität (Abstände zwischen einzelnen Filamenten).

Auf der Basis von umfangreichen experimentellen Daten, welche die Unterschiede zwischen verschiedenen Bindungsarten (Leinwand, Köper, Panama) offenbaren, wurde ein neues Modell zur Beschreibung der Penetration von Flüssigkeiten in die textile Strukturen entwickelt.

Außerdem wurde der Einfluss der Thermofixierung und Imprägnierung von Polyester Materialien mit Soil-Release-Polymeren auf die Topographie, Benetzbarkeit und Auswaschbarkeit für die drei wichtigsten Gewebeatarten untersucht, welche die gleiche Anzahl von Schussfäden haben.

Für die Charakterisierung des Verschmutzungsverhaltens von Textilien wurde eine so genannte Fleck-Analyse-Methode (spot analysis method) vorgeschlagen, welche es erlaubt, benetzungsdynamische Eigenschaften von Flüssigkeiten an Oberflächen mit anisotroper Topographie zu studieren. Diese Methode ist geeignet auch für Oberflächen mit anisotropen Rauheitsstrukturen und für poröse Materialien.

Der Effekt von Waschen/Trocknen-Zyklen auf die Topographie, Spreitung, Benetzung und Verschmutzung von Leinwandgewebe und Gestricke aus Baumwolle wurde zusätzlich untersucht.

In allen Spezialfällen diente die topographische Charakterisierung und die Interpretation der Ergebnisse auf verschiedenen Längenskalen zur besseren Verständnis von Benetzungsphänomenen.

Ein mathematisches Modell für die virtuelle Konstruktion von textilen Oberflächen wurde entwickelt, die das Studium der Effekte infolge topographischer Änderungen auf das Verhalten von Polymer- und Textiloberflächen ermöglicht. Oberflächen von Leingeweben und duromeren Verbundwerkstoffsystemen wurden mit der Fourier-

Synthese unter Zuhilfenahme verschiedener harmonischer Wellen mathematisch abgebildet. Die Topographie- und Konstruktionsparameter wurden bei der Fourier-Synthese zur Konstruktion virtueller Topographien genutzt. Im Falle der textilen Materialein wurde der Effekt von Waschen/Trocknen-Zyklen für die Baumwolltextilien sowie der Thermofixierung von Polyestertextilien auf ihre Meso- und Mikromorphologie auf der Basis gemessener Parameter für jede Topographie modelliert. Dieses Modell erlaubt auch die Vorhersage der Änderungen in der Porosität von resultierenden textilen Strukturen, ihres Benetzungs- und Anschmutzungsverhaltens. Mit dieser Methode ist es möglich, gewünschte Änderungen von textilen Konstruktionsparametern einzustellen und ihre Effekte auf die Topographie zu untersuchen.

Contents

1	Introduction and objective	1
1.1	Problem definition	1
1.2	Objective	2
2	Theoretical background	3
2.1	Surface morphology	4
2.2	Surface topometry	4
2.3	Traditional measurement methods for topography	5
2.3.1	Conventional measuring methods	8
2.3.1.1	Mechanical sensing measurement method	8
2.3.1.2	Measurement by the capacitance method	9
2.3.1.3	Measurement using ultrasound	9
2.3.2	Optical methods	10
2.3.2.1	Large range optical methods	10
2.3.2.2	Optical methods for very small roughness	11
2.3.2.3	Measurement methods using diffraction	12
2.3.2.4	Methods using the Speckle phenomenon	13
2.3.2.5	3D measurement by laser triangulation method	13
2.3.2.6	Stereo photogrammetry	14
2.3.3	Scanning microscopy	14
2.3.3.1	Scanning probe microscopes (SPM)	14
2.3.3.2	Scanning Electron Microscope (SEM)	15
2.4	Modern optical methods for topography	15
2.4.1	Scanning methods using laser	16
2.4.1.1	Confocal laser scanning optical microscopy (CLSM)	16
2.4.1.2	Conoscopic holography (CSL)	17
2.4.1.3	Digital holographic microscopy (DHM) and digital comparative holography (DISCO)	18
2.4.2	Scanning methods using white light	18
2.4.2.1	Confocal scanning optical microscopy (CSOM)	18
2.4.2.2	Chromatic confocal imaging (CWL)	19
2.4.3	Non scanning methods using VIS, NIR and/or UV	20
2.4.3.1	High-resolution scandisk confocal microscopy (SDCM)	20
2.4.3.2	White light interferometry (WLI)	21
2.4.3.3	Film thickness interferometry	22
2.4.3.4	Fringe projection imaging (FPM)	23
3	Topographic characterization techniques	25
3.1	Justification of the optical method used	25
3.2	Selection of the initial sampling conditions	27
3.3	Common pre-processing mathematical operations	28
3.3.1	Correction of surface plane	28
3.3.1.1	Centre arithmetical mean plane (Graphical Mean Plane)	29

3.3.3.2	Least squares mean plane	29
3.3.3.3	Minimum zone plane	30
3.3.2	Correction of invalid data	30
3.3.3	Segmentation of data	31
3.4	Characterization techniques	33
3.4.1	Statistical characterization	34
3.4.1.1	Statistical distribution	34
3.4.1.2	Areal autocorrelation function (AACF)	34
3.4.1.3	Spectral moment analysis	36
3.4.2	2D spectral analysis	36
3.4.3	Time series analysis	38
3.4.4	Functional characterization	38
3.4.4.1	DIN 4776	38
3.4.4.2	Motif combination	39
3.4.4.3	Volumetrical characterization	40
3.4.5	Visual characterization	41
3.4.5.1	Isometric plot	42
3.4.5.2	Contour plot	42
3.4.5.3	Greyscale image	43
3.4.5.4	Solid-coloured Image	44
3.4.5.5	Greyscale-coloured Image	44
3.4.5.6	Cross section profile plot	44
3.4.6	Fractal analysis	44
3.5	Mathematical and physical meaning of the common topographic characterisation parameters	45
3.5.1	Rough (morphologic) characterization parameters	47
3.5.1.1	Digital surface filtering	48
3.5.1.2	Fast Fourier transformation (FFT) filtering	48
3.5.2	Fine (topometric) characterization parameters	49
3.5.2.1	Cut-off length of sampling interval L_m	51
3.5.2.2	Profile height P_t	51
3.5.2.3	Rough height R_t	51
3.5.2.4	Wave height W_t (DIN EN ISO 4287, ASME B46.1) and waviness W_z	52
3.5.2.5	Mean rough height R_z (DIN EN ISO 4287, ASME B46.1)	52
3.5.2.6	Maximal rough height R_{max} (DIN EN ISO 4287, ASME B46.1)	53
3.5.2.7	Arithmetical mean roughness R_a (DIN EN ISO 4287, ASME B46.1)	53
3.5.2.8	Root mean square roughness R_q (DIN EN ISO 4287, ASME B46.1)	54
3.5.2.9	Porosity, surface porosity or surface mean void volume	54
3.5.2.10	Some considerations about cut-off length	54
3.5.2.11	Relationship between R_{max} , R_z and R_a	55
3.6	Calculating the optimal sampling conditions	55
3.6.1	Non-periodic surfaces	56
3.6.2	Periodic surfaces	59
3.7	Manipulation techniques and complementary characterization procedures	61
3.7.1	Visual manipulation operations	61
3.7.1.1	Exchange of axes	61
3.7.1.2	Rotate	61
3.7.1.3	Flip	62
3.7.1.4	Mirror	62
3.7.1.5	Zoom and Clip	62
3.7.2	Numerical manipulation techniques	62

3.7.2.1	Resample	62
3.7.2.2	Calibration	62
3.7.2.3	Despike	62
3.7.2.4	Remove peaks	63
3.7.2.5	Destep	63
3.7.2.6	Inversion	63
3.7.2.7	Truncation	64
3.7.3	Complementary characterization procedures	64
3.7.3.1	Profile analysis	64
3.7.3.2	Histogram and cumulative histogram	64
3.7.3.3	Comparison	66
3.7.4	Complementary characterization parameters	66
3.7.4.1	Grain size	66
3.7.4.2	Filling quantity	66
3.7.4.3	Wenzel roughness factor	67
3.7.4.4	Surface fractal dimension	69
4	Topographic characterization at different length scales	73
4.1	Sheet Moulding Compounds (SMC)	73
4.1.1	Topographic parameters	74
4.1.2	Moulding conditions and topographic transfer from mold to SMC surface	75
4.1.3	Effect of glass fiber content on micro-topography	79
4.1.4	Influence of moulding conditions on the long waviness	80
4.1.5	Characterization of short waviness	81
4.1.6	Effect of prepregs placement on macro- and meso-topography	82
4.1.7	Correlation between length scales and resulting topography	83
4.1.8	Application of the concept of length scales to topographic characterisation	84
4.1.8.1	A profile model to understand the cavities formation on SMC surfaces	85
4.1.8.2	Characterisation of cavities and prediction of coatability	88
4.1.8.3	Surface Relative Smooth parameter (SRS) to characterise the topographic modification of SMC surfaces	89
4.2	Textile materials	94
4.2.1	Textile macro-topography	95
4.2.2	Textile meso-topography	96
4.2.3	Textile micro-topography	98
5	New topographic concepts for the mechanistic understanding of wetting phenomena	100
5.1	Correlation of topography and wettability of SMC	102
5.1.1	Meso-topography and wetting	103
5.1.2	Micro-topography and wetting	105
5.2	Correlation of topography and wettability of textile materials	105
5.2.1	Polyester textiles	106
5.2.1.1	Influence of textile construction parameters on topography, spreading, wetting and cleanability	106
5.2.1.2	Influence of thermo-mechanical changes on topography, spreading, wetting and soiling	113

5.2.1.3	Influence of impregnation of Soil Release Polymers (SRP) on topography, spreading, wetting, soiling and cleanability	118
5.2.2	Cotton textiles	126
5.2.2.1	Wash cycles as surface modification process	126
6	Modeling of polymer surface topography by Fourier synthesis	138
6.1	Reconstruction of 2D-profiles using harmonic series	139
6.1.1	Topographical synthesis by Fourier Series	140
6.2	Virtual 3D construction of the topography selecting and modifying and topographic parameters	141
6.3	Application of model proposed to the study of polymer surfaces	145
6.3.1	Simulating surface modifications on polyester fabrics by thermofixing	145
6.3.2	Simulating surface modifications on cotton fabrics by wash-dry cycles	147
6.3.3	Simulating the effect of mould surface and mould/sheet separation on SMC topography	148
7	Conclusions	150
8	References	154

Glossary of symbols

a_1	amplitude of a primary wave (by sinoidal functions)
AACF	Areal Autocorrelation Function
AFM	Atomic Force Microscope
a_k, a_m	amplitudes of secondary waves (by sinoidal functions)
A_m	sampling area
ASPD	Areal Power Spectral Density
CLSM	Confocal Laser Scanning optical Microscopy
CSL	Conoscopic Holography
CSOM	Confocal Scanning Optical Microscopy
CWL	Chromatic (White Light) Confocal Imaging
CWL FT	Interferometric (White Light) Film Thickness Sensor
CWL IR	Infrared Film Thickness Sensor
$\Delta\Gamma$	relative cleanability
DHM	Digital Holographic Microscopy
DISCO	Digital Comparative Holography
ΔS	surface variation by relaxation/shrinkage of textiles
Δ_x, Δ_y	lateral resolution
Δ_z	vertical resolution
FD	fractal dimension
FFT	Fast Fourier Transformation
FPM	Fringe Projection Imaging
FTR	Thin Film Sensor
f_i	surface area fraction of patch i on Cassie-Baxter model
γ	threshold to calculate V_C and V_G
γ_s	interfacial tension of solid-gas
γ_{sl}	interfacial tension of solid-liquid
γ_l	interfacial tension of liquid-gas
Γ	surface cleanability
h	thershold to measure cavities volume by SMC
h_v	heigh limit value
k, m	harmonic coefficients
λ	distance between wefts of between warps by textiles
L_m, l_x, l_y	cut-off length, measure length or sampling interval
$L-W_z$	long waviness (by SMC)
M	number of sampling points in one trace
N	number of sampling traces in the sampling area
N_a	number of short waves or "micro" waves (by SMC)
N_z	number of long waves or meso waves (by SMC)
$P(x)$	sinoidal function
PDMS	polydimethylsiloxan
PET	polyethylene therephthalate
POET	polyoxyethylene therephthalate
P_t, sP_t	profile height

θ	static contact angle between gas-liquid and solid-liquid interfaces
θ_a	apparent contact angle
θ_i	contact angle of patch i on Cassie-Baxter model
R	Reflection coefficient
r.u.	repetitive units (by textile)
R_a, sR_a	arithmetic mean roughness
R_{max}, sR_{max}	maximal rough height
R_p, sR_p	distance between highest point and mean height line
R_q, sR_q	root mean square roughness
R_t, sR_t	rough height
R_v, sR_v	distance between deepest point and mean height line
R_z, sR_z	mean rough height, mean roughness
SAD	Soil Additional Density
SDCM	High-Resolution Scandisk Confocal Microcopy
S_{dr}	developed surface area ratio
SEM	Scanning Electron Microscope
S_k	core roughness depth
SMC	Sheet Moulding Compounds
S_{pk}	reduced summit height
S_{r1}	upper bearing area
S_{r2}	lower bearing area
SRP	Soil Release Polymer
sR_{rl}	Wenzel roughness factor
SRS	Surface Relative Smooth parameter
STM	Scanning Probe Microscope
STM	Scanning Tunneling Microscope
S_{vk}	reduced valley depth
T	period
TGA	Thermogravimetry
t_s	spreading time
t_w	total wetting time
V_C	cavities volume
V_G	grains volume
V_o	porosity, surface porosity or mean void volume
ω	frequency
WLI	White Light Interferometry
W_t, sW_t	wave height, waviness
W_z	waviness

1 Introduction and objective

The quantitative description of the microstructure and the surface topography is a research field which can provide a better understanding of the relation between surface topography, microstructure, and mechanical and physical-chemical properties.

Surfaces of polymer materials contain information about the mechanism of their formation as well as the factors that have influenced on this mechanism. Besides, the surface morphology of a polymer material can essentially influence on its functional character.

1.1 Problem definition

In many cases, a systematic surface characterization is necessary to set up quantitative correlations between production conditions and physical-chemical properties of engineering surfaces, to compare the resulting polymer surface with standards and to modelling the surface behaviour.

During the last 30 years, the possibilities for surface topography quantification have been broadened by the availability of new methods [1]. For the evaluation of topographical data, several mathematical operations such as calculation algorithms and standard parameters can be applied today [2]. For this reason, the selection of the correct methodology while evaluating of the data measured and the optimal use of the topographical information obtained are especially relevant.

For any type of modification of a technical surface, the interplay between topography and surface chemistry determines the surface properties. Therefore, topographic qualitative description (morphology) and its quantitative description (topometry) are of great importance.

Every modification can produce changes on the surface in a special way. Additional to the nature of the process (mechanical, optical, electrical, magnetic, chemical, biological), the duration of its effect and external mechanical/environmental influences must be considered generally [3].

The resulting topography correlates to nanoscopic, microscopic and macroscopic properties which in combination define the final surface properties.

1.2 Objective

The aim of the present study is to suggest new scientific contributions to the topographic characterization of polymer engineering surfaces and to apply them to the physical-chemical and mechanistic understanding of wetting phenomena.

2 Theoretical background

The surface of a material is a part of it representing the boundaries between it and its environment. Surfaces as physical entities possess many attributes, geometry being one of them. Surface geometry of real materials by nature is three-dimensional and its detailed features are termed topography. In engineering field, topography represents the main external features of a surface which is determined by the description of its morphology and topometry.

In practice, the notion of a surface extends to sub-layers of solid boundaries and the surface assumes certain internal features [2], e.g. hardness, residual stress, deformation, chemical composition and reactions, microstructure, capillary, hydrophobicity, that are often of foremost concern in an application. Surface topography often interrelates with these features in complicated manners and in three dimensions to define certain engineering properties. Surface topography is, therefore, significant for surface performance and the importance of its measurement as a means of functional analysis and prediction is obvious. Engineering surfaces are produced in various way, typically by machining, surface treatment and coating. Surface topography modification is therefore performed by material removal, transformation or addition. Combinations of various machining, treatment and coating operations are employed to produce surfaces with desired characteristics for a particular application. Surface topography, therefore, contains 'signatures' of the surface generation process and as such can be used to diagnose, monitor and control the manufacturing process. From an engineering perspective, the ultimate objective of a surface topography measurement, as a mean of control and knowledge, is to establish a correlation between an engineering surface transformation (e.g. wear, chatter, soiling, cleanability, permeability, etc.) and its topographical characteristics (e.g. waviness, roughness, porosity, fractal dimension,

etc.). Surface topography measurement, therefore, serves as a link between manufacturing, functional performance analysis and prediction, and surface design.

2.1 Surface morphology

Surface morphology qualitatively describes the form and structure of a surface disregarding of fine details (*Fig. 2.1(a)*).

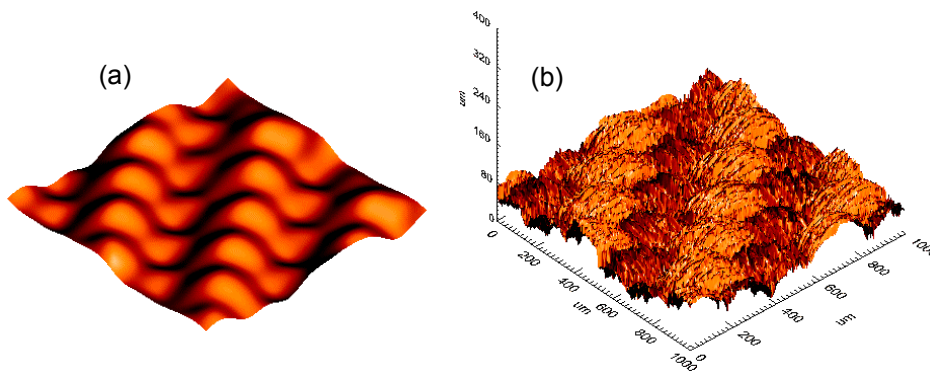


Figure 2.1: Topography of a polyester fabric (twill) represented as surface morphology(a) and topometry (b).

2.2 Surface topometry

If one speaks of the topometry of a surface, the exact coordinates of the separate points are meant. A topometric map in the geography among other things offers quantitative information by numeric contours of the earth's surface. In technology, one understands under a "topography measurement" the determination of x-, y- and z-coordinates of a set of representative points of the surface, as shown in *Fig. 2.2*.

Also the notions of roughness and waviness are found in the geography: so one speaks, for example, about a rugose mountain or about a wavy hill landscape. These notions are rather qualitative in the everyday life and return the first impression of the landscape. In technology, the notions roughness and waviness are of great value to the quantitative characterization of surfaces.

A simple isolated value cannot describe the surface extensively: the height of the highest mountain or the middle height of the mountains or the number of mountains are insufficient to describe a complete geographical scenery. Therefore, there is also in technology a multiplicity of characteristic values for roughness and waviness by which different types of combinations are applied to classify surfaces.

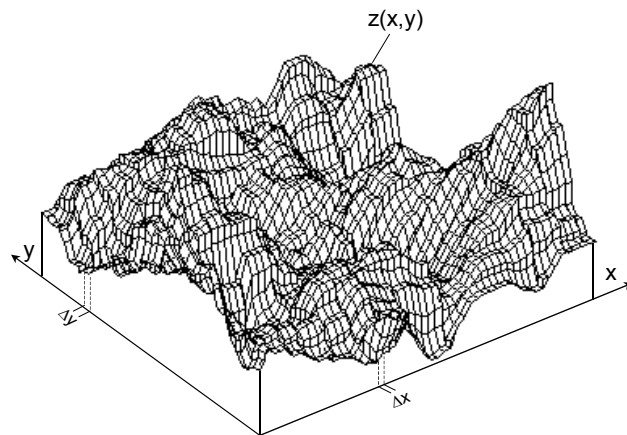


Figure 2.2 Coordinate system used for surface topography representation.

2.3 Traditional measurement methods for topography

The integrated study of surface topography calls for the integration of surface phenomena, measurement requirements and the measurement process. The main of a measurement process is to provide representations, numerical or graphical, which describe the surface. A quantitative 3D surface measurement invariably involves the use of computers in the measurement process due to the large amount of information involved. Computers are involved at various stages in the measurement process: control of data collection, data storage, processing, analysis and output of results. By necessity, a physical surface $z(x,y)$ must be digitised in the measurement process in order to enable storage, processing and analysis of topographic information. Therefore, in digital 3D surface analysis, a discrete surface height by $z(x_i, y_i)$ is denoted, where (x_i, y_i) is a discrete spatial point at the horizontal plane. A discrete surface $z(x_i, y_i)$ is obtained by sampling a continuous surface $z(x,y)$.

Measurement requirements determine the measuring methods and procedure to be employed and these are reflected at the various stages in the measurement process. A general procedure and measurement cycle for surface topography assessment is shown in *Fig. 2.3*. Given the specification of measurement requirements, a typical

measurement process includes data acquisition, pre-processing and characterisation:

a) **Data acquisition:**

Measurement systems for 3D surface topography data collection are often categorised by the physical principle used at the surface-sensor interface. A classification scheme based on this criteria is given in *Fig. 2.4*. In addition to the sensing principles for surface information and their capabilities (range, resolution, suitability of application, etc.), datum accuracy and digitisation strategy are of major concern in a 3D surface data acquisition system. Data acquisition datum is a

reference from which the three co-ordinates of a data point on the test surface is determined. Digitisation is necessary due to the use of digital techniques including sampling, quantisation and coding. These topics will be discussed in the present study.

b) **Pre-processing:** Following the storage of data collected at the previous step, some processing operations must be carried out before further analysis. Referring to *Fig. 2.3*, pre-processing includes levelling of surface data, and if necessary, form removal, data manipulations (truncation, segmentation, rotation, inversion, sub-area extraction, etc.) and filtering. Levelling refers to the removal of linear trend from the recorded surface data due to the misalignment of nominal surface plane and the data collection datum. In

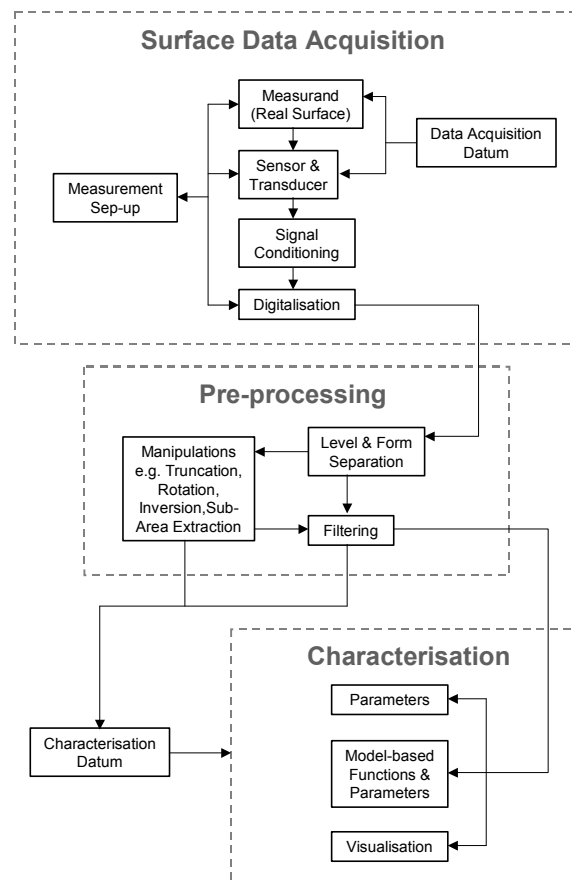


Figure 2.3 A general procedure and measurement cycle for a 3D topography assessment.

addition, different zeroing convention may be used in the coding of quantised surface heights. Form removal is necessary, if the surface is curved and the curvature does not participate in the surface phenomenon. Levelling and form removal are often preformed by least squares plane or surface fitting and can be carried in a single procedure. Filtering concerns the separation of different frequency components in the surface data. A surface filter should have zero or linear phase and a smooth weighting function. These two properties of a surface filter will help preserve the general features of the surface. A Gaussian filter satisfies both criteria and can be conveniently designed. The first and foremost principle for the use of filtering is its functional justification. The use of filters is particularly objectionable, when the functional significance of the different frequency components is not clear. The pre-processing operations collectively transform the data collection datum into a characterisation datum which form a basis for subsequent characterisation.

- c) **Characterization:** Surface topography, unlike other measurands (length, temperature, force, etc.), is a complicated measurement parameter. A one-to-one numerical representation is impossible. Parameter representation is invariably achieved on a many-to-one basis and is only effective from the engineering point of view when the implied information transformation and reduction process reflect the principle of functional significance, i.e. the representation(s) sought represent the engineering surface phenomenon to a practically satisfactory extent. On the next pages some typical and modern characterisation techniques for 3D surface topography analysis are reviewed and summarised.

In Chapters 3 and 4, special attention is paid to parametrical characterisation. Parameters discussed include those that are straight or modified extensions of 2D parameters and those that assume distinct 3D meanings. In Chapter 4, a characterisation procedure at different length-scales is proposed, which is based on an interdependency study of the existent parameters.

A bibliographic study of different topography measurements is presented on the following pages. A comparison between different technical specifications (measuring ranges and resolution) of the most important non-contact optical methods is detailed in [Table 2.1](#).

2.3.1 Conventional measuring methods

2.3.1.1 Mechanical sensing measurement method

These measuring instruments lead a fine needle over the surface of the measuring object and record the change of the height. In general, a stylus instrument profilometer takes only 2-D profiles of a surface [4]. The 3D surface texture measurement consists of the measurement of parallel profiles linked together in the orthogonal direction, and to a tangential reference line. Therefore a stylus measurement is made by an instrument allowing displacement of a surface texture probe in the both orthogonal horizontal x and y directions, and the measurement of the vertical amplitudes on the z axis with the probe [5]. The vertical movement of the sensor is changed into an analogue signal using either an inductive system (moving

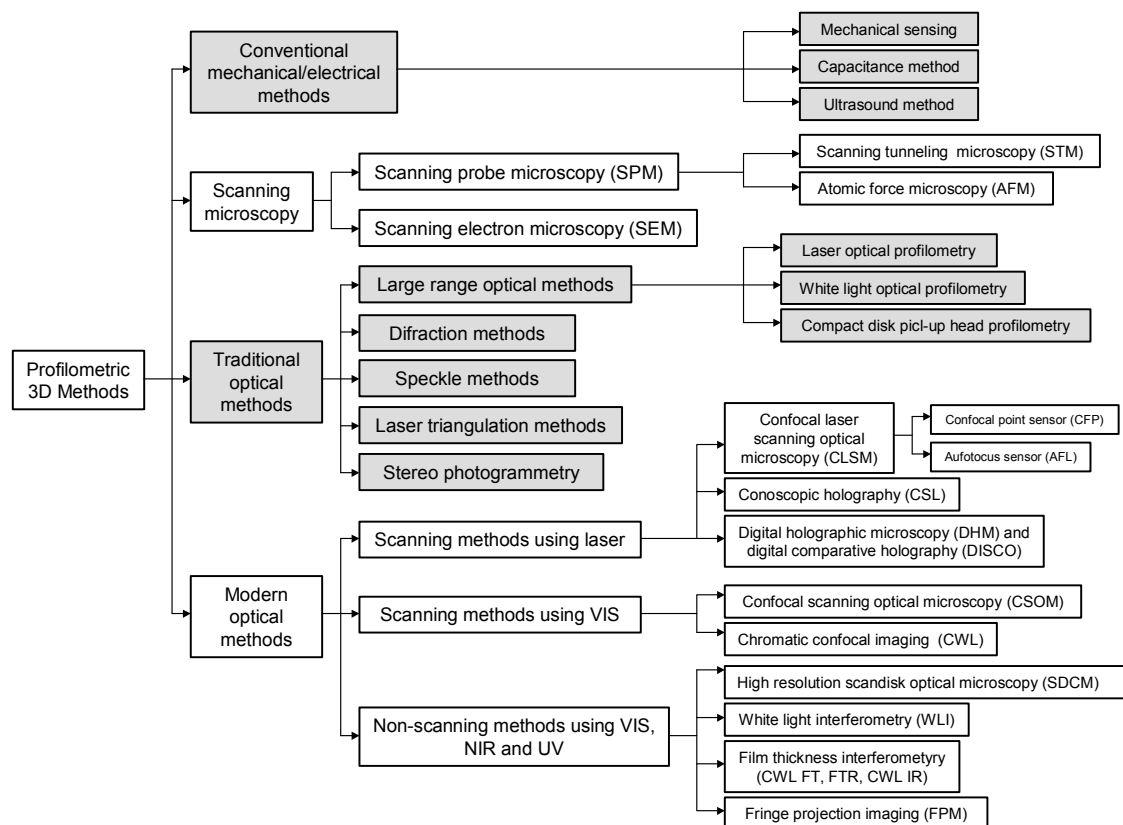


Figure 2.4 A classification of profilometric 3D methods based on sensing principle.

core in a fixed coil), or optical (displacement of a mechanical instrument in front of photo-electric cells) [2]. The quality of the measurement essentially depends on the accuracy of the mechanical translation unit, on the acquisition line and on external

disturbances. They directly limit the capability of the instrument to assess very smooth surfaces.

A special type of instrument combines the reliability of mechanical scanning with the precision of optical interferometry (by an integrated laser beam and Michelson interferometer) [6]. Signals generated either by reference or by the mechanical measurement arm are conveyed to photo diodes for interference fringe detection. The movement of the translational system (x direction) is measured by a second Michelson interferometer. This means, that the horizontal position of any point on the surface is also known, with a degree of precision which is free of any imperfection due to positioning of mechanical instruments. Under proper environmental control, this instrument is probably the most precise mechanical contact sensor for very large measurement scales (of the order of 5 mm).

2.3.1.2 Measurement by the capacitance method

The basic principle [7] is that a condenser should be formed between the sample to be measured and a thin electrode placed close to the surface. This thin electrode (with a thickness of approximately 0.3 μm) is made in such a way that only the local electric field in the immediate vicinity has any influence on it. The electrode is moved over the surface perpendicularly to its plane, the whole behaviour like a runner, so that the average distance between the electrode and the surface is practically constant. The spatial resolution depends on how does surface adjacent to the electrode affect the capacitance value. As the electric field is not only due to the surfaces facing it, the height measurement is balanced by the heights close to the electrode.

2.3.1.3 Measurement using ultrasound

Ultrasound back scattering can be a mean of measuring the surface topography of machined parts [8]. This system is normally based on a transducer which sends out a pulsed ultrasound signal and collects its echo, reflected off the surface. The surface profile is deduced from the time the signal takes to travel between the transducer and the surface under study. The ultrasound signal is sensitive to several factors such as ultrasound frequency coupling medium, angle of incidence, diaphragm aperture and distance from the surface.

2.3.2 Optical methods

2.3.2.1 Large range optical methods

Large range optical instruments refer to those whose peak-to-valley roughness is at least an order of magnitude higher than the wavelength of light. Low roughness surfaces refer to those whose peak-to-valley height is of the same order of magnitude as the wavelength of light or smaller. There are four types of large range optical instruments:

- a) **Laser optical profilometry**, that uses a wide aperture objective which focuses a laser beam onto the surface to be studied [9]. The light scattered back by the surface is collimated* on a photo detector which receives a maximum signal when the surface is at the focal point. A servo-control system controls the position of the objective until the signal reaches a maximum. The simplicity of the system is attractive, but it is rather slow, as each measurement point requires the beam to be focused, so the objective needs to be moved.
- b) **White light optical profilometer**, which works on the white light [10] but is based on a similar principle to that in (a) above. The main advantage is that it does not require any of the mechanical parts used to re-focus the beam to be moved. The light scattered back by the surface is received by two photo detectors which are symmetrical with regard to a separating cube. The values of light intensity collected by both photo detectors, the objective magnification and another values related with the geometry of the optical parts are used to calculate the height values. The depth of field and the lateral resolution depend on what objective is used.
- c) **Profilometer using a compact disc pick-up head** [11]. The focusing lens of the laser beam is mounted on a motorised system so that the beam can be re-focused according to local surface topography. Beam diameter and hence the spatial resolution, is comparable to that obtained with a classical contact profilometer. A motor displaces the optical instrument which focuses the beams; the signal delivered by photo detectors controls the movement.

* Collimated light is light whose rays are nearly parallel, and therefore will spread slowly as it propagates.

- d) **Profilometer for form measurement.** This system allows real time sample control and form defect measurement [12], gives some topographical information according to Beckmann Theory [13] as well as assumption of a Gaussian distribution of surfaces asperities. A laser lights the surface (parallel beam), and the light reflected by the surfaces is focused onto a bar-graph of photo diodes by triangulation^{*}; the spot formed on the surface moves according to the surface defects and the general form of the sample. This system is useful because of the size of its form defect measurement scale, but the information obtained from the light intensity distribution is incomplete and only approximate.

2.3.2.2 Optical methods for very small roughness

The principle involves bringing together two waves fronts originating either from a reference or from the surface to be studied. In the interference zone, the phase difference between two successive fringes is 2π . The classical interference method at best detects phase differences of $\pi/4$, hence the sensitivity of systems is wavelength-dependent. The type of interferometry used varies from author to author. In the implementation by Biegen and Smythe [14] a Fizeau interferometer is used. In this implementation, a He-Ne laser beam is focused on a diffusing disc in a way to form a source point of adjustable size. The beam is focused onto an objective focus after reflection of a polarising prism. The beam from the surface of the object to be analysed is taken up by the objective and crosses a quarter wave slide. Other authors have opted for a Mirau interferometer [15]. The Optics laboratory at the Faculty of Science in Besançon developed a three dimensional profilometer which uses heterodyne interferometry [16].

Michelson interferometers are also used for fast measurements of form deviations of smooth measuring objects with respect of a reference surface [4]. White light interferometry is also used to measure the surface topography [4]. This method has proven to be a very good tool to obtain good height measurements because of carefully selecting of two wavelengths of the spectra it is possible to greatly increase the dynamic range of the measurement over that can be obtained using a single

^{*} In trigonometry and geometry, triangulation is the process of determining the location of a point by measuring angles to it from known points at either end of a fixed baseline, rather than measuring distances to the point directly. The point can then be fixed as the third point of a triangle with one known side and two known angles.

coherent wavelength [17]. White light interferometers are nevertheless stationary lab devices, then measuring under difficult surroundings conditions is problematic. This methods will be discussed in more detail in Section 2.4.

Table 2.1 Measuring ranges and resolution of the most important non-contact optical methods for 3D topometry.

Method	Measure range		Resolution	
	xy	z	xy	z
Laser optical profilometry	up to 5 mm	4 mm	5 µm	8 nm
Compact disk pick-up head profilometry	1 mm - 5 mm	-	1 µm - 2 µm	1 µm
Diffracton methods	3 mm - 4 mm	-	3 µm	5 nm - 2 µm
Speckle methods	-	-	1 µm - 30 µm	20 nm - 70 nm
Laser triangulation methods	-	3 mm	10 µm - 20 µm	300 nm
Confocal laser scanning microscopy by confocal point sensor (CFP)	4 mm	1 mm	1 µm	20 nm
Confocal laser scanning microscopy by autofocus sensor (AFL)	2 mm	1.5 mm	1 µm - 2 µm	10 nm
Conoscopy holography (CSL)	25 mm - 100 mm	8 mm - 35 mm	12 µm - 35 µm	1 µm - 10 µm
Digital holographic microscopy (DSM) and DISCO	0.1 mm - 3 mm	1 mm - 10 mm	1 µm - 50 µm	0.75 µm - 3 µm
Confocal scanning optical microscopy (CSOM)	1 mm - 100 mm ^{*1}	20 µm	130 nm - 200 nm	50 nm ^{*1}
Chromatic confocal imaging (CWL)	up to 100 mm	300 µm - 25 mm	1 µm - 12.5 µm	3 nm - 250 nm
High resolution scandisk optical microscopy (SDCM)	114 µm - 1520 µm	up to 400 µm	0.198 µm - 1.98 µm	1 nm - 10 nm
White light interferometry (WLI)	0.24 mm - 1.6 mm	100 µm - 400 µm	4.8 µm - 32 µm	0.1 nm
Interferometric film thickness sensor (CWL FT)	9 - 26 mm ^{*2}	2 µm - 250 µm	5 µm - 20 µm	10 nm ^{*3}
Thin film sensor (FTR) using VIS	-	50 nm - 20 µm	200 µm - 800 µm	1 nm ^{*3}
Thin film sensor (FTR) using NIR	-	70 nm - 70 µm	200 µm - 800 µm	1 nm ^{*3}
Thin film sensor (FTR) using VIS/NIR	-	50 nm - 100 µm	200 µm - 800 µm	1 nm ^{*3}
Thin film sensor (FTR) using UV/VIS	-	10 nm - 20 µm	200 µm - 800 µm	1 nm ^{*3}
Thin film sensor (FTR) using UV/VIS/NIR	-	10 nm - 70 µm	200 µm - 800 µm	1 nm ^{*3}
Infra-red film thickness sensor (CWL IR)	23.5 mm ^{*2}	40 µm - 3500 µm	6.5 µm	200 nm ^{*3}
Fringe projection (FPM)	1.5 mm - 4 mm	0.5 mm - 1 mm	2 µm - 3 µm	0.1 µm

^{*1} by near-field scanning optical microscopy (NSOM)

^{*2} as scan-mode

^{*3} resolution thickness

2.3.2.3 Measurement methods using diffraction

Several methods have been developed over the last few years [18,19]. All of them where electromagnetic radiation is scattered by a rough surface – a phenomenon whose theory was studied by Beckmann [13] and Hingle et al [20] - use an optical device for the Fourier transformation of the surface based on a set of lenses which produce a coherent light source point. An array of photo diodes receives the diffraction of the sample. The power spectrum is made of three elements: the first one relating to the specular reflection on the sample and the two others to the diffracted light in relation to harmonic or random components of the surface. This apparatus is simple and measurement is rapid, but its main drawback is that it gives only the power spectrum of the surface, i.e. a magnitude which is difficult to link to the general surface topographical parameters.

There are variations of this apparatus, in particular that by Brodmann et al [21] which uses an infra-red source. The experimental apparatus proposed by Stover [22]

includes a goniometer on which a light detector collects the scattered beam (power scattered in a given direction).

2.3.2.3 Methods using the Speckle phenomenon

A Speckle pattern is a random intensity pattern produced by the mutual interference of a set of wavefronts. This phenomenon has been investigated since the time of Newton, but Speckles have come into prominence since the invention of the laser and have now found a variety of applications. If the analysed surface has asperities whose spatial distribution wavelength is almost the same as that of the light source, the light will be scattered in different directions in the space, leading to interference. The intensity observed will no longer be simply that predicted by geometrical optics, but will also include – to the detriment of the specular intensity - many diffuse components. The use of a coherent source reinforces this phenomenon, in which diffused wave interference will take place, leading to Speckle patterns.

Speckles form a Speckle figure which can be used to obtain topographical properties of a surface: the random nature of the speckle phenomenon means that the intensity distribution observed is a characteristic of a given surface. The techniques employed are very varied and have undergone considerable development. They all use an aperture detector which is small enough to allow individual analysis of each speckle. Special implementations of the same phenomenon are the correlation between surface roughness and size of laser spot [23], the use of interference between two speckle figures [24,25] and the use of polychromatic light [26].

2.3.2.5 3D measurement by laser triangulation method

This system uses the triangulation method, by focusing a laser spot on the surface to be studied [4]. Its relief can be reconstructed by analysing the defocalisation of the laser diode. Laser is focused on the object to be analysed, and the light diffused by the surface is focused on a photo detector. When the object is moved, the height variations encountered along the surface are expressed as a displacement of the spot on the photo diode. The position of the spot on the detector is converted into an electric signal which is proportional to the height of each point of the scanned profile. The resulting 2D slope map is numerical integrated and thus height information of the entire surface is obtained [27].

2.3.2.6 Stereo photogrammetry

The calculation of the 3D data by photogrammetry is carried out from images of (at least) two cameras [28]. They are condensed and observed in an analysing evaluation instrument, where they overlap and create a three-dimensional image, analogous to the human eye's spatial vision. With the help of a visible marker that is blended in, the observing operator follows the surface contours and thus transfers the surface structure data into a PC which evaluates their spatial co-ordinates and determines the typical surface parameters. To analyse the structure, the program can produce the image of the surface from various visual angles. It is shown in central projection so that a real impression of the structure is given. In addition, a layered map of the surface can be shown. Parts of the surface can also be zoomed for detailed information. Classical 3D measurement procedures based on photogrammetry causes systematic errors at strong curved surfaces or steps in surfaces.

2.3.3 Scanning microscopy

2.3.3.1 Scanning probe microscopes (SPM)

Scanning probe microscopes are a family of instruments used for studying properties of materials from the micron up to the atomic level. Two fundamental components that make scanning probe microscopy possible are the probe and the scanner. The probe is the point of interface between the SPM and the sample; it is the probe that intimately interrogates various qualities of the surface. The scanner controls the precise position of the probe in relation to the surface, both vertically and laterally [29]. In order to generate an SPM image, the scanner moves the probe tip close enough to the sample surface for the probe to sense the probe-sample interaction. Once within this regime, the probe produces a signal representing the magnitude of this interaction, which corresponds to the probe-sample distance. This signal is referred to as the detector signal.

- a) **Scanning tunneling microscopes (STM)** measure the topography of a surface using a tunneling current depending on the separation between the probe tip and the sample surface. STM is typically performed on conductive and semi-conductive surfaces. Common applications include atomic resolution

imaging, electrochemical STM, scanning tunneling spectroscopy (STS), and low-current imaging of poorly conductive samples using low-current STM.

- b) The **atomic force microscope (AFM)** or **scanning force microscope (SFM)** grew out of the STM and today is by far the more prevalent of the two. Unlike STMs, AFMs can be used to study insulators, as well as semiconductors and conductors. The probe used in an AFM is a sharp tip, typically less than 5 μm tall and often less than 10 nm in diameter at the apex. The tip is located at the free end of a cantilever that is usually 100-500 μm long. Forces between the tip and the sample surface cause the cantilever to bend or deflect. A detector measures the cantilever deflections as the tip is scanned over the sample, or the sample is scanned under the tip. The measured cantilever deflections allow a computer to generate a map of surface topography. Several forces typically contribute to deflection of an AFM cantilever. To a large extent, the distance regime (i.e., the tip-sample spacing) determines the type of force that will be sensed.

2.3.3.2 Scanning electron microscope (SEM)

Scanning electron microscopy is a method for high-resolution imaging of surfaces. The SEM uses electrons for imaging, much as a light microscope uses visible light. The advantages of this method over light microscopy include greater magnification (up to 100,000X) and much greater depth of field.

An incident electron beam is raster-scanned across the sample's surface, and the resulting electrons emitted from the sample are collected to form an image of the surface. Imaging is typically obtained using secondary electrons for the best resolution of fine surface topographical features [30,31]. Alternatively, imaging with backscattered electrons gives contrast based on atomic number to resolve microscopic composition variations, as well as, topographical information.

2.4 Modern optical methods for topography

In recent years, the possibilities for surface topography quantification have been broadened by the availability of new non-destructive, non-contact measuring methods [1], which are able to image surfaces three-dimensionally using the x-, y-

and z-axes in the orthogonal coordinate system. In resulting images, the height of each surface point is encoded as a grey value. This overcomes the three-dimensional characterization of surfaces by two-dimensional height profiles, obtained by sectioning fracture surfaces and drawing the profiles.

2.4.1 Scanning methods using laser

2.4.1.1 Confocal laser scanning optical microscopy (CLSM)

Laser scanning confocal microscopy is a recent optical microscope technique. In this type of microscope, a laser scans the surface point-by-point [32,33]; the emitted or transmitted signal is picked up by a detector and the image is reconstructed. A confocal diaphragm eliminates the effect of the upper or lower planes, in epifluorescence or in reflection. Compared to traditional microscopy, confocal microscopy with laser scanning has two main advantages: (1) the spatial and axial resolution are increased and (2) perfectly superposable images can be obtained of successive z-planes, of series of optical cross-sections, where the potential for 3D visualisation, reconstruction and quantification is enormous [2].

A recent innovation of this method uses a confocal point sensor (CFP) (United States Patent 7170075) [34-37], which measuring principle is as follows: an oscillating lens emits a focussed and punctiform laser beam onto an object's surface. The reflected light from the given measuring position passes through a half mirror onto a pinhole. Behind the pinhole sits a light sensitive detector. Every time the laser beam focuses on the object's surface, the maximum amount of the emitted laser light is able to pass the pinhole. In this moment, the position of the oscillating lens is measured allowing calculate the exact height information of the measured position. This method allows high-resolution measurements, precise results even with changes in the surface reflectance at different measurement positions and a fast measurements even on surfaces with very low reflectance. Typical applications are: fast topography and profile measurement even on sensitive and soft materials, measurement of microstructures, measurement of ground and polished optical components, control of electronic components, inspection of tools and products in the field of plastic injection moulding and inspection of dimensions, step-height etc. on printed circuit boards.

Another new method is the so called autofocus measurement (AFL) (United States Patent 6824056) [34,37,38], which is based on the principle of dynamic focusing. A movable lens is approached toward a point on the specimen until the emitted light spot of the sensor is in focus (controlled by focus detector). While scanning an entire surface, the lens is permanently moved up and down in order to keep the focus. By measuring the relative change of the height it is possible to determine the z-height at the measured position. The method allows high resolution and precision, small measuring spot, high lateral resolution, coaxial measurement, no shading effects, high sampling rate and the possibility of integrate a microscope for convenient selection of measurement position. Typical applications are: quality assurance in automotive industry (interior, cylinders, shafts, electronics, etc.), profile measurements of lens contours, profile and 3D measurements, roughness determination on technical surfaces (tools, cylinders, finished products, etc.), dimension measurement of (micro-)injection molding parts, measurement of water flatness, research and development in microelectromechanical systems and in medical technology (catheters, prostheses, etc.).

2.4.1.2 Conoscopic holography (CSL)

Conoscopic holography is a simple implementation of a particular type of polarized light interference process based on crystal optics. [34,39].

A laser beam is focused on the specimen. The light which is scattered in the measuring spot is captured by the sensor. A configuration of two polarizers and one uniaxial crystal splits the captured light into two light beams that pass the crystal with different velocities. This leads to a superposition on the detector. The distance between lens and specimen is evaluated from the resulting double slit interference pattern. This new technique has many advantages over classical holography [40]: uses concentric optics and is insensitive to the position of the key optical

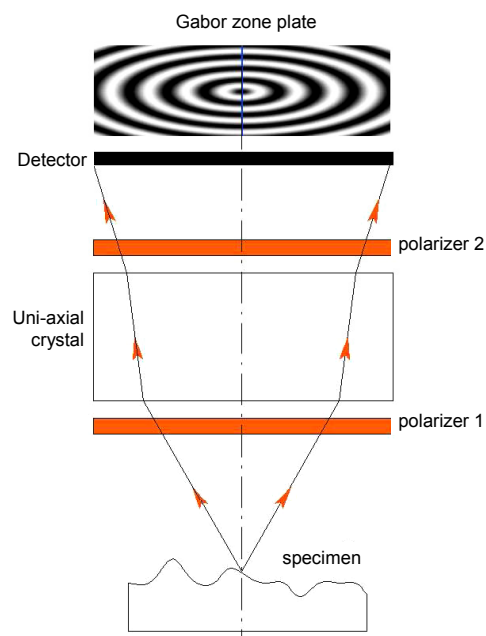


Figure 2.5
Schematic presentation of the measuring principle of CSL [34].

components, an interfringe distance adjustable to common CCD sensors, which facilitates the interface with computer system, and light need be only quasi-monochromatic (in practice, a 10 nm spectral bandwidth is enough) but not spatially coherent. Measuring features of this method are: wide working range and measuring bandwidth, very well suited for steep edges and coaxial measurement, no shading effects. Typical applications of conoscopic holography are almost the same of the autofocus measurement mentioned above.

2.4.1.3 Digital holographic microscopy (DHM) and digital comparative holography (DISCO)

Digital holographic microscopy (DHM) is an imaging technique, which can be applied to visualisation and metrology of microscopic objects [41]. This method is based on the classic holographic principle, with the difference that the hologram recording is performed by a digital image sensor, e.g. a CCD or CMOS camera. The subsequent reconstruction of the holographic image that contains information about the object wave is carried out numerically with a computer. The method provides quantitative phase contrast imaging that is suitable for high resolving investigations on reflective surfaces as well as for marker-free analysis of living cells. Results from engineered surfaces and living cells demonstrate applications of this method for technical inspection and life cell imaging [42].

For industrial applications, fast technologies for shape comparison between a master and a test object are needed. This task can be fulfilled with the help of comparative digital holography, which is the concern of the BMBF project DISCO (Distant Shape Control by Comparative Digital Holography) [43,44]. This 'comparison DHM' allows a straight comparison with a gauge provided by a manufacturer or customer. The phase subtraction between ideal and actual wavefront of the object provides data equivalent to those given by a Twyman-Green or a Mach-Zehnder interferometer [41].

2.4.2 Scanning methods using white light

2.4.2.1 Confocal scanning optical microscopy (CSOM)

Confocal scanning optical microscopy (CSOM) is an optical microscopic technique [32], which offers significant advantages over conventional microscopy.

In this confocal mode, an aperture, usually slightly smaller in diameter than the Airy disc pattern*, is positioned in the image plane in front of the detector, at a position confocal with the in-focus voxel** . Light emanating from this in-focus voxel thus through the aperture to the detector, while that from any region above or below the focal plane is defocused at the aperture plane and is thus largely prevented from reaching the detector, contributing essentially nothing to the confocal image. It is this ability to reduce out-of-focus blur, and thus permit accurate non-invasive optical sectioning, that makes confocal scanning microscopy so well suited specially for the imaging and 3D tomography of stained biological specimens.

2.4.2.2 Chromatic confocal imaging (CWL)

Unlike conventional microscopy, which images, simultaneously, all the points in the field of view, chromatic confocal microscopy images only one object point at a time. The field is reconstructed by (x,y)-scanning [45].

This novel optoelectronic setup based on a quasi confocal, z-axis extended field, proprietary design was developed for high resolution non contact 3D surface metrology including roughness characterization and surface flaw detection.

The instrument uses a chromatic white-light sensor (CWL) [4,37], which is based on the principle of chromatic aberration of light. White light is focused on the surface by a measuring head with a strongly wavelength-dependent focal length (chromatic aberration). The spectrum of the light scattered on the surface generates a peak in the spectrometer. The wavelength of this peak along with a

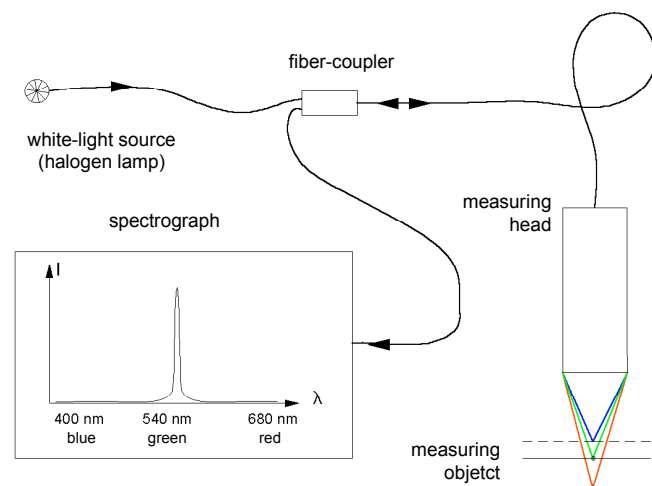


Figure 2.6 Schematic presentation of the measuring principle of CWL [34].

* In optics, the Airy disc (or Airy disk) and Airy pattern are descriptions of the best focused spot of light that a perfect lens with a circular aperture can make, limited by the diffraction of light. The diffraction pattern resulting from a uniformly-illuminated circular aperture has a bright region in the center, known as the Airy disc which together with the series of concentric bright rings around is called the Airy pattern. Both are named after George Biddell Airy, who first described the phenomenon. The diameter of this pattern is related to the wavelength of the illuminating light and the size of the circular aperture.

** A voxel (a portmanteau of the words *volumetric* and *pixel*) is a volume element, representing a value on a regular grid in three dimensional space. This is analogous to a pixel, which represents 2D image data.

calibration table reveals the distance from sensor to sample. The sensor works on transparent, highly reflective or even matt black surfaces [46,47]. It is extremely fast and has virtually no edge effects. This method allows very high resolution due to small spot and is suited for use in difficult ambient conditions. Additionally provides a coaxial measurement without edge effects. For these reasons this method is applied in quality checks in front-end and back-end fabrication of semiconductors, research and development and quality control in micro systems engineering, in medical technology and in automotive industry. Another fields of application are: quality checks of circuit boards, injection moulding of (micro-)parts and optical components and 3D measurements on heavily structured surfaces (e.g. tools, rollers, components).

Due to its modified optical setup and its superluminescent diode, a high-resolution version of this sensor (CWL-HR) provides the highest lateral resolution of the family (sub- μm). It works on highly reflective as well as light absorbing and rough surfaces. It may even be used to measure the thicknesses of thin transparent films, as well as in nanotechnology, medical technology and life sciences [48].

2.4.3 Non scanning methods using VIS, NIR and/or UV

2.4.3.1 High-resolution scandisk confocal microscopy (SDCM)

Scandisk confocal microscopy is an optical imaging technique used to increase micrograph contrast and/or to reconstruct three-dimensional images by using a spatial pinhole to eliminate out-of-focus light or flare in specimens that are thicker than the focal plane (United States Patent 6824056) [49].

The measuring principle [37] is that the light of a LED is focused by a movable objective on an object's surface, then reflected and finally captured by a detector. If the object is out of focus, its illumination and image on the detector are unsharp, which results in a very low output

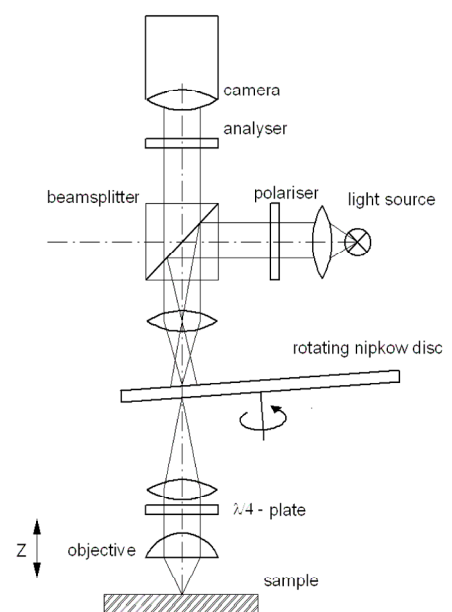


Figure 2.7 Functional principle of confocal microscopy [34].

signal. Once the object's surface is in the focus of the objective and the detector, a maximum signal is received. Very precise information on the height can be obtained by gradually moving the focal point (lens) in z-direction.

This punctiform principle can be extended into a field of view method by the use of a rotating Nipkow disc which distributes the incident light beam line by line over the object's surface to measure 3D topography, profiles and roughness [50-52].

This method allows fast 3D measurement of topography, structure and roughness with excellent height resolution and depth of field. Typical application fields are the semiconductor industry, microelectromechanical systems, optics, automotive industry as well as plastic and paper industries.

2.4.3.2 White light interferometry (WLI)

White interferometry (WLI) is a fast method to perform 3D topographical measurements [34]. It utilizes a light source with very low temporal coherence. By means of a beam splitter this light is separated into a reference beam (reflected to a reference mirror) and an object beam that strikes the surface to be measured. The light reflected from both, the reference mirror and the measured object is overlaid.

This interference pattern is captured by a camera. Whilst performing the topography measurement, the objective is gradually moved in small steps into z-direction. At

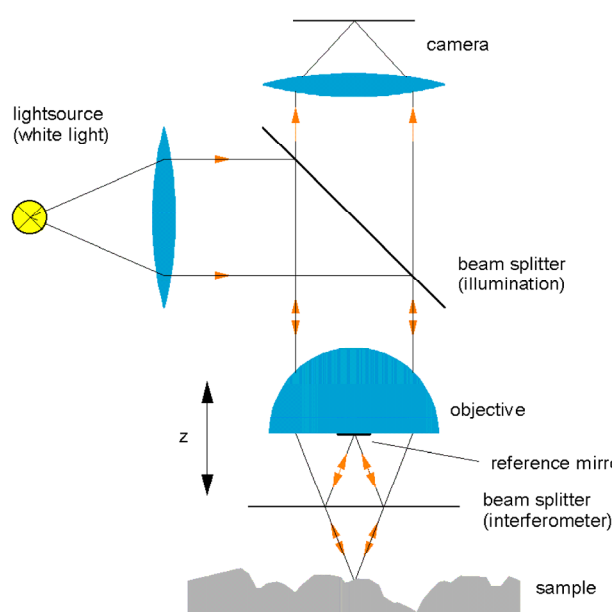


Figure 2.8
Schematic presentation of the measuring principle of WLI [34].

each position the camera takes a single image. Then, all images are compiled into an image stack, which is used to render the 3D topography. Due to the low temporal coherence of the white-light the WLI characterizes reflective and rough surfaces as well as step heights with very good height resolution, which is typical for interferometric measurements approaches [17].

Some measuring features of this method are sub-nanometer height

resolution, very fast 3D measurements and measurement of highly reflective, rough or structured surfaces. Typical applications are: roughness measurement in nm-range, e.g. on optical components such as mirror or lenses, evaluation of micro structures (e.g. microelectromechanical systems, microfluidics, microoptics), measurement of step-height in the field of semiconductors, measurement on different materials (e.g. metal, semiconductors, glass, plastics, paper, lacquers and coatings) and measurement on liquids [34,53].

2.4.3.3 Film thickness interferometry

Interferometry makes possible the determination of film thickness by different types of sensors.

- a) **Interferometric film thickness sensor (CWL FT)** allows a fast, non-contact and highly resolved thickness measurement of films and coatings [34,54,55]. Its function is based on the principle that at each boundary layer of a transparent film incident light is partially reflected. To measure film thickness with the CWL FT, light from a white light source (halogen bulb) is focussed onto the film and the spectrum of the reflected light is evaluated. Due to the interference of light from the boundary layers, the spectrum shows a typical waviness from which the sensor calculates the film thickness. Since the evaluated spectrum depends not only on the thickness, but also on the refractive index of the material, this parameter is included in the calculation of the thickness measurement. Using this method is possible to measure transparent films and coatings with application in the measurement of foils in the food industry, control of blister packaging, varnish measurement for the automotive industry and examination of multilayer systems such as air gaps below transparent covers and measurement. Additionally it is possible to integrate the sensor in a scanning system for application in thickness mapping on semiconductors, for example.
- b) **Thin film sensor (FTR)** [34] allows a high-resolution, non-contact measurement of single or multi-layer thin films by the superimposition of light beams reflected at the boundaries of a thin film. The evaluation of the spectral interference pattern of the superimposed light beams results in the film thickness. This measured reflectance spectrum is compared with a calculated

one, where the unknown thickness is systematically varied until both spectra match. The method allows the measurement of both, single and multi-layer films. Some applications are reported in measurement of thickness of oxides, nitrides, photoresist and other semiconductor process films, antireflection coatings and antiscratch coatings, measurement on opaque substrates (e.g. aluminium, brass, ceramics, copper, steel and plastics), thin films in the optics industry and lacquers and of lacquers and thin foils. New application fields of this method are reported on measurements of oil-film thickness [56] and in biology [57]. These instruments can work with different combinations of VIS, NIR and UV.

c) Infrared film-thickness sensor (CWL IR) [58] allows a high-resolution fast and non-contact film-thickness measurement by the spectral analysis of the interference of beams reflected at the boundaries of a transparent film on a substrate. The intensity of the reflected radiation shows a periodical waviness pattern that is dependent on the film thickness. From the intensity pattern and with the known refractive index of the film material the film thickness is calculated. A sensor provided by FRT Fries Research & Technology (Germany) [34] was developed especially for samples which are opaque in the VIS but are transparent in the near IR, like many semiconductor materials. This sensor is accompanied by a narrow band source with 1300 nm center wavelength. The method can be also used for measurement of film-thickness of objects on opaque carrier materials as well as for measurement of oil film-thickness [59]. Special measurement features are the high measuring range and the high local resolution. Adapted to a scanning system, this method allows the film-thickness mapping.

2.4.3.4 Fringe projection imaging (FPM)

This cost-effective instrument [34] type can be applied for very fast, precise and high-resolution topography measurements, because it allows the complete topography of a surface to be acquired during one single measurement within a few seconds. Scanning of the sensor over the sample is not required. The measuring method is based on the principle of fringe projection. From the distortion of a striped pattern

being projected on the sample, the sensor investigates the height of each measuring point.

To achieve a fringe projection, a digital micro mirror array is integrated into the instrument. Compared to similar methods, this procedure allows good light efficiency, very high fringe contrast as well as a distortion-free projection which contributes to high-precision and high-resolution surface measurements. From the measured topography data, waviness, roughness, radius of curvature as well as contours etc. can be determined. Because the higher vertical measuring range, but with some limitations of lateral resolution, this method is recommendable for surfaces such as textile materials and embossed plastic structures.

3 Topographic characterisation techniques

Nowadays reliability and versatility of non-contact optical characterisation methods for topography are widely recognized. Chromatic confocal imaging (CWL) and high-resolution scandisk confocal microscopy (SDCM) are at present the most used techniques of this type of instruments [60].

Before topographical characterisation, the adequate selection of the optimal measuring method and corresponding sampling conditions were of fundamental importance.

3.1 Justification of the optical method used

The selection of the optimal topographical measuring method depends on cut-off length, resolution, measure time and principally on optical sensibility. Another important criterion for the selection of the optical measure method is the necessity of a non-contact procedure, especially in case of textile materials, where the position of fibers and filaments is very sensible to mechanical contact.

Chromatic confocal imaging method was selected as measuring topographical method for the study of surface topography and correlating between it and other relevant surface properties of polymer materials. All samples were examined using a MicroGlider instrument (FRT, Germany) [34]. After measuring, topographical data obtained were processed by defined mathematical operations before the calculation of the characterisation parameters.

As shown in [Table 2.1](#), chromatic confocal imaging, depending on instrument characteristics, allows a lateral measure range and a vertical measure range up to 100 mm and 25 mm, respectively, and a lateral resolution and vertical resolution up to 1 μm and 3 nm, respectively.

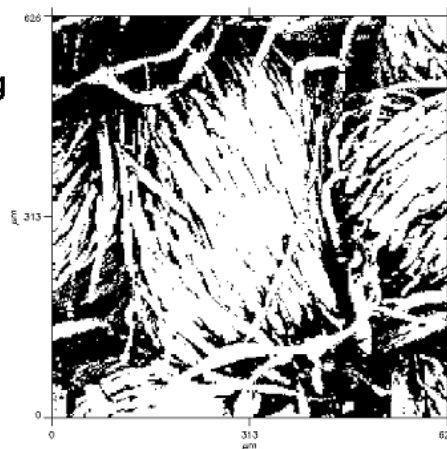
The most important advantages of CWL over SDCM are the longer lateral measure range (100 mm vs. 1.52 mm) and principally the wider vertical measure range (up to 25 mm vs. up to 400 μm), which makes the confocal microscope inadequate to measure surfaces with high roughness, for example textile materials, as can be seen in *Fig. 3.1*. By extremely low roughness, the topographical characterisation of light reflective surfaces (higher brilliancy) can demand much more sensitivity to focal detection than the available by a confocal microscopy.

The most important disadvantage of chromatic confocal imaging is the extremely long duration of the measurement, due to the point-by-point scanning process.

Chromatic confocal imaging

Distance between points = 1 μm
 Total number of points = 374,544
 Invalid points = 130,716 (34.9 %)

Duration of the measurement = aprox.
 100 minutes



High-resolution scandisk confocal microscopy

Distance between points = 0.8 μm
 Total number of points = 585,225
 Invalid points = 452,379 (77.3 %)

Duration of the measurement = aprox.
 5 minutes



Figure 3.1 Sensibility comparison between CWL and SDCM sensors by the same sample, which corresponds to a cotton fabric surface (sampling interval = 626 μm). White regions represent valid (measured) points, while black regions represents invalid (no detected) points.

According to *Fig. 3.1*, CWL provides much more data for a rough surface but after longer measure times. Because the most important selection criterium is sensibility, CWL was selected as measuring method to perform the present study.

3.2 Selection of the initial sampling conditions

3D surface characterisation is based on digital areal topographic data and, therefore, sampling conditions are represented by the sampling interval, Δx , Δy , the size of sampling matrix, $M \times N$, and the sampling area, $A_m = l_x \times l_y$ (see [Fig. 2.1](#)). Two of the three parameters are independent variables. The third parameter can be calculated from the other two. The relation between these three parameters is given as follows:

$$l_x = (M-1)\Delta x, \quad l_y = (N-1)\Delta y, \quad A_m = l_x \times l_y \quad (3.1)$$

The size of the sampling area and sampling interval are very important quantities, because they directly determine the long-wavelength and shortwavelength limits of the measurement.

Stout et al. [2] recommended the following procedure to select the initial sampling conditions:

- 1) The sampling area size is equal to the evaluation area. The assessment based on one sampling area is acceptable. An averaging of results from several sampling areas is not required.
- 2) The number of sampling points in one trace M and the number of sampling traces in the area N are required to be values of a power of two. For characterising isotropic surfaces, $M = N$ is necessary. N need not be equal to the number of sampling points for characterising anisotropic surfaces. The lowest limit for M in this case is $2^p = 128$ ($p = 7$), while the lowest limit for N is $2^q = 32$ ($q = 5$).
- 3) The determination of sampling interval series is based on many considerations. It is suggested that the sampling intervals, Δx and Δy , in the two orthogonal directions, x and y , be equal in characterisation of isotropic surfaces. If Δx is not equal to Δy is also acceptable for characterising anisotropic surfaces.
- 4) The sampling interval series is recommended to follow the rule 1, 2, 5, 10,.... Different units (nm, μm or mm) can be assigned to this series.
- 5) The practical sampling area is determined by the selected sampling size pair and the sampling interval pair. This area might be square or rectangular in case of an anisotropic surface.

The first recommendation supposes that the sample area is statistically representative for all the surface. Stout [2] based the second recommendation on the fact that advanced signal processing techniques, especially spectral analysis, correlation analysis and digital filtering, are very common and frequently used in processing areal topographic data. For convenience and high efficiency of data processing, the Fast Fourier Transformation (FFT) algorithm is inevitably employed to transfer the data from the time or space domain to the frequency domain and vice versa.

The use of optimal statistical sampling conditions depends however on a systematic calculation procedure. After defining the most important topographic characterization parameters (cf. Section 3.5), a calculation procedure of the optimal cut-off length (l_x , also called L_m) and resolution (Δx) for 3D measurements using values of waviness and roughness is presented and discussed (Section 3.6).

3.3 Common pre-processing mathematical operations

After measuring topography, usually some pre-processing mathematical operations are needed to the characterisation. These operations are in general for all type of topographic data, independent of the measuring method used.

Depending on material and measuring conditions, the raw measured data could present three typical problems:

- a) the geometrical plane of the measured surface is not perpendicular to the sensor light direction (see *Fig. 3.2.(a)*),
- b) some points could not be detected by sensor and remain as “invalid points” (cf. Section 3.1), and
- c) some higher or deeper points are undesirable due their connection with interferences (not interesting surface marks, dust particles, etc.)

3.3.1 Correction of surface plane

To adjust the measured surface plane, a reference plane is required to be perpendicular to the sensor direction. There are many planes which could be used for reference by 3D topography characterisation. However, the most common

reference planes are the graphical mean plane, the least squares mean plane and the minimum zone plane.

3.3.1.1 Centre arithmetical mean plane (graphical mean plane)

It is not difficult to extend the concept of the centre arithmetical mean *line* (graphical mean line) in standards [61-63] to the centre arithmetical mean *plane* to obtain “a reference plane representing the form of the geometrical plane and whose normal direction is parallel to the general normal direction of the plane within the sampling area, such that the sums of the volumes contained between it, and those parts of the plane that lie on each side of it, are equal” (Fig. 3.2). However, as specified in [61] and [63] the centre arithmetical mean line is defined and used for graphical convenience; defining the centre arithmetical mean plane would not be graphically convenient and such a defined plane is not unique for random surfaces.

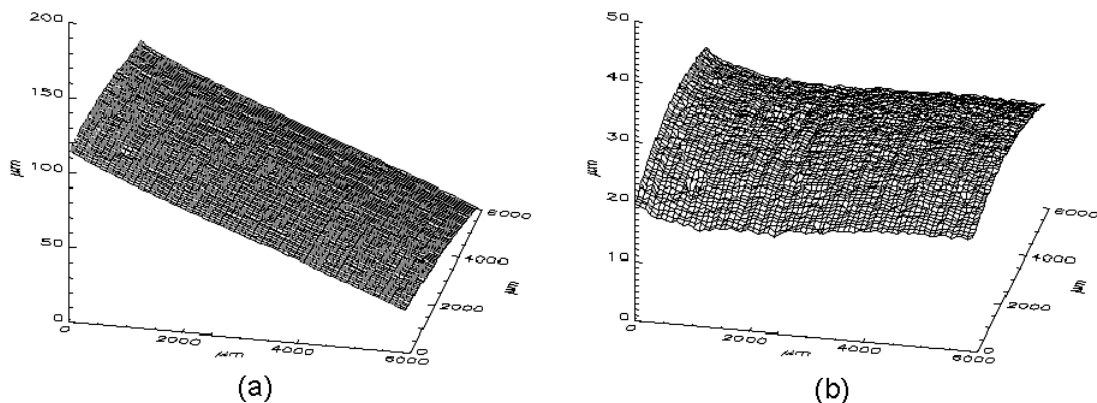


Figure 3.2 Centre arithmetical mean plane as a reference (to compare, note the different display range in z direction):

- (a) 3D representation of surface scanned with a montage slope of only 0.8°
- (b) The same surface transformed using the arithmetical mean plane as a reference.

3.3.1.2 Least squares mean plane

The least squares mean plane is very well defined in mathematics as a plane such that the sum of the squares of asperity departures from this plane is a minimum [64,65]. The normal direction of the least squares mean plane would change with the arbitrary starting points and number of cycles involved in the surface. However, most engineered and optical surfaces are non-periodic. Therefore, in most cases, with no significant outliers, the normal direction of the least squares mean plane would

conform to the normal direction of the measured surface. Thus, it can be used to remove the trend and to level the raw topographic data. In addition, the least squares mean plane is a special case of centre arithmetic mean planes, i.e. it has the attribute that the sum of material volumes above and below it are equal. Therefore, the residual surface which is obtained by subtracting the least squares mean plane from the measured surface has zero mean.

3.3.1.3 Minimum zone plane

The minimum zone plane is recommended in BS standard [66] and ISO standard [67], and is widely used to assess flatness and form errors of surfaces [68, 69]. It takes care of the maximum deviation of the flatness or form and minimises the distance between two parallel planes which just contain the surface. Although the smallest maximum peak and valley deviations can be obtained with respect to the plane, the normal direction of the plane is too sensitive to a few number of extreme outliers. The procedure has a very simple mathematical expression. However, there is no popular procedure or commonly-agreed ‘best’ method to determine the mathematical plane. Many approaches such as Monte Carlo, simples, spiral search and Powell [70], can be employed to find the minimum zone plane.

3.3.2 Correction of invalid data

All x-y coordinates that after the measure have no height value (z) are called “invalid data”.

For isolated invalid points, the easier correction procedure is the calculation of a z mean value using the z values of its neighbours (linear interpolation) [34].

If two or more invalid points are connected, the calculated surface mean height value (that corresponds to all the measured valid points) is assigned momentarily to the invalid neighbours while the calculation of each new value. Applying this procedure, the accumulation of invalid points produce, however, smooth corrected areas (*Fig. 3.3*), which morphology could contrast with the measured surface. In this case, depending on the size of the corrected surface, the necessity of a new measure with another sampling conditions is to consider.

In many cases, correction of invalid data leads to a better illustrations quality of the data (particularly in the case of images).

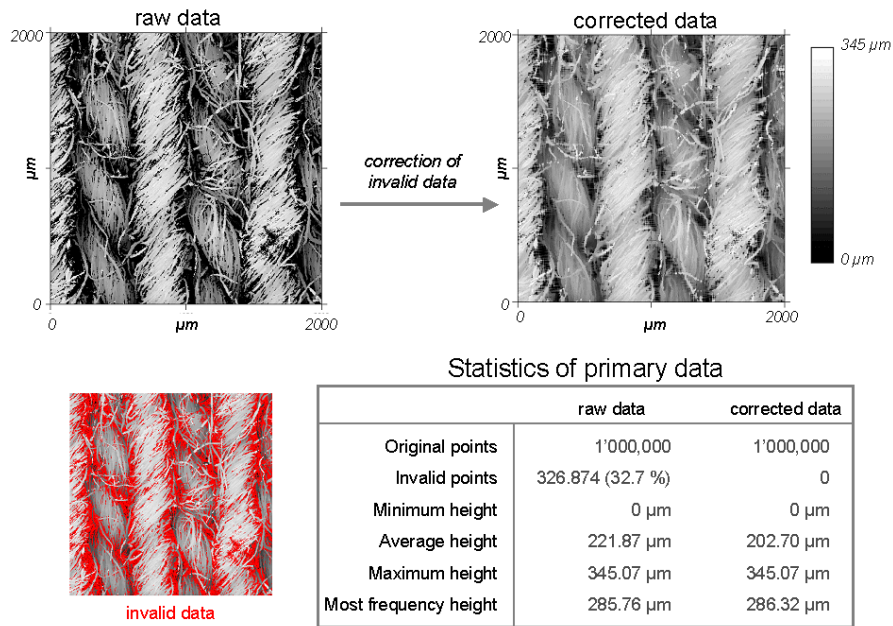


Figure 3.3 The correction of invalid points modifies the statistic of primary data, especially the average height.

3.3.3 Segmentation of data

Mathematical segmentation is the elimination of points or group of points commonly by using the histogram of frequencies or a contour map of the surface, or both as a graphical and numerical input (Fig. 3.4). After mathematical segmentation, new invalid data are produced. If desired, its elimination proceeds by the operation explained in Section 3.3.2.

With or without a posterior correction of invalid data, segmentation statistically modifies the collection of points (surface topography) and then many of resulting topographical and statistical parameters, depending on their mathematical definition.

There are two common purposes to segmenting the topographical data:

- a) **Correction of false points** or elimination of recognized false points, due to, for example, a dust particle or to some reference marks.
- b) **Morphological zooming** or vertical zooming, which can be defined as the mathematical isolation of a collection of height values that corresponds to a recognized morphology. Morphological zooming does not modify the measure area or surface of the map, only eliminates no interested surface topography according to defined scientific or technical criteria (Fig. 3.5).

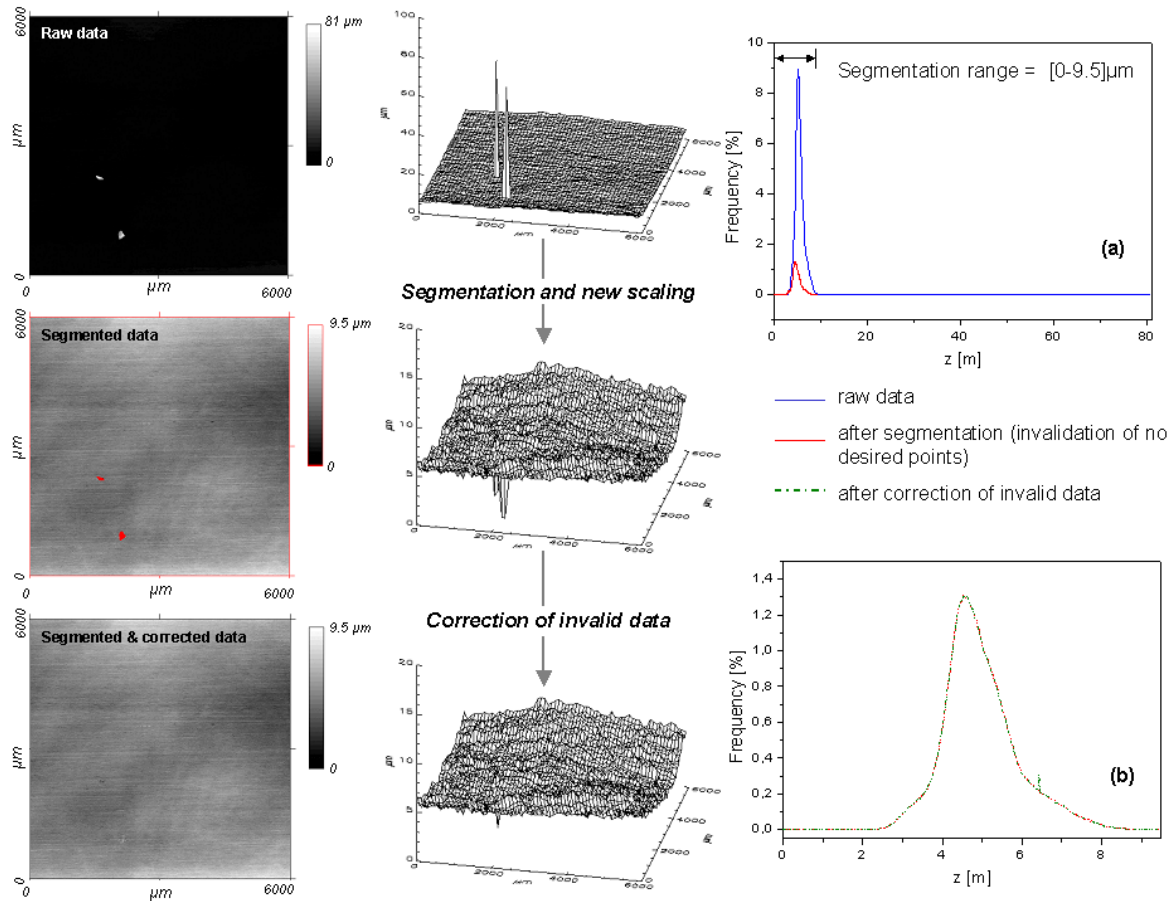


Figure 3.4 Segmentation process of raw data including not desired topographic information corresponding to two dust particles laying at the surface. Histograms of segmented and corrected data (b) show almost the same topography, due to the despicable importance of the invalid points (0.08% of all segmented data, in this case).

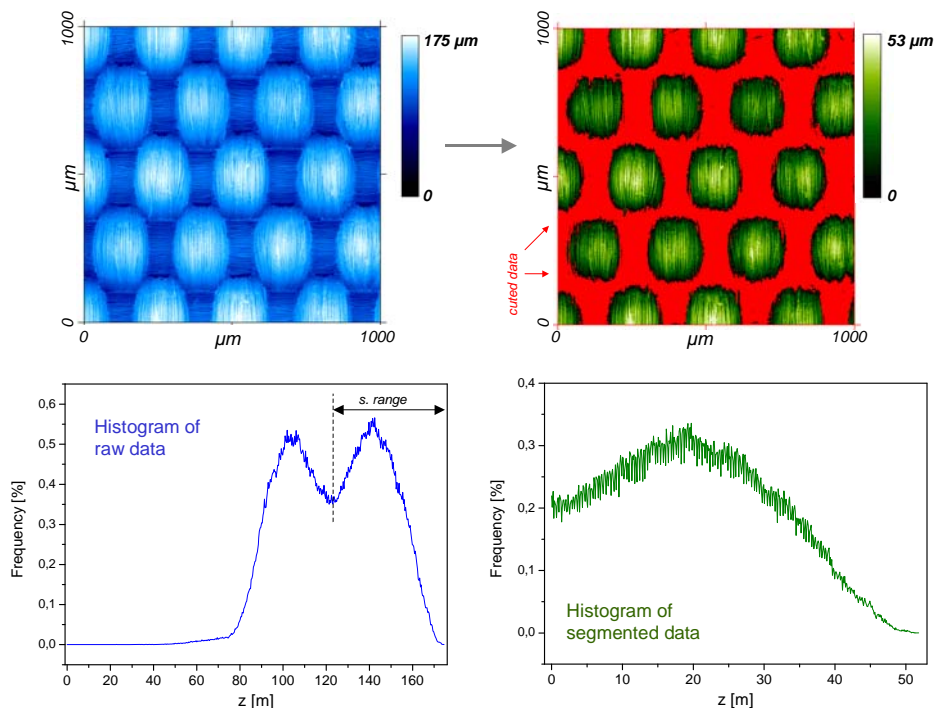


Figure 3.5 Example of a morphological segmentation of a textile surface: The process isolates the warps topography in a polyester woven plain surface. The resulting topography has a new height range and frequency distribution.

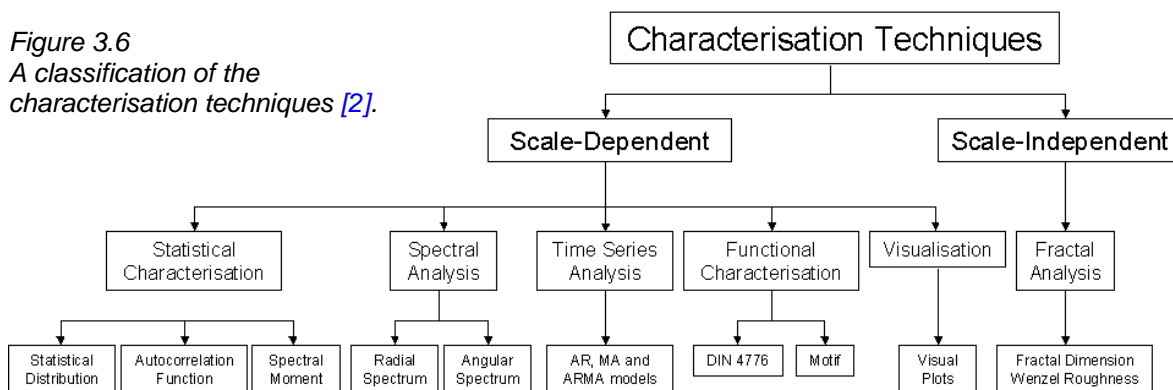
3.4 Characterisation techniques

Independent of the measuring method used to obtain topographical data, the main objective of the characterisation of surface topography is the use of different analysis techniques, such as statistical, mathematical and functional approaches, which provide a guideline for a fundamental understanding and interpreting topographical characteristics. As a consequence, the characterisation leads to quantify the surface topography with some parameters, and hence, to study the surface properties of materials, to control manufacturing process and, in general, to perform functional surfaces.

A general classification of various characterisation techniques from a mathematical point of view (see *Fig. 3.6*) can be subdivided into two main categories: scale-dependent and scale independent characterisation techniques [2].

A term ‘scale-dependent’ is used in recognition of the fact that the results obtained using these techniques are dependent on the measurement scale. With different measure scales, e.g. nanometric and micrometric, analysis results would be quite different. That is because a surface is composed of more than one length scale of roughness, that are superimposed on each other. Due to multiscale nature of surfaces, it was found that most conventional parameters defined by the International Standards [63,71,72] are scale-dependent. In some cases, they do not represent surface characteristics correctly enough.

In the category ‘scale-independent’, topography characteristics are independent of the measurement scale. In this case, a surface may be described by a fractal dimension or Wenzel roughness factor, i.e. a dimension with a non-integer value.



3.4.1 Statistical characterisation

The statistical characterisation of surface topography has been widely used in science, academia and industry. Since statistics is the best tool for processing random data, it is seen as a natural and meaningful method of analysis for surfaces especially in terms of the increased reliability of the analysis. There are three important forms of statistical characterisation: statistical distribution, 2D autocorrelation function and spectral moment analysis.

3.4.1.1 Statistical distribution

Statistical distribution models the topographic height, slope and curvature by the probability density function for both, continuous and discrete distributions. Generally the probability density function is described from four aspects, i.e. central tendency, dispersion, asymmetry and peakedness. There are many parameters, which can be used to characterise these four properties [73], for example, mean and standard deviation to describe the dispersion, skewness to describe the asymmetry and kurtosis to describe the peakedness.

3.4.1.2 Areal autocorrelation function (AACF)

This procedure describes the general dependency of height values of the data at one x-y coordinate on the values at another x-y coordinate. It was recognised, that the 2D version of AACF (autocorrelation function, ACF) is a very useful tool for processing random signals, because of providing basic information about the spatial relation and dependency on the data. When AACF is used for surface topographic assessment, it is a good method to indicate randomness and directionality of surface features [74-76].

The properties of AACF have not been fully investigated and applied to characterising engineering surfaces. However, with the aid of mathematical derivation it is possible to identify and summarize some interesting properties of the AACF surfaces:

- a) AACF is a real function;
- b) AACF with zero autocorrelation length in both orthogonal directions is the variance of a surface;
- c) The maximum value of AACF is at the zero autocorrelation length;

- d) If a surface is periodic in either one or two orthogonal directions, AACF is periodic with the same periodicity in either one or two orthogonal directions.

AACF helps to visualize the correlation of surface profile heights in different directions. The decay of correlation will be very slow in the direction of consistent surface height, whereas the decay will be very fast in the direction of more random surface height values. If a surface has periodicity, its decay will illustrate that periodicity [109].

Due to the properties mentioned above, AACF is preferably used to acquire topographic information related to the spatial properties of surfaces, specially to recognize their isotropy (*Fig. 3.7*).

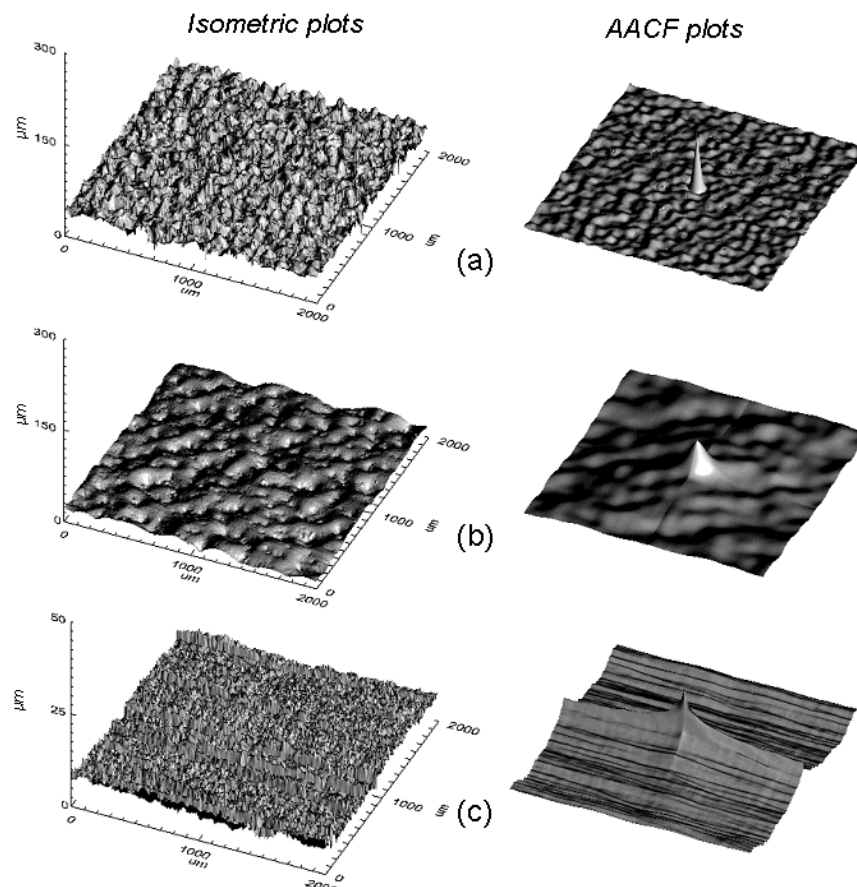


Figure 3.7
Isometric and AACF plots of different polymer materials used in automotive industry:
 (a) and (b) Polypropylene,
 (c) Sheet Moulding Compound (SMC) containing glass fibre and Polyester.
 AACF plot of (a) is periodic in both orthogonal directions, i.e. the surface is isotropic. On the contrary, SMC surface (c) is anisotropic.

3.4.1.3 Spectral moment analysis

This approach was first developed by Longuet-Higgins [77,78] for the 3D description of ocean surfaces. Later, it was applied to the characterisation of engineering surfaces by Nayak [79] and others [80,81]. The theory of spectral moments suggests that all relevant characteristics of a randomly rough Gaussian surface, such as the mean square height, mean square slope, average length of contour per unit area, and average density of maxima and minima per unit area can be obtained from the spectral moments which are derived in relation to the power spectrum of a random surface. In other words, the dominant characterisation parameters of the surface topography can be represented by the spectral moments.

Engineering surfaces are commonly anisotropic and non-Gaussian. For this reason, this characterisation method is rarely used.

3.4.2 2D spectral analysis

Areal spectral analysis reveals dominant frequencies in the texture patterns of a surface, by condensing data in the space domain into the frequency-based domain. By exploring the possible periodic nature of data, particular individual frequencies or wavelengths can be isolated as having primary contribution to the surface shape. In general, high and low spatial frequency components contribute to the roughness and to the waviness of the surface, respectively. The presence and density of these classes of frequencies provide insight into the surface's dominant features.

Wallach [106] used real spectral analysis directly as a mean to study the topography of engineering surfaces. In his paper he described how the technique could be employed to obtain the waviness. Sherrington [107] carried out extensive work on areal power spectral density (APSD) applied to characterising engineering surfaces.

Anisotropic surfaces have power densities that run perpendicular to their lay patterns [109]. If the lay pattern is highly ordered, the power will be concentrated at specific frequency intervals and harmonics thereof. In a random or isotropic surface, no discernable texture pattern exists and power is concentrated at the origin with almost instant decay in all directions. Then APSD, which is obtained as a radial layout, provide some significant information to characterise a surface topography:

- Low frequency components play an important role in surfaces' APSD. At large radial frequency, the energy of the APSD is negligible.

- For surfaces having periodicity in either one or two orthogonal directions, the main energy of APSD would be concentrated on the specific frequency the periodicity and along the same directions.
- For an isotropic random surface, APSD energy is approximately evenly distributed in circulation around the origin of frequency axes.
- For anisotropic surfaces, the main energy of APSD is concentrated on the direction perpendicular to the lay.

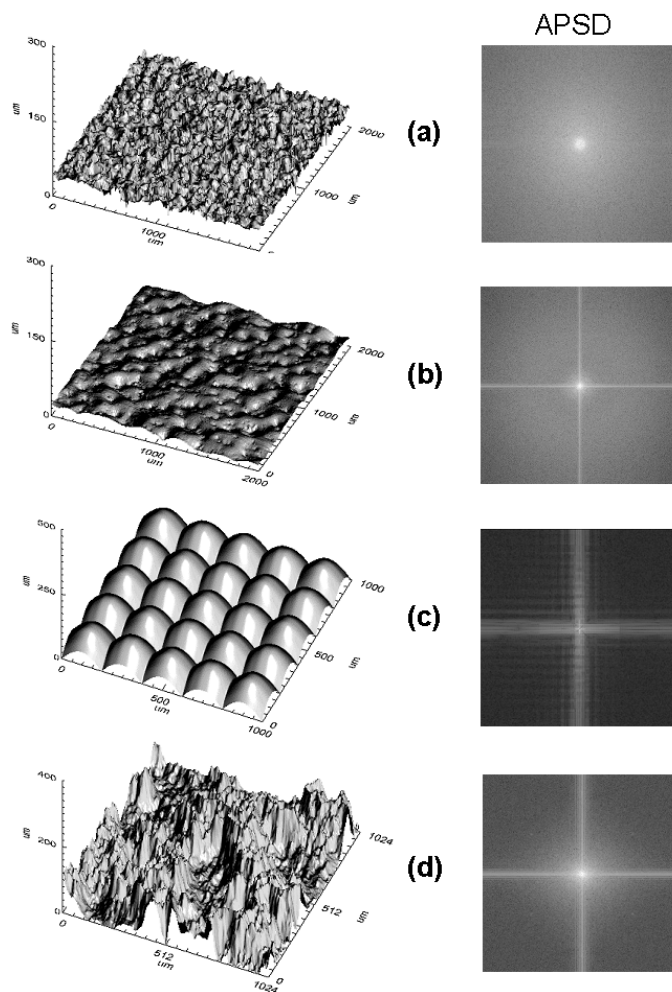


*Figure 3.8
Isometric and
APSD images of
different polymer
surfaces: (a) and
(b) Polypropylene
of Fig. 3.7, (c)
simulated
anisotropic sinoidal
surface and (d)
simulated fractal
surface
constructed by
random midpoint
displacement
algorithm.*

It is important to mention that since a sampling area is divided into two orthogonal directions, artificial frequency components are possibly introduced in the two orthogonal frequency axes, which is known as Gibbs* phenomenon [108].

* Gibbs phenomenon (also known as ringing artifacts) named after the American physicist J. Willard Gibbs, is the peculiar manner in which the Fourier series of a piecewise continuously differentiable periodic function behaves at a jump discontinuity: the overshoot does not die up as the frequency increases, but approaches a finite limit.

3.4.3 Time series analysis

Time series analysis is an analytical method to model a random signal [82]. It was systematically introduced into engineering and surface characterisation by Pandit and Wu [83], and it was further applied to surface profile and surface topography characterisation and simulation by other researchers [84-86].

The central idea of time series analysis is that a current data point can be represented by a combination of its previous data points and a residual noise in one of three principal mathematical models [2]. The process of time series analysis is to fit the random data into one of those three models with given orders. The coefficients of the models, that can be calculated in terms of the autocorrelation function by the least squares algorithm, are the resulting characterisation parameters for the surface.

3.4.4 Functional characterisation

This type of characterisation takes into account the functional requirements and applications of the surfaces.

There are two critical problems encountered in functional characterisation. The first is that there are a wide range of functional requirements according to the use and applications of the surface and it is difficult or even impossible to find a general functional characterisation method to cover all the range of functional requirements [87]. The second main problem encountered in functional characterisation is that engineering requirements for a particular surface are not fully appreciated and documented and, thus, a knowledge gap exists between features which have to be specified by designer and those which can be generated by an appropriate manufacturing processes.

There are two functional characterisation methods standardised, the German standard DIN 4776 [88] and the motif combination method in the French R&W industrial standard [89]. The volumetric characterisation method proposed by Davis et al [90] can be also considered too as a functional characterisation method.

3.4.4.1 DIN 4776

The functional characterisation method proposed by Bodschwinn [91] and standardised in DIN 4776 [88] is suitable for highly stressed surfaces which are relatively flat on the top and highly grooved or pored at the bottom. This standard is

defined for 2D profiles, but can be extended to 3D topography. The central idea of the standard is to define a series parameters, R_k (core roughness depth), R_{pk} (reduced peak height), R_{vk} (reduced valley depth), M_{r1} (first bearing area point) and M_{r2} (second bearing area point), called R_k parameters from the profile Abbott-Firestone curve as shown in Fig. 3.9, so as to assign to them different functional roles [91].

DIN 4776 is mainly suited for characterising surfaces which are flat on the top and are highly grooved or pored on the bottom. In other cases, DIN 4776 may result in unreliable information.

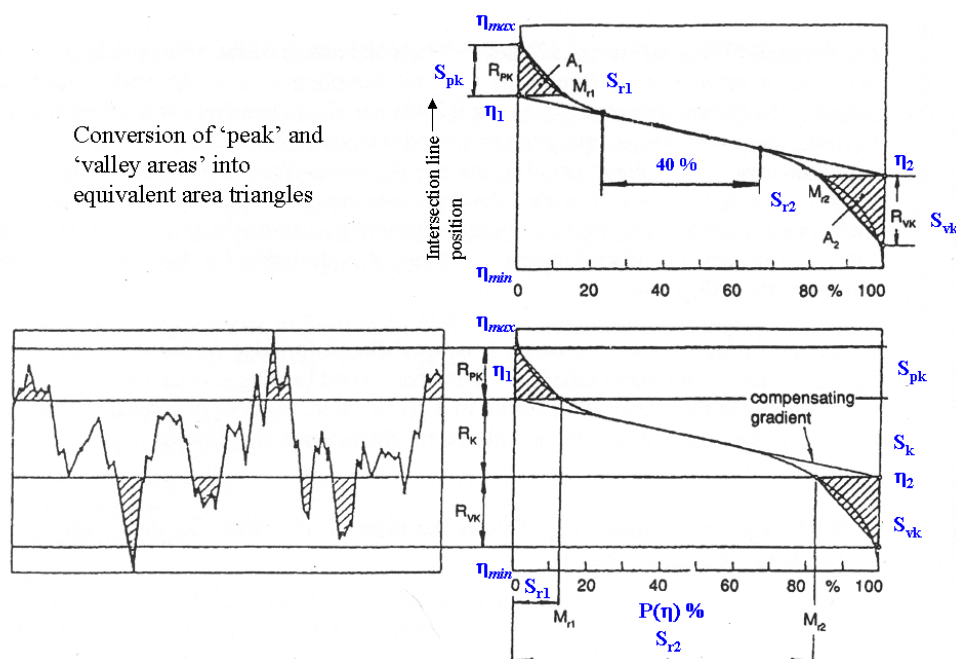


Figure 3.9
DIN 4776
parameters in
2D and in 3D
(blue) [88].

For highly stressed surfaces, it is recommended that R_k parameter be renamed to S_k parameter set as follows: core roughness depth S_k , reduced summit height S_{pk} , reduced valley depth S_{vk} , upper bearing area S_{r1} , lower bearing area S_{r2} .

As the same way to calculate the R_k parameters, in some cases a double step filtering or levelling process is needed to obtain S_k parameters (Fig. 3.9).

3.4.4.2 Motif combination

The motif is a profile part of a profile between two peaks [92]. The motif combination method emphasises that large profile peaks and valleys play an important role in functional applications. Therefore, this method extracts significant profile features and eliminates insignificant features that particularly hinder the determination of the

mean slope of the profile. The motif combination characterisation was reported to be a complementary approach to solve specific technical problems and be useful to characterise non-Gaussian height distribution surfaces and those where the upper part of the surface is important for the function.

The combination of the motifs is based on four fundamental rules (envelope, width, enlargement and relative depth) [93] as shown in *Fig. 3.10*.

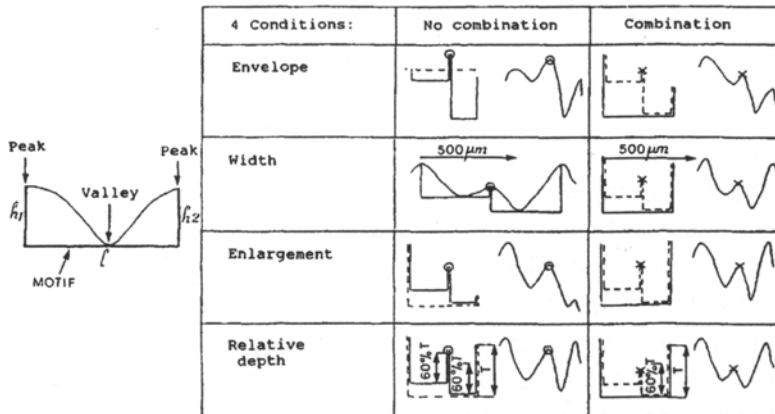


Figure 3.10
Four fundamental rules of motif combination [93].

The parameters which are provided by the motif combination are shown in *Fig. 3.11*. The most important ones are the mean motif depth and the mean motif spacing, which will be described later (cf. Section 3.5) as roughness and waviness, respectively.

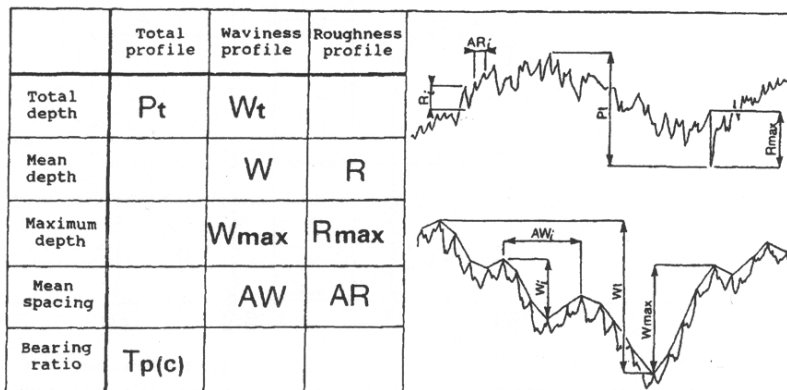


Figure 3.11
Motif parameters [93].

3.4.4.3 Volumetrical characterisation

This type of characterisation is actually a geometrical one, which calculates the debris volume of material and the void volume enclosed by a flat surface and material debris (*Fig. 3.12*). While both, material and void volume are directly related

to functional properties e.g. running in, friction and water or oil retention, Davis et al [90] used this technique to characterise engine bore surfaces.

In the present study, volumetrical characterisation was used as a method to study free volume available (porosity) as a function of depth.

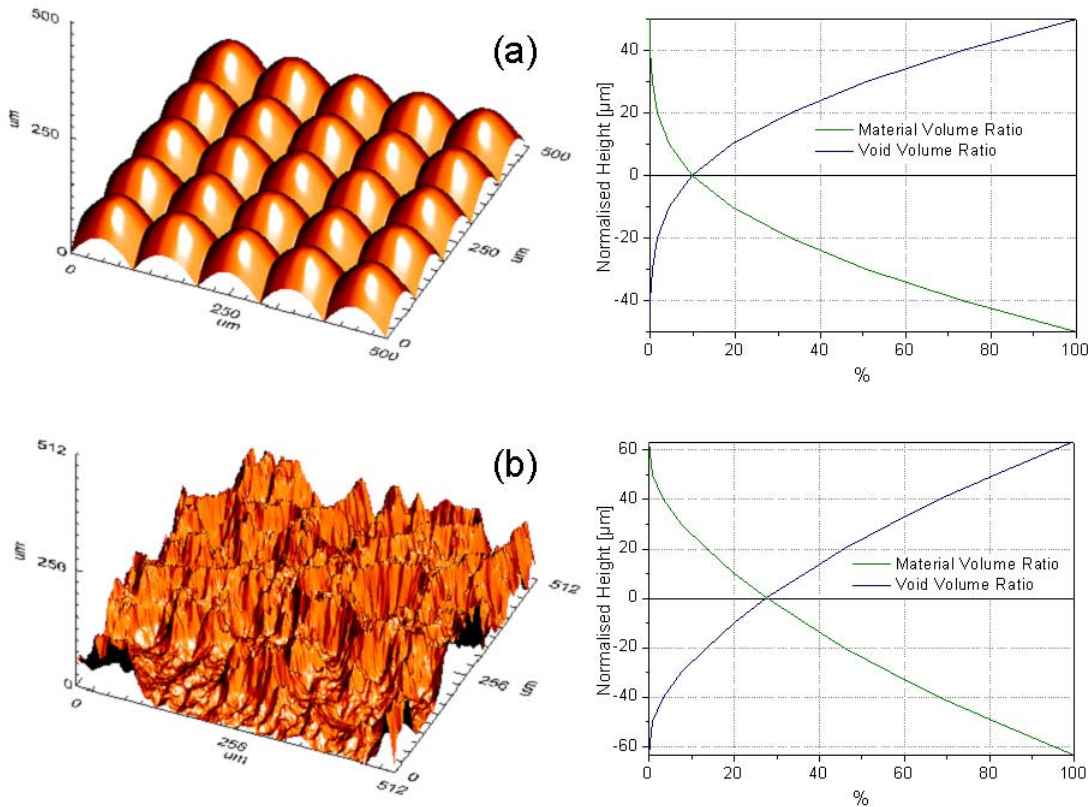


Figure 3.12 Volume ratios of (a) simulated sinoidal surface), (b) simulated fractal surface constructed by random midpoint displacement process.

3.4.5 Visual characterisation

Due to their great utility, visualisation techniques are far more important in 3D surface analysis than in 2D profile analysis. Using only the human eye as a powerful and versatile processor of information, it is possible to appreciate, valuate and compare complicated and ill-defined but patterned data. Sophisticated image processing and computer graphics techniques provide powerful and flexible tools for manipulating a large amount of topographic data.

The visualisation techniques do not include the presentation of mathematically processed topographic information such as the height distribution, bearing area function, auto correlation function and spectral decomposition. They are mainly concerned with visual presentations of raw or processed topographic data. There are six basic types of visual presentations: isometric projection, contour map, greyscale image, solid-coloured image, greyscale-coloured image and cross section profile plot, each one of them based on different graphical principles and exhibiting different visual aspects of topographic data (*Fig. 3.13*).

3.4.5.1 Isometric plot

An isometric plot is a projection of a 3D object on a 2D medium. An important property of this type of projection is that distances along the projection axes retain their original proportion. The data points can be interconnected with their neighbouring points by straight lines (grid), using a grey scale or simulating the presence of a light source, which can be positioned as convenience. All these three possibilities (*Fig. 3.13(a)*) are also available combining different colours by using modern specialized software.

The following three basic parameters can be assigned to the isometric plot:

- a) The **projection angle**, which is the angle between the viewing direction and the x-y plane,
- b) The **magnification of z** relative to x and y, and
- c) The **rotation angle**, the angle by which the x-y plane rotates around the z axis.

3.4.5.2 Contour plot

In a contour plot or contour map (*Fig. 3.13(b)*), lines are used to connect points of similar height in the same way as a terrain map is made. Except for the lines intersecting with the boundary of the mapped area, all lines are closed and do not intersect each other. The data points on the same line have the same height value.

This type of presentation of topographic data is particularly useful for identifying directional features.

The basic two parameters related to the plotting of the contour map are the number of contour levels and the frequency of their labelling by height values.

3.4.5.3 Greyscale image

In a greyscale image of a surface (*Fig. 3.13(c)*), the data points of the areal matrix are re-quantised to the resolution of greys available on the display device or media and displayed as greys proportional to the re-quantised surface height values. The basic parameter for this type of visual representation is the number of grey levels. Grey level numbers over 30 are usually unnecessary since the human eye can only detect about 30 greys.

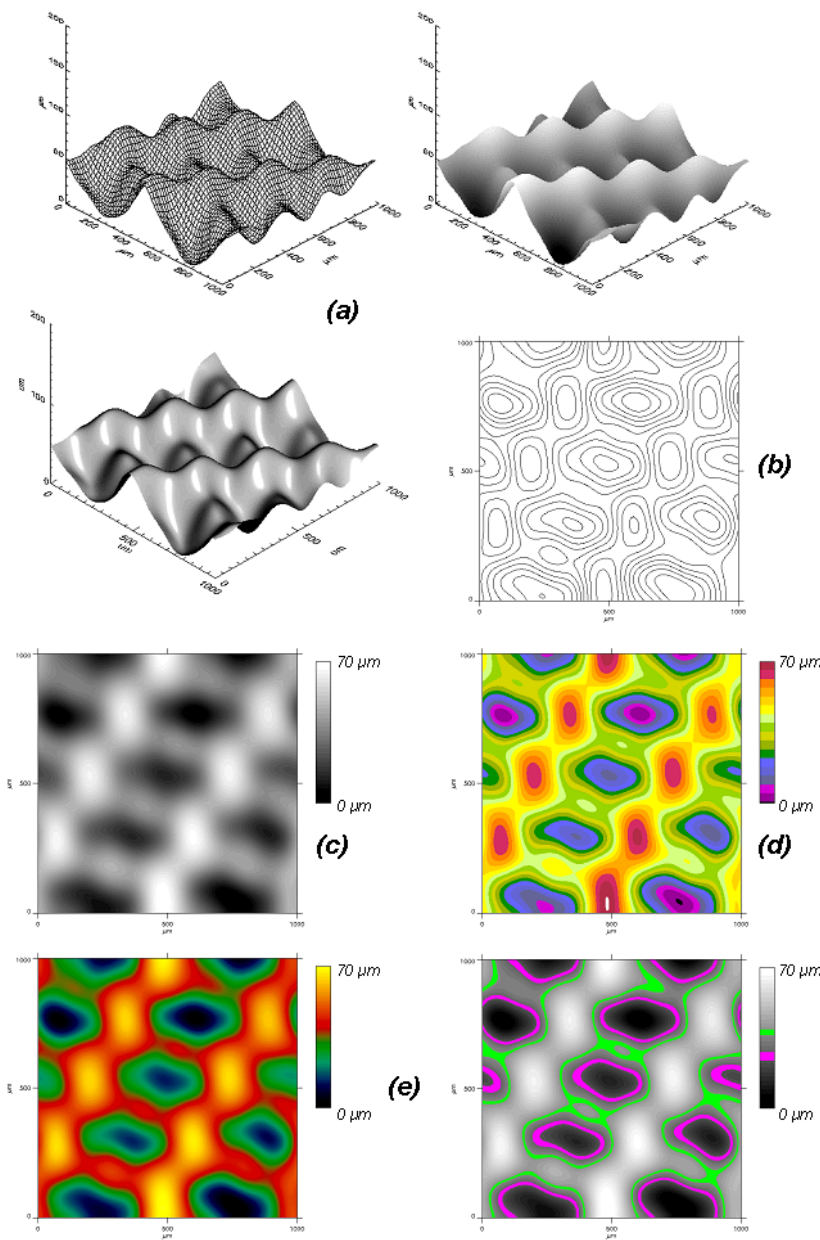


Figure 3.13
 a) Isometric plots,
 b) Contour plot,
 c) Greyscale image,
 d) Solid-coloured image
 e) Greyscale-coloured images

3.4.5.4 Solid-coloured image

Assigning solid colours to different intervals of height results in a useful image that can contrast different types of morphologies or point out defined regions in the same map (*Fig. 3.13(d)*).

3.4.5.5 Greyscale-coloured Image

This type of visual representation is a combination of greyscale and solid-coloured image (*Fig. 3.13(e)*). Its correct use makes possible to integrate in the map additional information that relates the topography with physical or chemical phenomenologies; for example the visualisation of film formation or deposition of solids at a textile or another rough surface.

3.4.5.6 Cross section profile plot

Individual profiles can be extracted from areal data and this can be from any specified direction and position where a sufficient number of data points allows useful plotting (*Fig. 3.14*). Relative scaling of x and z axes is normally used to control the differential magnification of the plot.

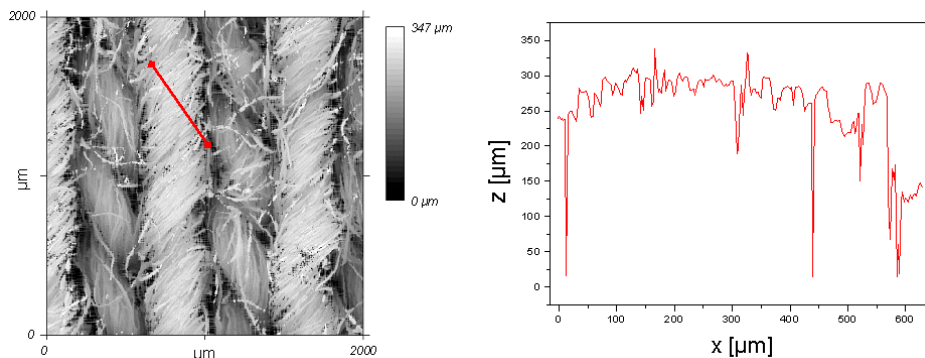


*Figure 3.14
Cross section
profile plot.*

3.4.6 Fractal analysis

Many authors [94-101] proved that engineering surfaces are fractal [103-105]. These surfaces are statistically 'self affine' i.e. the scales in the vertical and lateral directions are different rather than 'self-similar' which means that a self-similar random fractal has the same statistics in relation to the scale of observation for all scales in all directions.

Fractal analysis has been increasingly applied to surface modelling [94,95], surface characterisation [96,97], surface contact [98-100] and wear analysis [101,102].

However, the variation of fractal parameters in terms of surfaces and characterisation procedures has not been fully investigated yet.

In Section 3.7.4, some application examples of the fractal dimension as a characterisation parameter for surfaces is described and discussed.

3.5 Mathematical and physical meaning of the most common topographic characterisation parameters

A very important problem in surface-related research is choosing parameters characterising surface properties in such a way that they correlate with surface formation mechanism, morphology, topometry and functional behaviour [168]. The solution to this problem has been attempted by a range of characterisation techniques mentioned in Section 3.4.

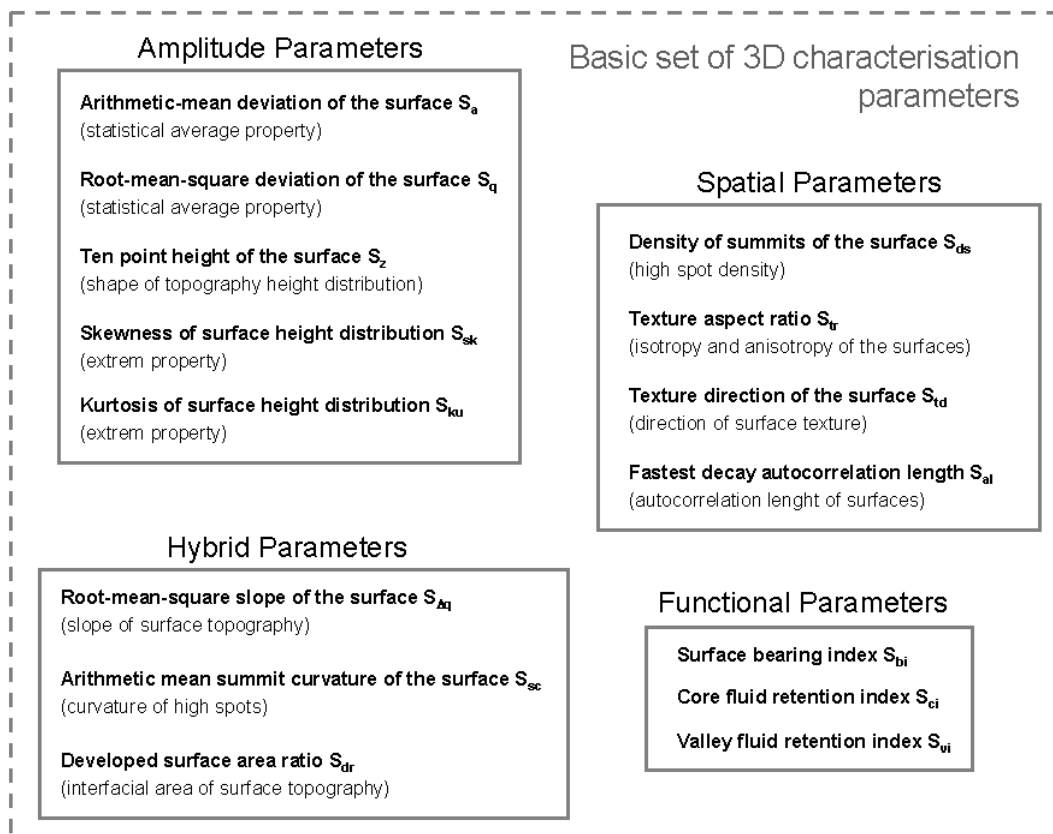


Figure 3.15 A basic set of 3D characterisation parameters proposed by Stout et al [2, 116].

A graphic or even a statistical description of the topography is not enough to characterise a surface. Many 2D parameters were already defined in many

International Standards [63,71,72], and commonly offer an attractive and realistic solution. However they cannot provide adequate and reliable information for the analysis of intrinsically 3D surface topography. Literature on some 3D parameters is spread diversely through research papers and product information [2,34,50-52]. Some 3D parameters are extended from their 2D counterparts, others are specifically developed for 3D surfaces. A draft proposal [2,116] for 3D parameters is based on a literature survey (1992). In that report, Stout et al have presented unambiguous definitions and algorithms for potential 3D parameters as a basic parameter set (*Fig. 3.15*) according to the following aspects:

- amplitude property,
- spatial property,
- hybrid property,
- area and volumes and
- some functional properties.

Although these aspects do not completely describe a surface, e.g. they do not specify the homogeneity of the surface, they are deemed, nevertheless to cover the breadth of useful parameters.

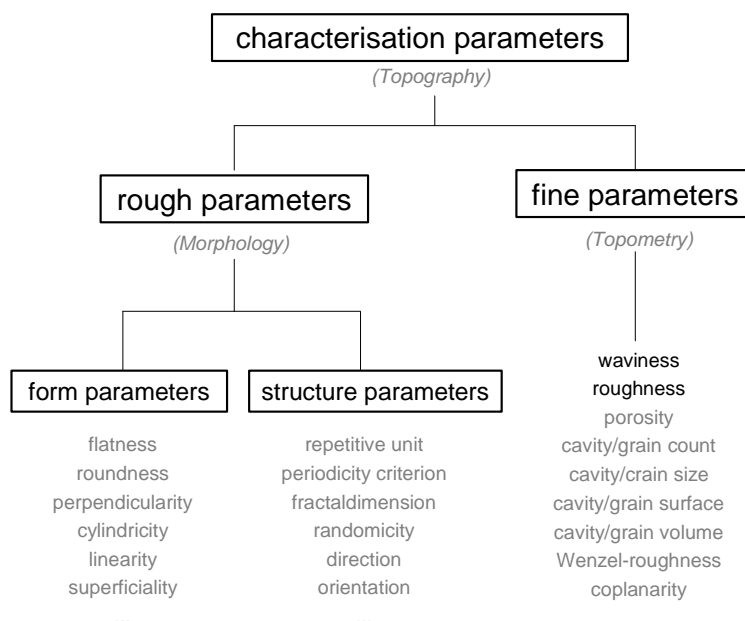


*Figure 3.16
Classification of
characterisation
parameters
proposed by
FRT [4].*

Another simpler classification proposed by researches at Fries Research & Technology [4] considers basically that each surface have to be described using

qualitative and quantitative characterisation parameters which are divided in rough (morphologic) and fine (topometric) parameters (Fig. 3.16).

3.5.1 Rough (morphologic) characterisation parameters

According to the researches of Fries Research & Technology [4], these parameters describe the form and structure of a surface. In spite of their relation with the morphology, they can also provide quantitative information.

Form parameters (flatness, roundness, perpendicularity, cylindricity, linearity, superficiality, etc.) characterise the surface geometry.

Structure parameters give information about the construction criterion of the surface. Size and geometry of eventual repetitive units, their periodic criterion (for fractal as well as for non-fractal surfaces), randomness, direction and orientation of irregularities are only some examples of these type of parameters.

In the present study both, areal autocorrelation function (AACF) and areal power spectral density (APSD) were taken into account to characterise the isotropy of surfaces by quantitative revealing of surface frequency contents. Additionally, to characterise the surface morphology, two mathematical procedures, digital surface filtering and FFT-filtering were applied to the topographical data after mathematical pre-processing explained in Section 3.3.

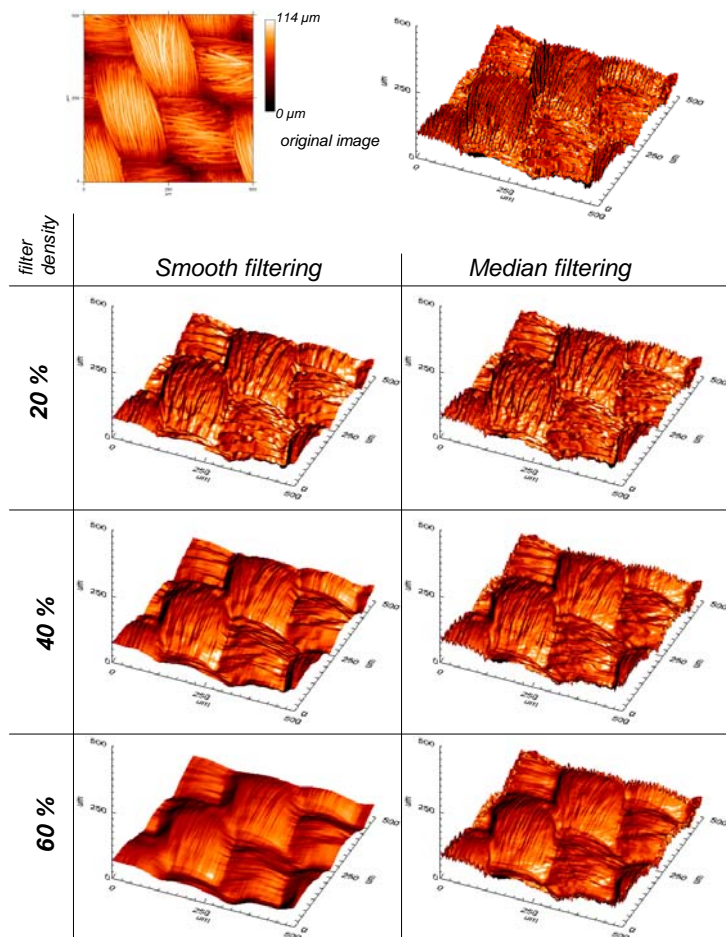


Figure 3.17 Smooth and median filtering using different filter densities.

3.5.1.1 Digital surface filtering

Two types of digital surface filtering were applied to the topographical data in the present study (*Fig. 3.17*):

- a) **Smooth filtering** calculates the arithmetical mean of each data point with its neighbourhood. A fit order (value) gives the number of its neighboring points, and consequently the density of the filter. *Fig. 3.18* shows the changes in a 2D profile of a yarn after smooth filtering.
- b) **Median filtering** replaces each point with the median value with its neighbourhood. The median filter clears noise (so-called “salt and pepper noise”), i.e. isolates high and low values. The median value will not be obtained by averaging the data but by sorting them out. The median value of 1, 10 and 4 is 4, while the arithmetical average value is 5. As in the case of smooth filtering, a fit order (value) gives the number of its neighboring points, and, consequently, the density of the filter. Compared to smooth filtering, median filtering has two important disadvantages: a longer computer time of calculation and impossibility of filtering the border points of the original image.

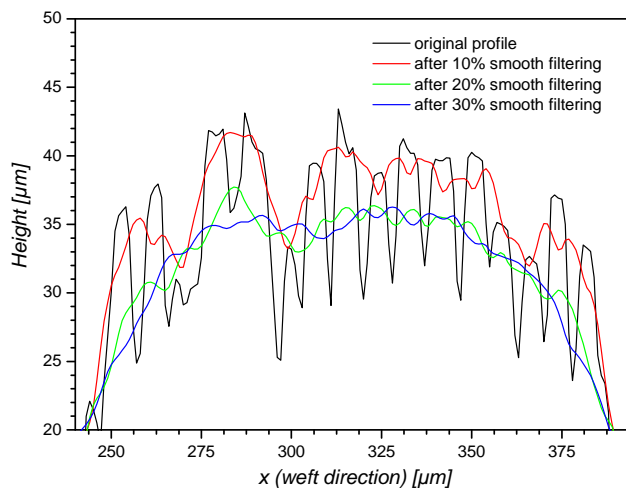


Figure 3.18
Evolution of smooth filtering a polyester warp yarn (2D profile).

3.5.1.2 Fast Fourier transformation (FFT) filtering

This digital filtering operation is defined by the convolution^{*} of the input and the impulse response function. The convolution operation involves a large number of operations [110] that combined by scalar multiplications [111] with functions of the

^{*} In functional analysis, convolution is a mathematical operation on two functions, producing a third function that is typically viewed as a modified version of one of the original functions.

Fourier domains allows a selection of defined frequencies and a construction of filtered surfaces [112].

FFT method is strongly recommended for high computational efficiency. The resulting collection of points permits the visual appreciation of the morphological waviness [113-115] and the posterior calculation of new parameters depending on the characterisation criteria as will be explained later.

By selecting the fundamental frequency to reconstruct the image, the resulting morphology is comparable with applying smooth filtering of high order (Fig. 3.19).

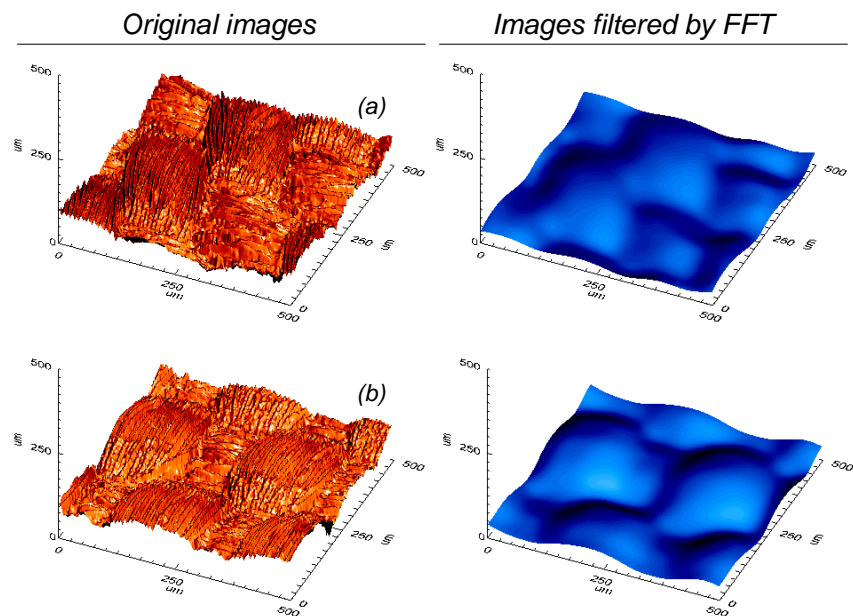


Figure 3.19 Fast Fourier transformation filtering. Surface of a twill polyester fabric (a), surface of a woven plain polyester fabric (b).

3.5.2 Fine (topometric) characterisation parameters

The most important topometric parameters are waviness and roughness. According to DIN 4760, fine characterisation parameters describe the topometry of a surface on four defined levels (Fig. 3.20 and Fig. 3.21) depending on the ratio between length and height of the surface studied.

To determine roughness and waviness of a 2D profile, FFT-filtering is applied to separate the long-wavy and short-wavy profile components. By filtering a measured profile (primary data, P-profile), a roughness filtered profile (R-profile) and a waviness filtered profile (W-profile) are obtained (Fig. 3.22).

The application of an equivalent mathematical procedure to a 3D topographical data [112] results on the separation of waviness and roughness surfaces (Fig. 3.23).

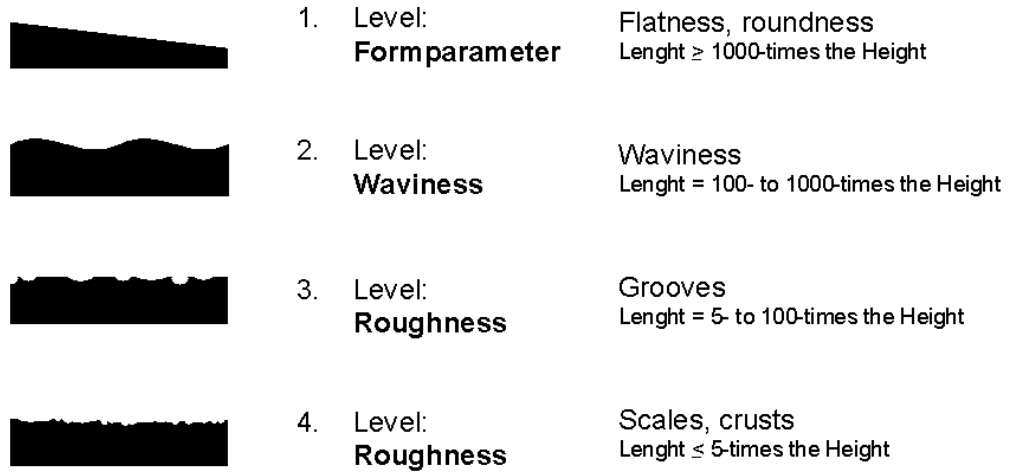


Figure 3.20 Level system of topographical irregularities according to DIN 4760.

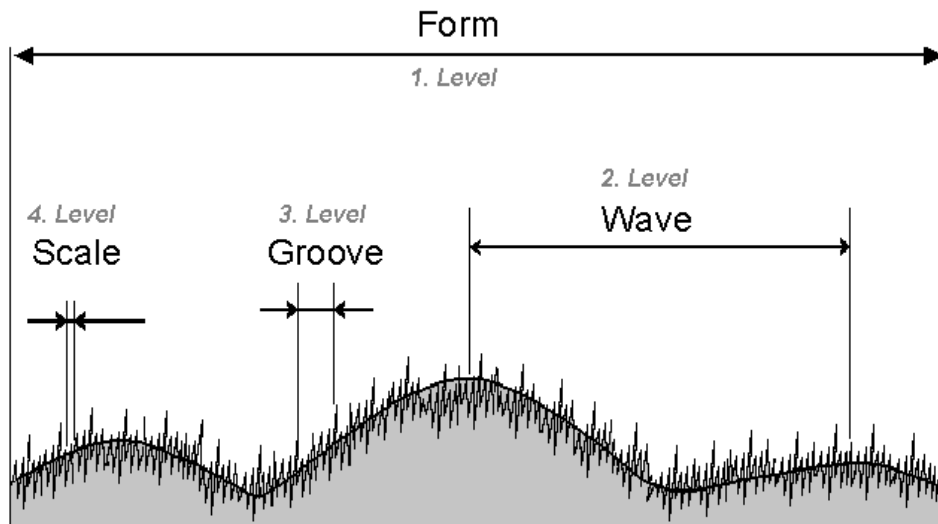


Figure 3.21 Graphic representation of the inhomogeneities of fine parameters up to 4th Level of a topographic profile.

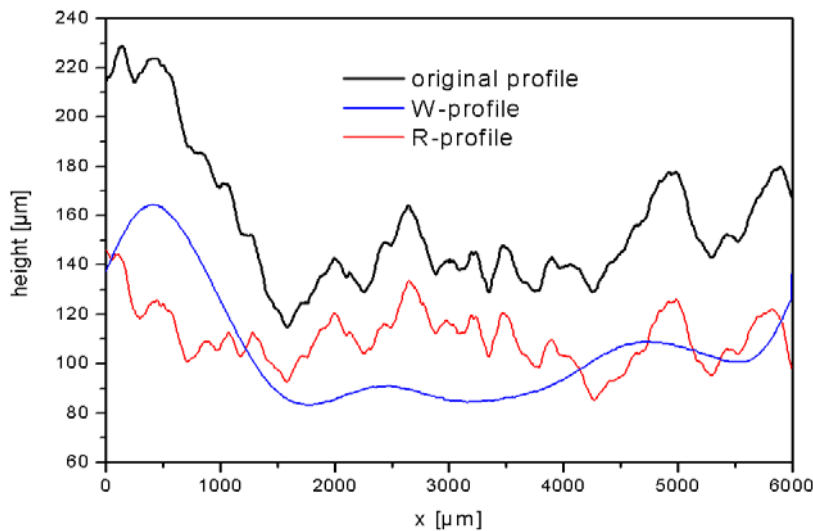


Figure 3.22 W-profile and R-profile obtained applying FFT-filtering (original profile at $y = 3000 \mu\text{m}$ of Fig.3.23 surface).

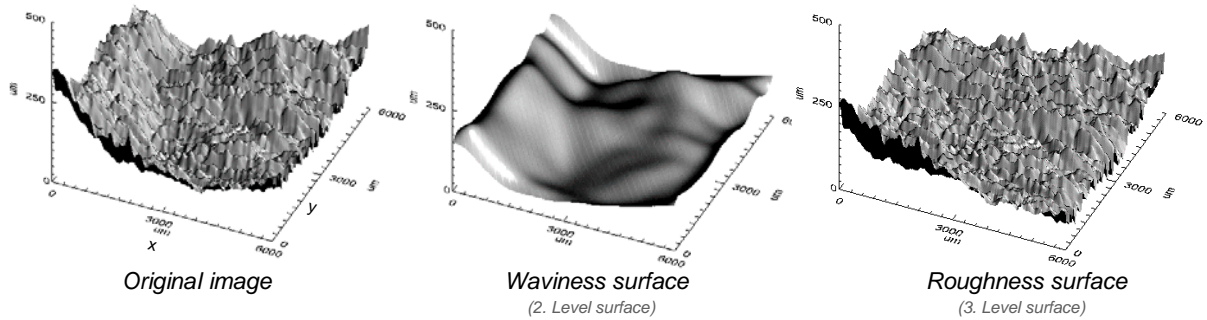


Figure 3.23 Waviness and roughness surfaces obtained applying FFT- filtering to the original topographic data.

3.5.2.1 Cut-off length or sampling interval L_m

Roughness and waviness are measured along a defined length range L_m . According to DIN 4768, this parameter is divided into 5 length units L_e . The length of L_e corresponds to the limit wavelength λ_c (also called L_c) used by roughness/waviness filtering [4].

3.5.2.2 Profile height P_t

At 2D profiles, the parameter P_t is the distance between the highest and the deepest points of P-profile (Fig. 3.24). Equivalent value for a surface is also called sP_t .

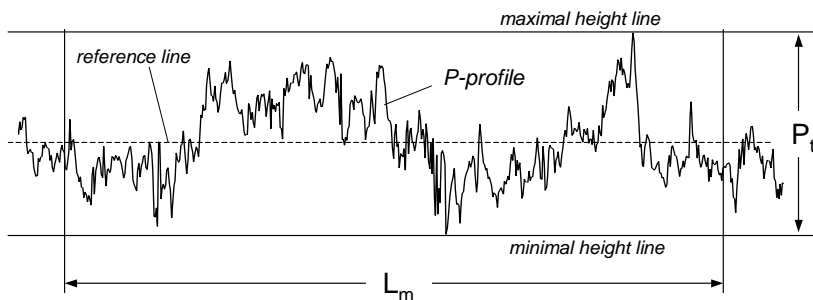


Figure 3.24 Profile height P_t .

3.5.2.3 Rough height R_t

Rough height R_t is the distance between the highest profile elevation and the deepest profile valley of a R-profile inside a defined length range L_m (Fig. 3.25). Additional parameters R_p and R_v are defined as distances between highest point - mean height line, and deepest point mean height line, respectively. Equivalent values for a surface are also called sR_t , sR_p and sR_v , respectively.

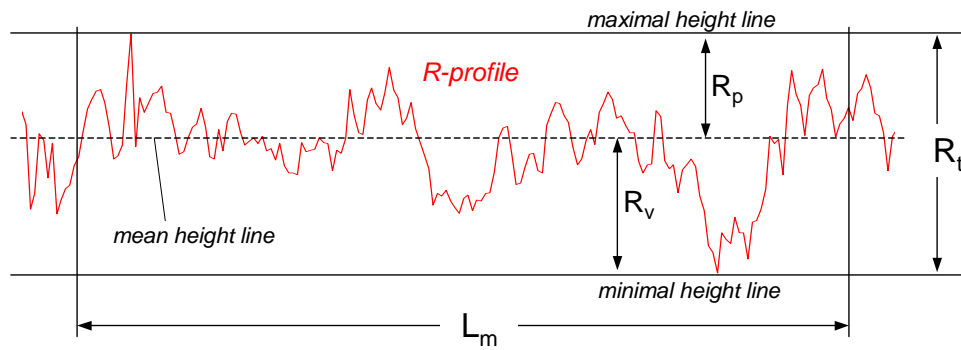


Figure 3.25 Rough height R_t , R_p and R_v .

3.5.2.4 Wave height W_t (DIN EN ISO 4287, ASME B46.1) and waviness W_z

Wave height is defined as the distance between the highest profile elevation and the deepest profile valley of a W-profile inside a defined length range L_m (Fig.3.26). Waviness W_z is obtained by the same procedure as R_z (cf. Section 3.5.2.5), but using a W-profile. Equivalent values for a surface are also called sW_t and sW_z , respectively.

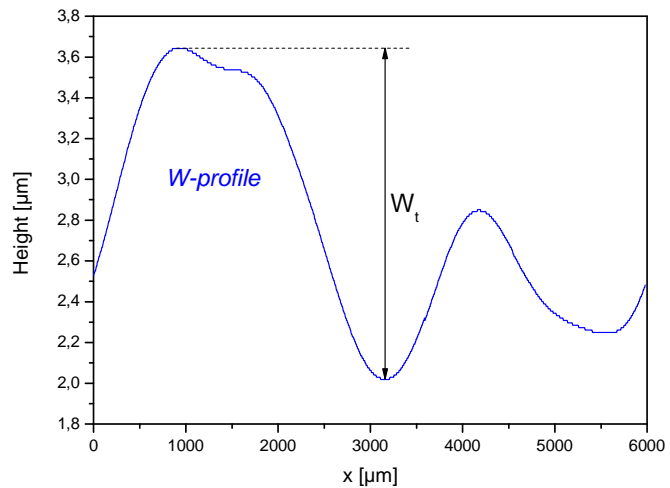


Figure 3.26 Wave height W_t .

3.5.2.5 Mean rough height R_z (DIN EN ISO 4287, ASME B46.1)

This characterisation parameter commonly called ‘mean roughness’ is defined as the arithmetic average of five R_{z_i} values, each one corresponding to the distance between the highest profile elevation and the deepest profile valley measured inside a length unit L_e of the R-profile (Fig. 3.27). Equivalent value for a surface is called sR_z .

$$R_z = \frac{1}{5} \sum_{i=1}^5 R_{z_i} \quad (3.2)$$

3.5.2.6 Maximal rough height R_{max} (DIN EN ISO 4287, ASME B46.1)

R_{max} is the largest R_{zi} of the five intervals L_e . This parameter is not identic to R_t . Normally, R_t is larger or equal to R_{max} (Fig. 3.27). Equivalent value for a surface is also called sR_{max} .

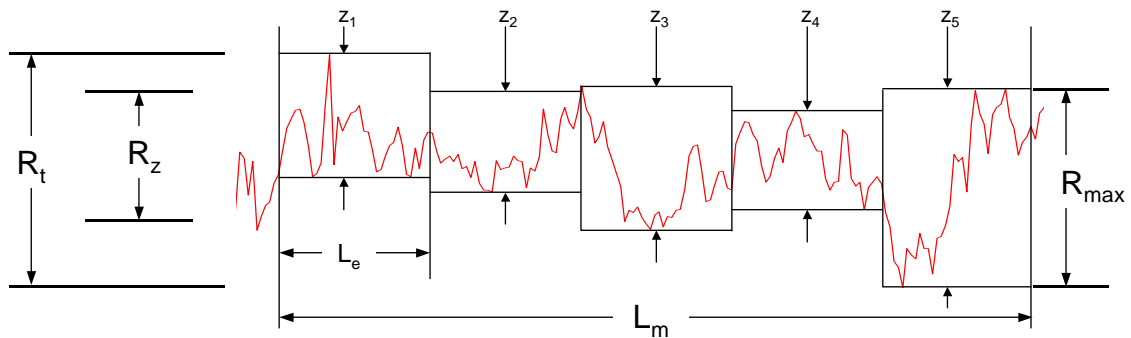


Figure 3.27 Mean rough height R_z and maximal rough height R_{max} ($R_{z5} = R_{max}$).

3.5.2.7 Arithmetic mean roughness R_a (DIN EN ISO 4287, ASME B46.1)

R_a is the arithmetic average of all distances between y -value and mean height inside a range length L_m (Fig. 3.28). Equivalent value for a surface is also called sR_a .

$$R_a = \frac{1}{N} \sum_{i=1}^n |y_i - \bar{y}| \quad (\text{Two dimensional } R_a) \quad (3.3)$$

$$R_a = \frac{1}{MN} \sum_{j=1}^M \sum_{k=1}^N |z_{jk} - \bar{z}| \quad (\text{Three dimensional } R_a) \quad (3.4)$$

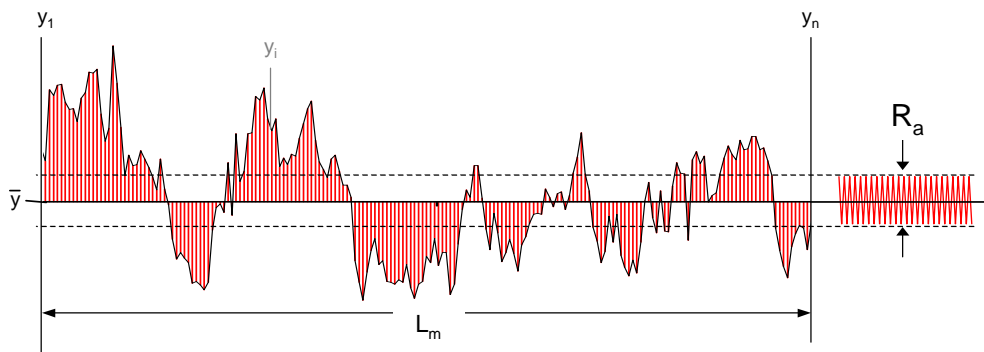


Figure 3.28 Arithmetic mean roughness R_a of a R -profile.

3.5.2.8 Root mean square roughness R_q (DIN EN ISO 4287, ASME B.46.1)

R_q is the square average of all distances between y-value and the mean height. The resulting value is quite larger than R_a . Equivalent value for a surface is also called sR_q .

$$R_q = \sqrt{\frac{1}{N} \sum_{i=1}^N (y_i - \bar{y})^2} \quad (\text{Two dimensional } R_q) \quad (3.5)$$

$$R_q = \sqrt{\frac{1}{MN} \sum_{j=1}^M \sum_{k=1}^N (z_{jk} - \bar{z})^2} \quad (\text{Three dimensional } R_q) \quad (3.6)$$

3.5.2.9 Porosity, surface porosity or surface mean void volume V_o

V_o , whose units are given as [volume]/[projected area], is defined in the present study as the volume contained between the true surface and the calculated mean-height plane, per unit area. Applying the criteria of volumetrical characterisation (Section 3.4.4.3), this parameter can be extended to the calculation of curves of material and void volume ratios to characterise the change of porosity as a function of deep measured from defined reference plane.

3.5.2.10 Some considerations about the cut-off length L_m

As have been shown in the previous pages, roughness and waviness are measured along a defined length range L_m . Calculated values of almost all characterisation

Periodic profile	Non-periodic profile		Measure length
R_{Sm} [μm]	R_z [μm]	R_a [μm]	L_m [mm]
0.01 – 0.04	< 0.1	< 0.02	0.4
0.04 – 0.13	0.1 – 0.5	0.02 – 0.1	1.25
0.13 – 0.4	0.5 – 10	0.1 – 2	4
0.4 – 1.3	10 – 50	2 – 10	12.5
1.3 – 4	> 50	> 10	40

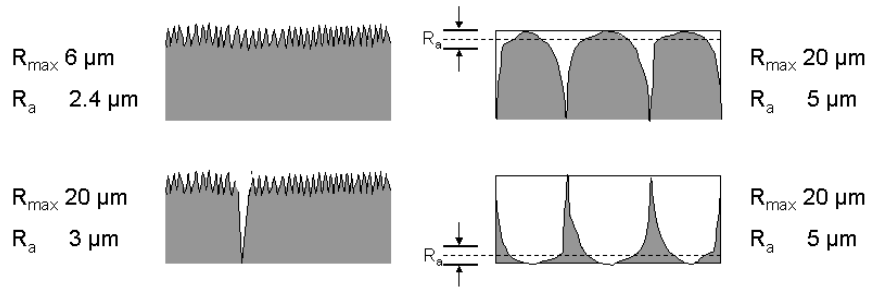
Table 3.1 Recommended cut-off length (L_m) depending on roughness.

parameters depend on selected L_m value, specially for periodic profiles. Some authors [4,117,118,120] recommend the observation of the expected roughness values or the application of power spectral analysis and fractal dimension as guide for the selection of the

optimal L_m . For periodic profiles, the scale-distance (R_{Sm}) (Fig. 3.21) is recommended as a input value for the estimation of L_m value. For non-periodic profiles, the relationship between R_a and R_z is recommended according to Table 3.1 [4].

Nevertheless, in the present study, a systematic statistical procedure for the calculation of an optimal L_m is presented in Section 3.6.

Figure 3.29
Comparison between R_a and R_{max} .



3.5.2.11 Relationship between R_{max} , R_z and R_a

According to its statistical nature, R_{max} is more sensitive to height inhomogeneities than R_z . R_a is statistically oriented to a mean value, then exceptional higher or deeper points have no important impact on calculated R_a (Fig. 3.29). Fig.3.30 shows the dependence of R_{max} , R_z and R_a on six different 2D profiles.

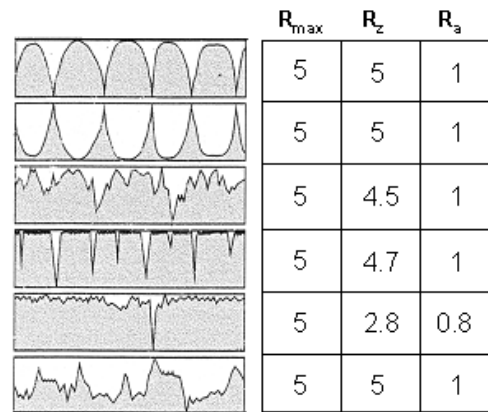


Figure 3.30
Comparison between values of R_{max} , R_z and R_a in respect to their information content [4].

3.6 Calculating the optimal sampling conditions

Cut-off length (L_m) and resolution (Δ_x , assuming that $\Delta_x = \Delta_y$) are the most important sampling parameters, which apart from particularly instrumental dependent ones, have to be optimally defined before characterising a topography.

Tsukada & Sasajima [119] and Yim & Kim [117] discussed the problem of an optimum sampling interval (L_m) by checking the variance of the root mean square height (R_q) of the surface under different sampling intervals. According to Stout et al. [2], recommendation of authors mentioned above for the choice of sampling interval are doubtful because of the fact that L_m seems to have some influence on the amplitude parameters (W_t and W_z).

The use of tables such as Table 3.1, that relate foreseen mean rough height (R_z), root mean square roughness (R_q) and arithmetic mean roughness (R_a) with L_m is frequently recommended to know the optimal value of L_m for periodic as well as non-periodic surfaces. However a choice proper sampling conditions for practical applications is not trivial. As optimal sampling conditions are strongly dependent on

the type of material to be characterized, experience is usually required. For this reason, a systematic procedure to define the optimal L_m and Δ_x values is proposed as follows:

- 1) Acquiring topographical data at the highest resolution available (minimal value of Δ_x) using different L_m values. Two procedures are recommended:
 - only one measure at the highest L_m and posterior zooming (sub-area extractions), and
 - independent measures using the same zero point position.
- 2) The use of statistical criteria in order to define the optimal value of L_m by analysing the calculated curves of W_z , R_z and R_a as a function of L_m .
- 3) Acquiring topographical data with the defined optimal L_m using different values of resolution.
- 4) The use of statistical and topographical criteria to analyse R_z and R_a as a function of Δ_x in order to define the optimal resolution.

3.6.1 Non-periodic surfaces

Application of steps according to the procedure described above, to sheet moulding compound (SMC) surface (see Fig. 3.7(c)), results in the curves shown in Fig. 3.31.

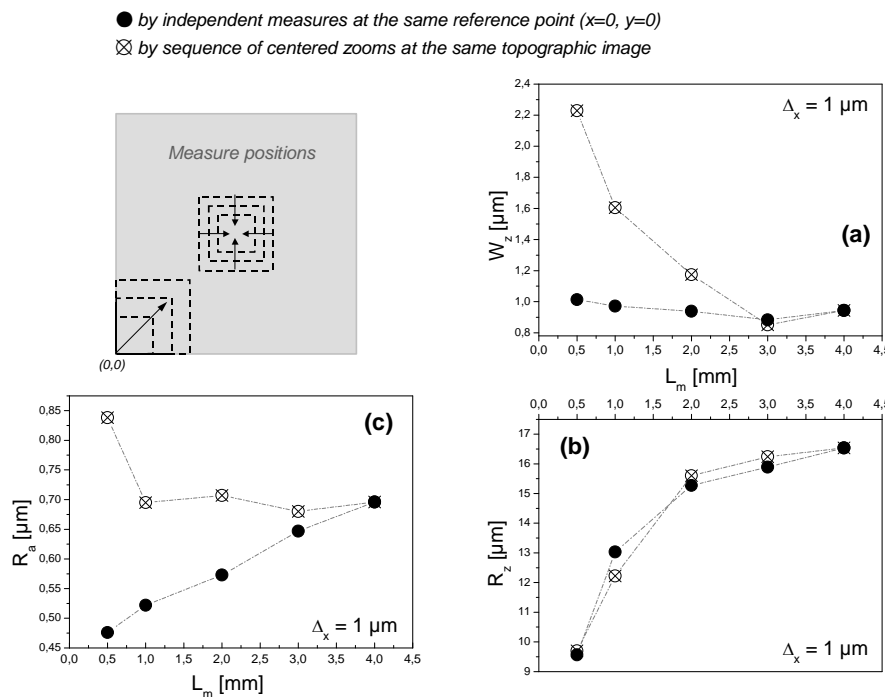


Figure 3.31
 Topographic parameters of a SMC surface as a function of L_m .

Calculated waviness values for the surface (*Fig. 3.31(a)*) measured using $\Delta_x = 1 \mu\text{m}$, show an important dependency on the cut-off length up to $L_m = 3 \text{ mm}$. As a result of FFT-filtering operations applied to the topographical data, waviness measured is always strongly dependent on a measurement scale. The waviness calculation of an idealized P-profile shown in *Fig. 3.32*, leads to a different waviness value depending on the cut-off length. Using a longer cut-off length (L_{m1}), the waviness (W_{z1}) of the filtered W-profile quantify the amplitude on the second level (cf. Section 3.5.2) of the P-profile. But using a shorter cut-off length (L_{m2}), FFT-filtering tends to describe the waviness of irregularities on the third level, which leads to a higher value of wave height (W_{z2}).

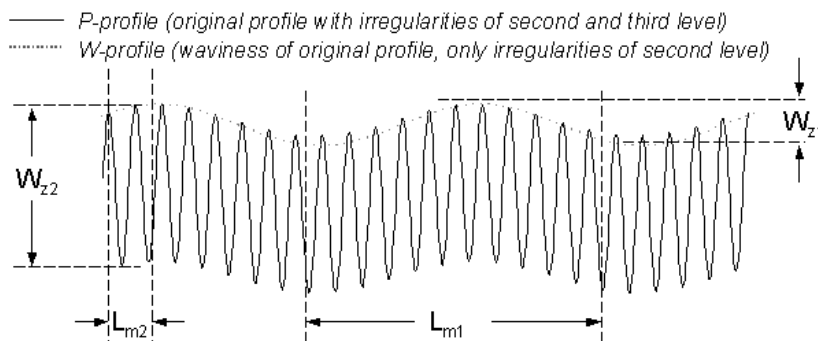


Figure 3.32
Dependency of
waviness on cut-off
length.

Depending on the type of surface and on the aim of characterisation, it is important to consider the previous explanation about the connection between waviness and measure or cut-off length in order to find and probe the optimal measure scale to describe the waviness.

In the same way as W_z , values calculated for R_z show an important dependency of L_m (*Fig. 3.31(b)*) with a tendency to a constant value of $16.5 \mu\text{m}$ at about $L_m = 3 \text{ mm}$. However, the velocity of this convergence is practically independent of measure position, because the surface irregularities between $z = 10 \mu\text{m}$ and $z = 17 \mu\text{m}$ (“grooves” on the third level according to DIN 4760) are regularly distributed over the surface. In other words, over of $L_m = 3 \text{ mm}$ the measured value of R_z becomes statistically reliable.

Values of R_a are highly sensitive to the measure position (*Fig. 3.31(c)*). By sub-area extractions, a clear tendency to a constant R_a value, when $L_m > 1 \text{ mm}$ is observed, because over the same region of the surface, irregularities on the fourth level (DIN 4760), also called “scales” or “crusts” ($z = 0.45 \mu\text{m}$ to $z = 0.85 \mu\text{m}$ in this case), have almost the same height. To characterize this surface it is important to note that the

mean height of “scales” and “crusts” depends on a measure region, probably due to two causes: the use of a not at all regular polished metallic mold during the production of the SMC samples and irregular glass fibres orientation.

Considering the behaviour of W_z , and R_z , the optimal L_m value for this type of surface is 3 mm. Results obtained by analysing the dependence of R_a on measure positions, show that the optimal characterization of this fourth level irregularities demands the study of the surface by different measure positions and to consider the topography of the metallic mould, as well as glass fibre content and their orientation.

Using the defined optimal cut-off length ($L_m = 3 \text{ mm}$), new topographical data were obtained applying different values of resolution. Fig. 3.33 shows the behaviour of R_z and R_a calculated as a function of resolution. The selection of the optimal resolution depends on two conditions: highest statistical reliability and shorter measure time, which is especially important in the case

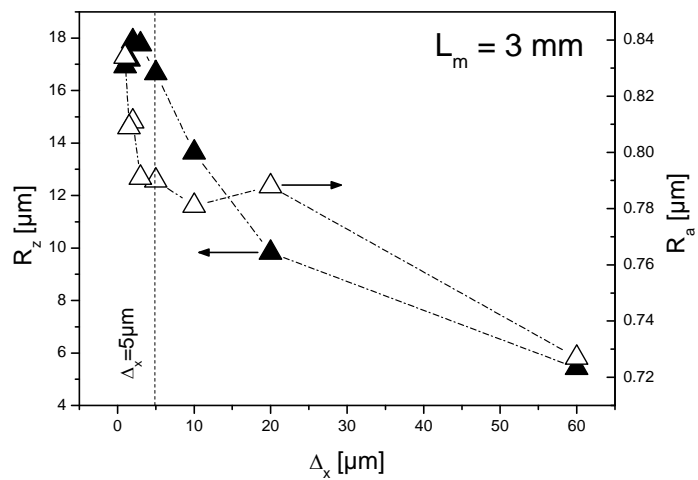


Figure 3.33 Characterisation parameters for the topography as function of Δ_x .

of scanning microscopy such as chromatic confocal imaging. Refining resolution (using smaller Δ_x) means the measure of more points in x- and y- direction and as a consequence longer measure time of the surface data (f -times more points means an increase of measure time in a factor of at least f^2).

From the statistical point of view, calculated R_z is reliable at resolutions finer than 5 μm . If the surface characterisation is oriented to the morphology of third level (“grooves” by

Parameter	Mean value	Standard deviation
W_z	0.951	0.242
R_z	17.228	4.082
R_a	0.763	0.066

Table 3.2 Calculated parameters of seven independent measurements.

DIN 4760), then $\Delta_x = 5 \mu\text{m}$ will be satisfactory. To characterise irregularities on the fourth level the recommended resolution is the finest available by the method used,

in this case $\Delta_x = 1 \mu\text{m}$. However, between resolutions of $5 \mu\text{m}$ and $1 \mu\text{m}$ the values of R_a show a difference of only 44 nanometers, about 5% of the measured arithmetic mean roughness at the finest resolution ($R_a = 8.34 \mu\text{m}$).

In order to probe the reliability of the optimized sampling conditions ($L_m = 3 \text{ mm}$ and $\Delta_x = 5 \mu\text{m}$), seven independent topographic measurements were performed in different regions of the sample surface. Standard deviation of the resulting parameters (Table 3.2) show that R_a is statistically more reliable than W_z and R_z . However, these results also show the dependency degree of topographic parameters on the measure position. The reasons will be analysed in the next Chapter.

3.6.2 Periodic surfaces

Polyester fabrics shown in Fig. 3.19 were used to probe the presented procedure to optimize sampling conditions in the case of periodic surfaces. Fig. 3.34 shows that the waviness of woven plain fabric is statistical reliable above $L_m = 2 \text{ mm}$, but in the case of twill fabric the optimal cut-off length must be higher than 3 mm. However this reasoning takes only in account the statistical behaviour of W_z . By applying FFT-filtering, calculated waviness images of Fig. 3.35 show that the mentioned almost constant values of W_z observed in Fig. 3.34 correspond in both cases to a quantification of plane irregularities (wrinkles) of the fabrics.

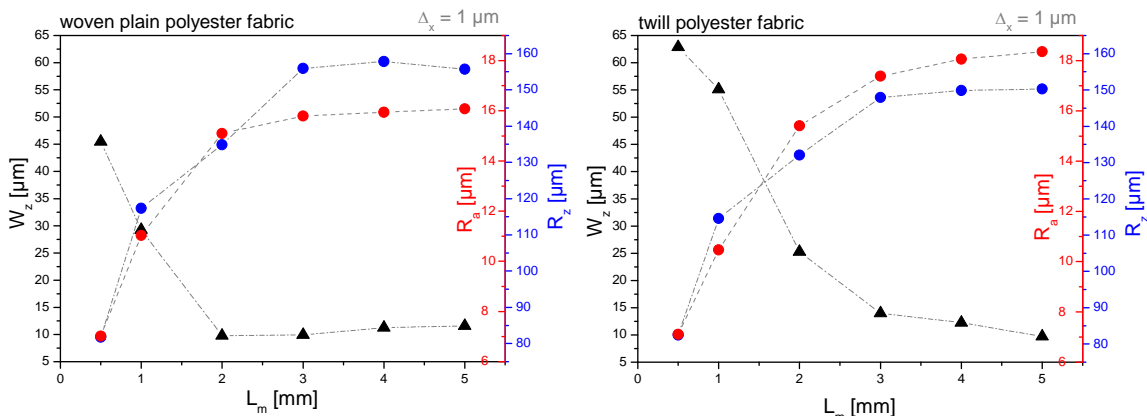


Figure 3.34 Topographic parameters of polyester fabric surfaces as a function of L_m .

If the characterisation is aimed to study the morphology due to the fabric structure, the calculation of waviness has to be realized using L_m in the range 0.5 to 1 mm by woven plain fabric, and from 1 to 2 mm by twill structure.

In the case of characterisation aimed to study the topography of the complete fabric surface without regarding the fabric structure (morphology), the recommended value of L_m is 3 mm for both fabrics, because over this cut-off length the values of R_z and R_a remain approximately constant.

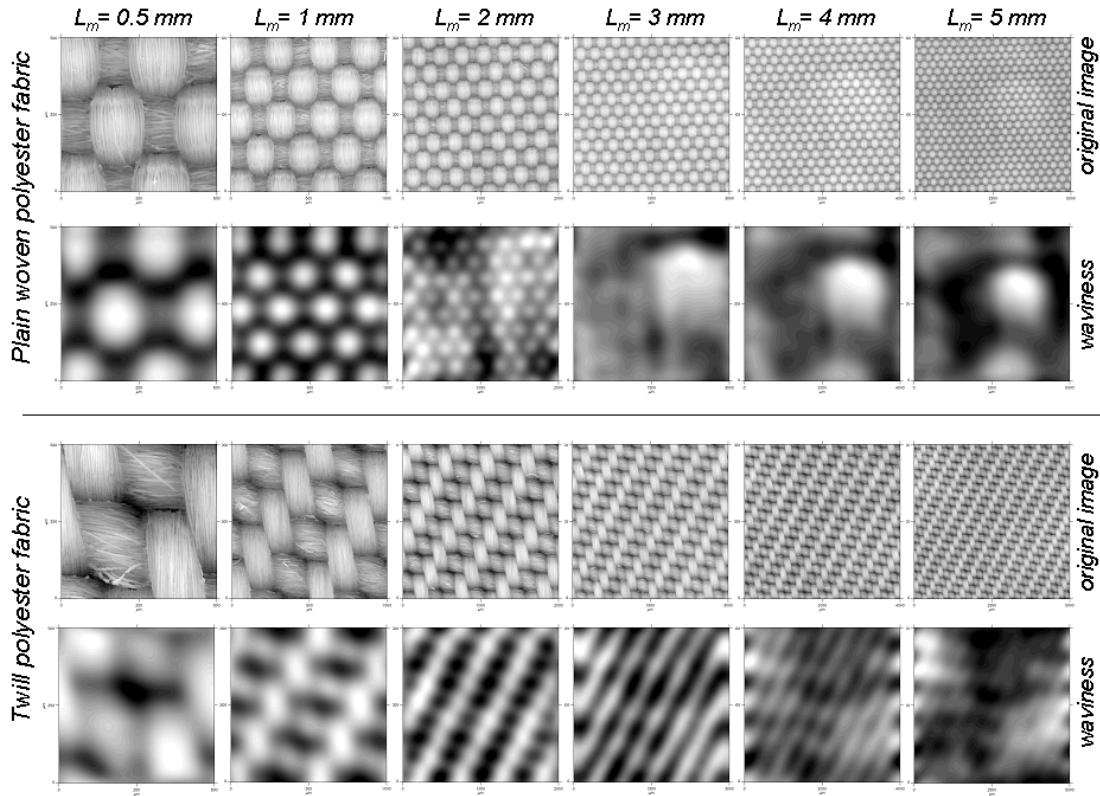


Figure 3.35 Waviness images of polyester fabric surfaces as function of L_m .

By $L_m = 3 \text{ mm}$, different values of resolution were used to obtain new topographical data. Fig. 3.36 shows that a resolution of $4 \mu\text{m}$ is enough to produce reliable information of R_z . On the other hand, values of R_a and their correspondent standard deviation (Table 3.3) show that using $L_m = 3 \text{ mm}$, the arithmetic mean roughness hardly depends on resolution. However, standard

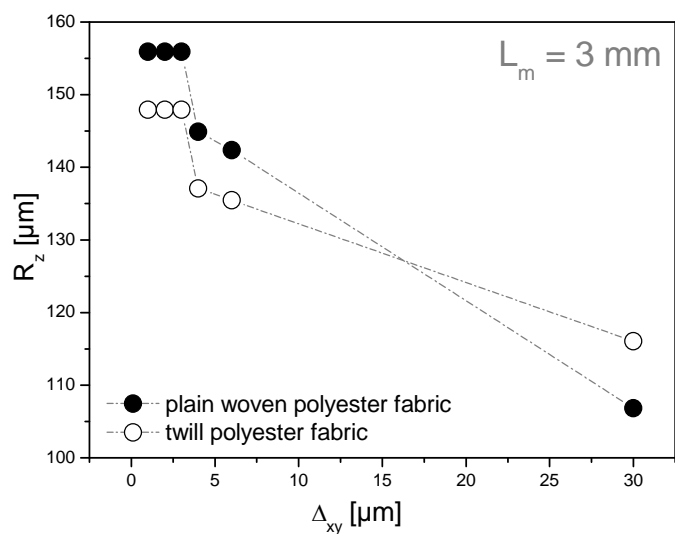


Figure 3.36 Mean roughness of polyester fabric surfaces as a function of Δ_x .

deviations of R_a for woven plain and twill fabric obtained using $L_m = 1 \text{ mm}$ are 0.51 and 0.62 respectively, clearly much more dependent on resolution.

$\Delta_x [\mu\text{m}]$	$R_a [\mu\text{m}]$	
	woven plain	twill
1	15.672	17.242
2	15.690	17.263
3	15.792	17.387
4	15.675	17.234
5	15.789	17.384
30	15.703	17.167
	$\sigma = 0.056$	$\sigma = 0.070$

*Table 3.3
 R_a for studied fabric surfaces
 by $L_m = 3 \text{ mm}$ are practically
 independent of resolution up to
 $\Delta_x = 30 \mu\text{m}$.*

3.7 Manipulation techniques and complementary characterization procedures

Techniques and parameters mentioned above are different ways to visualize and characterise topographic data. There are situations where topographic data need to be manipulated in certain ways to aid visual and numerical interpretation. There are almost limitless applicable techniques to this effect, for this reason it is important to realise the capabilities and limitations of these techniques and choose those that are useful for the intended purpose.

3.7.1 Visual manipulation operations

All of them are matrix operations that modify the relationship between x- and y-axes:

3.7.1.1 Exchange of axes

This function corresponds to a matrix transposition of original data that exchanges the values in $x \leftrightarrow y$ mantaining the original point and the points of diagonal $x = y$.

3.7.1.2 Rotate

This operation allows the original data to be rotated counter-clockwise, normally applying 90, 180 or 270°.

3.7.1.3 Flip

This function reflects the original data in the vertical y-axis ($y \leftrightarrow -y$).

3.7.1.4 Mirror

This function reflects the original data in the horizontal x-axis ($x \leftrightarrow -x$).

3.7.1.5 Zoom and Clip

It is sometimes necessary, in both visual presentation and data analysis, to extract a sub-area from the original area to either study the isolated area in detail (zooming) or to remove undesired data points outside the isolated area (clipping). While the original resolution remains constant, printed or new visual resolution is changed proportional to the lateral enlargement. To perform the visual resolution of a zoomed image, a resample (cf. Section 3.7.2.1) of the data is recommended.

3.7.2 Numerical manipulation techniques

3.7.2.1 Resample

By this function new x-y points and the correspondent height values are interpolated between the original data. On the contrary, the remove of data is often recommended if the data is too big, or if one simulate the effect of resolution on defined topographic parameters.

3.7.2.2 Calibration

By calibration a reset of x, y and z scale is performed. This operations are principally used by modelling and simulation of surfaces.

3.7.2.3 Despike

A “spike” is an isolated data point. Its z-value differs from its neighboring points extremely. To remove spikes from the original image two steps are necessary:

- 1) Selection of the x- or y- direction to compare each data point with its neighboring points on the left and on the right (x-direction), respectively at the top and the bottom (y-direction).
- 2) Input of a threshold value. A data point will be detected as a spike if the differences between the point and both neighboring points are superior to this

value. When a data point is detected as a spike, the medium value of its neighboring points will take its place.

3.7.2.4 Remove peaks

This filter removes all data higher or lower the threshold relating to the mean line. In contrast to the despiking filter larger ranges higher or lower the threshold can be removed with the remove peaks filter.

3.7.2.5 Destep

This function removes single steps of the original data. To remove a step is performed by:

- 1) Selection of the x - or y - direction to correct a step in the horizontal or vertical direction.
- 2) Selection of the desired area of the original image to destep.

3.7.2.6 Inversion

Inversion means to turn the surface upside down so that the pits, troughs and valleys become summits and ridges and vice versa ($z \leftrightarrow -z$). This helps to reveal topographic features located at the lower part of the surface and it is helpful for identifying pits and troughs. *Fig. 3.37* shows an isometric plot of an inverted ground surface; some pits and troughs are seen clearly.

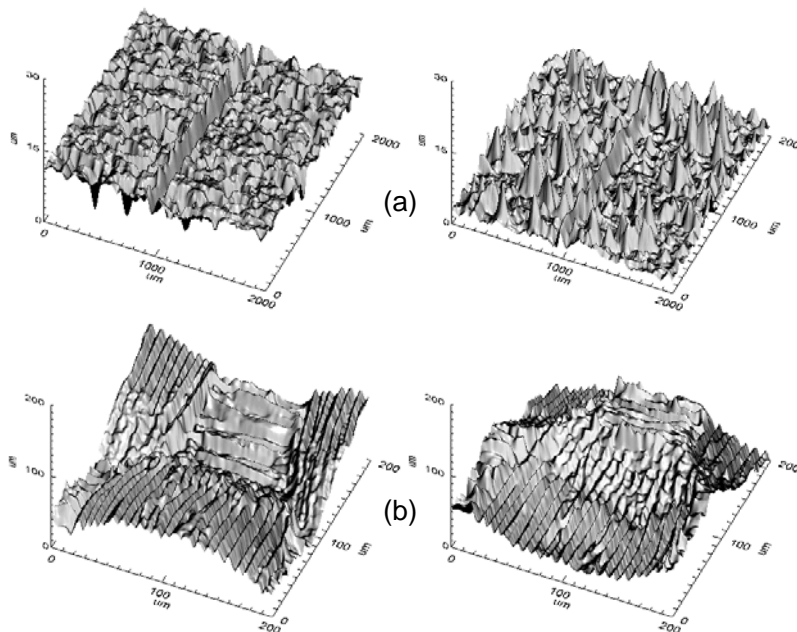


*Figure 3.37
Original surface (left)
and inversion of the
surface (right) of a
machined steel (a) and
of a polyester textile (b).*

3.7.2.7 Truncation

Truncation means to remove the material above a given plane being parallel to the mean plane. It is a special case of segmentation (cf. Section 3.3.3) if the aim is not a correction of invalid points, but the simulation of a wear process, in which case leaves the bearing area and contours visible, when plotted as shown *Fig. 3.38*. It may also be used to reveal features below a certain level that are otherwise invisible. The truncation level can

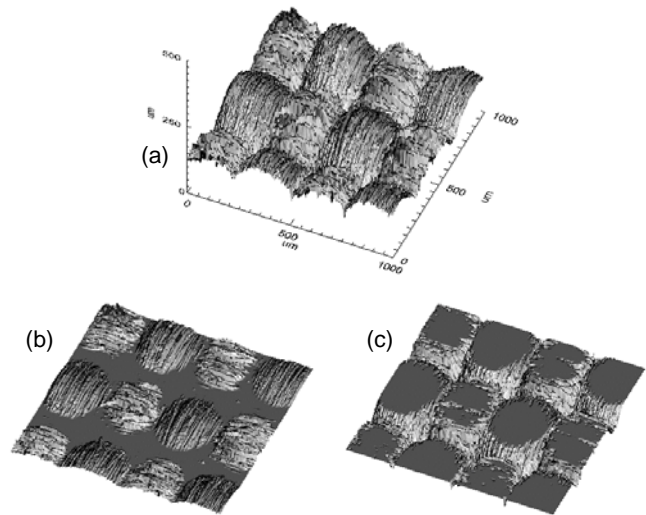


Figure 3.38
Original textile surface (a), truncation of all the points under a height value representing a 60% of the total height range (b), truncation of all the points upper a height value representing a 60% of the total height range (also called “40% truncation”) (c).

be specified either as a percentage value relative to the maximum summit or an absolute value (zero percent truncated surface corresponds to the original surface, and 100% truncated one corresponds to a flat surface).

3.7.3 Complementary characterisation procedures

3.7.3.1 Profile analysis

This analysis consists of a evaluation of all the possible geometrical elements of a 2D profile, e.g. distances point-to-point, distances point-to-line, angles and subtractions of lines and points. It is especially recommendable by studying the effect on topography by modifications if the same profile is studied before and after the modification.

3.7.3.2 Histogram and cumulative histogram

This analysis consists of an application of an histogram (a graphical display of tabulated frequencies, showing what proportion of height values fall into each of several categories, *Fig. 3.39*) and/or a cumulative histogram (mapping counting counts the cumulative number of observations in all height values up to the specified height) in order to visualize and compare a statistical distribution between surfaces or by a surface before and after defined topographic modification.

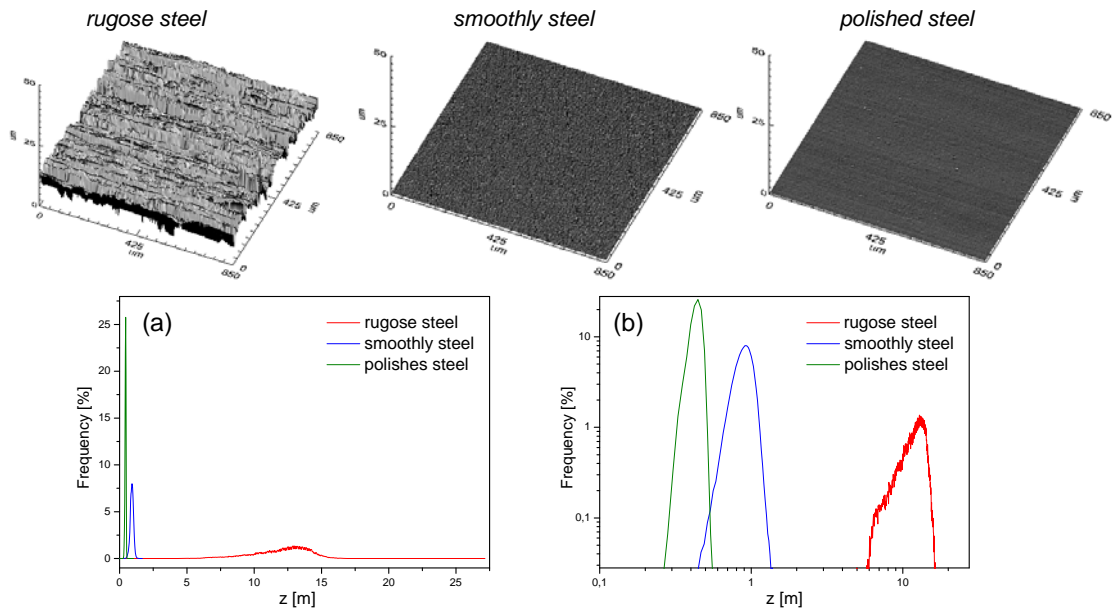


Figure 3.39 A comparison of topographic irregularities of three different steel surfaces by using histograms (a). For a better visualization of the curves it is recommended to use log-log scales (b).

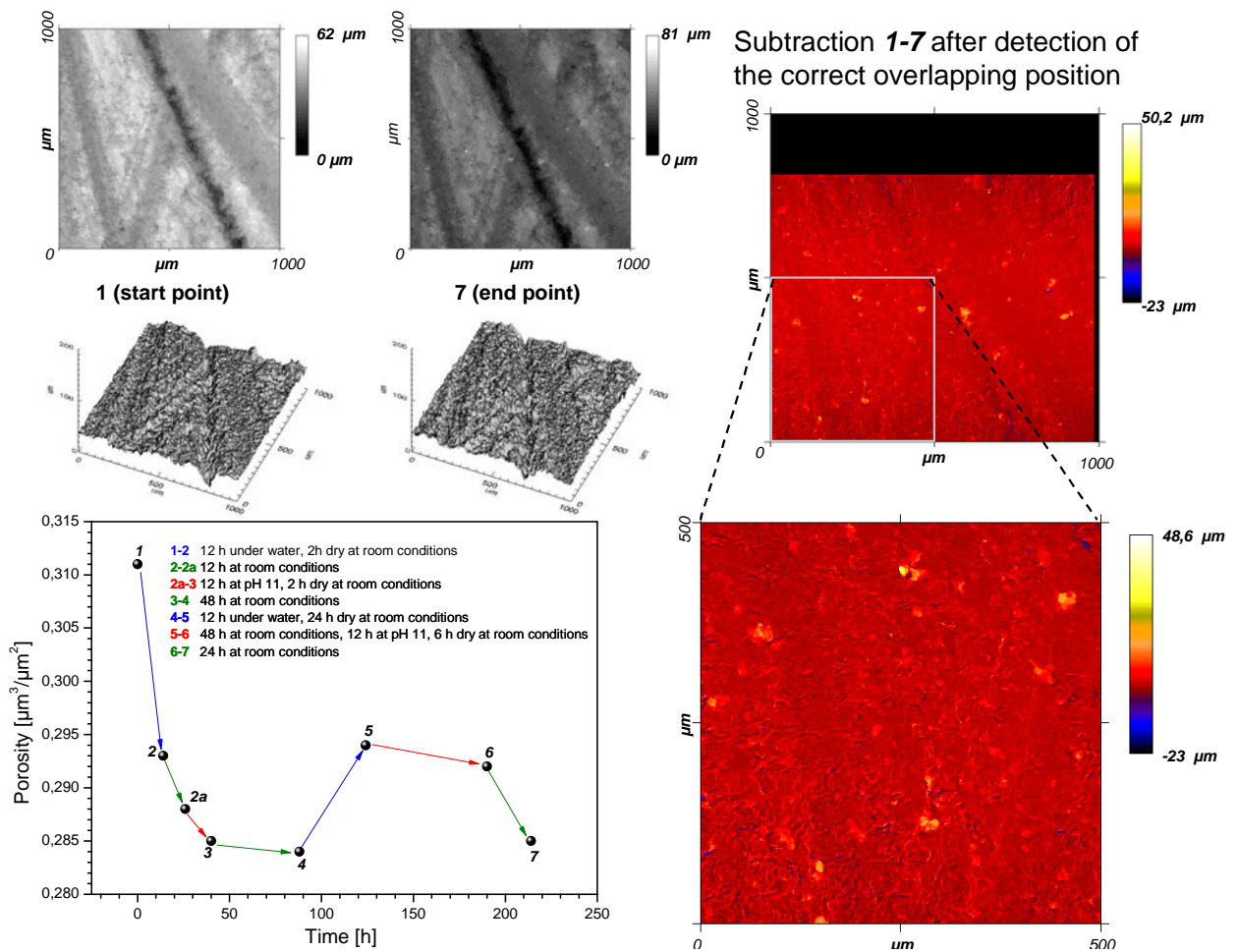


Figure 3.40 Surface subtraction (comparison) between initial and final conditions of a modified polyurethane surface.

3.7.3.3 Comparison

With this procedure it is possible to compare two images directly by addition, subtraction or by applying any other function. Before comparison, it is necessary to detect the overlapping position (at least two coincident points or a zero point and an angle).

This operation makes sense to compare a surface before and after its topographic modification (*Fig. 3.40*). In other cases, by different locations of a surface, the comparison of traditional topographic parameters is recommended.

By this procedure it is also possible to invert a surface by subtraction of the topographical data from a zero plane.

3.7.4 Complementary characterisation parameters

3.7.4.1 Grain size

This set of parameters represent the quantification of bumps, i.e. grains, from the original data over defined minimum z-height, so called threshold. Resulting parameters are: number of grains, grain-area average, grain-volume average, total area of grains, total volume of grains and the statistics of the grain size calculation (class versus percentage frequency), cf. *Fig. 3.41*.

3.7.4.2 Filling quantity

Quantification of filling is a special case of volumetric characterisation (cf. Section 3.4.4.3). This set of parameters represents the quantification of void volume, i.e. cavities from the original data under defined threshold (height level). Resulting parameters are: number of cavities, cavity-area average, cavity-volume average, total area of cavities, total volume of cavities and the statistics of the cavities size calculation (class versus percentage frequency), cf. *Fig. 3.41*.

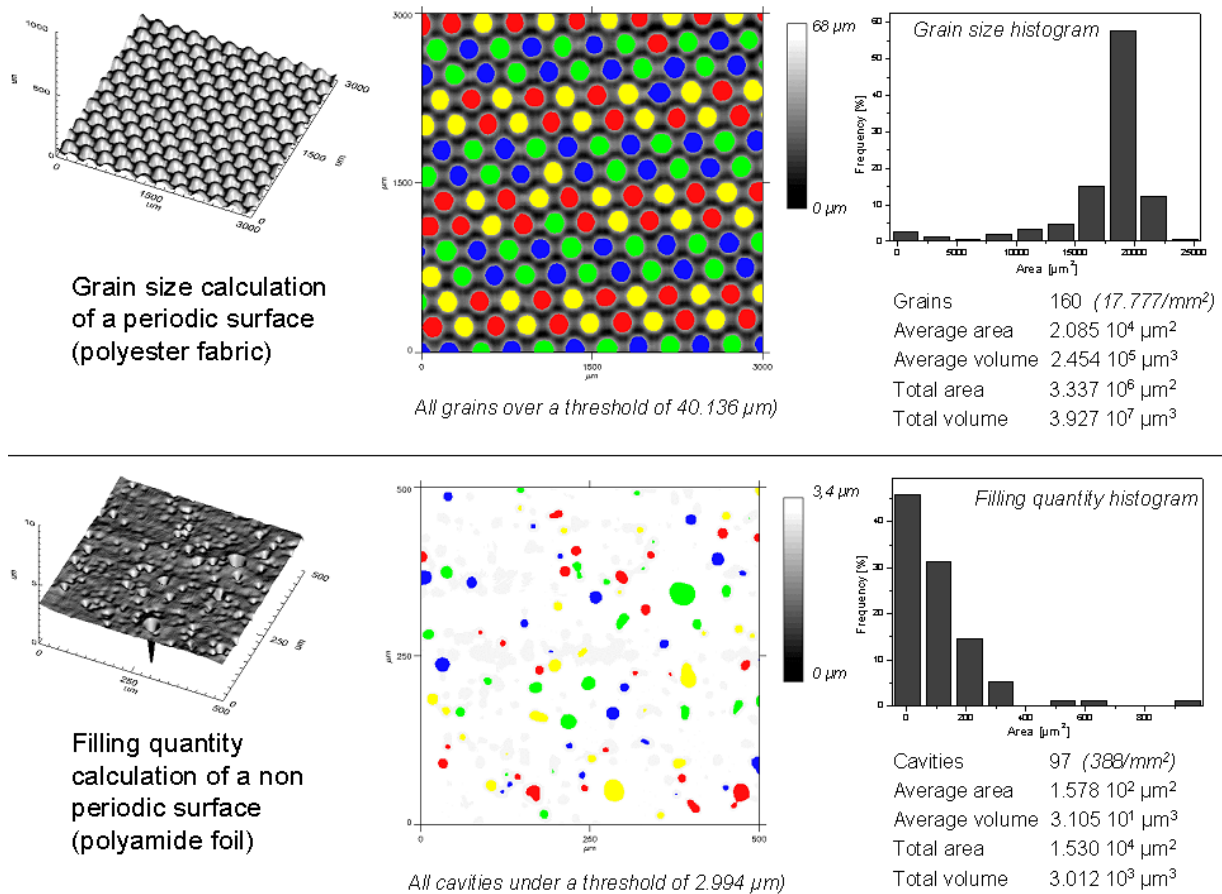


Figure 3.41 Volumetric characterization of the warp heads of a polyester fabric by grain size calculation and volumetric characterization of the pores (cavities) of a polyamide foil by filling quantity calculation.

3.7.4.3 Wenzel roughness factor

This hybrid parameter was introduced by Wenzel in order to discuss the influence of roughness on apparent macroscopic contact angle between solids and liquids [121, 122]. Wenzel roughness factor of a surface (sR_r) is the ratio between the a real (true, actual) surface (interface) area and the geometric projected (plain) area (Fig. 3.42).

As a geometrical parameter, Wenzel roughness factor of a surface by defined cut-off length (L_m), should depend on the total number of evaluated points of the image, and then on resolution. However, in the case of non natural periodic surfaces, such a generated surface by overlapping of sinoidal waves, shown in Fig. 4.43, the value of sR_r practically does not vary by resolution. On the other hand, Wenzel roughness factor of a simulated fractal (non-periodic) surface, produced by random midpoint displacement algorithm, is highly dependent on resolution. Other topographic characterisation parameters such as waviness, roughness (mean and arithmetical), porosity and fractal dimension calculated for both, periodic and fractal surfaces,

shown in Fig. 4.43, tend to a constant value with increasing measured data (number of evaluated points) and, hence, of resolution.

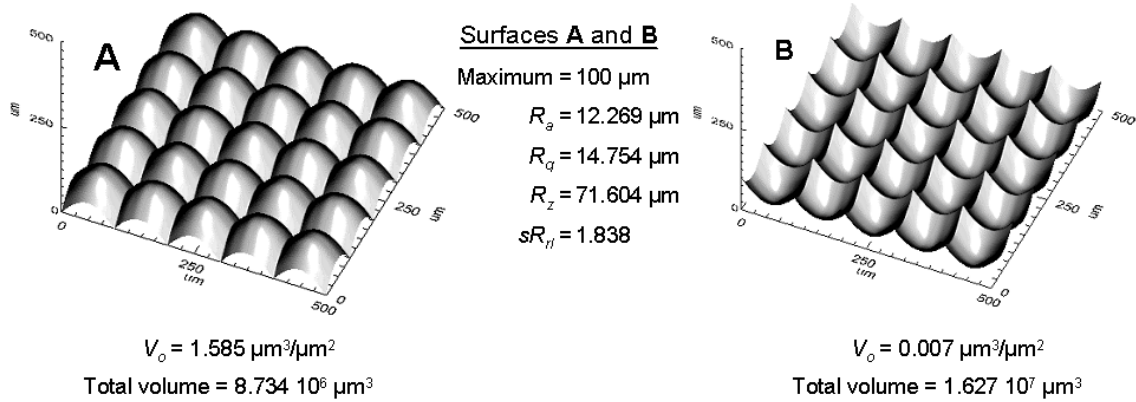


Figure 3.42 A comparison of characterization parameters and Wenzel roughness factor between a sinoidal simulated surface and its mathematically inverted image. Both surfaces have the same R_a , R_q , R_z and Wenzel factor (sR_{rl}). Only Porosity (V_o) and the total volume can characterise evident topographic differences.

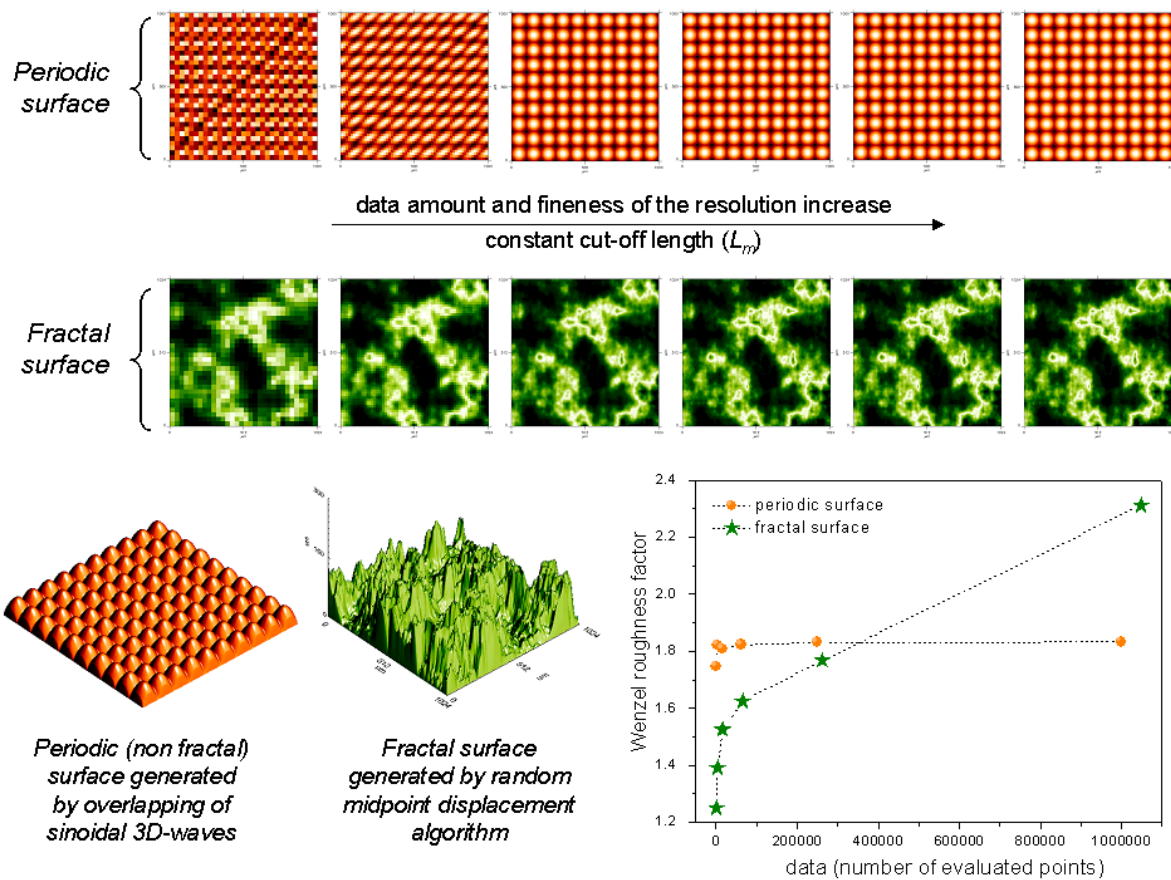


Figure 3.43 Dependency of Wenzel roughness factor on resolution (number of evaluated points having a defined cut-off length) by a periodic and non-periodic (fractal randomized) surfaces.

Since real surfaces could have some degree of periodicity as well as some degree of random, inclusive their fractal character (on a limited number of measure scales), dependency of Wenzel roughness factor on resolution should be investigated before the use of this factor as characterization parameter.

Some authors [2,116] express the Wenzel roughness factor as a percentage value called 'developed surface area ratio' S_{dr} (cf. Section 3.5, Fig. 3.15):

$$S_{dr} = \frac{\text{actual area} - \text{projected area}}{\text{projected area}} \times 100 \quad (3.7)$$

$$sR_{rl} = \frac{S_{dr}}{100} + 1 \quad (3.8)$$

3.7.4.4 Surface fractal dimension

The use of fractal dimension of a surface as a characterisation parameter (cf. Section 3.4.6) makes possible to quantify the degree of fracturing of the surface.

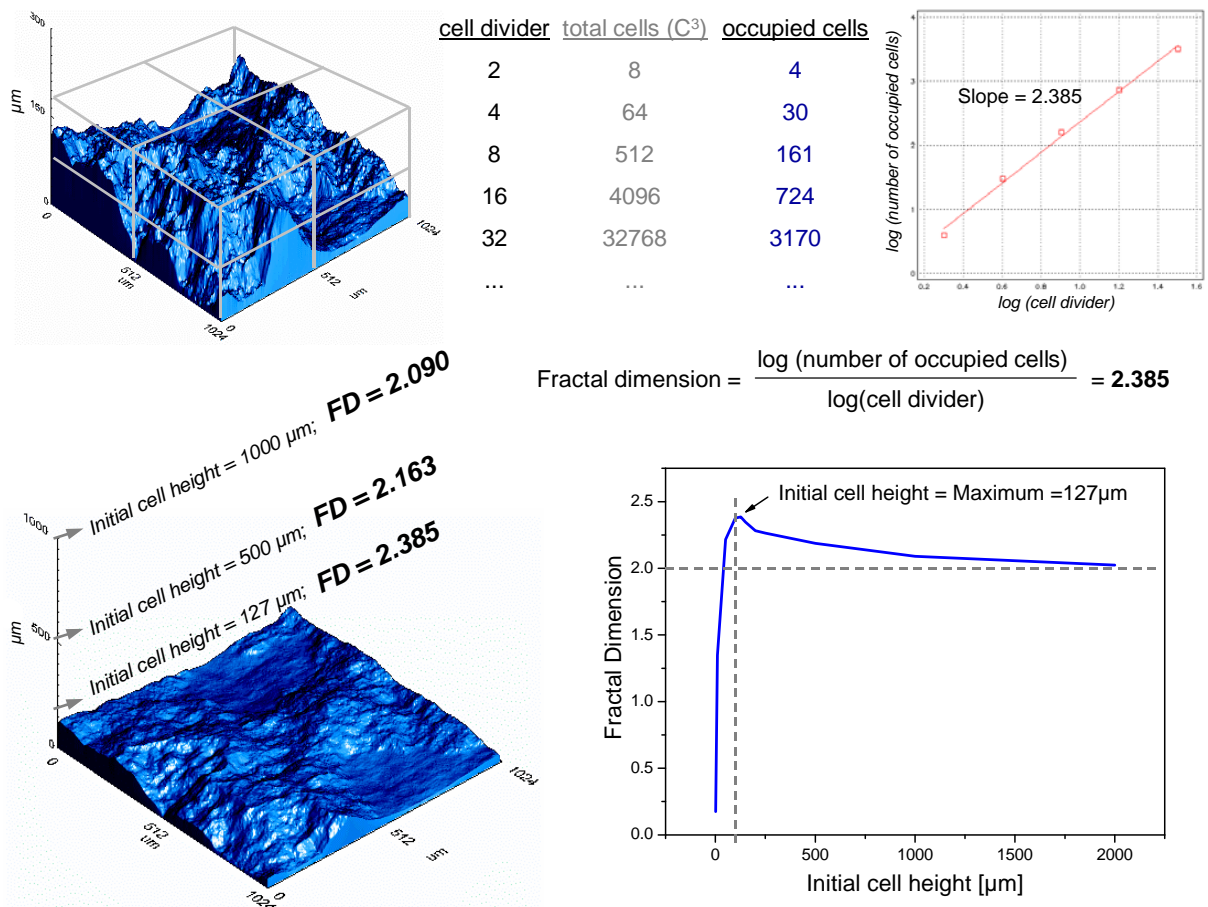


Figure 3.44 Calculation of the fractal dimension of a surface by 3D-box counting and dependency of fractal dimension on initial cell height.

Though the concept of fractal is defined for a self-affine object in any scale, the use of fractal dimension for non-fractal surfaces is possible by considering that many natural as well as man-made objects denote some ‘degree of fractality’. The calculation of fractal dimension of a surface is possible by 3D-box counting [123], consisting in sequential subdivision of the volume which contains the fractal surface in 3D-cells. By log-log plotting the number of cells occupied by the surface as a function of the cell divider factor, the slope value of the correlation straight-line curve corresponds to the value of fractal dimension. Usually a subdivision up to a cell divider of 32 is enough for a good correlation. *Fig. 3.44* shows the fractal dimension calculation of a generated plasma surface (random midpoint displacement surface) and the dependency of fractal dimension on initial cell height.

By comparison of fractal dimension values between surfaces it is important to decide one of the following selection criteria of the initial cell height (*Fig. 3.45*):

- Initial cell height is the maximum height of the highest surface to be compared; in this case, the calculated values for fractal dimension are affected by the surface waviness and are z-scale dependent.
- Each surface to be compared has a particular initial cell height corresponding to its maximum height. This case permits a comparison of fractal dimensions between surfaces independent of z-length scale. For this reason, this case reflects more clearly the non-scale dependency of fractal geometry.

Fractal dimension correlates with arithmetic mean roughness (*Fig. 3.46*), because R_a has no more information of wave fluctuations (waviness), which are strongly length-scale dependent (cf. *Fig. 3.35*).

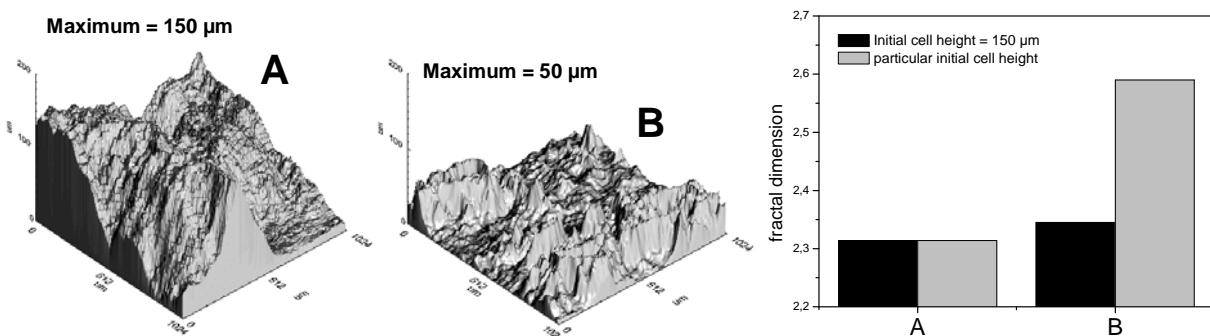


Figure 3.45 Different fractal dimension values using both selection criteria of initial cell height.

Calculated values of fractal dimension for a surface depend not only on initial cell height, but also on cut-off length. *Fig. 3.47* shows the effect of changing L_m on the calculated fractal dimension value by a constant number of evaluated points at a periodic surface. At longer L_m , fractal dimension tends to the value of 3, that corresponds to a volume due to the increase of number of evaluated repetitive units.

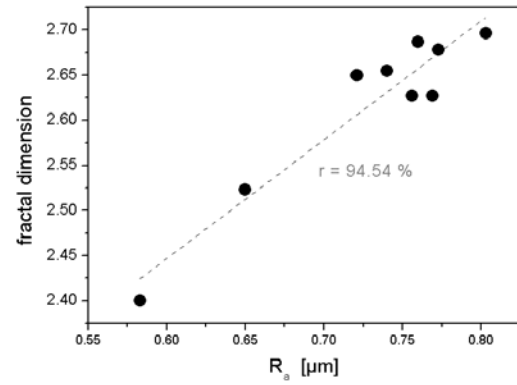


Figure 3.46
Correlation between fractal dimension and arithmetic roughness of a Sheet Moulding Compound (SMC) surface.

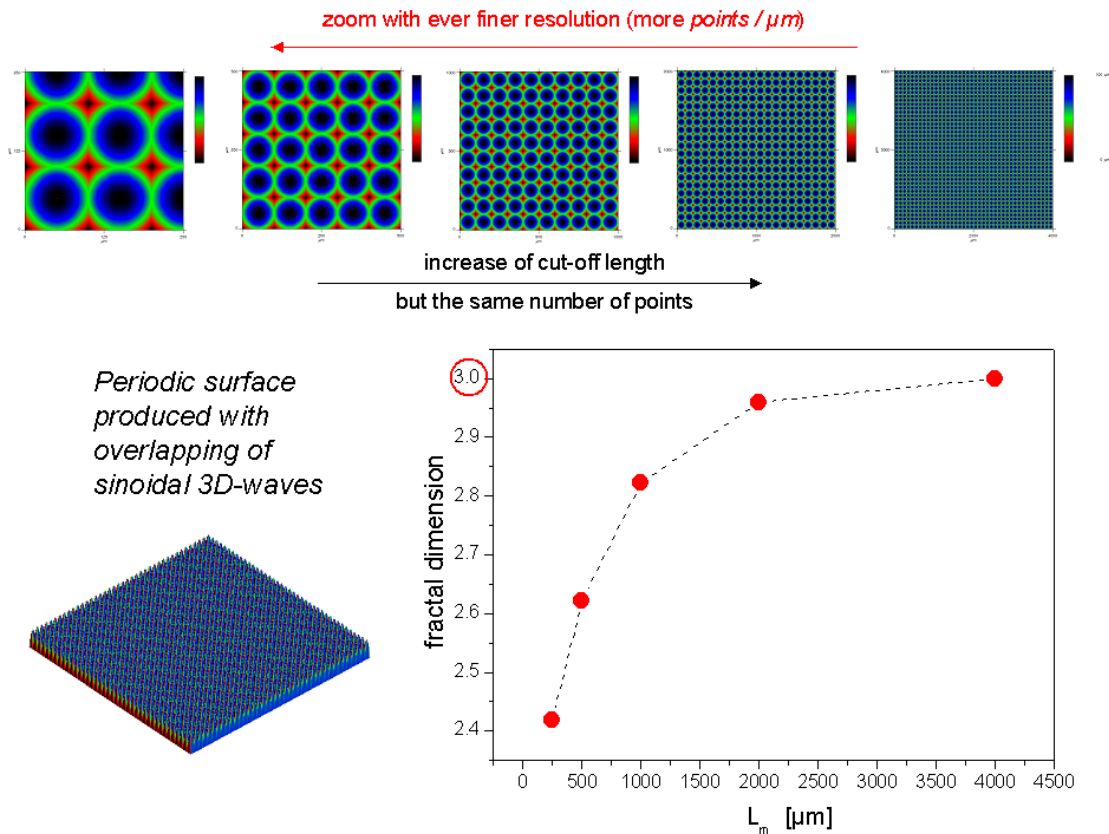


Figure 3.47 Dependency of calculated surface fractal dimension on cut-off length, by constant number of evaluated points.

Calculated value of fractal dimension for a real topographical data, for example the surface of a polyester twill fabric shown in *Fig. 3.48*, does not tend to 3 by an increase of L_m , but to a value slightly smaller than 3. In the case of a simulated fractal

surface, fractal dimension has almost the same value at any length scale, which precisely corresponds to the definition of a fractal object (self-affinity).

If the number of evaluated data remains constant, by real surfaces such as fabrics, shown in *Fig. 3.48*, Wenzel roughness factor slightly decreases with an increase of L_m because of the loss of details (increasing of Δ_x). For fractal surfaces, the dependency of Wenzel roughness factor on L_m (*Fig. 3.48*) and on Δ_x (*Fig. 3.43*) is considerable.

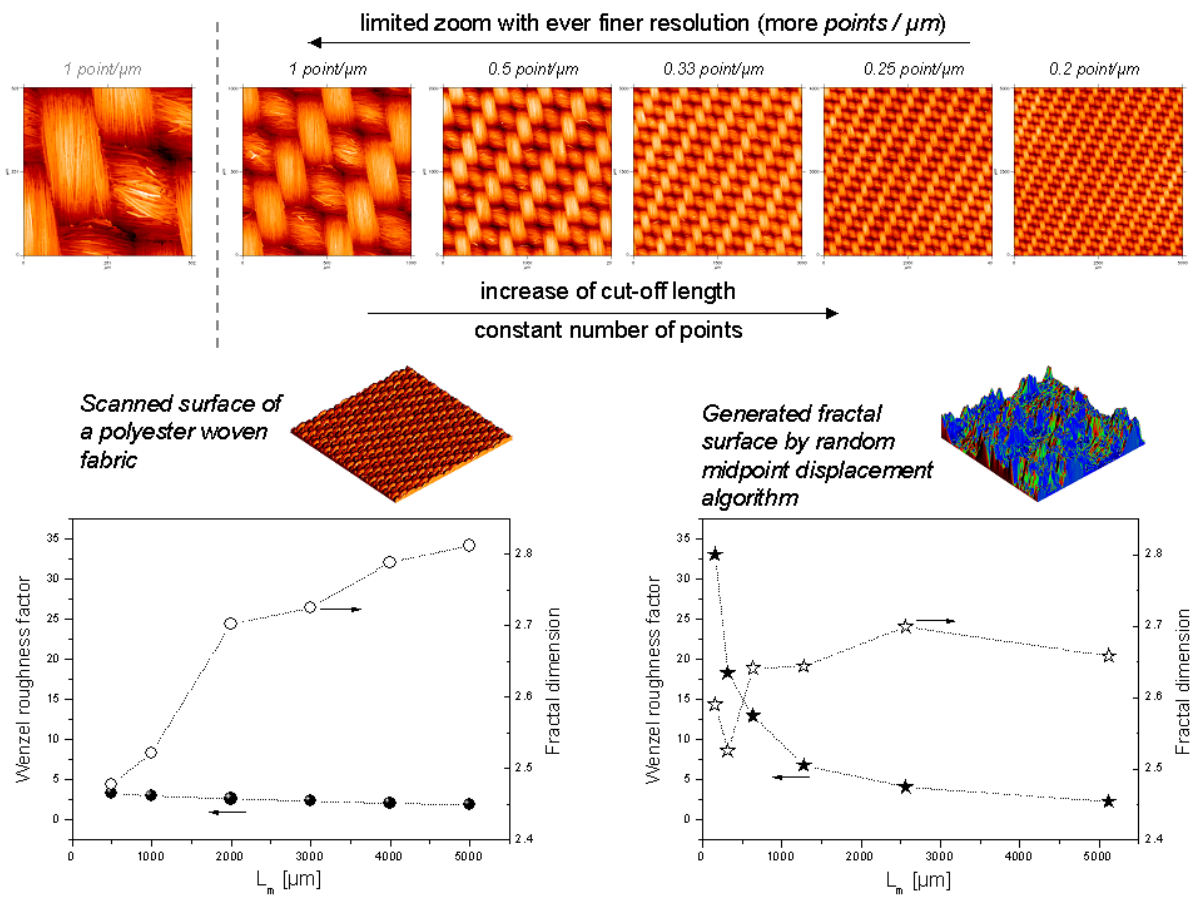


Figure 3.48 Comparison of fractal dimension and Wenzel roughness factor between a real textile surface and a generated fractal surface.

4 Topographic characterisation at different length scales

Calculating the optimal sampling conditions, the strong sensitivity of topographic parameters on the cut-off length was examined. Even if the statistical reliability of the parameters was achieved by using optimal values of L_m and Δ_x , the statistical and topographical meaning of the parameters obtained still depends on length scale, as shown in *Fig. 3.35*. In this illustration, by using $L_m = 5 \text{ mm}$ waviness surfaces obtained by FFT-filtering represent the morphology due to wrinkles and folds of textile materials, while by using $L_m = 0,5 \text{ mm}$ to $L_m = 1 \text{ mm}$ the same mathematical filtration provides the surface morphology due to the type of fabric structure (e.g. woven plain and twill).

In the present Chapter, the necessity of a topographic characterization at different length scales will be justified by using two different types of polymer surfaces: non-periodic surfaces of Sheet Moulding Compounds (SMC) and periodic surfaces of textile materials.

4.1 Sheet Moulding Compounds (SMC)

Owing to their light weight, good mechanical properties, corrosion resistance and design flexibility, fibre-reinforced composite materials are being used increasingly in automotive industry. A material commonly used for these applications is SMC which is based on glass fibre and a cross linking unsaturated polyesters / styrene matrix together with an inorganic filler. A typical formulation of SMC is given in *Table 4.1*. *Fig.4.1* shows a pressure-time diagram for the of *Table 4.1*, used to the calculation of the optimal conditions for the topographic characterization.

Due to topographic heterogeneities of SMC it is difficult to fulfil optical requirements of the automotive industry. By controlling the processing conditions, surface

properties of SMC can be optimized for subsequent coating. In order to qualify and quantify the coatability and the optical parameters of these surfaces, a systematic topographical functional characterization is required.

Samples of SMC were produced under defined temperature ($147.5 \pm 2.5^\circ\text{C}$), different conditions of pressure (3.5 to 14 MPa) and moulding time (60 to 360 s). Plates having 0%, 10%, 20% and 30% of glass fibres amount were studied. Both, placement procedure of prepregs under the press and morphology/topometry of the surface of the metallic mold cavity have been taken into account during the investigation.

*Table 4.1
Formulation of SMC used to the calculation of the optimal conditions for the topographic characterization.*

	wt. %
Unsaturated PES resin	13.3
Thermoplast	10.7
Thermoplastic solution in styrene	2.7
Initiator	0.3
Zinc stearate	0.8
Additives	0.6
Magnesium oxide	0.9
Calcium carbonate	50.6
Glass fibers, chopped	20.0

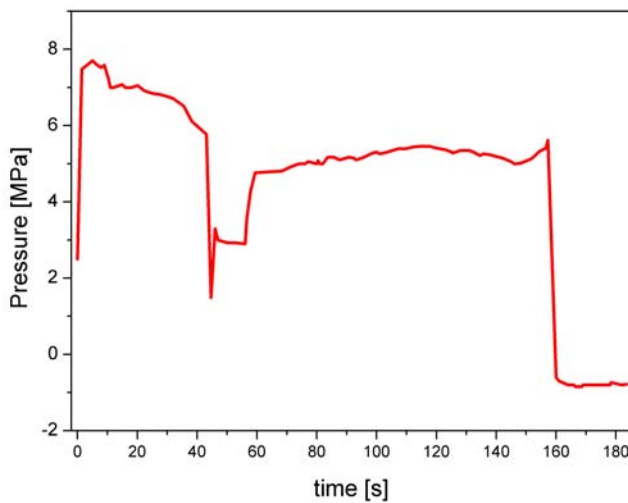


*Figure 4.1
Pressure-time diagram of SMC moulding process used to the calculation of optimal sampling conditions.*

4.1.1 Topographic parameters

Using the optimal parameters obtained (cf. Section 3.6.1), about 200 topographic measuring runs at the same and different coordinates of the SMC-plates (corresponding to identified positions of the metallic mould) were realized [124,125]. The resulting surface data were processed by FRT-Mark III Software (FRT, Germany) using mathematical filtering by Fast Fourier transformation method, whose graphical 3D representation can be seen in *Fig. 4.2*. Three meso-topographic parameters were calculated: short waviness (W_z), mean roughness (R_z) and number

of long waves on L_m (N_z). Three micro-topographic parameters were obtained: arithmetic mean roughness (R_a), number of short waves on L_m (N_a), and porosity (V_o). A description of the calculation process for N_z and N_a will be detailed in Section 4.1.8.

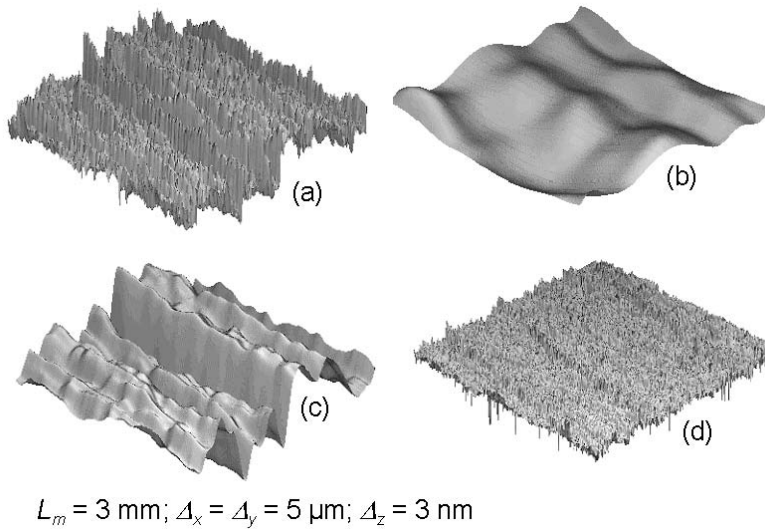


Figure 4.2
Total SMC topography (a), isolated short waviness (b), isolated mean roughness (c) and isolated arithmetic mean roughness (d).

Additional, long waviness ($L-W_z$) using $L_m = 100 \text{ mm}$ and $\Delta_x = 100 \mu\text{m}$ was measured in order to study the macro-morphology of surfaces.

4.1.2 Moulding conditions and topographic transfer from mold to SMC surface

In order to correlate R_a values to study roughness effects on SMC surface quality, Schubel [135] used microscopic and stylus profiling methods. In the present study, three different SMC plates manufactured under defined moulding conditions (pressure and moulding time) were selected. At the surface of each type, topography of sixty defined positions were characterised using $L_m = 3 \text{ mm}$ and $\Delta_x = 5 \mu\text{m}$. From a statistical point of view, mean values of W_z , R_z and N_z could characterise the topography as a function of moulding conditions, as shown in Fig. 4.3. Results reveal that moulding conditions control the meso-topography of SMC surfaces under investigation and apparently don't control the micro-topography characterised using R_a values.

By comparing topographic parameters measured between plates at the same position (Fig. 4.4), it is clear that the topography of the metallic mold controls the

resultant meso-topography of SMC surfaces more specifically than moulding conditions, by transference of its surface irregularities or third level (grooves).

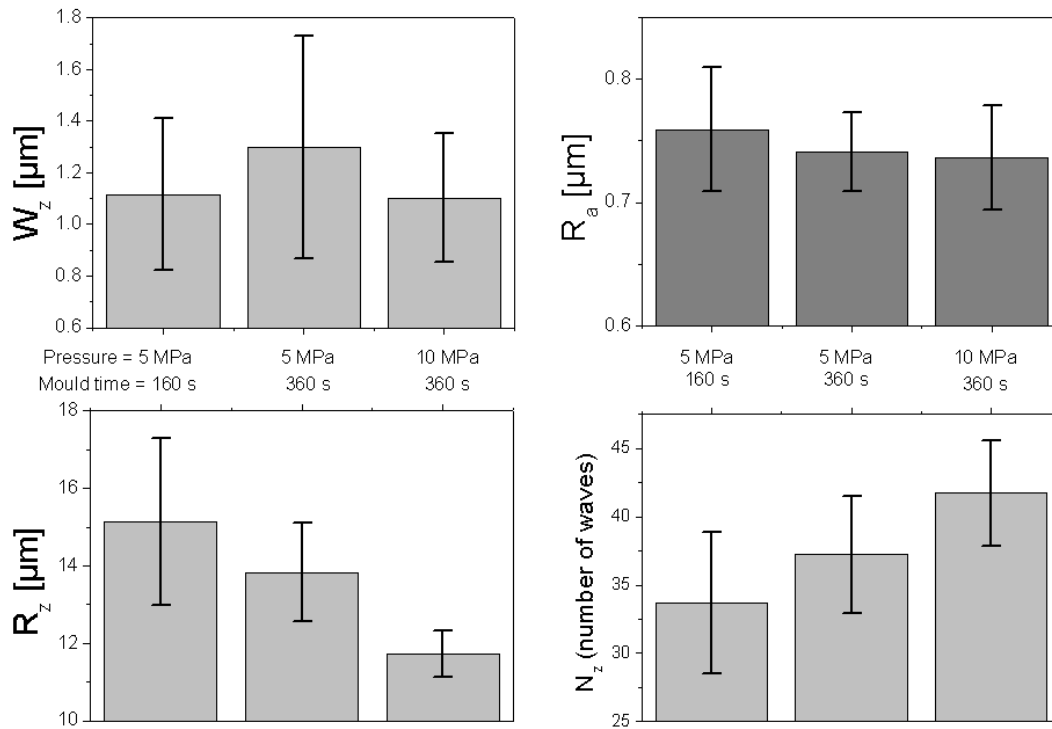


Figure 4.3 Influence of moulding conditions (different pressure and moulding time) on meso (W_z , R_z , N_z) and micro topography (R_a).

First important conclusion, is that by SMC any topographic characterisation of surface modification processes (such as cleaning by powerwash as an example) have to be realized by comparing topographical changes in identified mold-plate positions. For a systematic study of the mold influence on resultant SMC surfaces, it is necessary to previously measure the topography of the metallic mold.

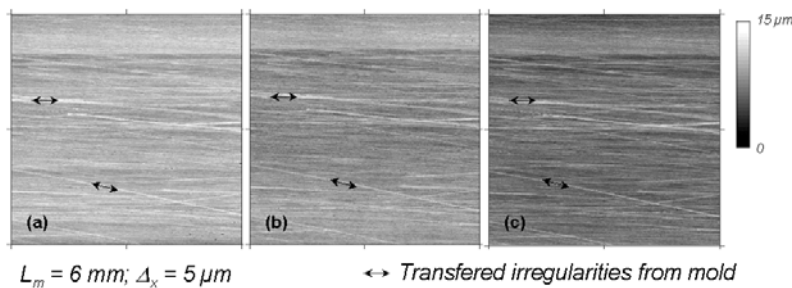


Figure 4.4 Transference of mold grooves defines the meso-topography of third level (DIN 4760) of SMC surfaces. Moulding conditions: 5 MPa and 160 s (a), 5 MPa and 360 s (b), 10 MPa and 360 s (c).

However, a direct measurement of the mold topography was not possible because of the size and weight of the metall piece. For this reason, a transfer print of the mould surface was obtained using polydimethylsiloxan (PDMS) (Fig. 4.5), which is proved to reproduce nanoscale structures with great reliability [126]. Before applying this

process to the metallic mold, an experimental probe as well as a calibration of this procedure were realized by measuring the topography of a small metallic piece of the same material of the mold and by comparing its measured topography with the topography of the obtained PDMS surface.

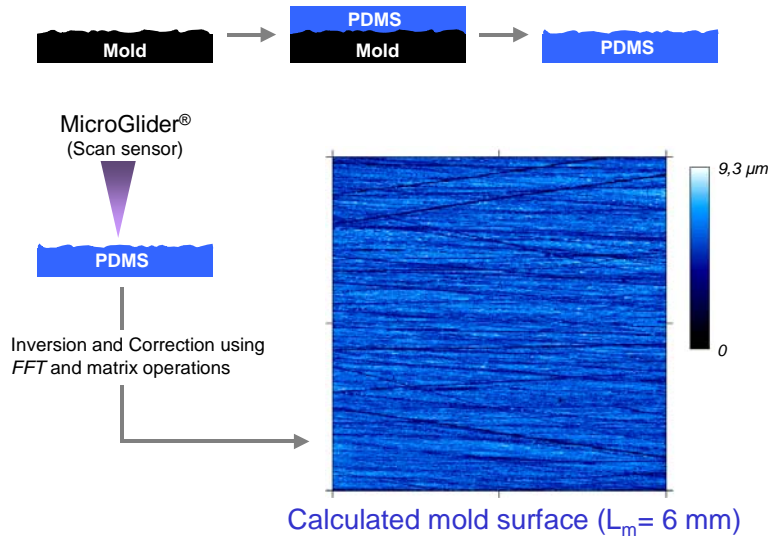


Figure 4.5
Indirect calculation of mold topography by transfer in PDMS.

According to the results, the transference of micro-topographic irregularities from mold to SMC surface is relatively low (Fig. 4.6). The calculation of Wenzel roughness factor [121,122] shows, that the mold effective area is only 1 % larger than the effective area of SMC surface, at the calculated optimal resolution of $5 \mu\text{m}$. However, the transference of meso-topography, characterised through R_z is high, principally because of a notable increase of the short waviness from mold to SMC surface, presumably due to adhesion during separation (Fig. 4.7), that could be responsible for a ‘shrinkage effect’ of P-profiles observed by Schubel et al. [135] and attributed to the mold surface and to a volumetric resin shrinkage.

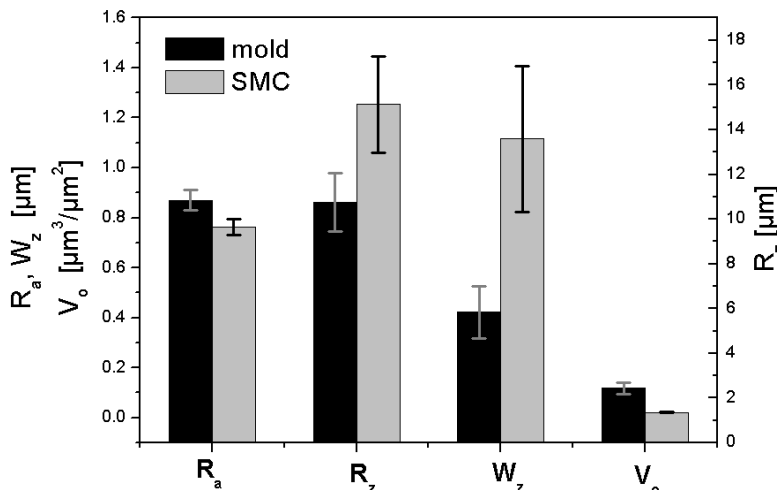


Figure 4.6
Topographic transfer from metallic mould to SMC surface.

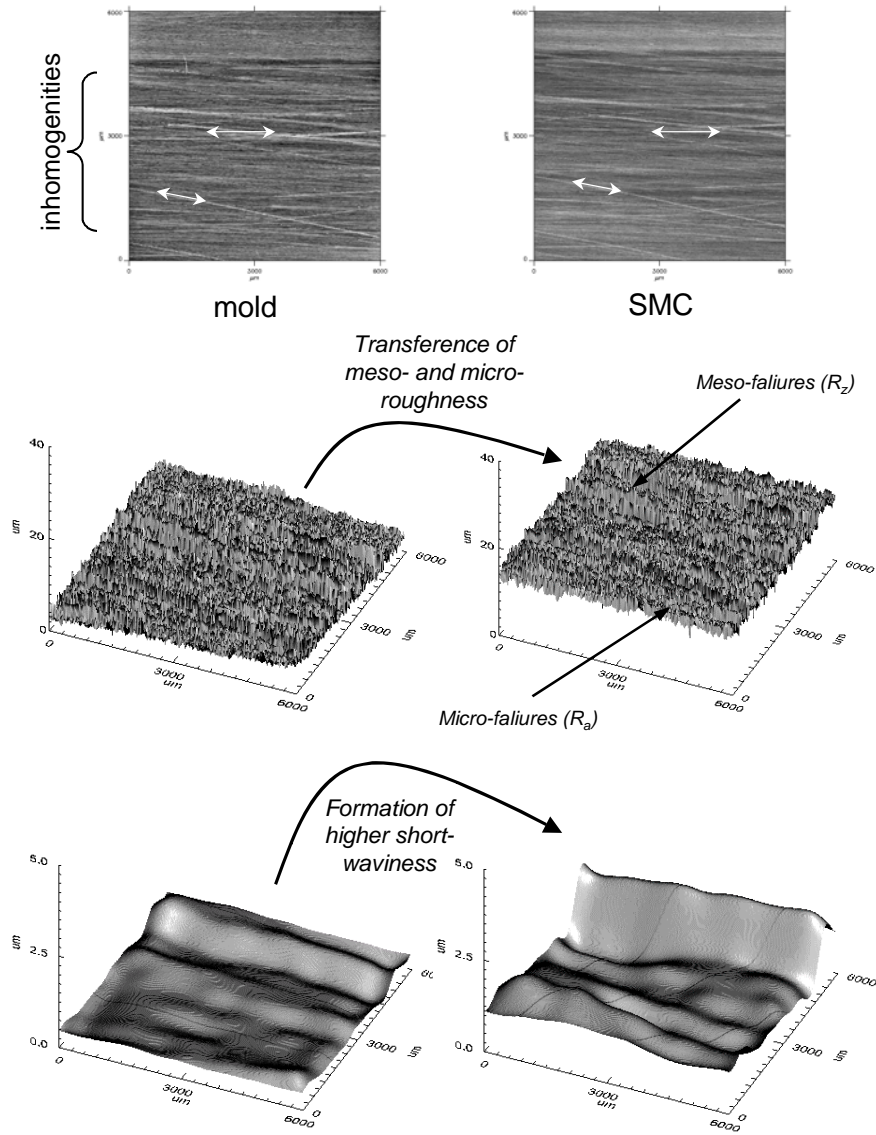


Figure 4.7 Transfer of meso- and micro morphologies from mold to SMC surface.

The transfer of meso-waves is only about 57% (see N_z in Fig. 4.8), but the transference of their height (characterized through R_z) is about 141 % due to a notable increase of short waviness (Fig. 4.6). After measuring of 15 identified positions at ten different twin SMC plates (manufactured with the same moulding conditions: 5 MPa, 160 s), it was possible to compare the influence of mold topography on the statistical reliability of the topographic parameters obtained. Fig. 4.9 shows that mold topography strongly influence the SMC meso-topography (R_z and N_z notably vary from position to position). By fixing a position at 10 twin plates, R_z and N_z are statistically more reliable. Only the effect of glass fibres orientation

(prepreg orientation) reflected in porosity (V_o) seems to control the meso and probably micro-topography of each measured area.

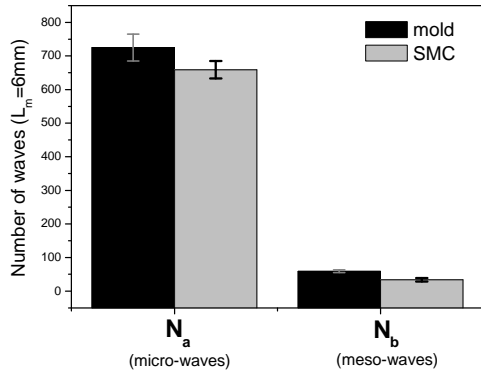


Figure 4.8 Meso- and micro-waves transfer from mold to SMC surface.

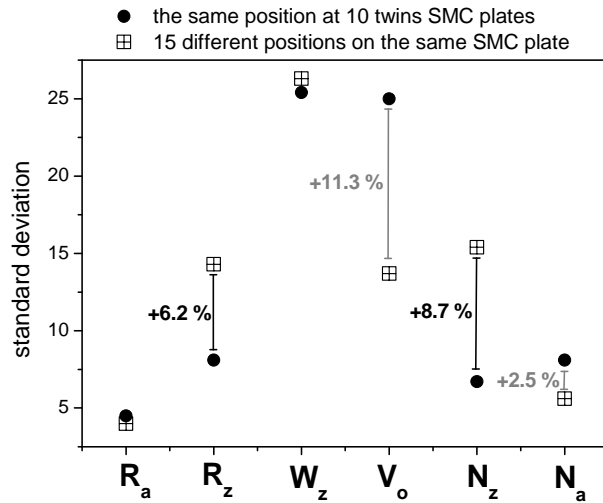


Figure 4.9 Impact of sampling (positioning) criteria on statistical reliability.

4.1.3 Effect of glass fibre content on micro-topography

Le [136] studied the internal microstructure and porosity of SMC. Orientation and content of glass fibres influence not only the internal structure but also the micro-topography of the SMC surface (cf. Section 4.1.2).

To consider the presence of glass fibres, the topography of 4 different recipes of SMC plates were analyzed containing 0 % and 10% of glass fibre amount.

According to the results, glass fibres increase the porosity of three types of SMC surfaces (Fig. 4.10). A more detailed analysis of short waviness will explain later the particular case of SMC-3, in which the whole porosity (which includes the short waviness effect) was not

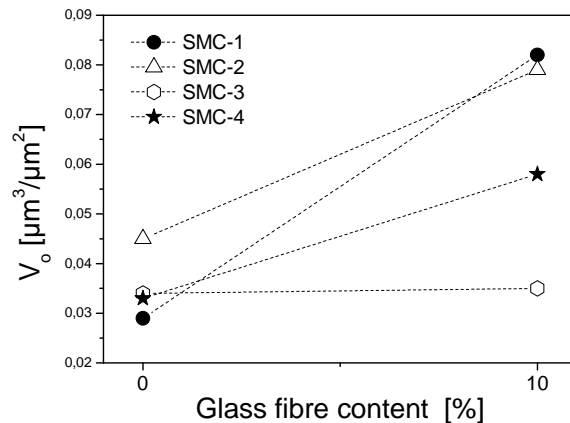


Figure 4.10 Effect of glass fibre content on topography of 4 different recipes of SMC. Before calculation of porosity (V_o), short waviness was removed. The values of porosity in this diagram are not influenced by short waviness, as well.

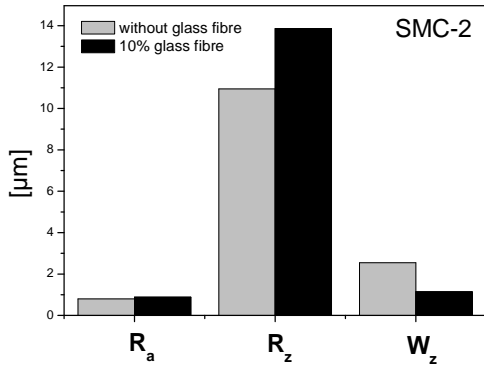


Figure 4.11
Effect of glass fibre content on topography parameters of SMC-2.

influenced by glass fibre content.

A detailed study of the SMC-2 case shows (Fig. 4.11) that the microtopography (characterized with R_a) is practically not influenced by glass fibre content. In this case, the mesotopography was modified by increasing of R_z and as a consequence of V_o . A decrease of short waviness is a result of increasing viscosity of a prepreg during moulding, cooling, drying and shrinkage,

and, especially, of decreasing of adhesion between mold and SMC surface during separation, presumably due to the presence of glass fibres.

4.1.4 Influence of moulding conditions on the long waviness

Surface long waviness ($L-W_z$) values of 4 different formulations of SMC materials manufactured under different conditions (different pressure and moulding time) were measured using $L_m = 100\text{ mm}$ and $\Delta_x = 100\text{ }\mu\text{m}$.

In general, long waviness reaches a constant value with increasing moulding time. Fig. 4.12 shows the special case of SMC-2. According to the results, pressure applied during moulding controls the resulting long waviness of the SMC recipes studied. Fig. 4.13 shows the behavior of long waviness as a function of pressure applied after 60 seconds of moulding. In the case of recipes 1, 2 and 4 pressure values, producing relative minima of long waviness, were identified. In

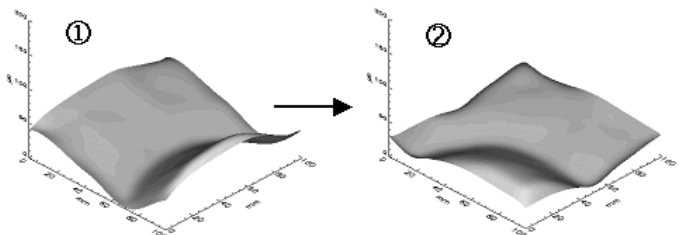
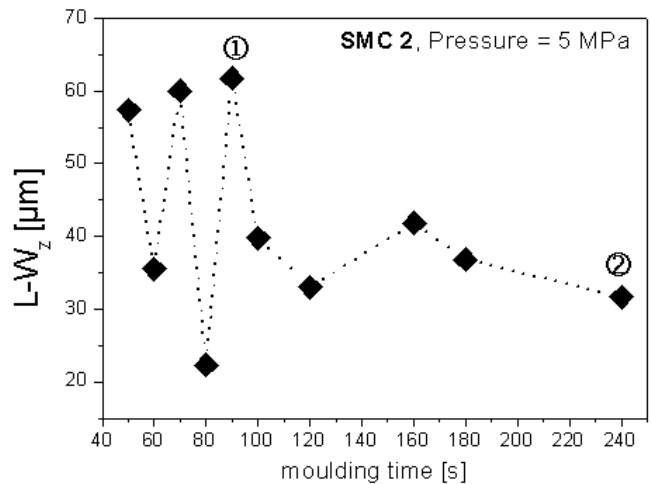


Figure 4.12
Effect of moulding time on long waviness of SMC-2.

the case of recipe 3, a pressure value of 8 MPa results in a relative maximum of long waviness.

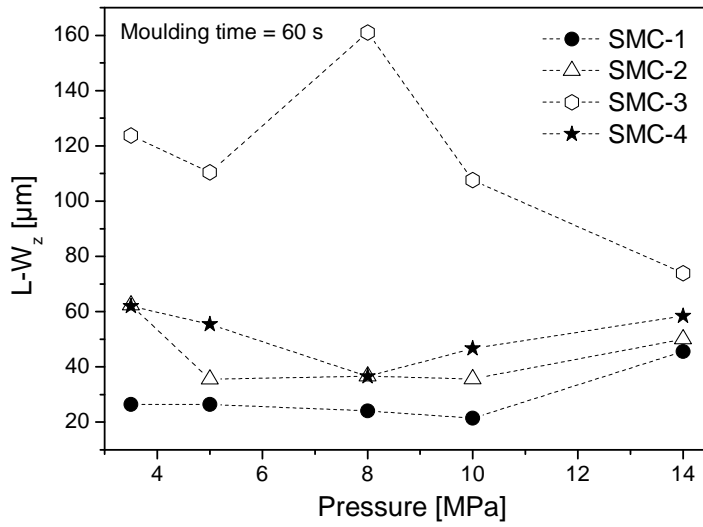


Figure 4.13
Effect of moulding pressure on long waviness at $L_m = 100$ mm and $\Delta_v = 100$ μ m.

4.1.5 Characterization of short waviness

The meso-topography ($L_m = 3$ mm to 6 mm) of SMC surfaces, resulting from different formulations, is represented by the short waviness obtained by FFT-filtering of the topographic data, shown in Fig. 4.14. SMC-3 shows the highest value of W_z for 4

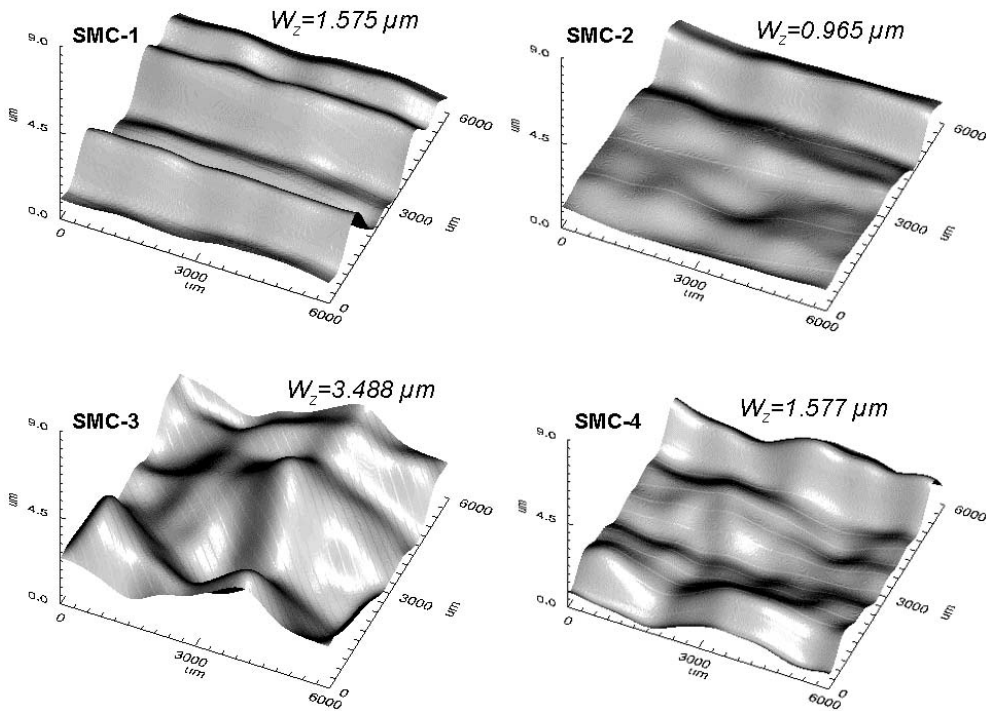


Figure 4.14 Meso-topography of different SMC formulations by a pressure value of 5 MPa after 60 seconds of moulding.

recipes studied. This is the reason that the resulting porosity of this SMC type depends mostly on meso-topography and not on glass fiber content, as has been suggested in Section 4.1.3.

Under pressure of 5 MPa, the meso-topography of SMC-1 shows the strongest dependency on moulding time (highest standard deviation of W_z values), as shown in *Fig. 4.15*. For all SMC recipes, resulting W_z decreases with longer moulding time, as illustrated in *Fig. 4.16*, for the case of SMC-2.

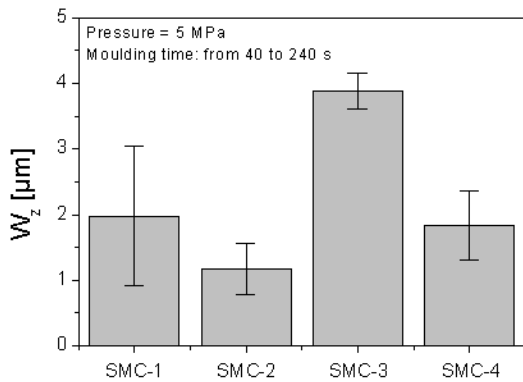


Figure 4.15
Short waviness average of different SMC formulations by pressure of 5 MPa after different moulding times.

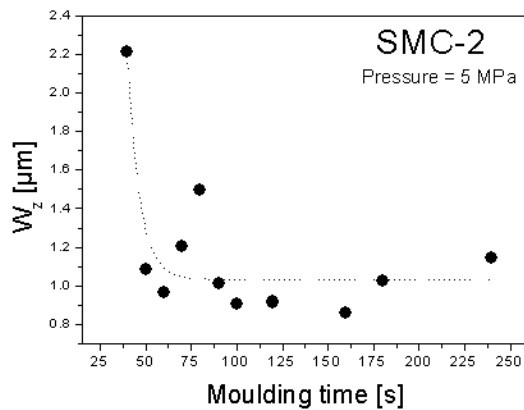


Figure 4.16
A decrease of short waviness with increasing moulding time.

4.1.6 Effect of prepregs placement on macro- and meso-morphology

It was found, that the placement procedure of prepregs influence not only the long waviness (macro-morphology) of the resulting SMC surface, but also the short waviness (meso-topography). *Fig. 4.17* schematizes two different placement procedures of prepregs before molding and their effect on the resulting macro-morphology ($L_m = 100\text{ mm}$) of SMC surfaces. In case of the second placement procedure, a meso-morphologic failure is produced on the resulting surface, which has an pronounced effect on measured short waviness.

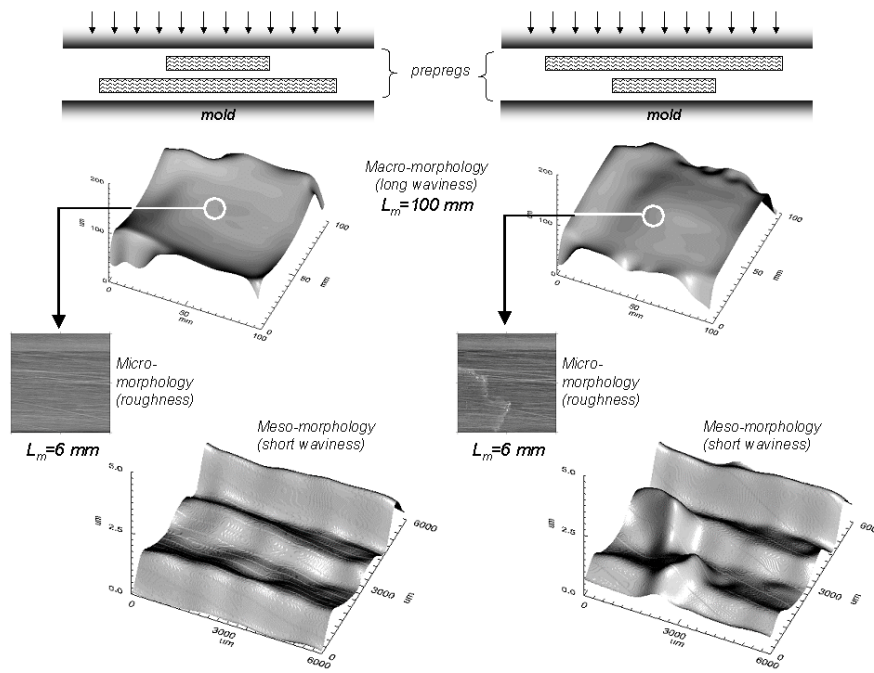


Figure 4.17
Effect of prepreg
placement
procedure on
macro-, meso-
and micro-
morphologies.

4.1.7 Correlation between length scales and resulting topography

After analysing topographic parameters calculated on macro-, meso- and micro-length scales of SMC surfaces manufactured by constant temperature ($147.5^{\circ}\text{C} \pm 2.5^{\circ}\text{C}$), it is possible to conceptualize the influence of each one of the most important moulding conditions on the topographic variables and, as a consequence, on the quality of the resulting surface, as schematized in *Fig. 4.18*.

The most important conclusions are:

- By a constant temperature, rheology during moulding, controlled by pressure and moulding time, defines the resulting long waviness (macro-morphology studied by $L_m = 100\text{ mm}$), which is simultaneously controlled by the mold form and prepregs placement procedure.
- Mold morphology and prepregs placement also directly control short waviness (meso-morphology studied by $L_m = 3\text{ mm}$), due to adhesion between mold and SMC surface during detaching.
- Orientation and size of glass fibres can in some cases affect the short waviness through adhesion during detaching, but in general control the meso topography (characterized with R_z).

- Mold surface always defines the meso topography (R_z) but, depending on mold inhomogeneities can also influence the micro topography (characterized with R_a).

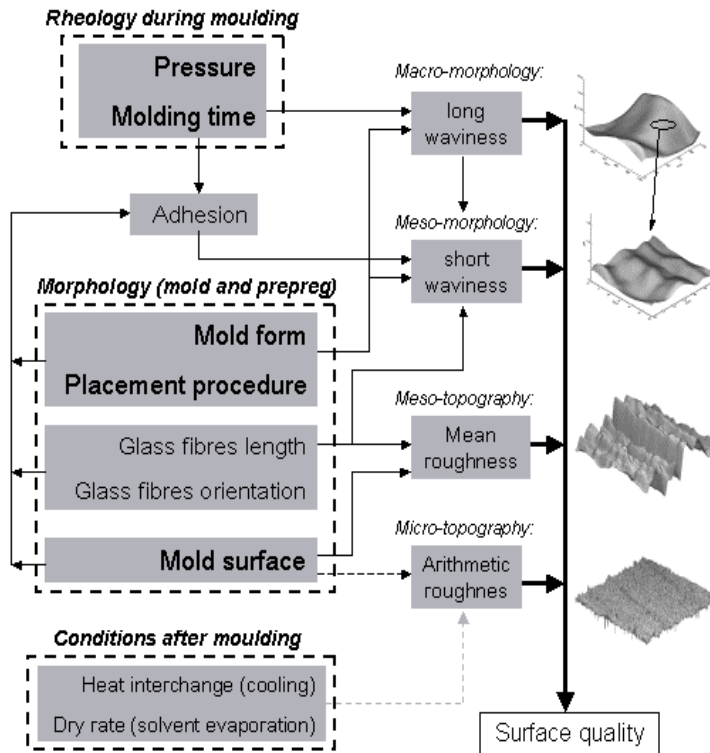


Figure 4.18 Schematization of the influence of production variables on the resulting quality of SMC surfaces trough the modification of the topography on different length scales.

Heat interchange (cooling) and conditions of residual volatiles evaporation already mentioned by Schubel et al. [137] after moulding, were not considered in the present study, but they can be presumed to be important in the definition of resulting micro-topography.

4.1.8 Application of the concept of length scales to topographic characterisation

Due to the topographic heterogeneities of SMC surfaces, it is difficult to fulfil optical requirements of coated SMC surfaces for technical applications, especially for the automotive industry. It was demonstrated, that preregs compositions, moulding and post-moulding conditions define the resulting surface topography by controlling surface morphology on different lengths scales.

Cavities (pores) of SMC surfaces are usually considered to retain air and produce failures (air bubbles) after coating. From a topographic point of view, a “coatable” SMC surface should be anisotropic, having no spikes and almost same-sized, not too deep, with regularly distributed micro-cavities.

In order to quantify the surface coatability, additional parameters can be considered: fractal dimension [138], number of cavities, cavity-area average, cavity-volume average, total area of cavities, total volume of cavities and cavities histograms. But the attention to all the topographic parameters mentioned for a reasonable quantification of coatability is very difficult. The resulting multivariable system is complex. The results of the present study reveal that a quantification of the surface quality using only one or two parameters seems to be a reasonable way. However, this approach requires a better understanding of the mechanism of surface formation. For this intention, a simple 2D structure model was developed [127].

4.1.8.1 A profile model to understand the cavities formation at SMC surfaces

Though SMC surfaces are non-periodic ones, i.e. they do not show any repetitive units compared to textile materials, some periodicity due to regular polish of the metallic mold permits the use of a periodic profile model in order to understand the formation of cavities as a result of the combination of the mould inhomogeneities with moulding and post-moulding conditions.

The following approach to develop a structural model does not take into account the short waviness. Only mean roughness and arithmetic roughness are considered to conform the total SMC topography (Fig. 4.2). Modelled profiles consist of triangular periodical waves of two length scales: the first scale describes the mean roughness R_z and the second one the arithmetic mean roughness R_a filtered by FFT, as shown in Fig. 4.19. Using calculated values of surface Wenzel roughness factor (sR_{rl}), the number of long waves (N_z) and short waves (N_a) can be obtained:

$$N_z = \frac{L_m}{2R_z} \sqrt{(sR_{rl(z)})^2 - 1} \quad (4.1)$$

$$N_a = \frac{L_m}{2R_a} \sqrt{(sR_{rl(a)})^2 - 1} \quad (4.2)$$

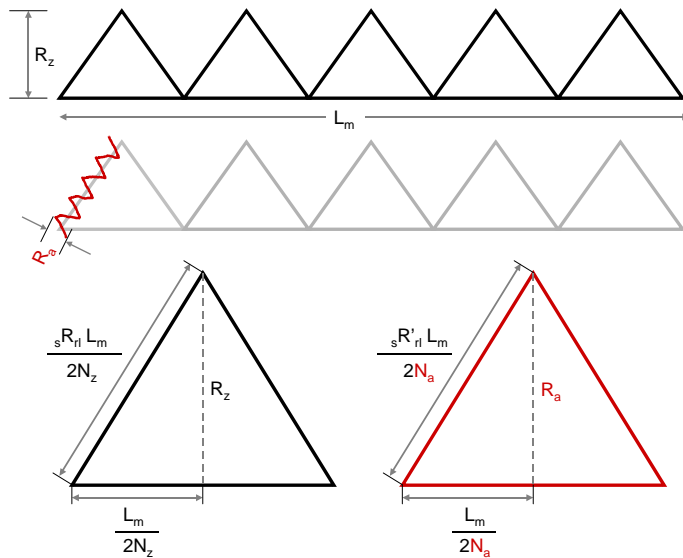


Figure 4.19
2D profile using triangular waves to describe the formation of long and short waves and their relation to R_z and R_a .

The quantity of cavities and their mean area were calculated by applying ‘filling quantity’ operations (cf. Section 3.7.4.2), with a threshold value of $6 \mu\text{m}$, measured under the highest point of the surface after filtration of short waviness (Fig. 4.20).

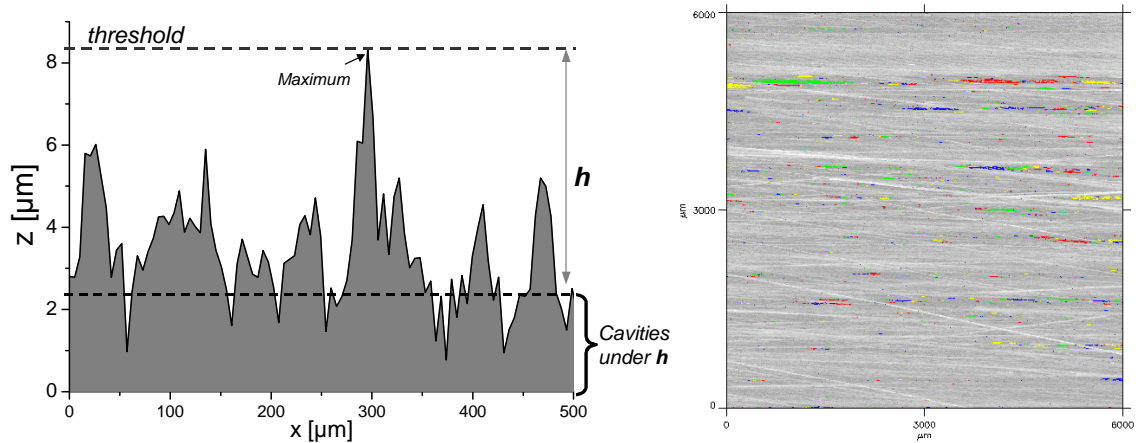


Figure 4.20 Quantification of cavities (coloured areas) by ‘filling quantity’ operation under $6 \mu\text{m}$ of highest point.

The threshold is an arbitrary value that depends on surface morphology. The purpose is to take a reference plane that can serve as “failure”- limit for all the surfaces to be studied and compared. As will be shown in Section 4.1.8.3, the volumetric characterisation of SMC samples produced by another better polished metallic mold demands the use of a threshold of only $2 \mu\text{m}$.

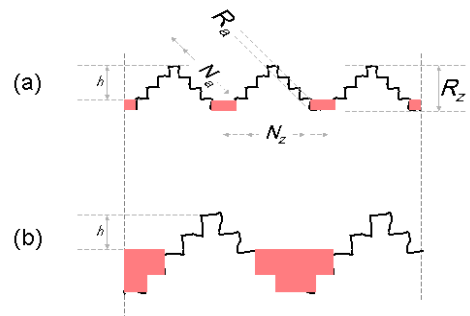


Figure 4.22
Modelled SMC-1 profile before moulding (a), schematization of predicted profile after 240 s of moulding (b). Sizes are not scaled.

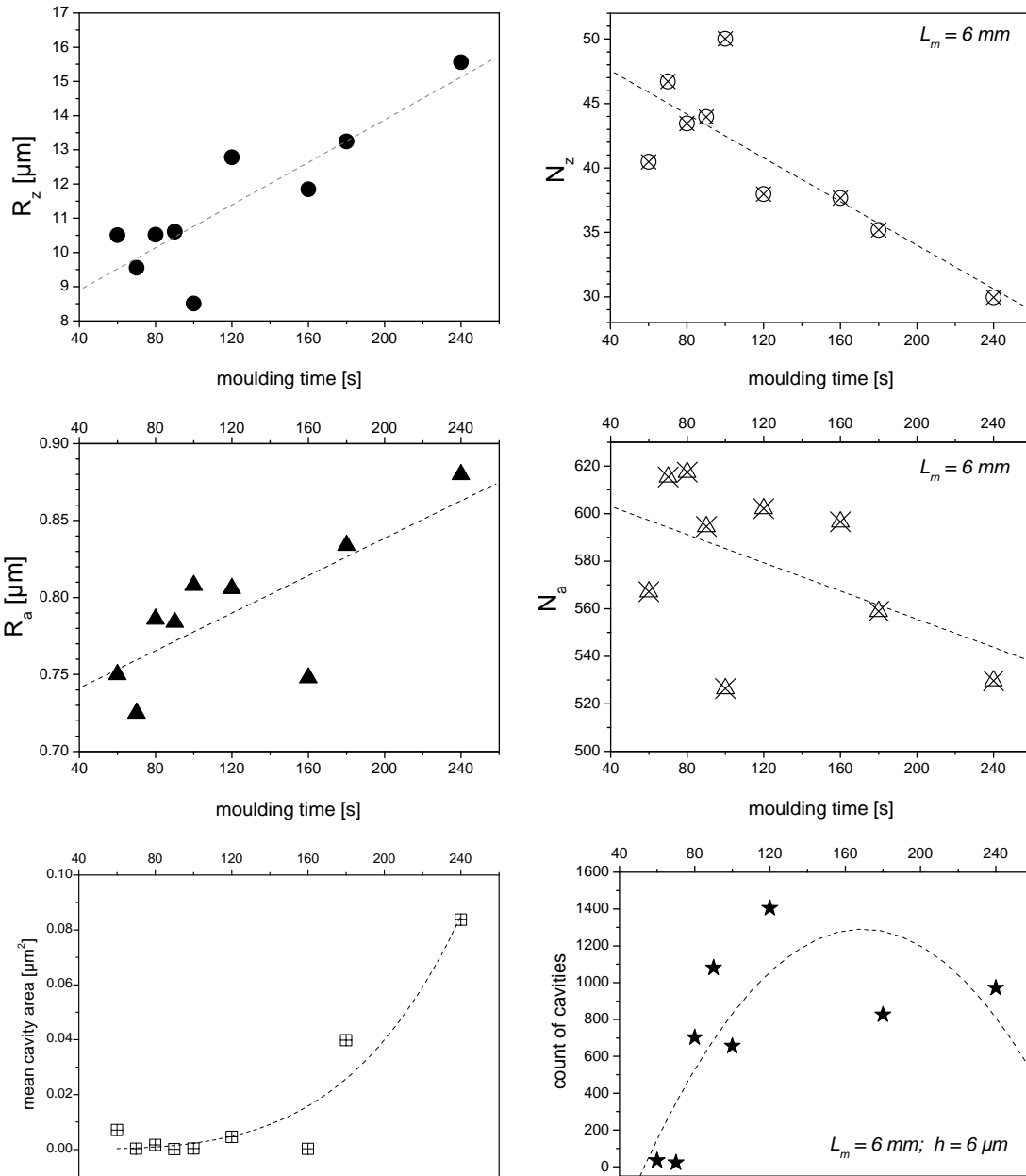


Figure 4.21 Measured values (R_z , R_a , mean cavity area and count of cavities) and calculated N_z and N_a as function of moulding time for a SMC-1 surface.

Applying the model for a surface of SMC-1 manufactured by pressure of 5 MPa, resulting quantity of cavities and their cross-sectional mean area (Fig. 4.21) could be predicted schematically by R_z , N_z , R_a and N_a , as functions of moulding time (see Fig. 4.22). In this case, moulding time increases R_z and R_a . At the same time, long and short waves decrease in their number. This process results in an increase of cavities cross-sectional area (as a mean value), which is predicted by the conceptual model described above. However, a decrease of cavities count, predicted by the model, occurs only for the last 120 seconds of moulding.

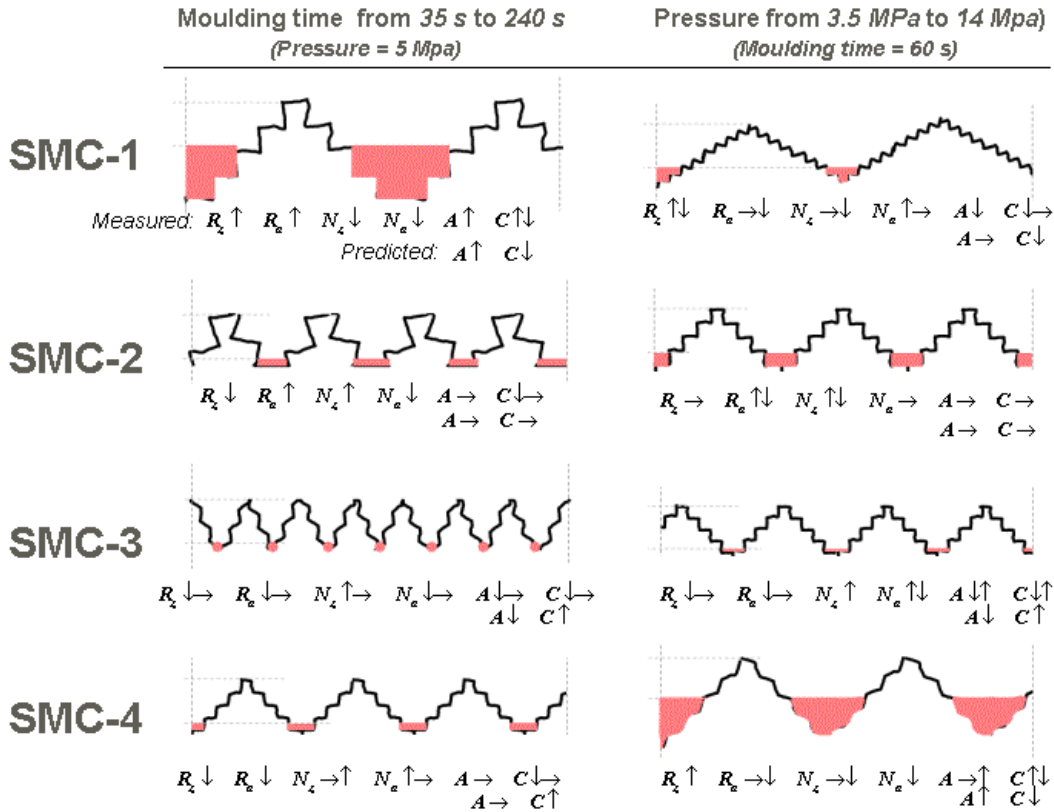


Figure 4.23 A qualitative comparison between measured and predicted parameters. A: mean cavity area, C: count of cavities. \uparrow denotes increase, \downarrow denotes decrease, \rightarrow denotes no change.

The same analysis, applied to other SMC recipes, for different moulding time and pressure values, shows (Fig. 4.23) that the model can conceptually predict the morphological modification of the profiles. In the case of SMC-3 at different moulding times, the effect of short waviness (cf. Section 4.1.5 and Fig. 4.14), does not allow the successful application of the model. The best prediction was obtained for SMC-2, for which measured W_z is the smallest for the recipes investigated.

4.1.8.2 Characterisation of cavities and prediction of coatability

The number of cavities under defined threshold and their mean area in a defined sample area ($L_m \times L_m$) can be used to compare and qualify the coatability of SMC surfaces. By using both parameters, the frequency and size of structural failures can be quantified. Fig. 4.24 shows the quantification of cavities in order to characterise the coatability of a SMC-2 surface.

According to this characterisation method, at a pressure of 3.5 MPa and a moulding time of 300 s the best coatable surface is formed. Only one cavity was found under a threshold of $6 \mu\text{m}$, whose area is about $75 \mu\text{m}^2$. Lower pressure values leads to

lower adhesion during the separation of a SMC surface from the metallic mould; as a consequence, resulting topography is more regular.

At the highest pressure (14 MPa), only 2 cavities were found after 300 s of moulding and 4 cavities after 360 s. However, by this duration of moulding, mean area of the cavities increased dramatically from $75 \mu\text{m}^2$ to $3000 \mu\text{m}^2$.

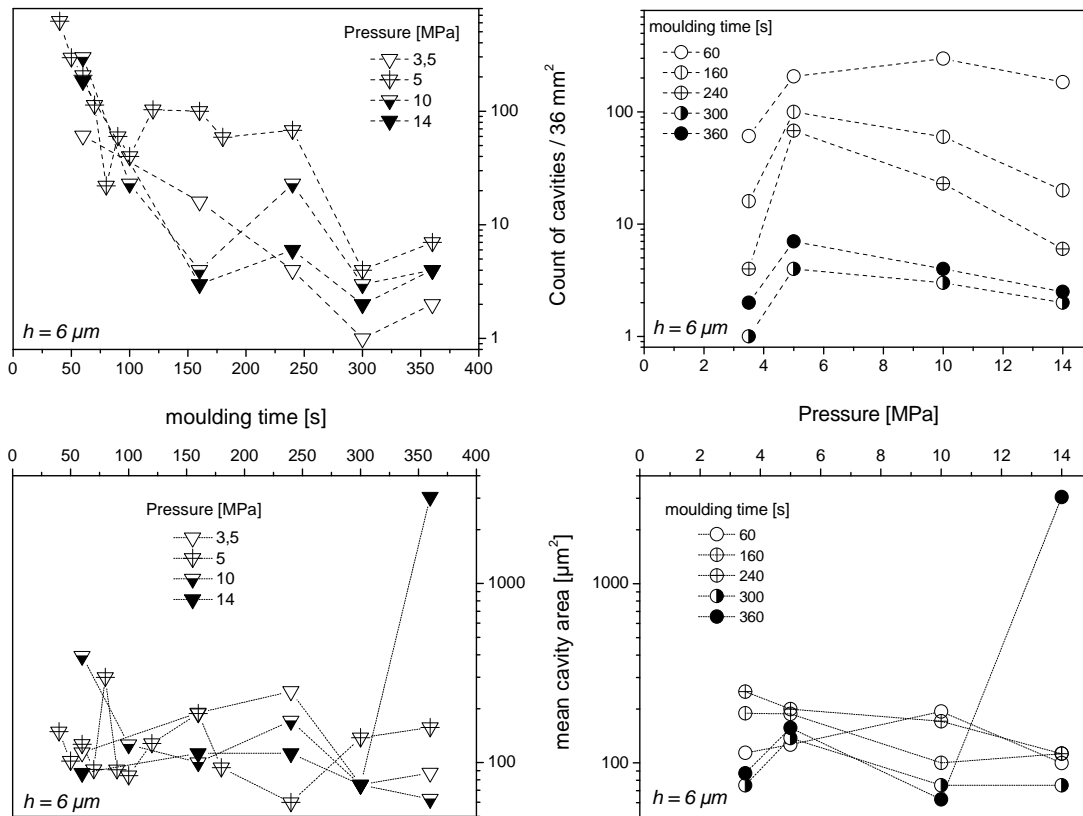


Figure 4.24 Count of cavities and mean cavity area under $6 \mu\text{m}$ from the highest point by different pressures and moulding durations for SMC-2 surfaces. Samples studied (36 mm^2 , $L_m = 6 \text{ mm}$) correspond to the same position of metallic mold.

4.1.8.3 Surface Relative Smooth parameter (SRS) to characterise the topographic modification of SMC surfaces

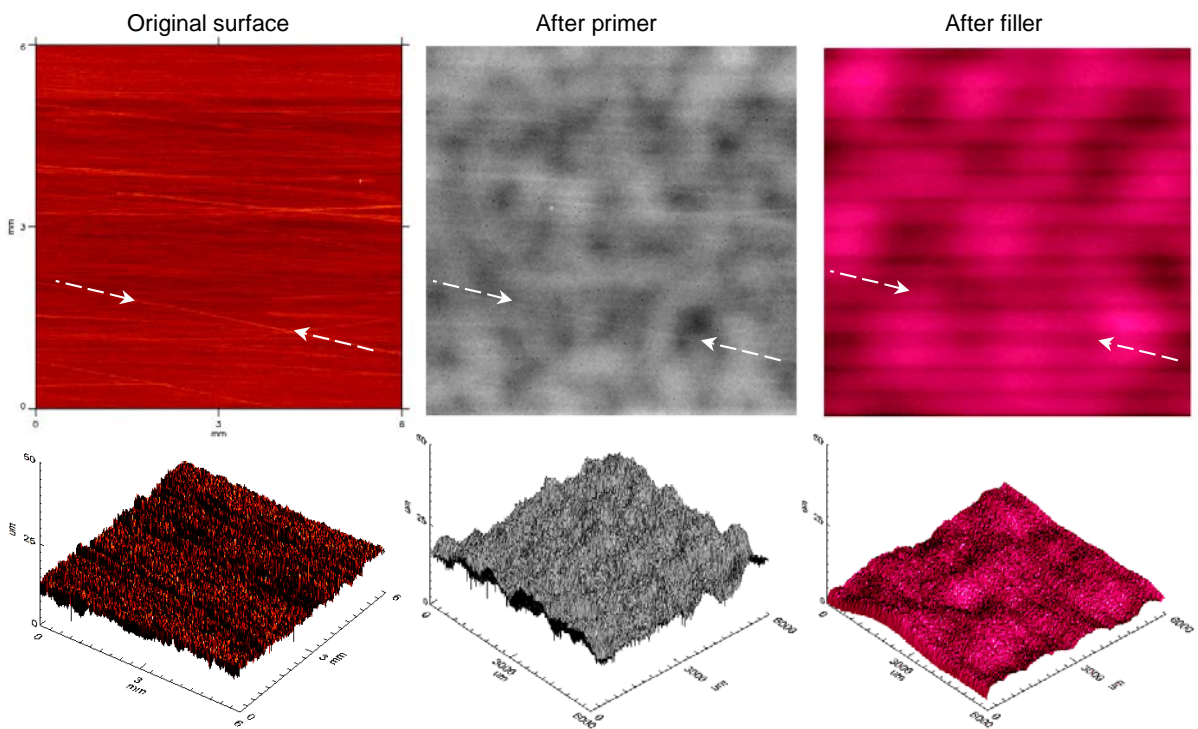
By using the count of cavities and their mean area as characterisation parameters only deep points are considered as potential causes of surface failures after coating by formation of undesired air bubbles. However, experiences demonstrate that grains (peaks), which are normally produced in deeper regions on the metallic mold, could not successfully be coated. Fig. 4.25 shows that after the first two steps of the

coating process, Primer (B1402 + Härter B1426 Wörwag) and Filler (7245 Anthrazit Hammelrath) respectively, some grooves remain at the surface.

To quantify the cavities as well as the grains of SMC surfaces, a critical parameter is needed. Taking the statistical mean height as a reference surface height value, it is possible to calculate the quantity and volume of all irregularities above a positive threshold ($+\gamma$) and under a negative threshold ($-\gamma$), according to *Fig. 4.26*. Knowing the total cavities volume (V_C) and the total grains volume (V_G) it is possible to characterise quantitatively the topographic modification of a surface by any treatment using the Surface Relative Smooth parameter (*SRS*) [127] defined by the equation:

$$SRS = 1 - \frac{V_{Cf} + V_{Gf}}{V_{Ci} + V_{Gi}} \quad (4.3)$$

where i and f denotes *before* and *after* a topographic modification respectively. For a practical application of this parameter, it is recommended to use percentages. In this case, a *SRS* value of zero denotes no topographical changes and 100% means a total surface smoothing (elimination of all cavities and grains). Negative values of *SRS* mean the formation of a more rugose surface after treatment.



$L_m = 6 \text{ mm}$; same mold position

Figure 4.25 Peaks marked by arrows, produced by mold irregularities, remain after application of primer and occasionally after filler.

When SRS parameters are used it is highly recommended to compare them in the same sample area. The election of a value for the threshold γ depends on surface topography; as a first approach $\frac{1}{2}R_a$ can be acceptable. In this case, all cavities and grains are formed by points located above or below the R_a amplitudes; shown in *Fig. 3.28*. The most important condition is that γ allow to perceive topographic differences before and after treatment and be maintained constant during the topographic characterisation. Comparison between SRS values makes sense only if γ value used was the same.

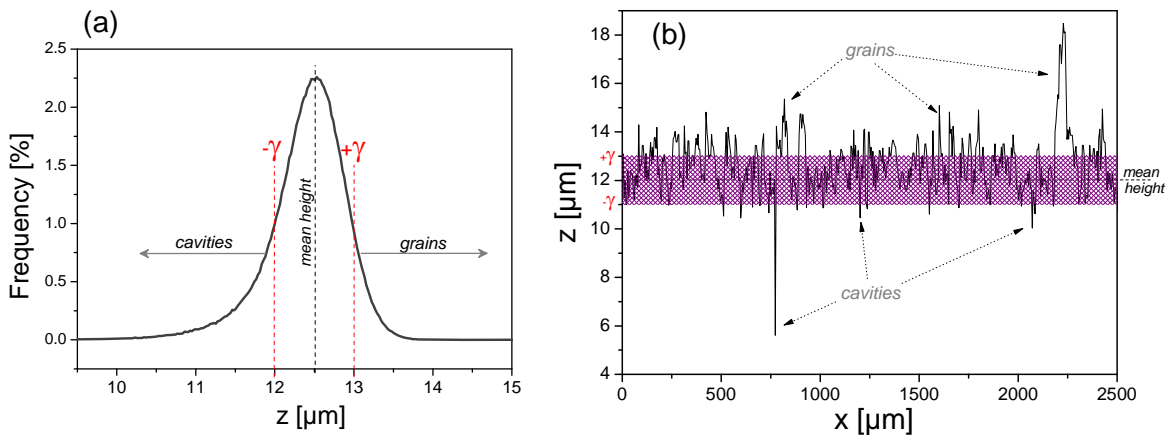


Figure 4.26 Thresholds $+\gamma$ and $-\gamma$ define cavities and grains in a heights histogram (a), cavities and grains in a surface profile (b).

SRS is very sensitive to small changes in topography. For example, after mechanical cleaning (rubbed with cloth) of a SMC surface by a mixture of benzene and ethanol (50% - 50% in volume) the topography changes. *Fig. 4.27* shows the profile modification measured over the sample SMC-2, maintaining the measure coordinates.

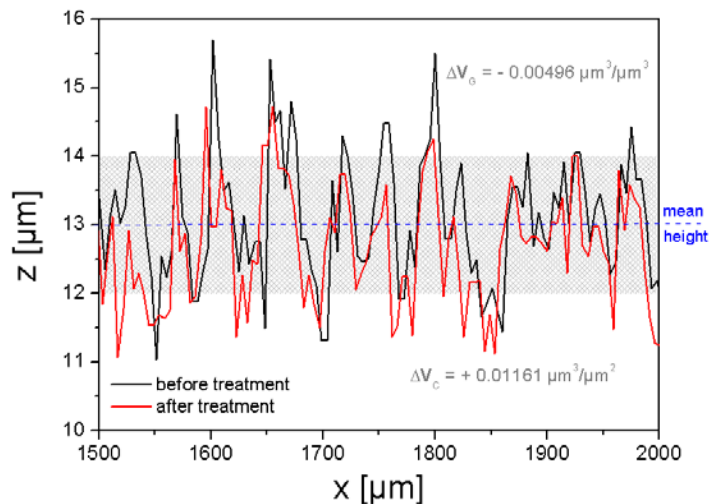


Figure 4.27 Modification of a SMC surface by cleaning with benzene-ethanol. Both profiles correspond to the same coordinates.

A complete analysis by SRS should also consider an increase or a decrease of counted cavities and grains. Fig. 4.28 shows the values before and after surface treatment of a fixed area of 30.6 mm^2 .

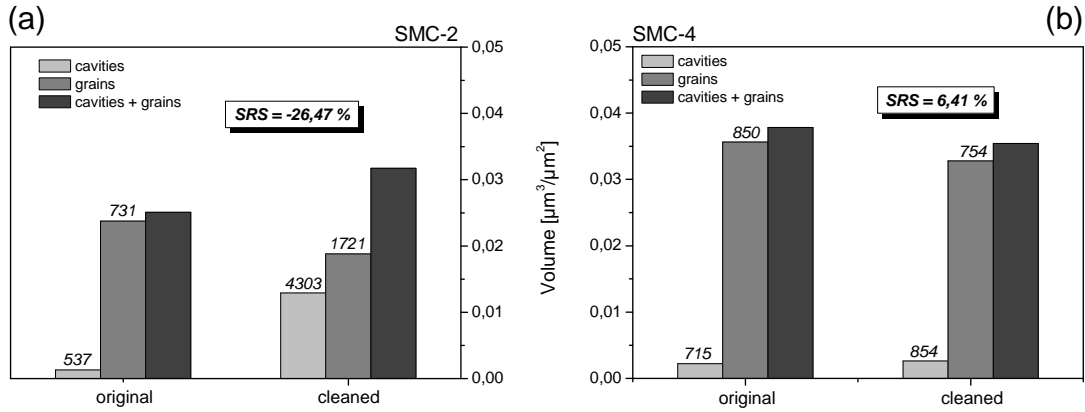


Figure 4.28 Complete characterisation and comparison of a modification by cleaning with benzene-ethanol between SMC-2 and SMC-4 surfaces. Evaluated area was 30.6 mm^2 . $\gamma = 1 \mu\text{m}$. Values above bars denote cavities and grains counted.

In the case of SMC-2 (Fig 4.28(a)), results of the volumetric characterisation indicate that solvents mixture removes monomer rests from deeper points resulting in more and larger cavities. From the same reason, solvents increase the number of grains, while friction during mechanical cleaning reduce their total volume by wear. The effect of solvents prevail on the effect of mechanical wear resulting in a more rugose surface ($SRS = -26,47\%$). On the contrary, SMC-4 is more resistant to solvents mixture as can be seen in Fig. 4.28(b). During treatment, mechanical wear removes grains in number and volume, leading to a smoother surface ($SRS = 6.41\%$).

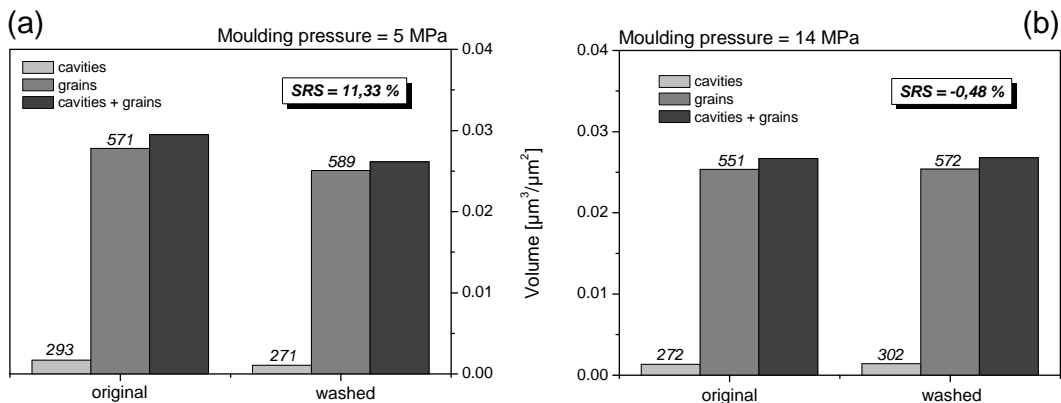


Figure 4.29 Complete characterisation and comparison of modification by power-wash. Both surfaces were moulded during 160 s under two different pressures. Evaluated area was 30.6 mm^2 . $\gamma = 1 \mu\text{m}$. Values above bars denote cavities and grains counted.

The effect of moulding conditions on the quality of a surface could be characterised by SRS. Fig. 4.29 shows the volumetrical characterisation of a SMC-2 sample produced by 5 MPa and 14 MPa of moulding pressure after treatment by powerwash (50°C, 3 bar, 2 min, 1% ESKAPHOR N 6502 B). According to these results, SMC-2 moulded under higher pressure (14 MPa, Fig. 4.29(b)) seems to be more resistant to power-wash treatment (water pressure washing), because almost no change in SRS value was observed (SRS = - 0.48%).

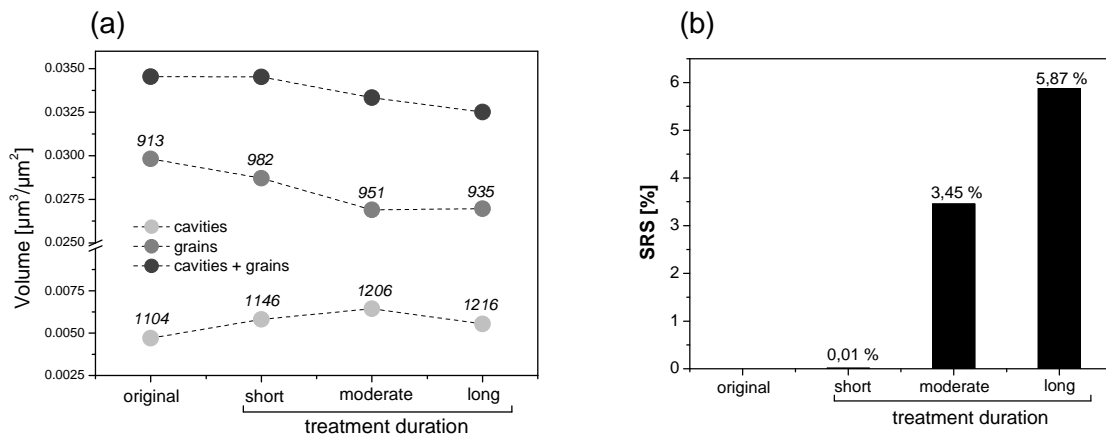


Figure 4.30 Sequential smoothing by CO_2 pressure applied on a SMC-4 surface moulded during 160 s and 5 MPa.

Besides of the use of SRS values to compare the behaviour of different surfaces under defined type of treatment, the parameter can be used to compare the effectiveness of different treatments on defined surface. Fig. 4.30 shows the effect of different treatment intensities (by qualifying treatment duration) of the same CO_2 pressure (2 bar) applied to SMC-4 surfaces previous moulded during 160 s under 5 MPa of pressure. The results indicate that the treatment improves smoothing of the surface depending on its duration. CO_2 pressure increases the number of cavities and its volume, but at the same time compresses the grains volume, which controls the smoothing of the surface. Values of cavities and grains volumes after long-term treatment don't follow the same behaviour because of the mean height position is modified to a lower plane after two sequential treatments. However the total volume (cavities and grains) sufficiently describe volumetrical changes occurred.

SRS values should be always accompanied by cavities and grains count information in order to suitable evaluate the topographical changes produced by modification. By comparing SRS values measured with a traditional topographic parameter such as

arithmetic mean roughness, the effectiveness of the characterisation method presented is evident. According to [Table 4.2](#), information provided by values of R_a before and after treatment and the difference ($R_{af} - R_{ai}$) are insufficient to describe the topographic transformations occurred.

*Table 4.2
Traditional topographic characterisation using R_a and SRS parameters in comparison.*

Treatment	Process	Surface	conditions	R_{ai}	R_{af}	$R_{af} - R_{ai}$	SRS
				μm			
cleaning	Benzin-Ethanol	SMC-2	cloth	0.736	0.852	0.1160	-26.47%
		SMC-4		0.737	0.735	-0.0020	6.41%
whasing	Power-wash	SMC-2	5 Mpa	0.728	0.728	0.0000	11.33%
			14 Mpa	0.725	0.730	0.0050	-0.48%
			no treatment	0.808	-	-	-
cleaning	CO ₂ pressure	SMC-4	short	0.808	0.869	0.0610	0.01%
			middle	0.808	0.863	0.0550	3.45%
			long	0.808	0.823	0.0150	5.87%

4.2 Textile Materials

Recent studies [\[128-130\]](#) shown that textile construction parameters such as fineness of filaments and yarn, warp and weft density as well as the type of weave, control the texture, surface topography and morphology of fabrics. Fabric topography affects the porosity and strongly influences the textile characteristics such as fabric mass, thickness, draping ability, stress-strain behaviour or air permeability. Moreover, there are significant differences between the soiling behaviour and soil release of textile materials with different topographic structures despite the similarity of their chemical nature [\[131-133\]](#).

In the studies cited above, a large number of roughness and waviness parameters were obtained, which do not take into account the scaled-morphologic periodicity of each surface studied and its influence on the whole topography. As periodic surfaces, all textile materials show some horizontal and vertical repetitive unities, therefore, different length scales have to be taken into account for a proper interpretation of the topographic data measured [\[134\]](#).

As shown in [Fig. 3.35](#), topographic parameters obtained by FFT-filtering provide different type of information depending on the cut-off length used. Due to their

structural diversity, a classification of textile materials according to their unit size and morphology of several length scales is necessary. A suggest to general range values of L_m in order to identify different measurable length scales is not possible. However, the specification of at least three different length scales (macro-, meso- and microscale) is absolute necessary by morphologically relative homogeneous textile groups. From a conceptual point of view, each one of the length scales proposed for a textile structure must provide specific information about the surface morphology and topometry of the materials. In all cases, the highest available resolution by confocal chromatic imaging ($\Delta_x = 1 \mu m$) was used, while the value of L_m was the parameter used to determine the length scale to be studied.

4.2.1 Textile macro-topography

Macro-morphological irregularities of textiles such as folds and wrinkles can be studied using FFT-filtering of the topographical data measured by large values of L_m (cf. Section 3.6.2). L_m value larger than 3 mm was suggested to quantify plane irregularities (waves and wrinkles) of fabrics. According to the large amount of topographical data measured at three different types of woven polyester textile surfaces (plain, twill and Panama), a total measured area ($L_m \times L_m$) should cover at least 169 (13^2) repetitive units (r.u.) in order to provide the macro-topographical information desired. 3D-waviness diagrams and their corresponding W_z values (Fig. 4.31) can be used as macro-morphological parameters, especially in order to characterise changes occurred after treatment. In this case, the characterisation have to be accompanied by a quantification of the 2D relaxation/shrinkage (cf. ISO 5077:2007) occurred by wetting, by mechanical processes, or by a combination of both.

Dimensional changes (relaxation/shrinkage) of fabrics at macro scale influence their meso- and micro-topography due to modification of repetitive unit dimensions and therefore the distances between yarns, filaments and fibres.

In Fig. 4.31, only macro-waviness diagram of woven plain does not show any morphological influence of repetitive units morphology, in this case $r.u. > 13^2$. Optimal L_m values for twill and Panama types of weave have to be larger than 5 mm in order to characterise their macro-topography.

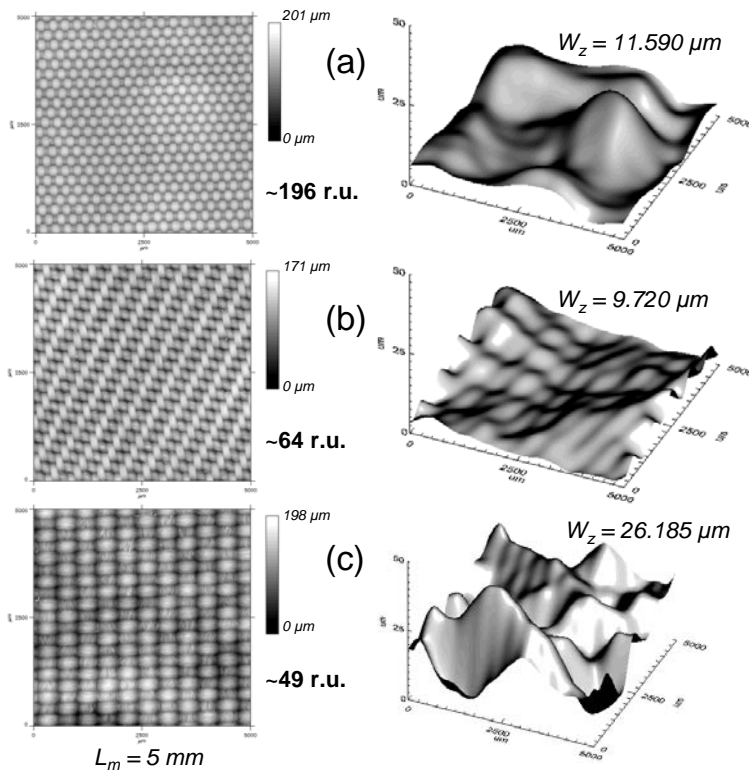


Figure 4.31
2D images (left) and 3D
waviness diagrams
(right) with W_z values of
woven plain (a), twill (b)
and Panama (c)
polyester fabrics.

4.2.2 Textile meso-topography

Meso-scale of textile materials should describe the surface topography produced by the type of weave and yarn used, without attending previous defined macro-topographic irregularities and details corresponding to fibers or filaments. A study of fabric surface topography at mesoscopic scale using FFT-filtering starts with the selection of a new optimal L_m value, which basically depends on the size of fabric repetitive unit. From a large amount of experimental data on polyester fabrics studied, a sample area ($L_m \times L_m$) should cover about 8 repetitive units (see [Table 4.3](#)).

Another way to construct meso-topographic diagrams is the use of digital surface filtering as described in Section 3.5.1.1. Filter density used depends on fabric characteristics and must be able to produce a surface without topographical details of fibres or filaments. [Fig. 4.32](#) shows the construction of meso-topographic surfaces by using FFT-filtering and Smooth filtering. In order to compare the

Table 4.3
 L_m containing about 8 repetitive units are
optimal to characterise the meso-topography.

	unit area mm^2	L_m mm	r.u.
woven plain	0.126	1.0	7.94
twill	0.396	1.8	8.18
Panama	0.478	2.0	8.37

morphologies and W_z values obtained, L_m and the filtering method used must be the same during the characterisation process.

An application of the study at this length scale is to know the relative z-distances between warps and wefts by woven fabrics and the amplitude of their wave (sinoidal) trace. As shown in *Fig. 4.32*, wefts describe almost a linear trace (their amplitudes are small). As a consequence, the first contact of a solid with the fabric surface takes place by the warps (“hills”) and the penetration of fluids on the fabric surface takes place principally on wefts (“valleys”). This result plays a very important role of the wetting behaviour of textile materials (cf. Section 5.2).

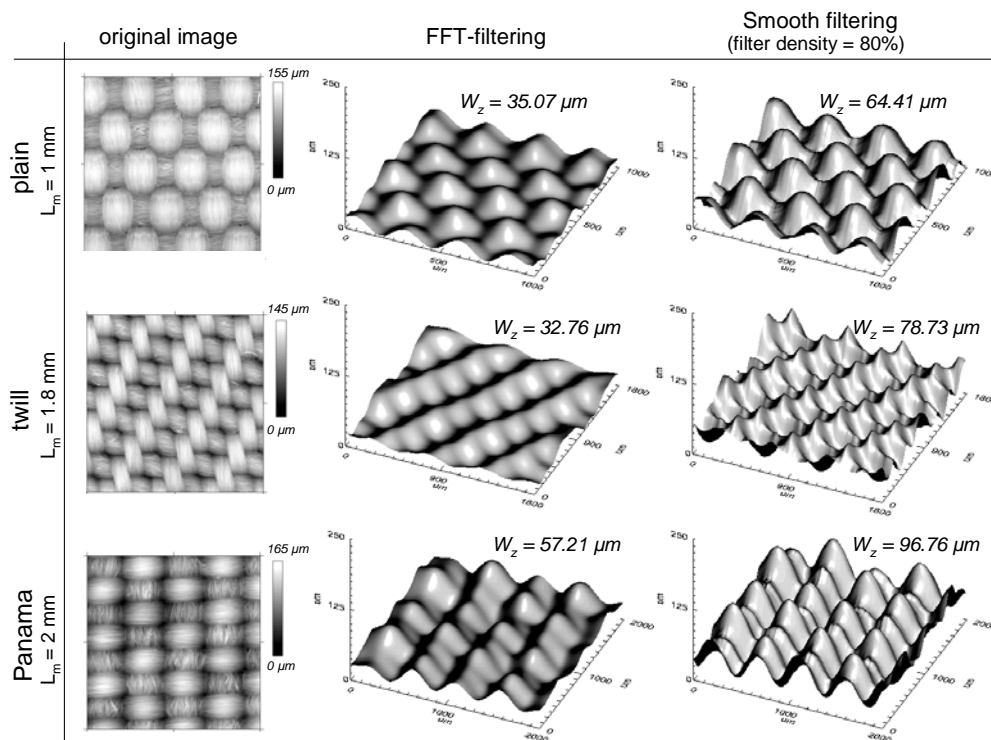


Figure 4.32 Meso-topography of different polyester fabrics after FFT-filtering and Smooth filtering.

Finally, the application of volumetrical characterisation criteria allows to investigating topographical conditions for fluids spreading over the surfaces (a connection between meso-morphology and spreading will be presented in Section 5.2.1). A height value (h_v) can be found to divide all data points in two groups: those that form ‘mountains’ and those that form ‘canals’ between the ‘mountains’. There are two conditions for h_v : (i) to be as small as possible and (ii) the canals be connected in order to allow flowing in all possible directions. In the case of twill and Panama fabrics, due to their more anisotropic morphology, independent but endless canals

can be formed. In the case of woven plain, all canals are connected to each other (Table 4.4).

Table 4.4
Volumetrical characterisation parameters obtained by dividing z-range according to h_v criteria. Smooth filtering (80%) was used to obtain the meso-topography. Different colored areas represent unconnected cavities.

	plain	twill	Panama
L_m [mm]	1	1.8	2
W_z [μm]	64.41	78.73	96.76
h_v [μm]	31.94	46.66	41.36
canals z-range (h_v/W_z) [%]	49.6	59.3	42.7
canals area [%]	58.0	66.4	40.5
canals volume [$\mu\text{m}^3/\mu\text{m}^2$]	6.787	10.083	5.300

4.2.3 Textile micro-topography

Unlike macro- and meso-scales, micro length scale reveals the influence of filaments and fibres characteristics on the resulting topography. Profile, fineness as well as natural or machined texture of these elements or distances between them are only some of the possible characteristics that as a whole define the resulting morphology

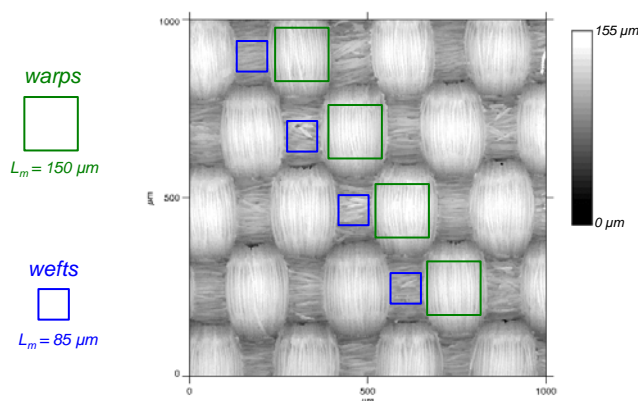


Figure 4.33
Optimal L_m values for the characterisation of warps and wefts micro-topography separately at a surface of woven plain polyester fabric.

and topometry at this length scale.

The selection of the optimal cut-off length in this case not longer depends on some statistical or mathematical criteria as seen in macro and meso length scales, rather on the size and location of the set of filaments or fibres by type and orientation. To study the micro-topography of woven plain fabrics, warps and wefts have to be zoomed

(sub-area extraction, cf. Section 3.7.1.5) separately. Optimal L_m values of warps and wefts depend on the type of weave and construction parameters such as yarn types, their diameters, warp densities, weft densities, etc. Depending on textile structure, more than one L_m value could be necessary for a complete micro-topographical characterisation, as can be seen in *Fig. 4.33*.

The number of sub-areas to be isolated depends on topographical parameters studied and on the standard deviations of their mean values. Usually five different zooms should be enough to characterise polyester monofilament fabrics. Depending on the characterization criteria, the elimination of micro-waviness, a consequence of yarn profile and fabric meso-topography, is possible by FFT-filtering, as can be seen in *Fig. 4.34*.

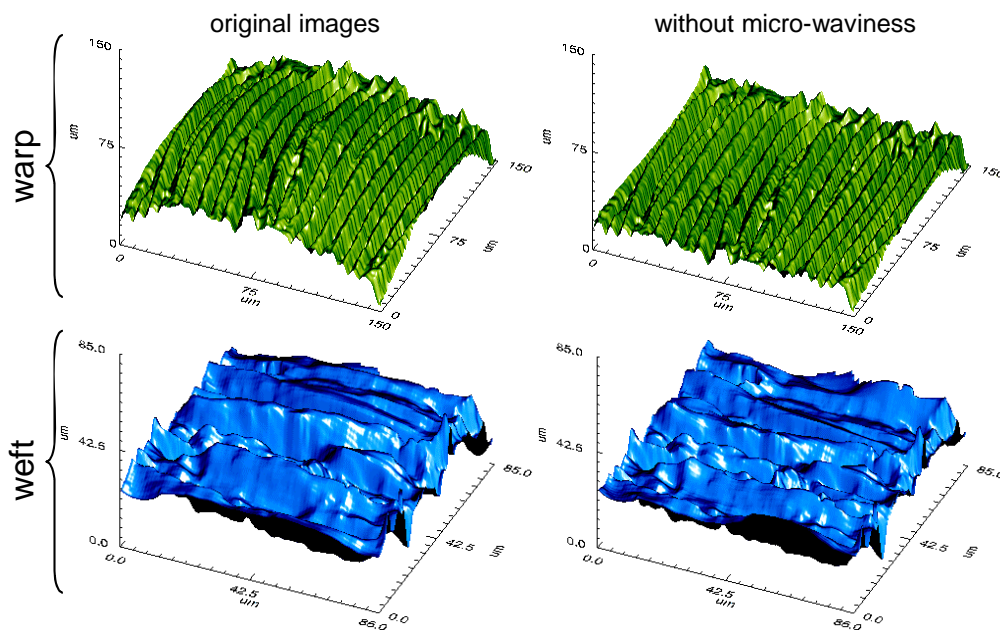


Figure 4.34 Micro-topographical images of a warp and a weft. The elimination of micro-waviness was possible by FFT-filtering.

Using the new topographical data generated, it is possible to calculate any micro-topographical parameter by profiling or by using the whole surface. The volumetrical characterization is a useful possibility through the evaluation of porosity or filling quantities at different deep heights. The calculation of SRS proposed in Section 4.1.8.3 can be important for the study of some surface modification treatments such as by thermofixing or plasma ones. Fractal dimension or Wenzel roughness factor could be important to characterise micro-topographical modifications of natural fibres, such as the caused by enzymatic action.

5 New topographic concepts for the mechanistic understanding of wetting phenomena

It is well known, that the surface topography of a solid significantly affects its wettability. Wetting behaviour is governed by two factors [144]; the chemical composition and the roughness of the solid surfaces. In terms of the contact angle θ a between the gas-liquid and solid-liquid interfaces, the wettability of an ideal *flat* solid is depicted by Young's equation [169-171],

$$\cos \theta = \frac{\gamma_s - \gamma_{sl}}{\gamma_l}, \quad (5.1)$$

where γ_{sl} , γ_s , and γ_l represent the interfacial tensions of solid-liquid, solid-gas, and liquid-gas interfaces, respectively. In the absence of surface roughness, Young's equation indicates that the nature of wetting is determined by the relative affinity of the solid for the liquid or gas phases, as illustrated by the difference between solid-gas and solid-liquid interfacial tensions in Eq. (5.1). The interfacial tensions γ_{sl} and γ_s are intrinsic properties associated with a surface and they can be controlled by chemical modification. As $\gamma_s - \gamma_{sl} > 0$, the contact angle is less than 90° (hydrophilic surface), whereas $\theta > 90^\circ$ (hydrophobic surface) for $\gamma_s - \gamma_{sl} < 0$.

Real solids are actually rough and, thus, their wettability is significantly influenced by the geometrical structure of the surface roughness. In other words, wetting replaces an area of the solid-gas interface by an equal area of solid-liquid interface and is generally also accompanied by an extension of the liquid-vapour interface. These surface relations vary with the conditions of the system and may change progressively as wetting proceeds depending on surface morphology and topometry. As each interface has its own specific surface energy content, wetting, with its

accompanying change in the extent of each interface, results in a net decrease or increase in total interfacial energy. For the point of view of thermodynamics, the magnitude of the free energy change involved determines whether or not wetting will proceed spontaneously, at what rate and how far it can progress against the external forces that may be brought into play to resist it, or, alternately, how large an external force may be needed to overcome the initial resistance to wetting.

The earliest work on the wetting of rough substrates was addressed by Wenzel [139, 168] and later by Cassie and Baxter [140]. Wenzel assumed that the liquid filled up the grooves on the rough surface and generalized Young's equation to obtain the apparent contact angle θ_a ,

$$\cos \theta_a = sR_r \cos \theta, \quad (5.2)$$

where sR_r is the "Wenzel roughness factor" defined in Section 3.7.4.3 as the ratio of the actual area of a rough surface to the geometric, projected area on the horizontal plane. Evidently, the effect of the roughness results in the improvement of the wetting for $\theta < 90^\circ$ but enhances the hydrophobicity for $\theta > 90^\circ$. Cassie and Baxter considered the wettability of a composite surface, composed of two types of homogeneous patches that have different solid-fluid interfacial tensions. The apparent contact angle is then given by

$$\cos \theta_a = f_1 \cos \theta_1 + f_2 \cos \theta_2, \quad (5.3)$$

where f_i and θ_i represent the surface area fraction and the contact angle of patch i , respectively.

For porous or corrugated surfaces, the roughness is mainly filled with air. The openings of the pores can be regarded as nonwetting patches with $\theta_2 = 180^\circ$. Since $f_2 = 1 - f_1$, Eq. (5.3) becomes

$$\cos \theta_a = f_1 (1 + \cos \theta_1) - 1 \quad (5.4)$$

In accord with Eq. (5.4), if surface hydrophobicity (θ_1) and surface roughness (f_1) are appropriately combined, a water droplet deposited on such a superhydrophobic surface can remain nearly spherical.

Besides the roughness factor (sR_r) and the wetted area fraction (f), the Wenzel and Cassie-Baxter theories are essentially independent of the geometrical characteristics of the roughness (the shape of the pore). For a given roughness geometry, these

theories may predict different apparent contact angles. The wetting state is usually believed to be in either Wenzel or Cassie-Baxter state. However, it is not decisively clear on which theory should be employed and when. A simple criterion is that the wetting state corresponds to the one with a lower free energy. In general, it is accepted that the Wenzel state (wetted groove, cf. *Fig. 5.4*) prevails for $\theta < 90^\circ$, while the Cassie-Baxter state (air pocket) dominates for $\theta > 90^\circ$.

Nakae et al. [141] reported about the effect of the surface roughness on the wettability at a constant Wenzel roughness factor using two kinds of models, the hemisphere close packing model and the hemiround rod close lining model. Nevertheless, the pitch is proportional to the height in these models (see *Fig. 3.42*). Therefore, they could not independently discuss the influence of roughness height and roughness pitch on the wettability. Nakae et al. recently reported [142] about the development of new models which can independently describe the influence of the surface roughness height and the roughness pitch on wettability. The authors used, however, idealized periodic surfaces for their models.

By definition, surface tensions, like specific energy values, are related to one unit of actual surface. But when a liquid spreads over a surface or a real solid, the forces that oppose each other along a given length of the advancing periphery of the wetted area are proportional in magnitude, not to the surface tensions of the respective interfaces but to their total energies per unit of geometric surface (this must be true if surface tensions themselves are characteristic properties, unaltered by surface roughness). As a consequence of this reasoning, topography of the surface plays a crucial role in its wettability.

In the present Chapter one pretends to understand the wetting phenomena of non periodic (SMC) and periodic (textiles) surfaces by applying the topographic characterisation methods using different length scales, as described in Chapter 4.

5.1 Correlation of topography and wettability of SMC

Static contact angle measurements of de-ionized water using a contact angle device (DataPhysics OCA40 micro) were used to correlate the wettability of SMC surfaces with measured topographic inhomogeneities. Sessile water droplets of 9 μL volume were applied at different positions of SMC samples.

In Section 4.1.2 it was shown that, in the case of SMC materials, topographic characterisation have to be realized dependent on mould-plate position, due to a strong influence of mould topography on resulting SMC surfaces.

To correlate topography of SMC surfaces with their wettability, topographical data (using $L_m = 6 \text{ mm}$, $\Delta_x = 5 \text{ }\mu\text{m}$) and the value of static water contact angle were measured in two different ways:

- a) 15 different positions on the same SMC sample (manufactured by 5 MPa during 100 s), distributed in a 4 x 8 cm grid (single measurements separated by 2 cm from each other), and
- b) one defined position (related to a defined position of the metallic mould) on 10 different SMC samples, which were moulded under the same conditions of pressure and time (5 MPa, 100 s).

The following results show that defined meso- and micro-topographies (Section 4.1.1) of SMC differently influences the wetting behaviour.

5.1.1 Meso-topography and wetting

Measured R_z and calculated N_z at 15 different positions at the same sample show a larger standard deviation compared to single measurements at the same position of 10 different samples, as can be seen in [Table 5.1](#). This fact verifies that R_z depends strongly on mould topography as concluded previously in Section 4.1.2.

Table 5.1 Topography and wettability: 15 different positions of the same sample (a) and the same position of 10 different samples.

		(a)		(b)	
		average	σ	average	σ
Mesotopography	R_z [μm]	15.07	1.86	13.72	1.06
	N_z	33.72	4.82	39.77	3.21
Microtopography	R_a [μm]	0.750	0.048	0.752	0.035
	N_a	672	49	704	48
Static contact angle	θ [$^\circ$]	76.2	6.0	83.2	4.1

Fig. 5.1 shows that the static contact angle correlates better with the meso-topography if their parameters (R_z , N_z), are constant due to the same influence of the mould (experiment b, *Fig. 5.1(b)*). In this case, the morphology can

be described as presented in *Fig. 4.2(c)*: each SMC sample, at the measured position, has the same morphology, but slightly different amplitudes (R_z) and calculated numbers of waves (N_z) due principally to the effect of glass fibers orientation, adhesion during mould-sample separation and chemical inhomogeneities

[124]. In another case (experiment a, *Fig. 5.1(a)*), different morphologies due to different mould positions result in a poor correlation.

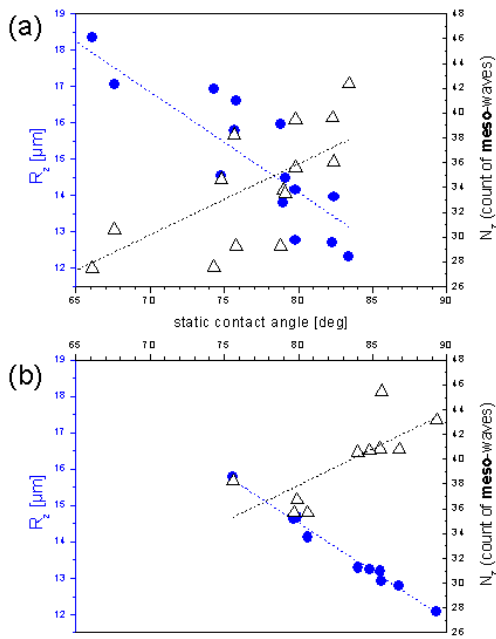


Figure 5.1 Meso-topography and wettability of SMC surfaces.

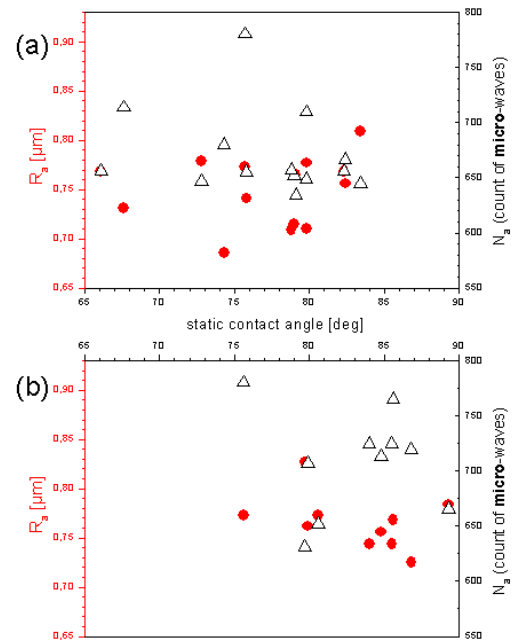


Figure 5.2 Micro-topography and wettability of SMC surfaces.

Independently of the mould position, a linear relationship between wetting and meso-morphology is observed by both experiments: higher amplitudes (R_z) and less number of waves (N_z) lead to more hydrophilicity (lower water contact angles). In other words, larger pores decrease the contact angle (see *Fig. 5.3*), that corresponds to the Wenzel regime of surface wetting (see *Fig. 5.4*).

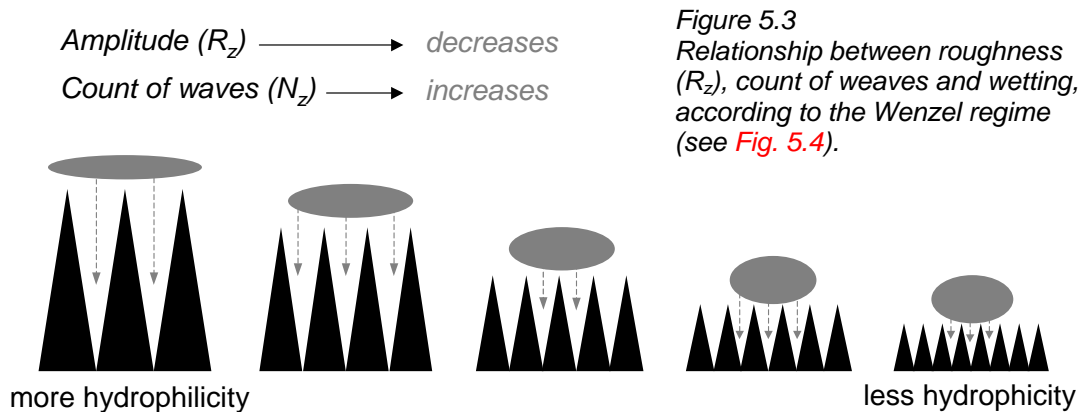


Figure 5.3 Relationship between roughness (R_z), count of waves and wetting, according to the Wenzel regime (see *Fig. 5.4*).

5.1.2 Micro-topography and wetting

The analysis of microtopography by R_a (as a micro amplitude) and the number of micro-waves (N_a), graphically presented in *Fig. 4.2(d)*, does not reveal any correlation with the wetting behaviour of water (*Fig. 5.2*). But less values dispersion observed by the same sample position (experiment b) reveals a connection and a slightly dependence of micro-topography on meso-morphology.

5.2 Correlation of topography and wettability of textile materials

In [132], it was shown that there are significant differences between the soiling behaviour and cleanability of polyester textile materials with different topographic structures despite the similarity of their chemical nature. Toward a better mechanistic understanding soil removal effects as well as quantitative correlations between them and topographical non-identity of fabrics, roughness and dynamic wetting results [131,132], were analysed in respect of liquid transport driven into a porous system by capillary forces. In general, wetting of a fibrous assembly, such as a fabric, is a complex process. Particularly, capillary flow is not determined by a constant advancing contact angle, as frequently assumed [145], but it depends on a dynamic contact angle corresponding to the instantaneous velocity of the moving meniscus.

In this study, it was found that measured dynamic contact angle of water, as a consequence of wetting, is less expressive in respect to changes in the topographic structure of textile surfaces. Moreover, wicking (*Fig. 5.4(d)*) occurring within the spaces

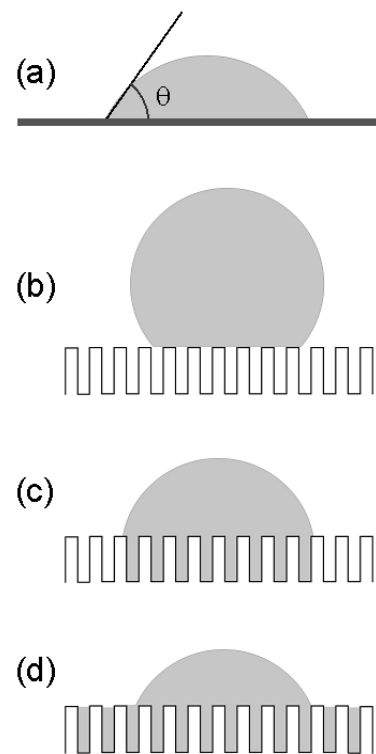


Figure 5.4
Wetting as a displacement of a fibre-air interface with a fibre-liquid interface (a), Cassie-Baxter regime (b), Wenzel regime (c), and wicking as the spontaneous flow of liquid in a fibrous assembly driven by capillary forces (d).
Johnson & Dettre in "Wettability", Ed. by John C. Berg, 1993).

between fibres, being previously wetted, strongly controls the fabrics cleanability. As most textile processes, including their detergency, are time-limited, the rate and direction of wicking is therefore important. It is known that the wicking rate is not solely governed by interfacial tensions and the fibres wettability but it also depends on capillary substrate dimensions and the liquid viscosity [145,167].

In Section 4.2, it was justified the necessity of a topographical characterisation of textile materials using different length scales. The methodology presented in Section 4.2 will be applied and discussed in the following pages.

By textile structures, morphological and chemical differences between synthetic filaments and natural fibres are decisive for wetting behaviour. For this reason, the following cases of study are divided into to groups of materials: polyester and cotton textiles.

5.2.1 Polyester textiles

Polyester fabrics of three different types of weave (*Fig. 5.5*) were manufactured at the Institute of Textile and Clothing Technology at the Technische Universität Dresden [128,130,146] using microfilaments produced by meltspinning of the same material (polyethylene therephthalate). Warp yarns were formed from flat filaments, while wefts from filaments texturated by three different processes (*Table 5.2, Fig. 5.6*).

Table 5.2
Textile parameters of polyester filaments produced according to [146].

Yarn	Number of filaments	Structure	Filaments fineness [dtex] ¹	Filaments diameter [µm]	Yarn fineness [tex] ¹
A	128	flat	0.78	6,0	9.9
B	128	textured, tangled	0.92	7,5 ²	11.5
C	256	false twist, textured	0.78	6,5 ²	16.3
D	384	textured, tangled	0.67	6,5 ²	24.6

¹ measured according to DIN EN ISO 1973.1996; ² before texturing

5.2.1.1 Influence of textile construction parameters on topography, spreading, wetting and cleanability

For this study, 14 different fabrics corresponding to plain, twill and Panama [146] structures were used (cf. *Table 5.3*).

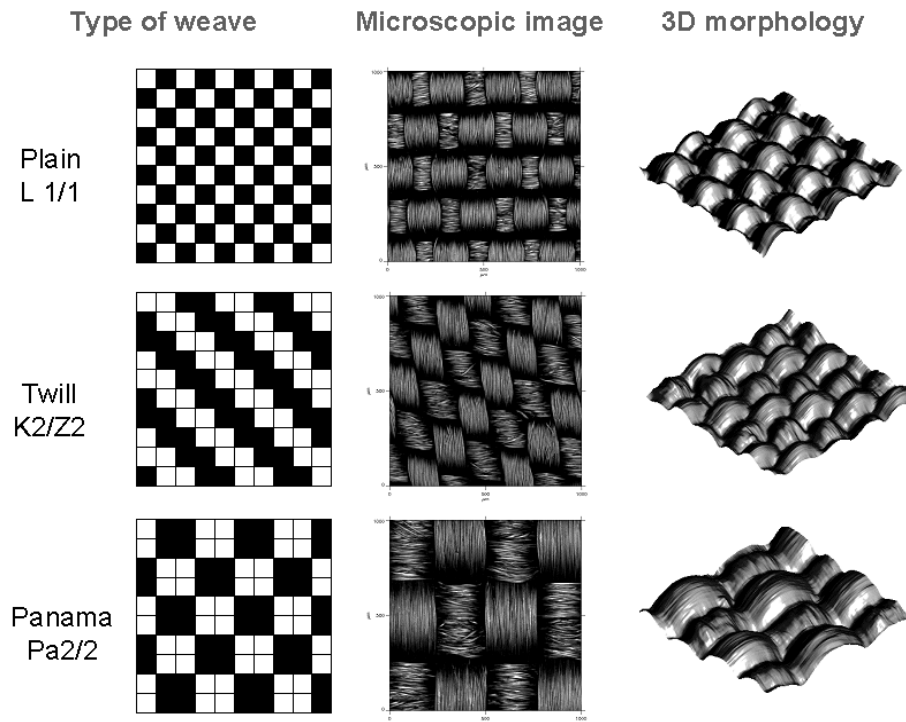


Figure 5.5 Polyester fabrics used in the present study.

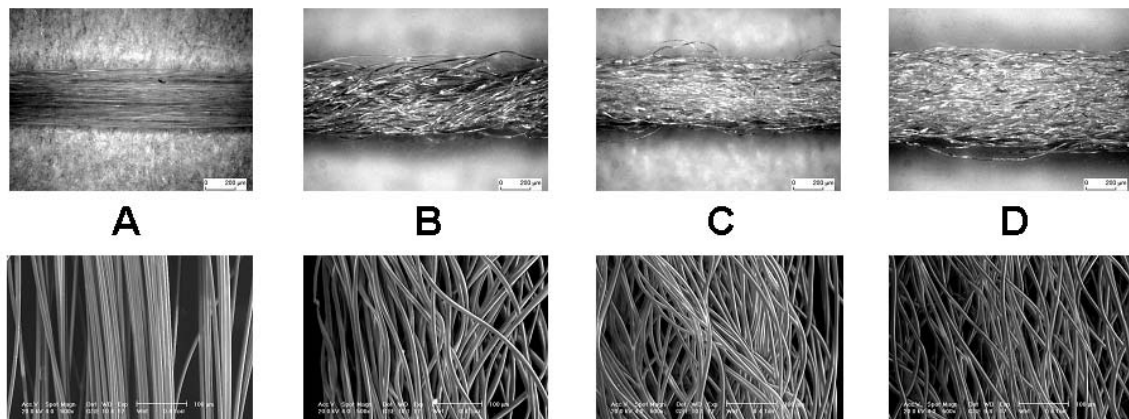


Figure 5.6 Microscopic images of yarns (above) and filaments (below) [146].

Dynamic contact angle measurements were carried out with a Fibro DAT 1122 dynamic contact angle tester (Fibro this equipment over other contact angle measuring procedure are detailed in were applied to the surface under electromagnet. The strength of the effects. After deposition, the droplet was data were collected thereafter for 30 s. temperature-controlled laboratory $40 \pm 2\%$ was kept constant.

were carried out with a Fibro DAT 1122 System, Sweden). Some advantages of measuring systems as well as the [147]. Water droplets of $10 \mu\text{m}$ volume investigation by a short stroke from an stroke was minimised to avoid oscillation stabilised on the surface and reliable The instrument was located in a maintained $23 \pm 1^\circ\text{C}$. Relative humidity of

On the basis of macroscopic water drop base changes, the wetting behaviour of the water drop can be divided into three different regimes (*Fig. 5.7*): dynamic wetting, defined as growing of the drop diameter depending on time (also know as spreading), the quasi-static wetting, here the drop diameter remains approximately constant, and penetration, which is marked by liquid drop absorption into fabrics depending on time.

For a better understanding of the wetting dynamics of textile surfaces it is important to attend at the meso-topography of the three different types of weave, previously studied in Section 4.2.2. By using the waviness as meso-topographical parameter, it is evident that the meso-topography of the fabrics controls the spreading rate of a liquid drop (*Fig. 5.8*). For the plain weave, an increase of the waviness depth causes a decrease of the spreading rate; warp yarns ('hills') slow down the liquid motion (*Fig. 5.9*). For twill weave, an increase of the waviness depth causes formation of deep and long domains of weft yarns ('canals') with small 'islands'. As a consequence, an increase of the spreading rate is observed. Finally, for Panama weave, an increase of the waviness depth causes formation of long and quasi-endless (without 'islands') deep domains ('canals'). Consequently, the waviness depth and spreading rate are proportional to each other.

At a smaller scale, by zooming (cf. Section 4.2.3) of warps and wefts separately (*Table 5.4*), topography measurements provide important information about changes in textile microstructures. Using this information, the behaviour of a liquid drop on a fabric surface during the wetting process can be explained.

Table 5.3
Yarn combinations and weft densities of the polyester fabrics used.

type of weave	warp	weft	weft/cm
Plain L1/1	A	B	38
			40
		C	31
			35
		D	25
			28
Twill K2/2Z	A	B	50
			53
		C	42
			46
		D	35
			38
Panama Pa2/2	A	B	40
			44

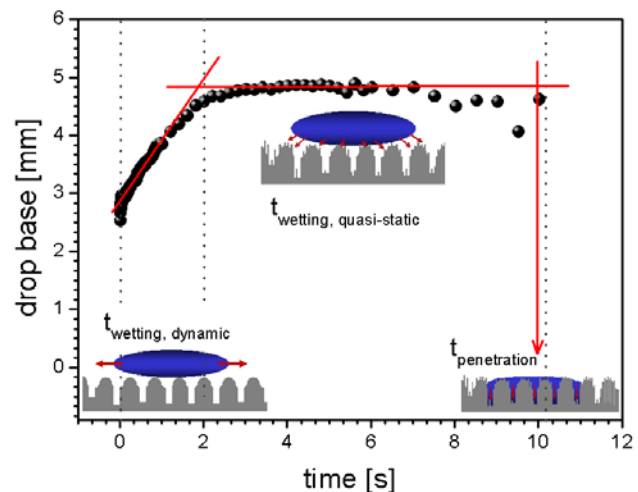


Figure 5.7 Three different wetting regimes of a textile surface.

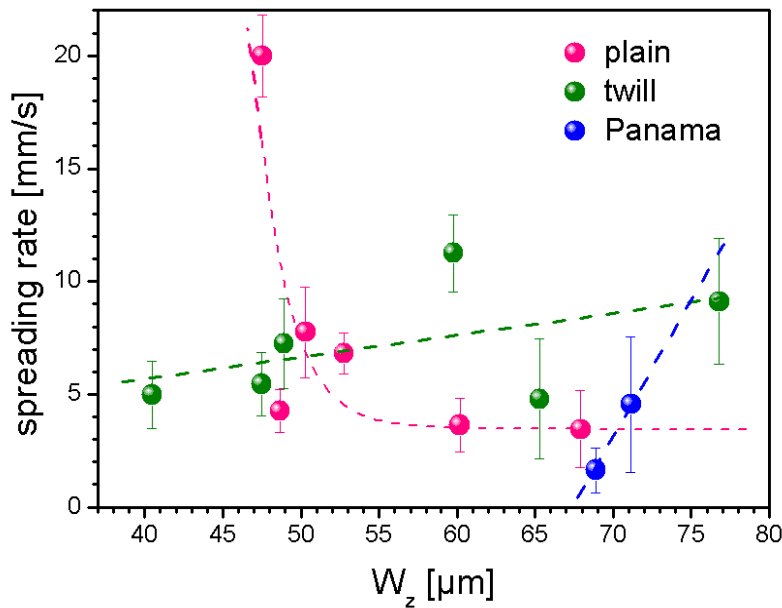


Figure 5.8
Dynamic wetting: meso-morphology controls the spreading rate of a liquid drop on a textile structure.

For a theoretical treatment of capillary flow in fabrics, the fibrous assemblies are usually considered to consist of a number of parallel capillaries [148]. The movement of a liquid in a non-homogeneous capillary system, such as fabrics, however, is discontinuous for another reason, as well: the wetting front advances into the capillary system in small jumps, because the irregular capillary spaces have various dimensions. Therefore, wicking – the spontaneous flow of a substrate, driven by capillary forces [145] – is affected by the morphology of the fibre surface as well as by the structure of corresponding capillary system depending on construction parameters such as fineness of filaments and yarn, warp and weft density and the type of weave.

While a textile surface consists of parallel horizontal und vertical capillaries, the surface micro-roughness controls, according to experimental results, the wetting behaviour of a liquid drop (Fig. 5.10).

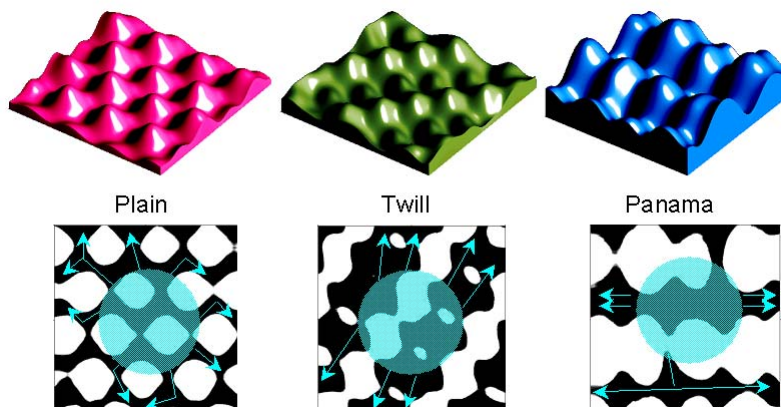


Figure 5.9
Respective textile morphology on meso-length scale controls the spreading rate. Above: morphology; below: spreading directions of a water drop.

There is a limiting value of micro-roughness (about $21 \mu\text{m}$), from which the wetting behaviour drastically changes from hydrophobic to hydrophilic. This phenomenon observed for

Table 5.4
Cut-off length and length of sub-area extractions (L_i) to characterize the fabric micro-topography.

type of weave	L_m [μm]	L_i warp [μm]	L_i weft [μm]
woven plain	1000	150	85
twill	1800	150	160
Panama	2000	240	220

hydrophobic surfaces can be explained using approaches according to Cassie-Baxter [143,144]: at the left side of the graphics in Fig. 5.10, an increase of micro-roughness leads to an increase in hydrophobicity if the spaces between filaments are small (Fig. 5.11, in contrast to in Fig. 5.3, where the spaces between peaks changed

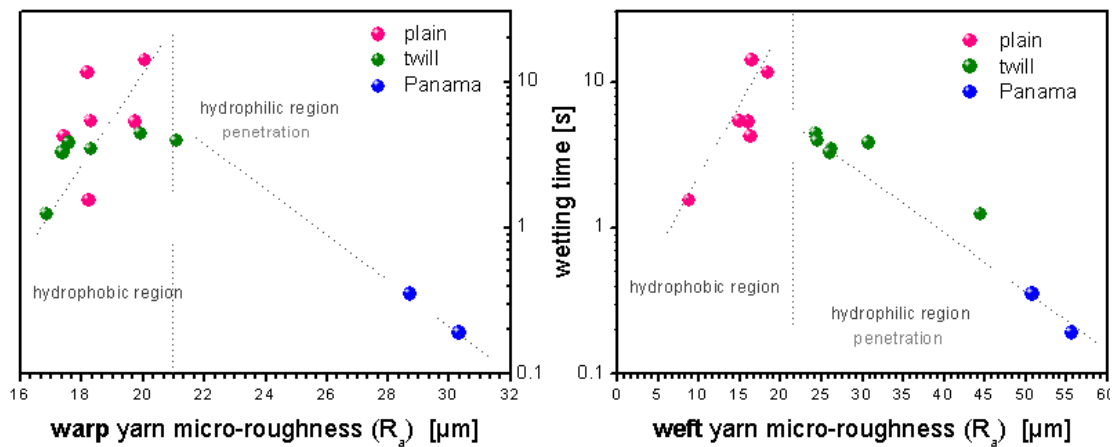


Figure 5.10 Liquid flow in warps and wefts directions occurs by two different regimes, depending on micro-topography.

proportionally with the roughness). Then, in case of the warps and wefts surfaces studied, if $R_a < 21 \mu\text{m}$ the rougher the surface, the less contact points (less solid fraction in Cassie-Baxter model) between textile surface and water droplet, therefore, more pronounced hydrophobic character. If yarn roughness exceed the value of about $21 \mu\text{m}$, larger free spaces between filaments leads to water absorption by capillarity (on right side of the graphics in Fig. 5.10 and Fig. 5.11).

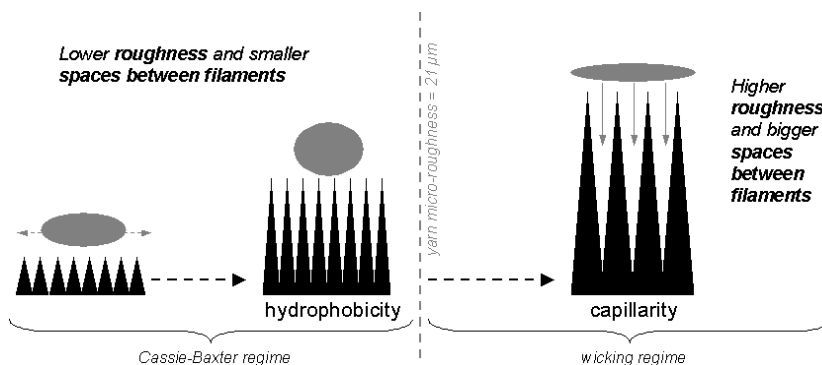


Figure 5.11
Yarn roughness and morphology make the difference in fabric wetting behaviour.

These two different kinds of behaviour were examined experimentally (*Fig. 5.12*) by considering only the topography due to the superior points up to 20 and 60 μm depth.

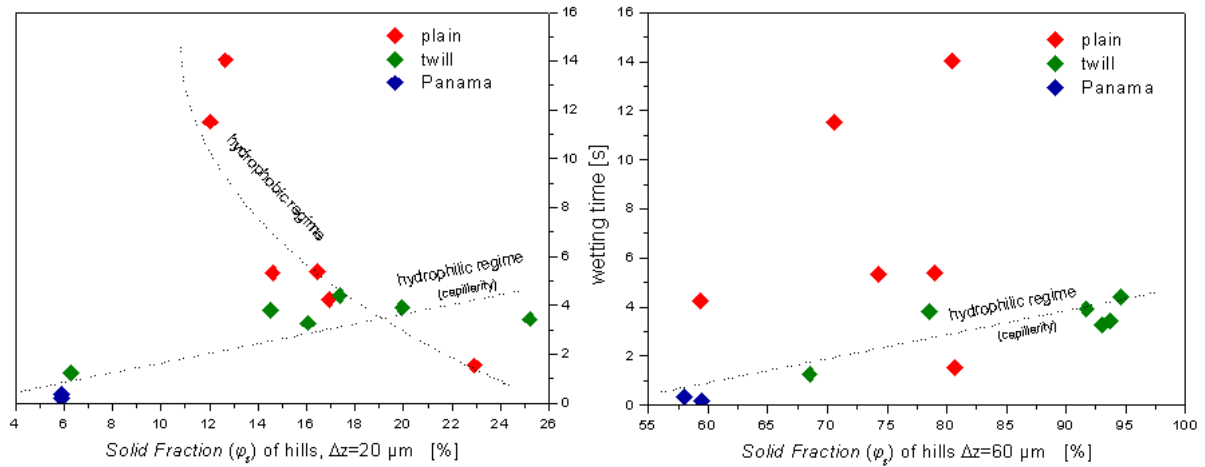


Figure 5.12 Solid fraction (contact points) of the wefts.

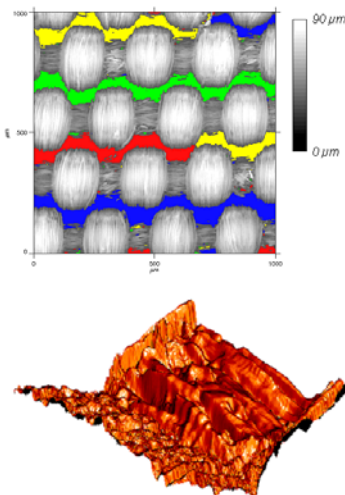


Figure 5.13
Above: spaces between filaments in a plain weave.
Below: spaces 3D-morphology.

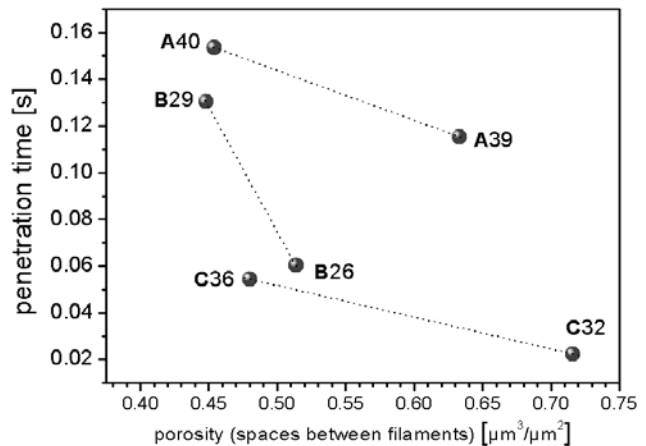


Figure 5.14
Absorption time for woven plain structure with different yarns (A, B, C) and weft densities (26 to 40 weft/cm).

Microtopography of spaces between filaments (*Fig. 5.13*) provides valuable information for understanding the fast wetting and penetration behaviour of a liquid drop. Plain weave fabrics reveal, for instance, larger spaces between filaments than them of twill weave. Then, the number and size of spaces between filaments (*Fig. 5.14*) in the case of the plain weave determines the fast water absorption time in spite of the hydrophobic character of this fabric type.

The wicking conceptual model suggested was verified in respect to the soil release of textiles according to the procedure used in [131,149] and described in Section 5.2.1.3 and Fig. 5.34. Results (Fig. 5.15) show that:

- warp yarns topography hardly affect the cleanability
- spaces between fibres make the plain weave surface oleophil. The larger they are, the more stain penetrates.
- spaces between fibres make the twill weave surface oleophobic. The larger and deeper they are, the more stain penetrates and the worse their cleanability.
- the weft yarn roughness controls the hydrophobicity or hydrophilicity of fabrics and, as a consequence, their cleanability.

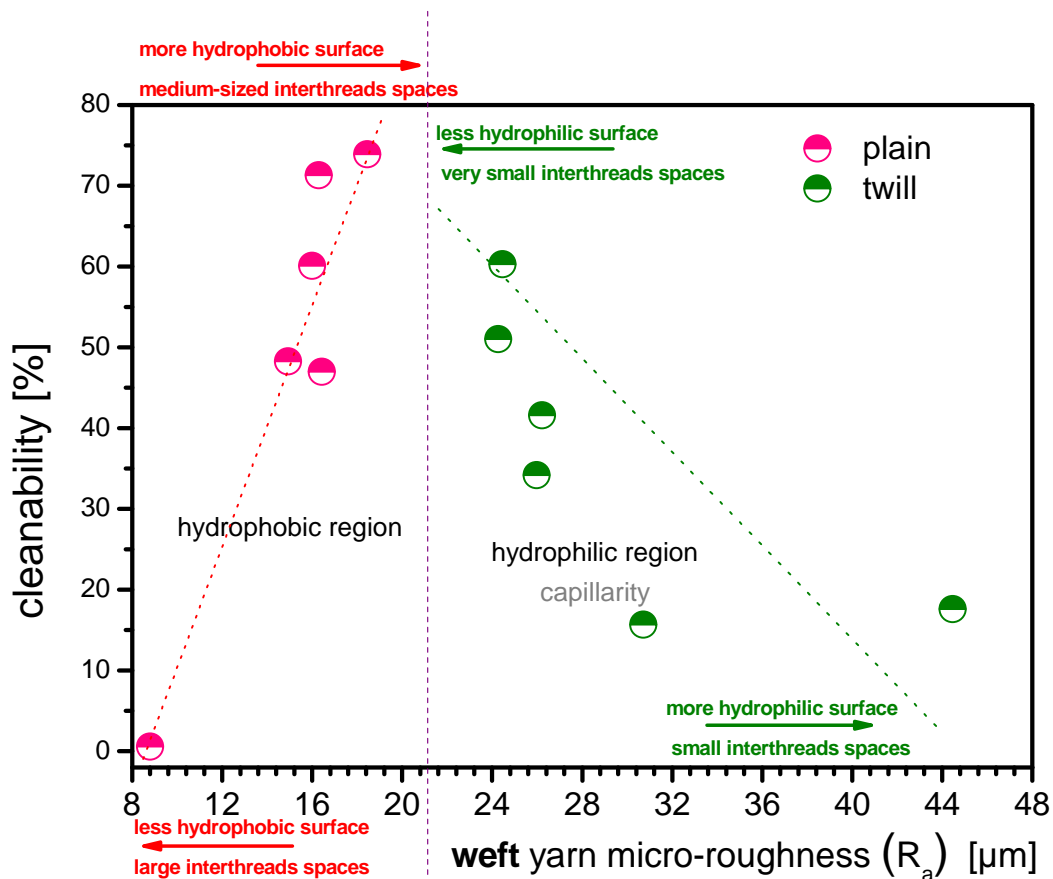


Figure 5.15
The conceptual model proposed allows a better understanding the cleanability phenomenon of polyester fabrics.

5.2.1.2 Influence of thermo-mechanical changes on topography, spreading, wetting and soiling

For this study, polyester fabrics with 3 types of weave: plain, twill and Panama were used, corresponding to the filaments combination warps(A)-wefts(B), all of them by the highest weft densities of 40, 53 and 44 weft/cm (Table 5.3).

Thermofixing were conducted below glass transition temperature at 70°C during 20 s using an industrial Carter AP-2 device [150,151].

Table 5.5
Dimensional change (difference between final and initial area) of fabrics due to thermofixing.

type of weave	Δ area [%]
woven plain	-2.47
twill	0.62
Panama	3.66

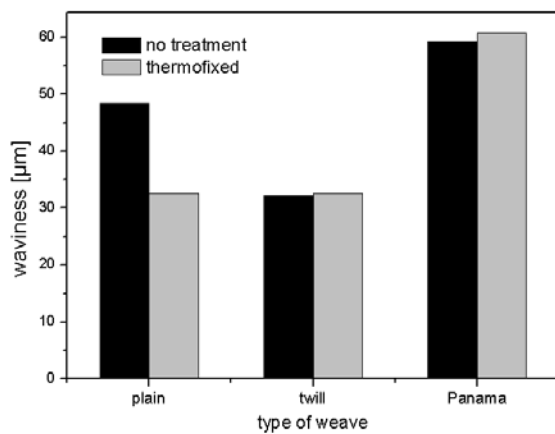


Figure 5.16
Effect of thermofixing on meso-topography.

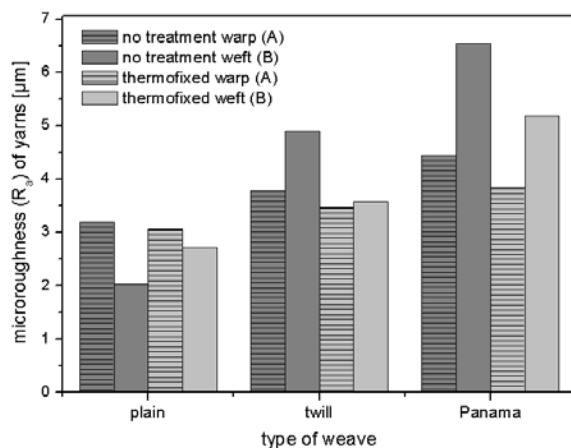


Figure 5.17
Effect of thermofixing on micro-topography of fabric yarns.

The process leads to measurable changes in macro-morphology through relaxation/shrinkage of the fabrics. The twill seems to be the most stable textile structure (Table 5.5).

The waviness (W_2) decreases for plain weave but remains almost constant for twill and Panama structures (Fig. 5.16).

Twill and Panama are mechanically more stable textile structures, then the thermofixing process does not lead to any significant change in their waviness. Additional, in contrast to plain, for twill and Panama structures, their warps and wefts are at the same height. During process, both yarns, A and B, experienced the same thermal conditions. More roughly textured tangled wefts (B) were probably not completely affected by the thermofixing because some of their high points at “hills” remain.

By analysing changes in micro-roughness (R_a) of warps and wefts separately, it is evident, that the topographic effect of thermofixing strongly depends on filaments characteristics (*Fig. 5.17*). For the plain weave structure, warp yarns describe a sinusoidal path, in contrast, wefts describe an almost linear path. Therefore, thermofixing leads to smoothing the surface through elimination of some exceptional height irregularities of the “hills” of flat warp yarns. At the same time, thermofixing leads to a yarn expansion (increase of roughness) of textured wefts for this type of weave (*Fig. 5.18*).

However, twill and Panama show a statistical decrease of micro-roughness (R_a) of warps and especially of wefts after thermofixing. The process smooth warp yarns profile (*Fig. 5.19*) and, as a consequence, the value of roughness is reduced, but not the values of high points who usually affect the waviness.

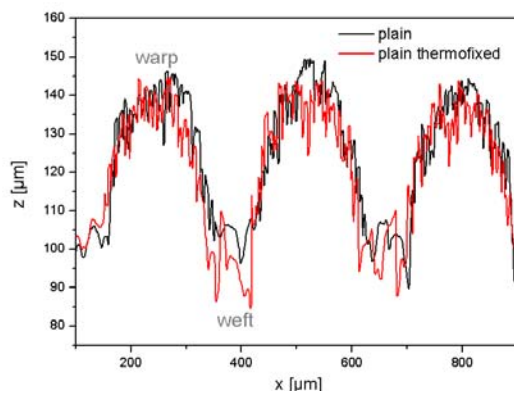


Figure 5.18
Effect of thermofixing on woven plain yarns.

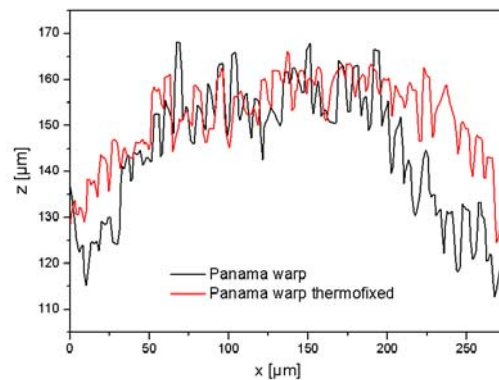


Figure 5.19
Effect of thermofixing on Panama yarns.

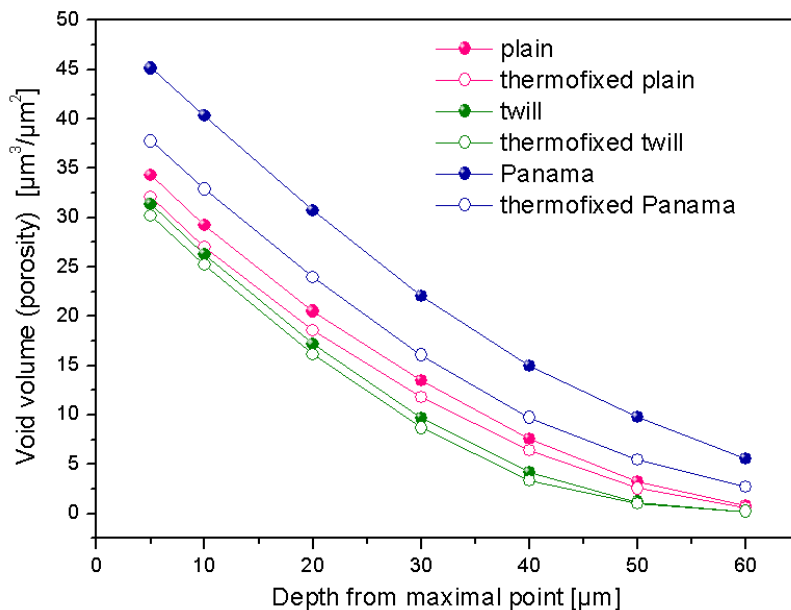


Figure 5.20
Effect of thermofixing on porosity.

According to volumetrical characterisation, Panama weave shows the most significant decrease of porosity after thermofixing (Fig. 5.20). Twill does not show any significant change in porosity.

Results show that the morphology of each type of weave determines a degree of influence of the thermal and mechanical process on the resulting waviness and roughness of the fabrics.

Dynamic wetting measurements were carried out with water droplets (cf. Section 5.2.1.1). After thermofixing, all the fabrics present smaller spreading rates and extremely longer wetting times (Fig. 5.21). The modification of meso-topography (waviness) and micro-topography of yarns (R_a) during the process, were supposed to produce these dramatic changes in wetting by all the fabrics studied.

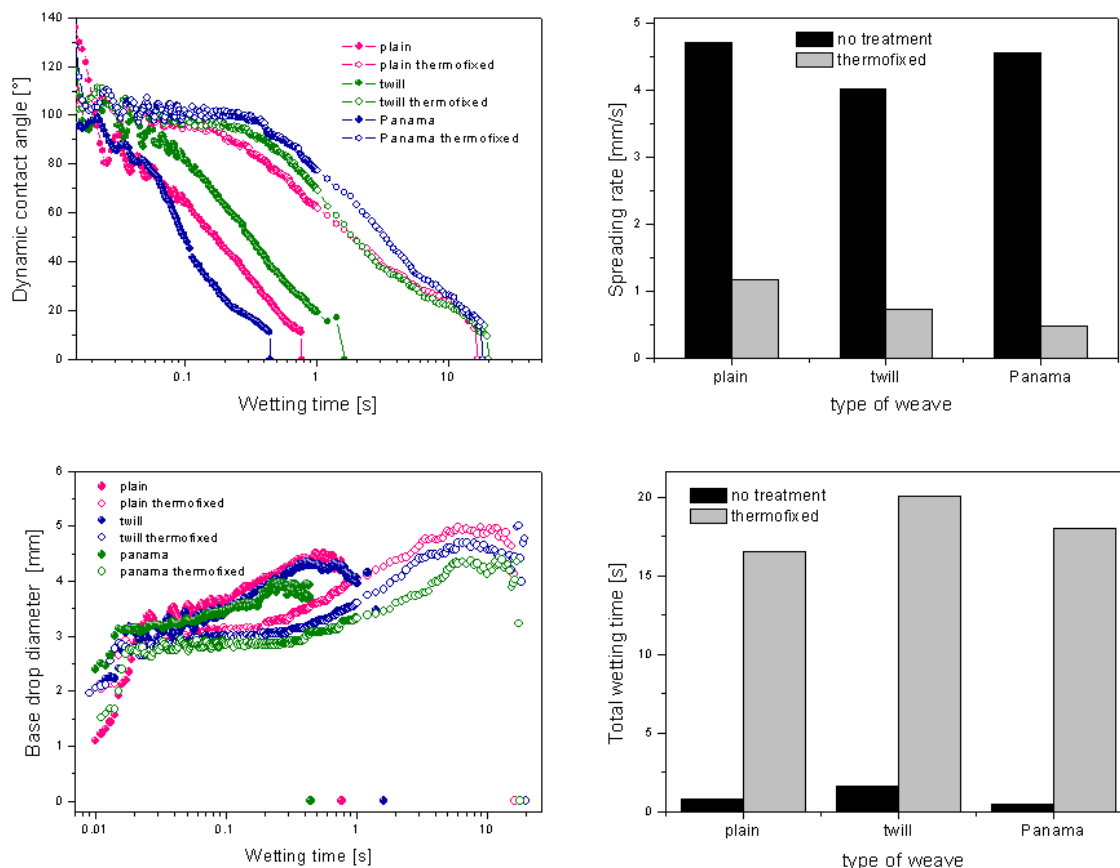


Figure 5.21 Effect of thermofixing on wetting behaviour of fabric surfaces.

In order to investigate a relationship between topographical changes due to thermofixing and wetting, a study of soiling behaviour was carried out by comparing the morphology of water soluble ink spots at untreated and thermofixed textile

surfaces. 5 μL drops of water soluble ink were applied under the same conditions for height and stroke pulse at the fabrics using Fibro DAT 1122 (cf. Section 5.2.1.1). Images of the spots were analyzed with a commercial scanner with a capture density of 1200 dots per inch and OriginPro 8G software.

Ink drops at untreated plain weave fabrics form an almost perfect circle. (*Fig. 5.22*). The formation process of an ink spot at the thermofixed plain structure takes place slower due to the following facts observed:

- a) lower roughness, that leads to a decrease of liquid absorption,
- b) shorter spreading time,
- c) slower spreading rate and
- d) longer wetting time (longer capillary).

In other words, after thermofixing the morphology of woven plain fabrics is better defined (waviness of the fabric and roughness of warps and wefts are smaller) and the consequence is that the ink spot formed is no longer a perfect circle, but almost an hexagon according to the causes described in *Fig. 5.23*.

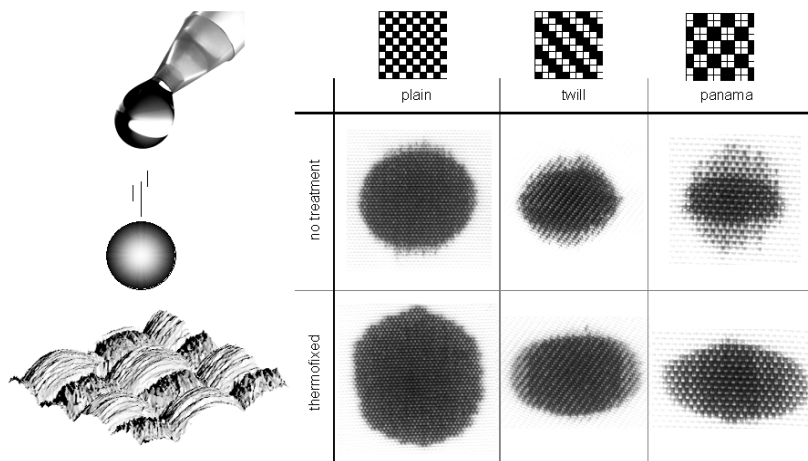
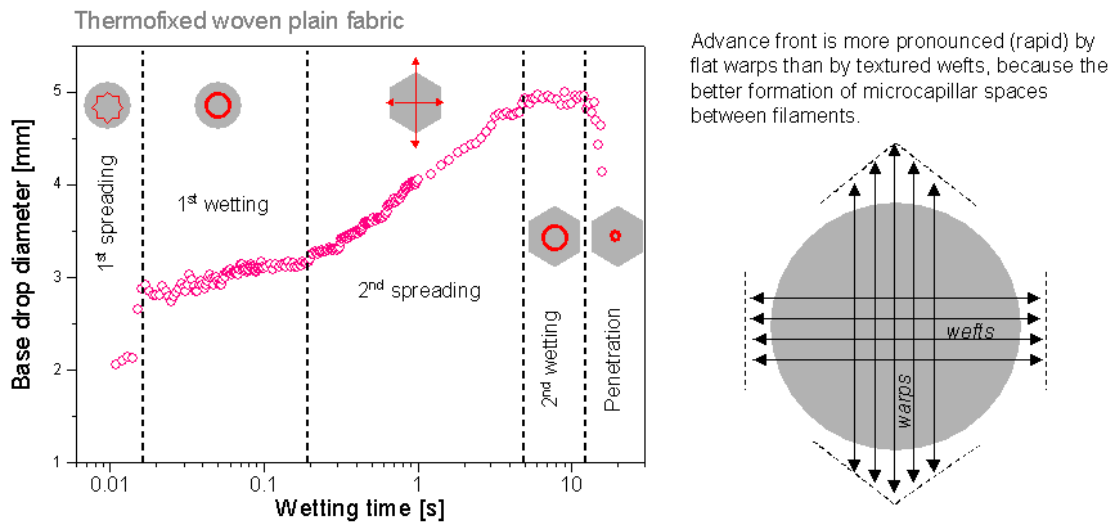


*Figure 5.22
Ink spots formation
over untreated and
thermofixed fabrics.*

In the case of Panama fabrics, micro-roughness values for warps (vertical direction in *Fig. 5.22*) before treatment and wefts after treatment are 4.45 μm and 5.19 μm respectively. With these micro-roughness the capillarity of yarns is better in contrast to the values of 6.54 μm and 3.83 μm which correspond to wefts before treatment and warps after treatment, respectively. According to the spot analysis, yarn micro-roughness between 4.45 μm and 5.19 μm leads to optimal conditions for capillary flow. In this way, the differences between the ink spots of Panama weave can be

explained, which show a marked horizontal (warps) diffusion before treatment and vertical (wefts) diffusion after treatment (cf. *Fig 5.22*).



Step	Δt [s]	Explanation
1 st spreading	0 to 0.017	Shorter and slower spreading over a more defined meso-morphology
1 st wetting	0.017 to 0.2	Slow penetration in flat warps and textured wefts
2 nd spreading	0.2 to 5	Capillarity of flat warps and of textured wefts with different advance fronts
2 nd wetting	5 to 14	End of horizontal capillarity; slow and deeper penetration in textured wefts
Penetration	14 to 16.5	Rapid penetration in deep spaces between yarns

Figure 5.23 Influence of yarns micro topography on spot formation.

Thermofixing leads to changes in the wetting behaviour of water on fabrics depending on their type of weave, morphology, topography and yarn characteristics. These changes clearly influence on the soiling behaviour, which results in longer but superficial spots (*Fig. 5.24*).

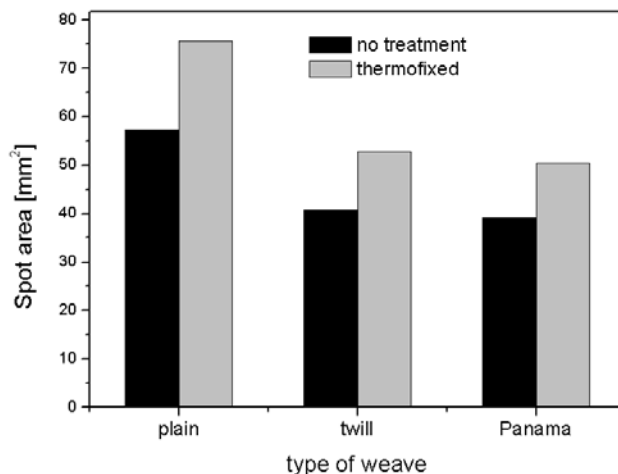


Figure 5.24 Effect of thermofixing on spots area.

5.2.1.3 Influence of impregnation of fabrics with Soil Release Polymers (SRP) on topography, spreading, wetting, soiling and cleanability

For this study, three different woven plain polyester fabrics (cf. Section 5.2.1.1, *Fig. 5.3*) were used, corresponding to the higher weft densities of each warps-wefts combination: A-B (40 weft/cm), A-C (35 weft/cm) and A-D (28 weft/cm). The soil release polymer chosen for the investigation was polyethylene-polyoxyethylene copolymer (MARLOQUEST SL), produced by Sasol Germany GmbH. This SRP is partly insoluble in water, having a constant solid content of 32.3%. A 1 g/L solution of the polymer in deionised reagent-grade water was used for impregnation of the fabrics. The equilibrium surface tension and pH value of the solution were measured to 57 mN/m and 6.3, respectively.

Testing pieces of each fabrics of 4.5 mm x 4.5 mm size were immersed into the aqueous SRP solution for 5 minutes. Without rinsing and wringing, the samples were dried overnight at 24°C in open air.

Dimensional changes by relaxation/shrinkage measured as surface expansion/contraction due to the impregnation with SRP depend on wefts structure and their yarn density (*Fig. 5.6*) as shown in *Fig. 5.25*.

The relationship between waviness and spreading rate of untreated fabrics was described in Section 5.2.1.1. The conceptual model presented there suggests, that for woven plain structures, an increase of the waviness depth causes a decrease of the spreading rate: warp threads (“hills”) slow down the liquid motion.

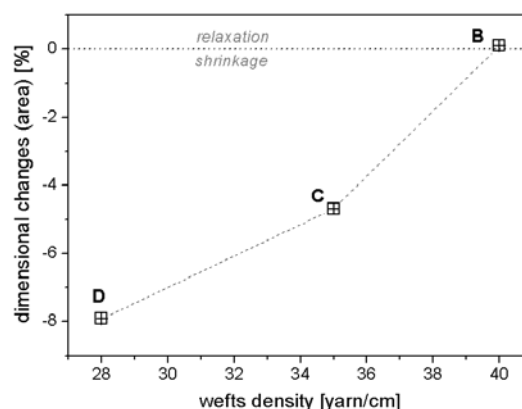


Figure 5.25
Effect of SRP on macro-morphology depending on wefts characteristics.

After impregnation with SRP, a notable increase of spreading rate was measured by all woven plain fabrics (*Fig. 5.26*). The new data do not correlate well with the original curve presented previously in *Fig. 5.8* for treated woven plain surfaces (*Fig. 5.27*). I.e., changes in the dynamic wetting behaviour after impregnation with SRP are obviously not only a consequence of meso-morphological changes, but of a chemical effect after impregnation with SRP. However, the inverse relationship

between waviness and spreading rate of impregnated fabrics supports the validity of the conceptual model proposed in Section 5.2.1.1.

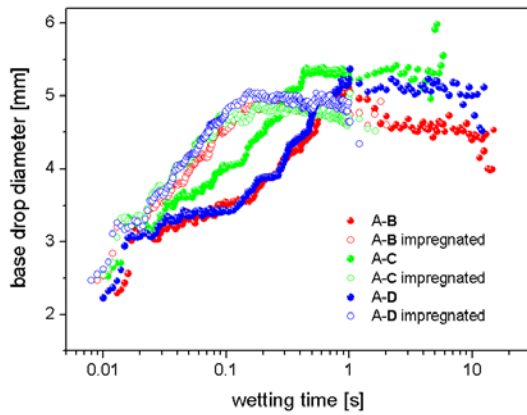


Figure 5.26
Effect of SRP on water wetting dynamic of woven plain fabrics (A-B, A-C and A-D denote yarn combinations).

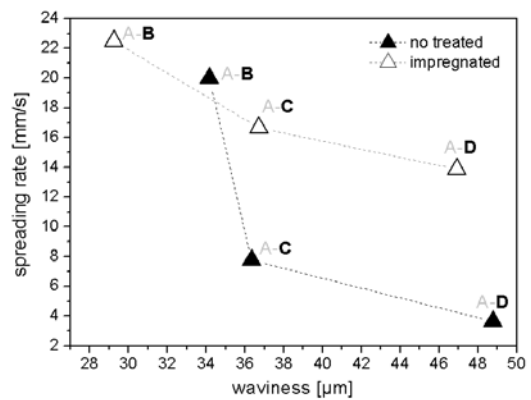


Figure 5.27
Effect of impregnation with SRP on the spreading rate of water (A-B, A-C and A-D denote yarn combinations).

Additionally to the meso-morphological changes due to the SRP impregnation, spreading rate could be affected by fabric contraction (Fig. 5.25) and roughness of deeper weft surfaces (Fig. 5.28). For fabrics A-C and A-D, the impregnation smoothes wefts surfaces decreasing their micro-roughness and closing spaces between filaments which leads to fabric contraction. That allows a more rapid spreading before the quasi-static wetting. This observation is similar to that described in Section 5.2.1.1 (Fig. 5.11) about the effect of roughness on wetting according to the Cassie-Baxter model. In the case of fabric A-B, impregnation leads to a significant increase of wefts micro-roughness, without dimensional change. If the roughness does not exceed the measured critical value of about $21 \mu\text{m}$, should retard the spreading by hydrophobization, according to the Cassie-Baxter model. If the micro-roughness is larger and exceed the critical value, according to wicking regime, the effect predicted is the begin of penetration by capillarity. Nevertheless in this case, near the critical value, only a small increase of spreading rate was measured (Fig. 5.27).

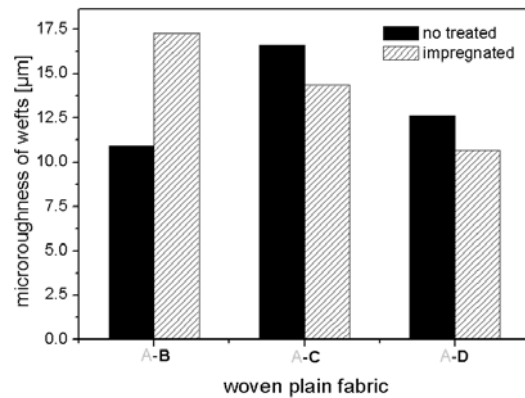


Figure 5.28
Effect of impregnation on wefts microtopography.

Measured wetting time is significantly shorter for impregnated fabrics (Fig. 5.29) and does not correlate with changes in micro-roughness of wefts as presented in Fig. 5.10 for untreated fabrics. The total wetting time strongly depends on the chemical modification due to the SRP impregnation.

The cleanability was examined by using two different types of soil: a liquid-solid mixture and a liquid. A liquid-solid soil was a combination of two kinds of soil materials: paraffin oil and acetylene black in the ratio 97.98:2.02, respectively [152]. A drop of 10 μL volume containing the oil-black soil was applied by a dropper to a testing surface in the untreated state and after its impregnation with SRP. For each fabric, 10 testing pieces were prepared by staining and drying at 24 °C in open air for 72 hours. An aqueous mixture (0.5 g/L) of non-ionic surfactant MARLIPAL 24/60, a Dodecyl- and Tetradecylalkohol with 6 ethoxy groups produced by from Sasol Germany GmbH, was used as a washing detergent. The samples were washed in the detergent at room temperature for 10 min. After washing, they were rinsed many times with deionised water and dried overnight at room temperature.

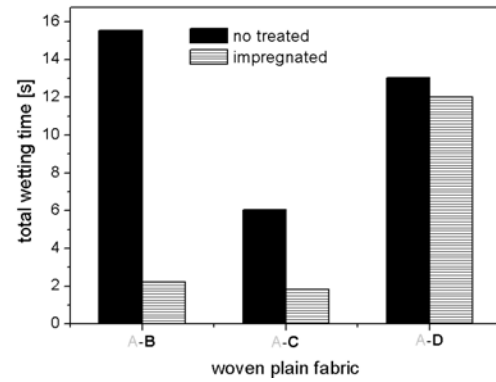


Figure 5.29
Effect of impregnation on total wetting time.

The combined soil can be considered as a dry soil (acetylene black) in a liquid vehicle (paraffin). The spot of acetylene black at the fabric surface was optically characterized using a Chroma Sensor spectrophotometer (Applied Color Systems, USA). From the measured reflection coefficient R (i.e. reflection ability), soiling additional density (SAD) can be obtained using the equation [132,153]

$$SAD = \log \frac{R_{reference}}{R_{soiled/washed}} \quad (5.5)$$

where $R_{reference}$ is the reflection coefficient of a surface before soiling, $R_{soiled/washed}$ is the reflection coefficient after soiling or washing. Surface cleanability is defined as [154]

$$\Gamma = \frac{SAD_{before washing} - SAD_{after washing}}{SAD_{before washing}} \cdot 100\% \quad (5.6)$$

The SAD_{before} washing value will be determined according to Eq. 5.5 using R_{soiled} , whereas SAD_{after} washing will be calculated using R_{washed} . In order to compare the cleanability of different substrates, the relative cleanability $\Delta\Gamma$ was considered:

$$\Delta\Gamma = \Gamma_{impregnated} - \Gamma_{untreated} \quad (5.7)$$

On the other hand, paraffin oil drops of $10\mu\text{L}$ were applied to the fabric surfaces using the Fibro DAT 1122 instrument by controlled conditions (cannula height and stroke pulse), before and after surface impregnation with SRP. For each fabric, 10 testing pieces were prepared by dropping with the soil followed by a drying time of 72 hours at 24°C in open air. Aqueous mixture of non-ionic Marlipal 24/60 (0.5 g/L) was used as detergent. The samples were washed in the detergent at room temperature for 10 minutes. After washing, they were rinsed many times with deionised water and dried overnight at room temperature. For the cleanability characterisation of paraffin oil spots, spreading rate values of water droplets ($10\mu\text{L}$) were measured with a Fibro DAT 1122 instrument at no soiled fabrics (untreated, impregnated) and exactly on the paraffin spots of soiled ones (untreated, impregnated). Then, SAD values were calculated by comparing the spreading rate before and after treatments (soiling, washing) by:

$$SAD = \log \frac{\left(\frac{2dr}{dt}\right)_{reference}}{\left(\frac{2dr}{dt}\right)_{soiled/washed}} \quad (5.8)$$

Where $2dr/dt$ is the correlated (linear) slope of base drop diameter vs. time by each dynamic wetting (spreading) interval.

The surface cleanability (Γ) and relative cleanability ($\Delta\Gamma$) were obtained applying the Eq. (5.6) and (5.7) to the calculated SAD values.

Surface cleanability values for a soil mixture were measured to be almost the same for untreated fabrics (Fig. 5.30(a)), but release of paraffin spot is more effective for untreated fabric A-D (Fig. 5.30(b)). In Section 5.2.1.2, it was discussed that the formation of larger but rather superficial spots by horizontal capillary between filament spaces correlate with a decrease of spreading rate, decrease of spreading time and in principle with the increase of total wetting time (more time to horizontal capillary between filaments). Therefore, larger but rather superficial spots depend on meso- and micro-topographical conditions (waviness and micro-roughness of wefts

respectively). Wetting parameters (cf. Section 5.2.1.1) for untreated fabric A-D surface (*spreading rate* = 3.64 mm/s, *spreading time* = 1.02 s and *total wetting time* = 13.03 s) according to the data represented in [Table 5.6](#), could lead to predicted larger and rather superficial spots, resulting in a better soil release. At this fabric, paraffin is less concentrated in the spot centre. This fact could explain the lowest static water contact angle (41.5°) measured at the paraffin spot position.

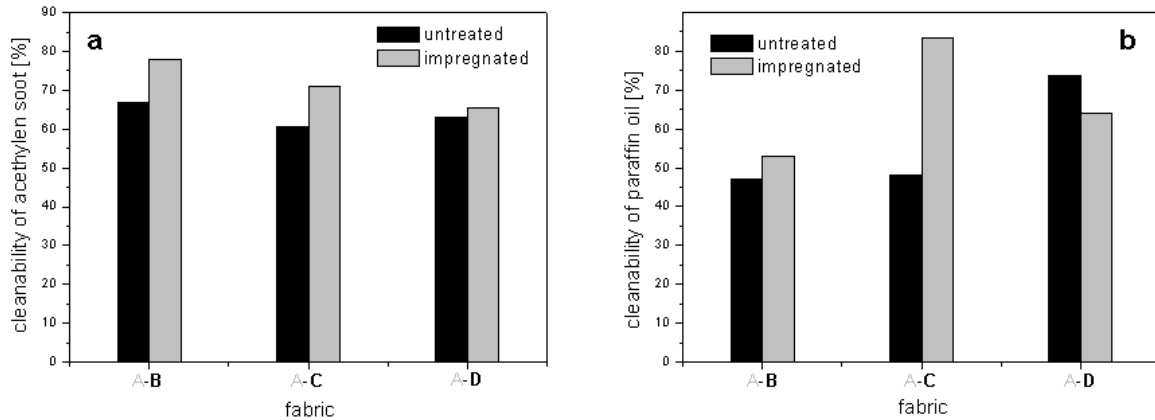


Figure 5.30 Surface cleanability of acetylene soot (a) and paraffin oil (b).

Table 5.6 Effect of impregnation on wetting parameters of fabrics and on their cleanability.
⁽¹⁾weft density measured for untreated fabrics, t_s spreading time, t_w total wetting time, θ static contact angle if occurs.

fabric	weft/cm ⁽¹⁾	treatment	$2dr/dt$ [mm/s]	t_s [s]	t_w [s]	θ [°]	Cleanability
A-B	40	untreated	19.99	1.00	15.54	-	$SAD_{soiled} = 2.483$
		soiled	0.07	9.53	-	64.7	$SAD_{washed} = 1.316$
		washed	0.97	2.82	10.03	-	$\Gamma_{untreated} = 47.0\%$
		impregnated	22.48	0.14	2.22	-	$SAD_{soiled} = 2.145$
		soiled	0.14	7.53	26.05	-	$SAD_{washed} = 1.010$
		washed	1.95	0.98	5.63	-	$\Gamma_{impregnated} = 52.9\%$
A-C	35	untreated	7.76	0.45	6.03	-	$SAD_{soiled} = 2.306$
		soiled	0.04	24.54	-	54.8	$SAD_{washed} = 1.192$
		washed	0.50	2.82	22.54	-	$\Gamma_{untreated} = 48.3\%$
		impregnated	29.57	0.17	1.82	-	$SAD_{soiled} = 2.574$
		soiled	0.02	5.03	15.54	-	$SAD_{washed} = 0.429$
		washed	2.89	0.72	4.63	-	$\Gamma_{impregnated} = 83.3\%$
A-D	28	untreated	3.64	1.02	13.04	-	$SAD_{soiled} = 1.618$
		soiled	0.09	8.03	-	41.5	$SAD_{washed} = 0.423$
		washed	1.38	1.42	12.03	-	$\Gamma_{untreated} = 73.9\%$
		impregnated	13.89	0.16	1.42	-	$SAD_{soiled} = 0.814$
		soiled	0.56	3.42	5.43	-	$SAD_{washed} = 0.292$
		washed	1.86	0.86	4.02	-	$\Gamma_{impregnated} = 64.1\%$
							$\Delta\Gamma = 5.9\%$
							$\Delta\Gamma = 35.0\%$
							$\Delta\Gamma = -9.8\%$

The untreated fabric A-B presents more closed filaments (higher weft-density) and lower micro-roughness of wefts than the others. This conditions lead to a short spreading time (1 s) with faster spreading rate (20 mm/s). During wetting, which is the longest (15.53 s) compared to the other textiles, water tends to penetrate slowly and does not flow by horizontal capillary between filaments. If the same occurs with paraffin oil, its wetting process could lead to smaller but deeper less cleanable spots compared to fabric A-D.

Untreated fabric A-C has the highest micro-roughness of wefts. That tends to stop spreading, which occurs only during 0.45 s and leading to a faster penetration and horizontal capillarity, resulting in the shortest wetting time (6.03 s) compared to other fabrics under study. In this case, penetration and capillarity are going to compete, resulting in cleanability (48.3 %) equivalent to that evaluated for fabric A-B (47 %).

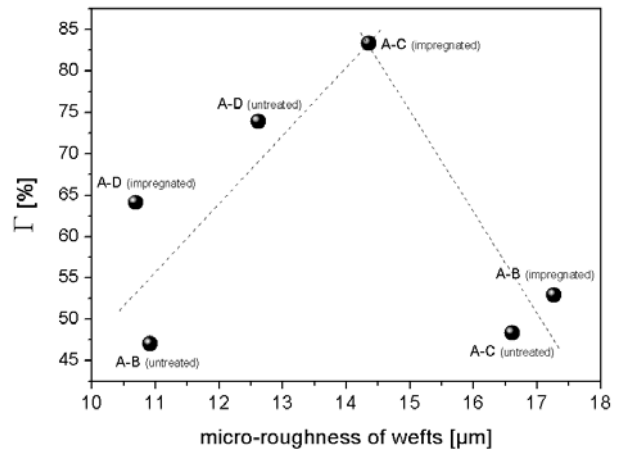


Figure 5.31
Effect of micro-topography of wefts on surface cleanability (Γ) of paraffin oil.

From topographical data for micro-roughness of wefts (Fig. 5.28), untreated fabric A-D is an intermediate state between A-B and A-C. This fact leads to the optimal conditions for growing of more superficial paraffin oil spots by horizontal capillarity and a moderate penetration in the textile structure. The consequence is a better soil release of 73.9% (Fig. 5.30(b)).

Using a soil mixture consisting from acetylene black and paraffin oil, acetylene black particles tends to penetrate into the fabric structures without regarding of differences in wetting dynamics of the liquid vehicle (paraffin oil). Almost the same cleanability of black spots of acetylene soot were measured for the untreated fabrics (Fig. 5.30(a)).

Impregnation with SRP is supposed to produce chemical changes on the surface recovering of the filaments surface by a thin PET layer. The topographical characterisation did not detect any film formation or SRP agglomeration in the spaces between filaments as in the cases reported in [132] and [134] respectively.

Additionally, impregnation with SRP leads to micro-topographical changes in the spaces between filaments, especially in wefts, whose micro-roughness controls the wetting dynamics as described above. Wetting characteristics, in turn, control the penetration of soil and the resulting cleanability. *Fig. 5.31* shows that, independent of wefts characteristics (filament type, filament fineness, yarn density) or impregnation with SRP, micro-roughness of wefts seems to control cleanability of paraffin oil. According to results, a critical micro-roughness ($R_a = 14.4 \mu m$) of impregnated A-C fabric is responsible for a maximum of cleanability and the best measured effect of impregnated fabric with SRP on cleanability ($\Delta\Gamma = 35\%$) (cf. *Fig. 5.32*)

For fabric A-D, which showed a better cleanability being untreated, the effect of impregnation on hydrophilicity is relevant: wetting time of a water drop reduces 9 times (from 13.03 to 1.42 s), however, the effect on cleanability is the worse ($\Delta\Gamma = -9.8\%$) because micro-roughness of wefts decreases during the process (from 12.61 to 10.69 μm , see *Fig. 5.31*).

Hydrophilisation of the surface due to impregnation with SRP is usually associated with positive effects on the resulting cleanability. Nevertheless, according to the results showed in *Fig. 5.33*, a decrease in wetting time does not lead to any better release of paraffin oil spots. Only the effect of the impregnation on micro-topography of wefts (*Fig. 5.31*) leads to a better cleanability.

Cleanability of acetylene black is in all cases enhanced by impregnation with SRP, especially for fabrics A-B and A-C (*Fig. 5.34*).

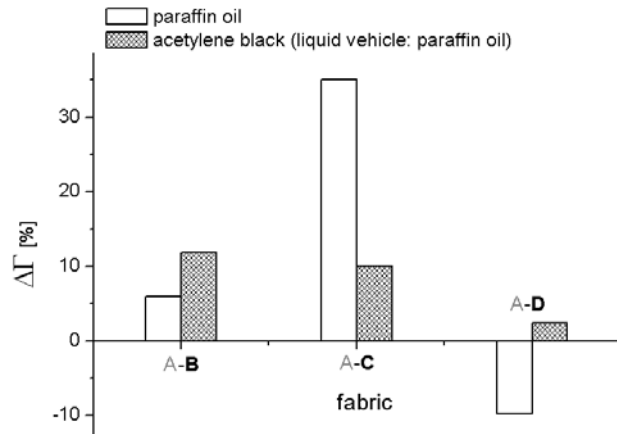


Figure 5.32
Relative cleanability (effect of impregnation on cleanability).

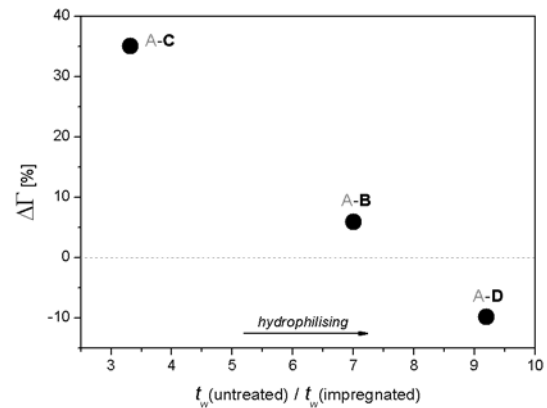


Figure 5.33
Hydrophilisation due to impregnation with SRP does not perform cleanability of paraffin oil.

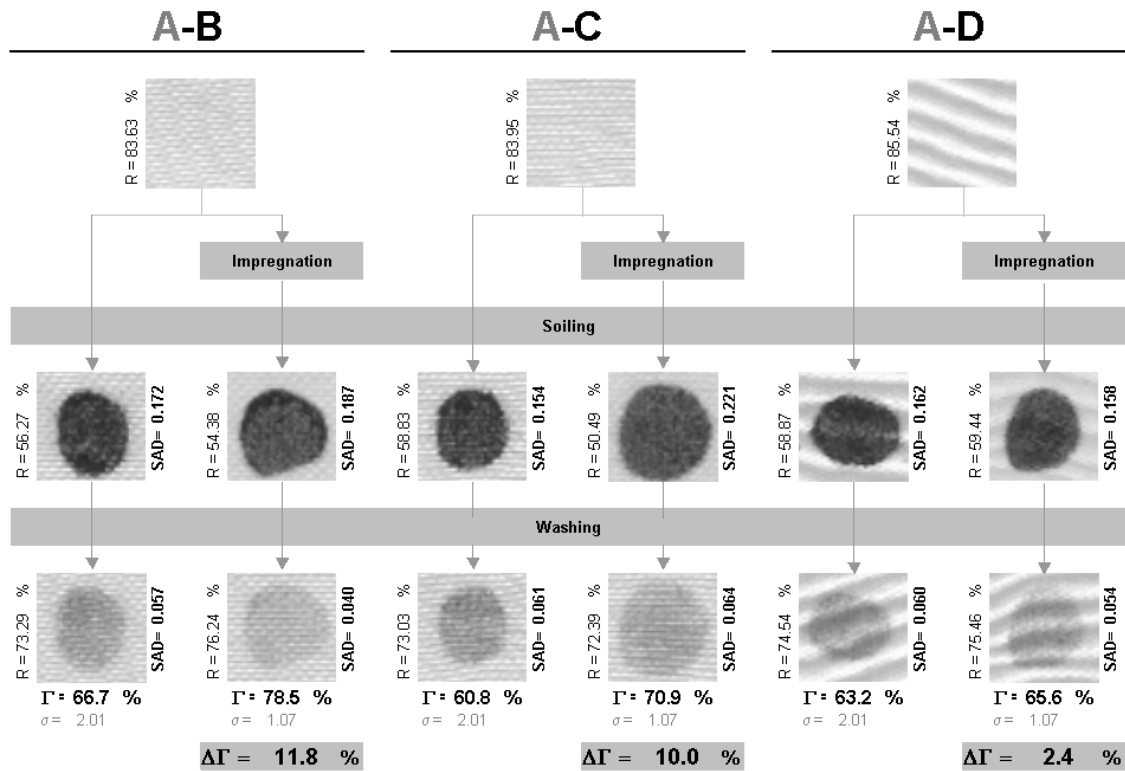


Figure 5.34 Surface and relative cleanability of acetylene black for untreated and impregnated fabrics.

A-D is more porous than A-B and A-C, and impregnation does not significantly change this value (Fig. 5.35). In this sense, impregnation does not help to the mechanical removing of dry soil (acetylene black) while washing. That explains a low effect of impregnation on cleanability of dry soil ($\Delta\Gamma = 2.4\%$) for this type of fabric.

It is important to note, that impregnation of A-C closes its pores from 0 to 35 μm depth and opens the pores laying deeper than 35 μm (Fig. 5.36). This effect could be related with a better removal of paraffin oil from this kind of fabric. Closing of

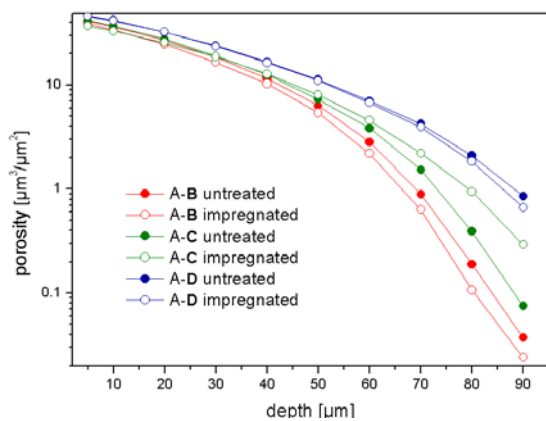


Figure 5.35 Effect of impregnation on porosity (void volume calculated from maximum point).

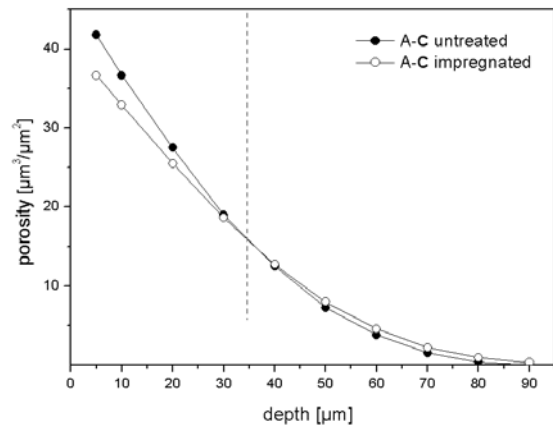


Figure 5.36 Impregnation by A-C closes pores from 0 to 35 μm and opens deeper ones.

superficial spaces reduces the effect of soiling (wet soil remains more superficial). Opening of pores laying deeper makes the penetration and action of the washing solution easier.

5.2.2 Cotton textiles

Woven and knitted fabrics (*Fig. 5.37*) used in this study were purchased from Testfabrics (USA). Their characteristics are summarized in *Table 5.7*.

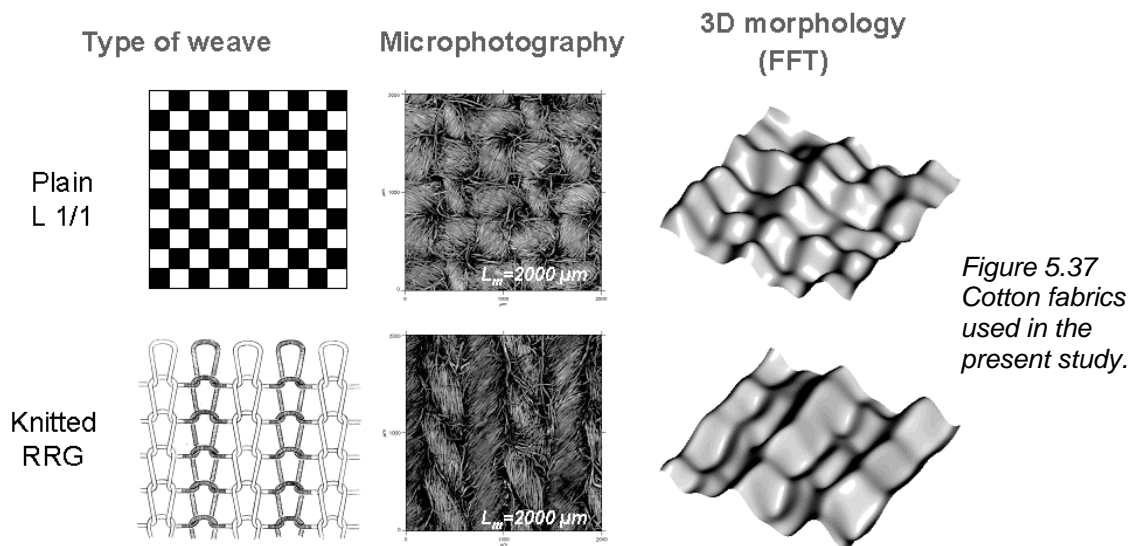


Figure 5.37 Cotton fabrics used in the present study.

5.2.2.1 Wash-dry cycles as surface modification process

Testing pieces of each fabric ($50\text{ cm} \times 50\text{ cm}$) were washed only with water at 23°C , using a drum washing machine D403/1-3 SDL Atlas Inc. (USA) during 20 minutes by 40 RPM . After washing, they were dried at room temperature overnight. Samples were submitted to different number of wash-dry cycles in order to study the cumulative mechanical effect on the resulting topography, wetting and soiling.

Table 5.7 Characteristics of fabrics used.

Fabric type	Weight [g/m ²]	Pick count [pick/dm]	Weave	Yarn count [dtex]
woven plain	170	270/270	L1/1	295/295
knitted (double jersey)	329	160/127	RRG	220

Dimensional changes by relaxation and/or shrinkage were measured as an increase or a decrease of marked areas ($10 \times 10\text{ cm}$) after the first, fifth and tenth wash-dry cycle. Washing leads to dimensional changes in the case of both fabrics. As can be seen in *Fig. 5.38*, a knitted fabric is relatively more stable than a woven plain one.

Dimensional modifications during washing are associated with gravimetric changes. The fabric density as a total fabric weight per square meter was determined at controlled laboratory conditions (23°C and 55% RH) for all fabrics (Fig. 5.39(a)).

During the process, fabrics are going to lose material (fiber) and to gain or lose humidity. Using the information

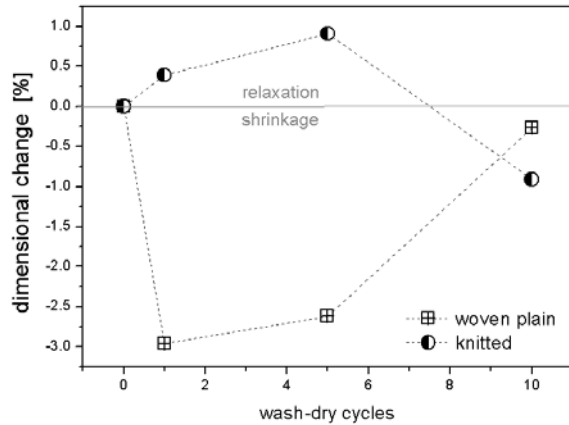


Figure 5.38 Dimensional change of fabrics as a consequence of washing and drying with respect to the untreated fabrics.

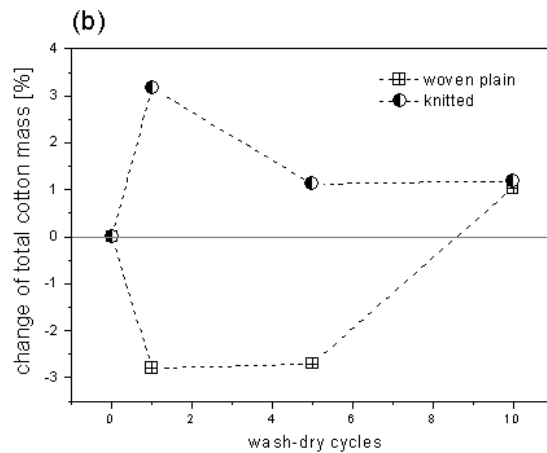
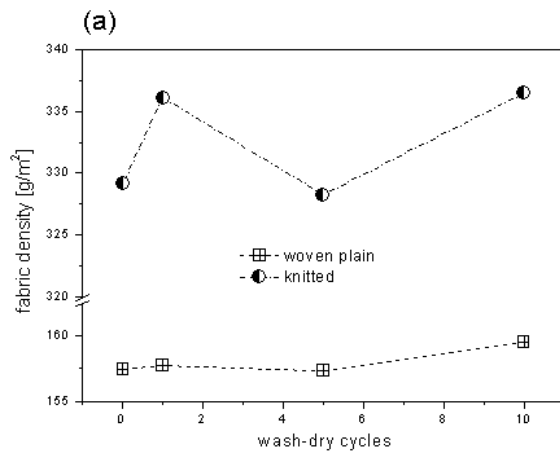


Figure 5.39 Dependence of fabric density on wash-dry cycles (a), and cotton mass gain/lose with respect to untreated samples depending on wash-dry cycles (b).

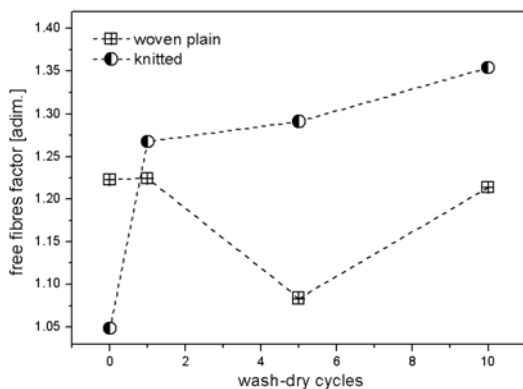


Figure 5.41 2D representation of the calculation of free fibers factor to quantification of pilling, by smooth filtering.

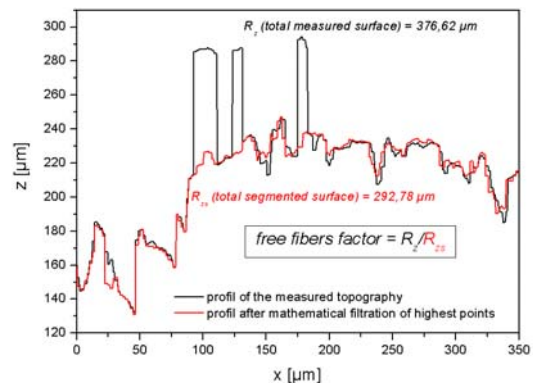


Figure 5.40 Pilling effect of washing and drying can be quantify by free fibers factor (R_z/R_{zs})

about dimensional and gravimetric changes, it was possible to calculate the total gain/lose of cotton fibre as a function of wash-dry cycles (*Fig. 5.39(b)*).

Topographic measurements by MicroGlider make possible to quantify changes in meso-roughness (R_z) and to relate it with the abrasion during washing causing the fiber to unravel and the loose ends ball up on the fabric surface (pilling). For this purpose, two values of roughness were obtained: the first one using topographical parameters measured as is, and the second value after a digital surface filtering (smooth filtering, cf. Section 3.5.1.1) of all the points that were above the mean line of yarns contour (*Fig. 5.40*). The surface tear effect of washing reduces pilling of woven plain fabric after five cycles, but more washings cycles lead to a new tear of surface fibres resulting in a new increase of pilling, as can be seen in *Fig. 5.41*. At knitted fabric, abrasion of a first wash cycle leads to a distinctive pilling; following cycles hardly increase pilling.

The topographic characterization of woven plain fabric shows that macro-morphological changes (relaxation and shrinkage) influence not only the meso-topography but also the micro-topography, measured as meso-porosity (spaces

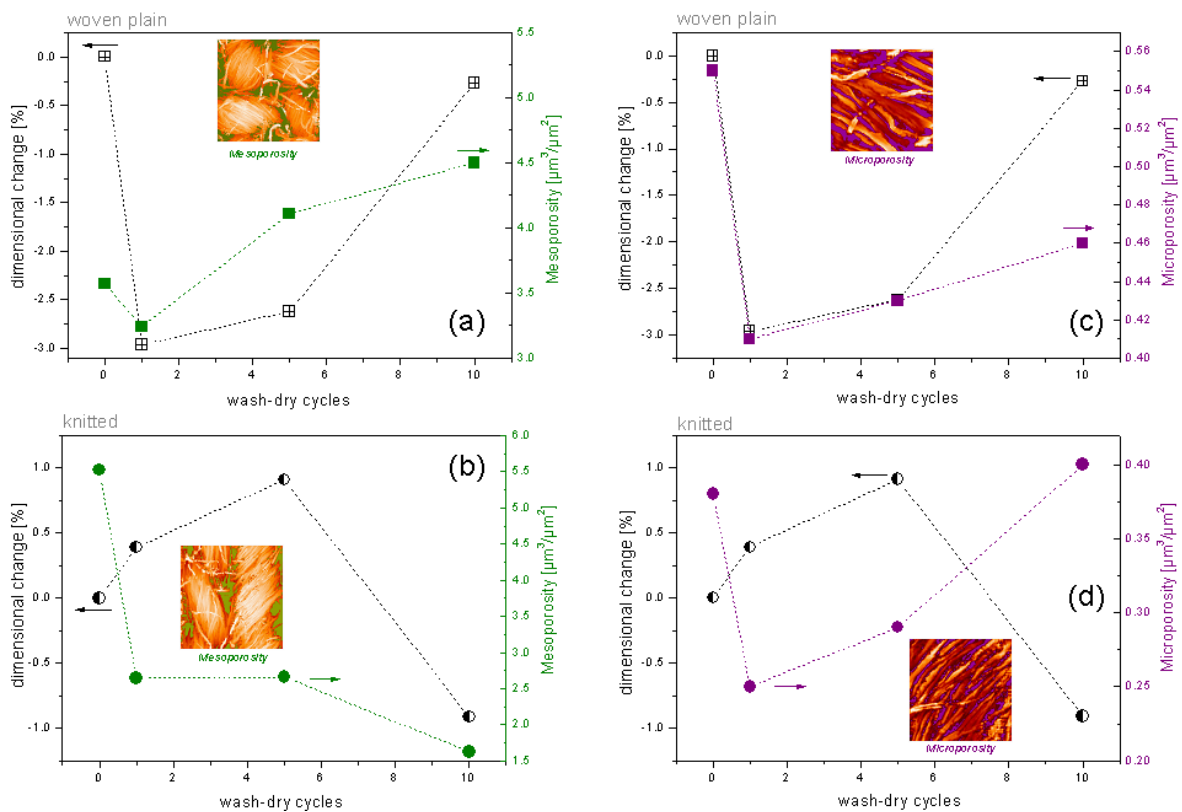


Figure 5.42 Relationship between dimensional changes and resulting topography as consequence of washing and drying.

between yarns) and micro-porosity (spaces between fibers), respectively (*Fig. 5.42(a)* and *Fig. 5.42(c)*), due to changes on volume of spaces between yarns. Topographic parameters meso- and micro-porosity are less influenced by macro-morphological changes of knitted fabric (*Fig. 5.42(b)* and *Fig. 5.42(d)*).

Mechanical effect of washing tends to sequentially increase the meso-porosity of a cotton woven plain structure but tends to decrease the meso-porosity of a knitted one, while for both structures micro-porosity decreases after the first wash and then sequentially increases.

The mechanical effect of wash cycles also leads to surface tear and pilling that, combined with the relaxation-shrinkage effect, can produce additional changes not only in the meso- but also in micro-porosity of the fabrics.

Moisture adsorption mechanism by cellulose fibres consists of three steps [155-157]: (1) the selective adsorption of water molecules by hydrogen bonding to the free hydroxyl groups in non-crystalline or intermicellar regions; (2) the adsorption of water into the lattice of the crystalline regions in those particular cellulose structures exhibiting changes in cellular dimensions with moisture adsorption; and (3) capillary condensation or “multiple-layer formation” in those spaces in the cellulose fibre which permit occupancy by additional water molecules. Water adsorbed according (1) and (2) may be considered as ‘bound’ [158] with energies greater than those involved in the water-to-water hydrogen bond. Conversely, the water taken up by capillary condensation might be expected to behave similarly to bulk.

Another interesting physical model of moisture distribution in cellulose [159] is based on the detection and identification of four types of water incorporated in cellulose: (i) *primary bounded water*, which molecules are connected by strong hydrogen bonding with active surface sites on the cellulose structure which may be unsatisfied hydroxyl groups (in the case of low ordered amorphous regions and highly ordered crystalline areas); (ii) *secondary bonded water*, bounded by penetration of the fiber bundles or internal surface hydroxyl groups in the amorphous areas; (iii) *free water*, which is formed as multilayers; and (iv) *bulk water*, which is defined as additional water that fills the large volume external to the cell wall (lumen). Assuming that fabric samples consist only of cellulose and water and washing and drying don't lead to any modification of cellulose cristallinity, i.e. crystalline/amorphous ratio, changes in the water content should be only due to adsorption of *free* and *bulk* water by multilayer

formation -capillary condensation- and filling of interfibers spaces respectively , as consequence of a combination of dimensional, gravimetric and topographical changes.

With intention of prove previous experimentally based argumentation [159] and of applying it to the mechanical modification studied for cotton fabrics after several wash-dry cycles, the total water content of the fabrics were investigated by Thermogravimetry (TGA), using a Thermogravimetric Analyzer Q500 von TA Instruments (USA). After preconditioning the samples during 48 hours under controlled conditions (23°C, 55% RH), they were heated in Nitrogen atmosphere at 30°C during 15 minutes (isothermal interval) and then with a constant heating slope of 8.5°C / minute.

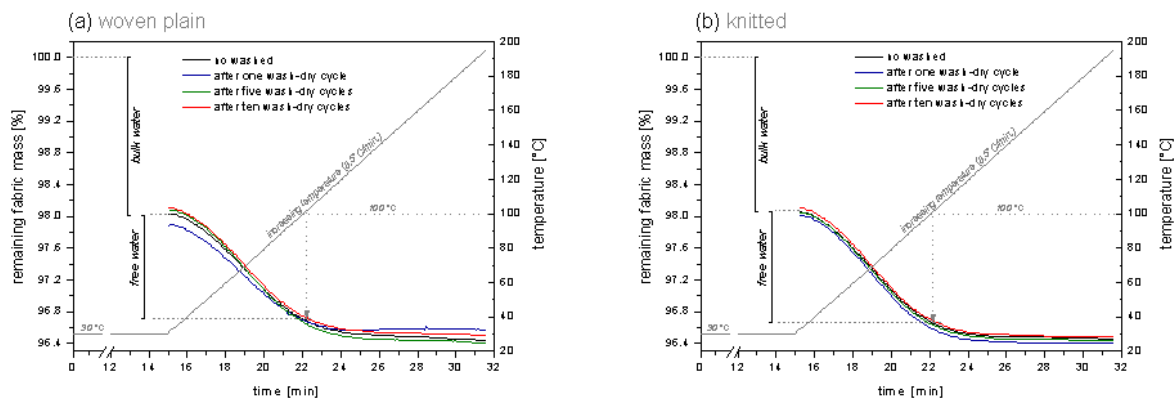


Figure 5.43 TGA graphs of woven plain (a) and knitted (b) fabric. Bulk water is supposed to be removed from spaces between fibers during isothermal (30°C) interval. Constant heating up to boiling point is supposed to remove all free (multilayered) water from fibers micro and nano inhomogeneities.

Results presented in Fig. 5.43 and Table 5.8 show that during isothermal interval by 30°C fabrics lose about 2% of their mass in form of bulk water. Constant heating up to water boiling point leads to an additional lose of weight in form of free water.

Important shrinkage by woven plain fabric (Fig. 5.38) and close of spaces between fibers (decrease of micro-porosity, Fig. 5.42c) after the first wash-dry process allows more retention of bulk water (2.12%). After 10 wash-dry

Table 5.8 Bulk and free water content of both fabrics after washing and drying.

fabric	wash-dry cycles	bulk water [%]	free water [%]	bulk + free water [%]
woven plain	0	1.97	1.33	3.30
	1	2.12	1.19	3.31
	5	1.93	1.41	3.34
	10	1.90	1.36	3.26
knitted	0	1.94	1.39	3.33
	1	1.99	1.42	3.41
	5	1.95	1.41	3.36
	10	1.90	1.41	3.31

cycles, woven fabrics relax, i.e. mesoporosity increases, *Fig. 5.42(a)* and its microporosity slightly increases (*Fig. 5.42(c)*). The consequence is less retention of *bulk* water after drying (*Table 5.8*).

In the case of knitted fabrics, an increase of total cotton mass observed after the first wash-dry cycle (*Fig. 5.39(b)*) correlates well with *bulk* and *free* water values in *Table 5.8*. In this case, the knitted structure tends to relax, i.e. a sequentially increasing of spaces between yarns (*Fig. 5.38*) up to the fifth wash-dry cycle but at the same time to close the spaces between fibers, i.e. decreasing microporosity, *Fig. 5.42(d)*). The effect is the tendency to more retention of *free* and *bulk* water after drying. After the tenth wash-dry cycle, knitted fabrics shrinkage leading to a decrease of distance between yarns and opens the spaces between fibers, leading to increasing of microporosity). The consequence is less retention of *bulk* water, as detailed in *Table 5.8*.

Pilling studied for both types of weave has no effect on *free* and *bulk* water retention after drying.

A relevant topic is the investigation of the effect of topographical modification of fabrics on their water uptake by capillarity when the fabric is in contact with an endless liquid source. An increase in weight can be measured by a method known as Wilhelmy plate technique [129,160]. Water uptake measurements were carried out with a DCAT 21 tensiometer von Dataphysics (Germany). A fabric sample (40 x 10 mm size in vertical position with the longer side as height) is connected to a micro balance.

Before the fabric sample touches the water surface, its weight contribution is zeroed by the calibration routine of the balance. In the case of knitted double jersey fabric, yarns were oriented in a vertical position (*Fig. 5.44*). After the fabric sample has penetrated into water, the balance records the weight gained caused by the wetting of the textile and the water uptake into the fabric due to capillary effects.

The weight gained over time is measured. It is strongly dependent on the hydrophilic-hydrophobic properties of the surface. The influence of the fabrics modification can be detected by comparing differently modified samples. A defined immersion depth of 1mm was used. The

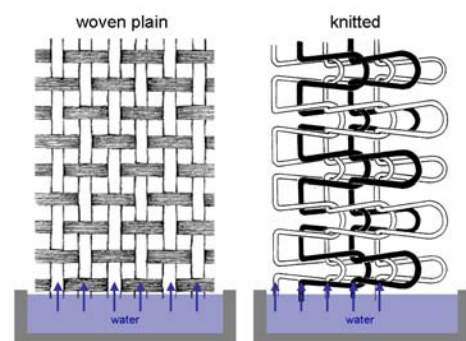
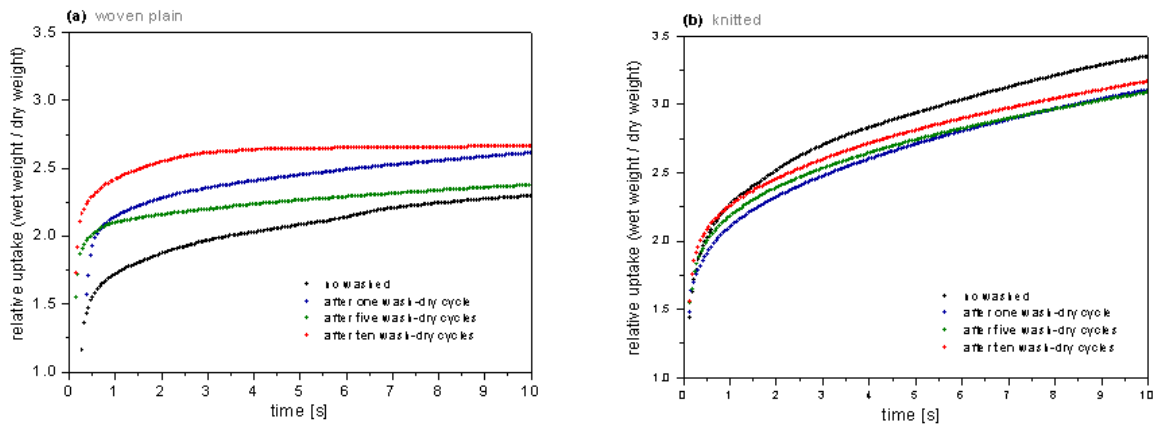


Figure 5.44
Orientation of fabric yarns during water uptake experiment.

water uptake rate is determined according to [161] from the linear part of the mass vs. time curve (Fig. 5.45).



Figures 5.45 Water uptake of woven plain (a) and knitted (b) fabrics during the first 10 seconds.

More or less presence of free water inside the fabrics does not determine the water absorption capability by capillarity. Fig. 5.45 shows that for each type of weave no dependence is observable between *bulk* and/or *free* water and absorption rate of water by capillary during the first 10 seconds.

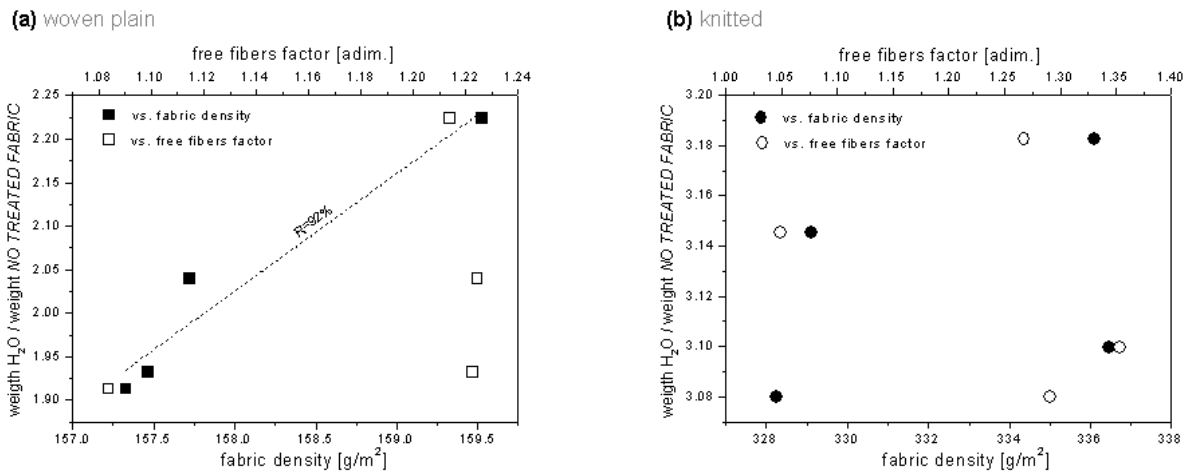


Figure 5.46 Total water absorption of woven plain (a) and knitted (b). Only by woven plain a correlation with fabric density was found.

According to the results showed in Fig. 5.46 for both fabrics, the total amount of water absorbed after 300 seconds (all the absorption curves tend to constant values after about 150 seconds, Fig. 5.45), does not depend on pilling. In all cases, total water uptake values were calculated using each particular fabric weight as a reference. Nevertheless, for woven plain, the fabric density controls the total water

absorption capability (Fig. 5.46(a)). In this case, after 10 wash-dry cycles, an increase of mesoporosity (spaces between yarns) results in optimal geometrical conditions for capillary flow.

On the other hand, intricate geometrical structure of knitted fabrics (they are not parallel yarns compared to the woven plain) makes difficult to interpret the optimal conditions for capillarity. For this weave, capillary flow results in better absorption in terms of total water uptake, if the sample was washed and dried only one time. In this case, the optimal conditions are reached after closing spaces between yarns (decrease of mesoporosity, Fig. 5.42(b)) and between fibers (decrease of microporosity, Fig. 5.42(d)).

Spreading and wetting with 10 μL volume water drops were measured on all fabrics using FibroDAT 1122 HS instrument according to the method described in Section 5.2.1.1.

The spreading rate, i.e. the of increase of the base drop diameter, reveals that each type of weave defines a specific behaviour of water at textile surfaces during the first instant of contact. Topographic modification of the surface leads to an increase of spreading rate for the woven plain (Fig. 5.47(a)) after several wash-dry cycles. On the contrary, a decrease of spreading rate is observed for knitted fabrics.

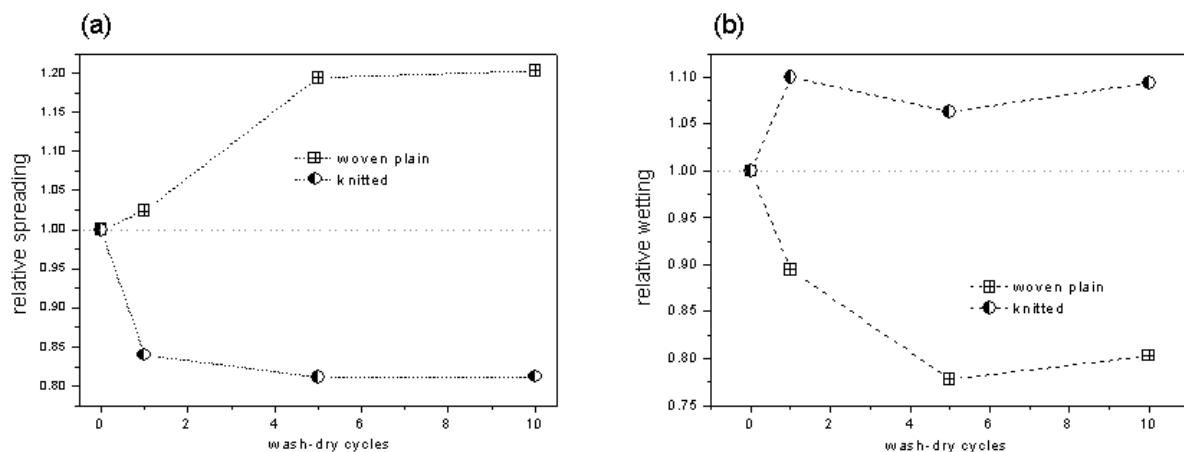


Figure 5.47 Relative spreading ($\text{spreading rate}_{\text{washed}}/\text{spreading rate}_{\text{reference}}$) (a), and relative wetting ($\text{wetting time}_{\text{washed}}/\text{wetting time}_{\text{reference}}$) (b), of both fabric types.

According to the results shown in Fig. 5.47(b), the total duration of wetting process - dynamic wetting or spreading, quasi-static wetting and penetration-, is accelerated for the woven plain structure and retarded for knitted fabrics after washing and drying.

For both types of weave, especially at the woven plain structure, an increase in volume between yarns (mesoporosity) leads to more rapid spreading, because fluid finds wider canals for its motion (Fig. 5.48(a)). At the same time, these spaces control the total wetting time of the liquid at textile surfaces: the larger mesoporosity the shorter wetting times (Fig. 5.48(b)).

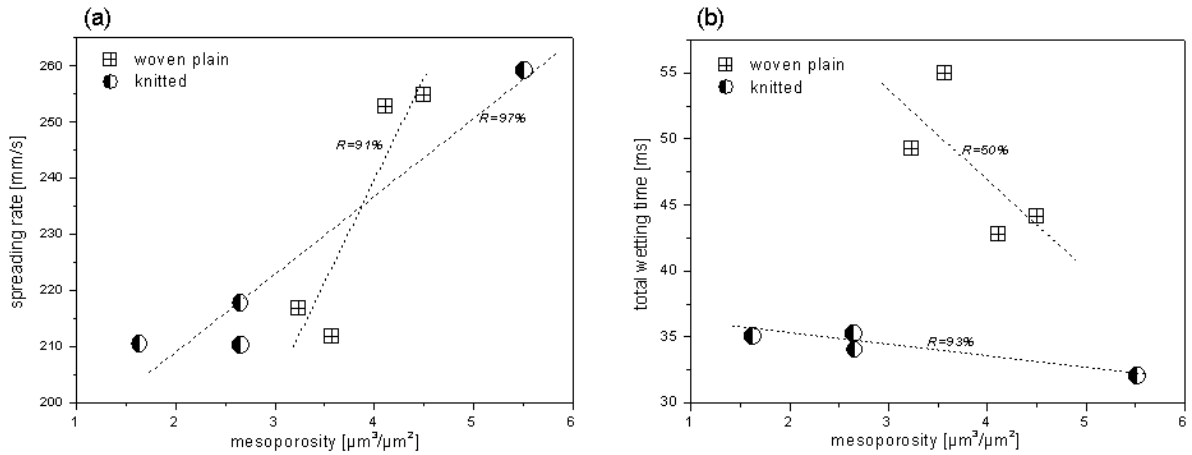


Figure 5.48 Fabrics mesoporosity controls the spreading rate (a) and the total duration of wetting process.

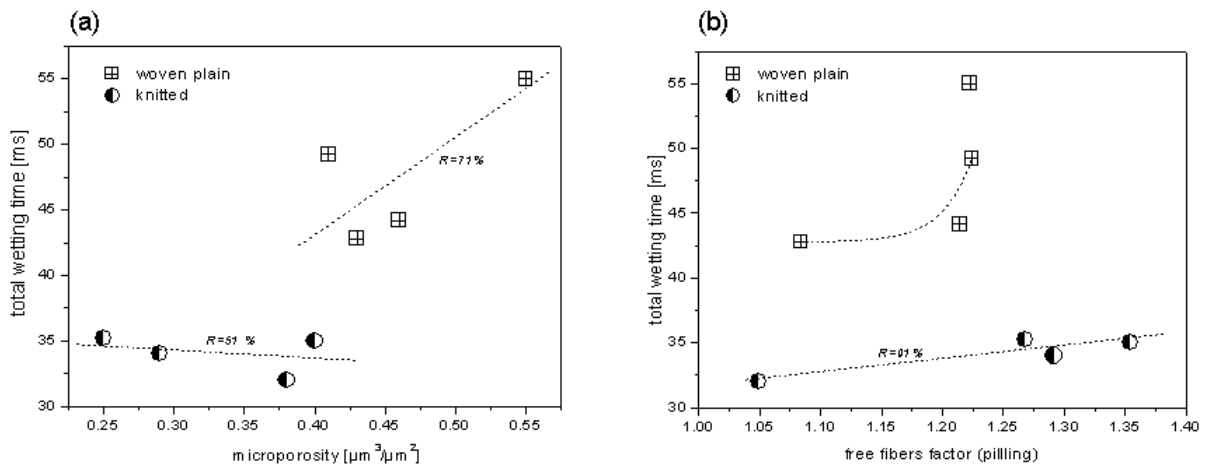


Figure 5.49 Microporosity (a) and free fibers (b) of woven plain influence strong on its water uptake by capillary.

A new concept to understand the relationship between wetting time of textile surface structures and textile topography at three different length scales was presented in Section 5.2.1.1, [151] and [162]. Applying this conceptual model to the woven plain surface, it presents an hydrophobic behaviour of wetting controlled by the solid fraction of the textile in contact with the liquid, that corresponds to Wenzel-Cassie model (Fig. 5.4): a higher microporosity means less points of contact, i.e. less solid

fraction between surface and water drop, leading to a more hydrophobic behaviour resulting in longer wetting times (*Fig. 5.49(a)*). If microporosity increases, the model mentioned predicts the existence of a state in which pores are large enough to enhance capillary, then the hydrophilic regime (wicking) begins and the slope of the curve turns negative; however, the value of the mentioned point depends on the surface morphology. Knitted fabric surfaces show a negative slope corresponding to the wicking regime, where capillary controls wetting.

In *Fig. 5.49(b)* an effect of pilling on wetting time of fabrics is noted: for knitted, free fibers tend to retard capillary. The same effect on the woven plain is exponential up to a maximum value of free fibers factor (*Fig. 5.40*). The effect of pilling is more important for woven plain compared to knitted fabrics, because for knitted fabrics free fibers do not represent any important mass compared to its more voluminous internal structure.

To investigate the effect of topography and wetting behaviour on soiling, an experiment with 5 μL drops of water soluble ink was performed. FibroDAT instrument was used to apply the soil on all the fabrics at the same measuring conditions having the same height and stroke pulse. 5 drops were applied on each sample. After drying, stained areas were averaging using a commercial scanner (1200 dpi) and OriginPro 8G image processing application software. Spots on woven plain fabrics have in average about 3 times more area than on knitted fabrics (*Fig. 5.50*).

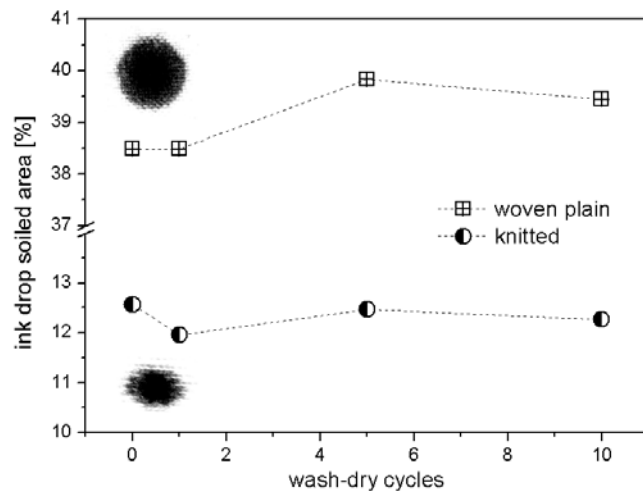


Figure 5.50
Soiling on woven plain fabrics leads to larger spots than on knitted fabrics.

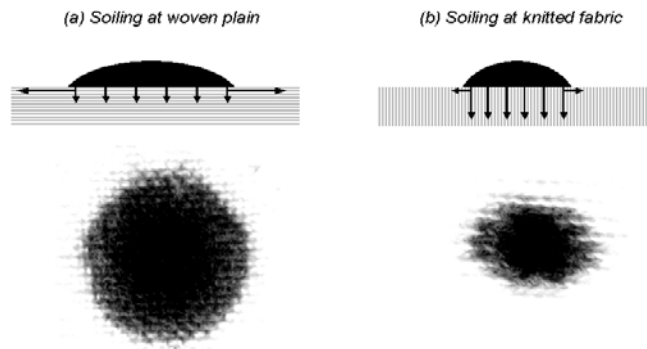
As can be seen in *Fig.5.48(a)*, spreading rate values for both fabrics are in the same interval (210 to 260 mm/s). However, for woven plain fabrics, longer wetting times (*Fig.5.48(b)*) indicate that horizontal diffusion of the drop ink by capillarity between yarns and fibers prevails over a rapid vertical penetration (*Fig.5.51*). As a consequence, larger and more superficial spots are observed. On the other hand,

shorter wetting times measured for knitted fabrics indicate a rapid penetration of ink drops into the structure, then smaller spot areas and deeper penetration. In both cases, the resulting spot area is controlled by macro-morphology –responsible for relaxation/shrinkage, yarns topology and pilling-, mesoporosity, and microporosity.

Figure 5.51

Topography of textile surfaces controls soiling.

- (a) longer wetting times indicate that horizontal diffusion of the ink drop by capillarity between yarns and fibers prevails over a rapid vertical penetration. Larger and more superficial spots.
- (b) Shorter wetting times measured by knitted fabrics indicates rapid penetration of ink drops into the structure. Smaller and deeper spots.



The woven plain morphology determines the surface to build larger and more superficial spots leading to a better soil release for woven plain fabrics. To prove this prediction, surface cleanability (Γ) of acetylene black (paraffin oil as liquid vehicle) was measured for both untreated fabrics according to the procedure described in Section 5.2.1.3. The surface cleanability of untreated woven plain calculated ($\Gamma = 60.97\%$) is two times larger than the obtained for untreated knitted fabrics ($\Gamma = 30.40\%$).

To investigate the correlation between the topographical effect of wash-dry cycles and soil release, the calculation of surface cleanability was done also for each modified woven plain surface. According to the results shown in *Fig. 5.52*, the topographical characteristics produced after 5 wash-dry cycles, perform the largest drop area and the best cleanability.

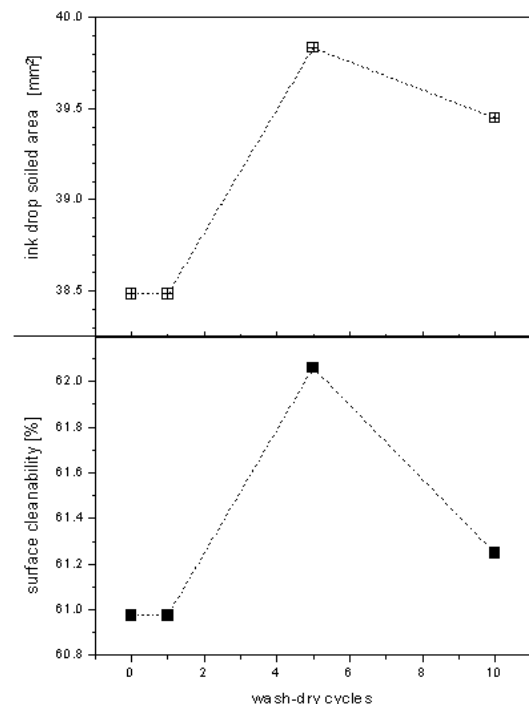


Figure 5.52
Effect of soiled area on cleanability at woven plain fabrics

High shrinkage and low pilling were observed for woven plain submitted to five wash-dry cycles. Shrinkage is the result of a considerable close of spaces between fibres, but the simultaneous effect is an increase of spaces between yarns. In other words, measured macro-morphological shrinkage is due to the contraction of yarns structure, that causes an increase of mesoporosity. These topographical changes are responsible of a higher spreading rate and shorter wetting time -rapid horizontal capillary-. The consequence is the formation of larger but superficial spots during soiling, resulting in better cleanability (*Fig. 5.53*).

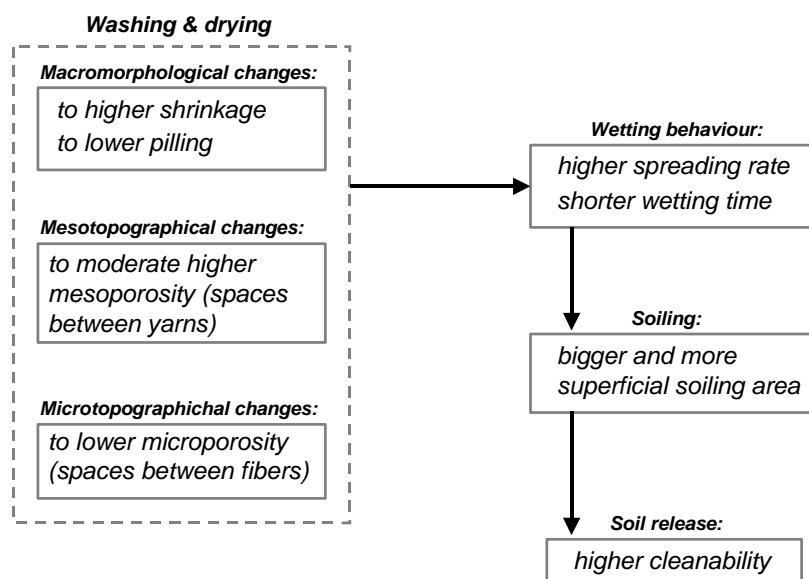


Figure 5.53
Topographical changes during wash-dry cycles that perform cleanability of woven plain cotton fabrics.

Sequential washing and drying or any kind of mechanical process lead to important topographical changes on textiles. For this reason, during the study of the effect of surfactants on soiling release, or the efficiency of textile reactive dyes [163], is very important to recognize independently the mechanical effect of the process from the physical-chemical effect of detergency or dyeing respectively. The present study is aimed to contribute to the investigation of this important topic by means of the topographical characterisation on different length scales.

6 Modelling of polymer surface topography by Fourier synthesis

In Section 4.1.8.1 a 'profile model' was used to study the cavities formation on SMC surfaces. Using periodic triangular waves, it is possible to study the effect of moulding time and pressure on topographic parameters and, therefore, on the resulting surface morphology.

Chapter 5 and other related recent studies [128,129] showed that textile construction parameters such as fineness of filaments and yarn, warp and weft density as well as the type of weave control the texture, morphology and surface topography of fabrics. Topography controls the surface porosity, which in turn strongly influences the textile characteristics such as fabric mass, thickness, draping ability, stress-strain behaviour or air permeability. Moreover, there are significant differences between the soiling behaviour and soil release of textile materials with different topographic structures despite the similarity of their chemical nature [130-132,134].

All semi-periodic and periodic surfaces, like modelled SMC and textile materials, show scaled horizontal and vertical repetitive unities, therefore, different length scales have to be taken into account by interpreting the topographic data measured, as demonstrated in [125,133], Chapter 4 and 5. In the present study, a novel wicking model was conceptually developed [162] on the basis of experimental results revealing differences in various fabric weave types in respect to water penetration. This model considers several length scales of surface roughness attributed to macro-, meso- and micro-regimes. The isolation and topographic characterisation on these length scales was possible by application of Fast Fourier Transformation (FFT) techniques, which are applied by the characterization of surface topography of solid materials [112-114].

Nicoll [164] synthesized textile textures using the concept of fractional Fourier analysis to perform a fully automatic separation of a global regular structure from an irregular structure. The synthesis is performed by generating a fractional Fourier texture mask from the extracted global regular structure, which is used to guide the generation of irregular texture details. However, this method enables only a realistic visualisation of structures, but does not give information about the resulting topography. Finckh [166] used a much more complicated numerical simulation of 3D fabrics by an explicit Finite Element Method.

Towards to a better understanding the relationship between polymer surfaces topography, their technical/construction parameters and interfacial phenomena such as adhesion and wetting, as well as to simulation and probing new related models, it is important to construct surfaces digitally by manipulating their parameters. The aim of the present Chapter is to show the potential of the Fourier synthesis in this respect.

6.1 Reconstruction of 2D-profiles using harmonic series

Topographic parameters of woven plain polyester fabrics used in Section 5.2.1.1 were characterized on three different length scales and studied in connection to the classical textile parameters:

- a) Macro-topographic scale, characterized by the average of distances between warps and wefts. Corresponding textile parameters are warp and weft densities.
- b) Meso-topographic scale, characterized on the basis of waviness and wave height (according to DIN EN ISO 4287), but using waviness (amplitude) values for warps and wefts separately. A textile parameter that describes relative heights of warps or wefts or their amplitudes is not available, but topographic characterization of woven fabrics have shown (cf. Section 5.2.1.1) that relative z-distances between warps and wefts and their wave (sinoidal) 'trajectory' influence strongly the fabric topography. According to measurements on woven, twill and Panama fabrics, wefts describe almost a linear 'trajectory' (their amplitudes are rather small). As a consequence, the first contact of any material with the fabric surface takes place by the warps surface and the final

penetration (or capillary) by fluids on the fabric surface takes place on wefts. This fact plays a very important role in the wetting behaviour of textile materials and shows how important is the characterisation of the meso-topography.

- c) Micro-topography was characterized by the mean height roughness (R_z) and arithmetic mean roughness (R_a), both measured according to DIN EN ISO 4287 for warps and wefts separately. Additionally, surface porosity (V_o , cf. Section 3.5.2.9) were included in this measure scale. Since the characterization of these topographic parameters was made after FFT-filtering of waviness over zoomed images of warps and wefts, R_z is related to the mean height of filaments, V_o represents the mean void volume between filaments and R_a characterizes the surface micro-topography of filaments. Then, R_z and V_o are controlled by the filament fineness and R_a by the filaments profiles.

6.1.1 Topographical synthesis by Fourier Series

For a woven plain structure, profiles of warps and wefts can be constructed separately by using the following sinoidal function, as a first approximation:

$$P(x) = a_1 \sin \omega x + a_k \sin k \omega x + a_m \sin m \omega x \quad (6.1)$$

$$\omega = \frac{2\pi}{T} \quad (6.2)$$

For each yarn profile, frequency ω and period T are used to control the macro-morphological scale and, thus, the yarn density, as explained previously. In the case of studying modification processes by washing, impregnation, ironing, thermofixing, plasma, etc., these values depend on the measured or expected relaxation/shrinkage.

The amplitude a_1 of a primary wave, which corresponds to the meso-morphological waviness described above, simulates the waviness depth of the yarn.

Porosity (V_o), which depends on the distance between filaments, can be simulated by the parameter $k > 1$, that generates a secondary wave. Mean rough height (R_z) can be simulated by the secondary amplitude a_k . Finally, another higher harmonic defined by the coefficient $m > 1$ and its correspondent amplitude a_m can be used to simulate the arithmetic mean roughness (R_a), which statistically represents the filament profile irregularities.

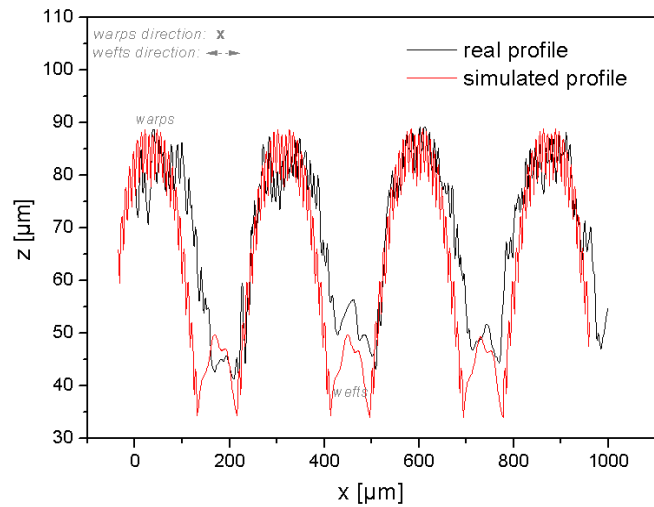


*Figure 6.1
Profiles of real (measured) and its simulated surface corresponding to a woven plain structure. Profile cut was made in wefts direction.*

Fig. 6.1 shows a comparison between a real (measured) profile and its simulated surface by using equations 6.1 and 6.2. and the input parameters given in *Table 6.1*.

6.2 Virtual 3D construction of the topography selecting and modifying topographic parameters

The generation of sinoidal cursor-functions, oriented in warps and wefts directions respectively, is necessary to describe the ‘trajectory’ of yarns in the 3D space. For a woven plain structure, the ‘trajectory’ of each yarn describes a maximum at the same time that it neighbors describe a minimum. For this reason, an alternated diphas of cursor waves is necessary by the warps as well as by the wefts [165]. This fact gives an additional advantage of simulate fabrics containing two different wefts and two different warps (*Fig. 6.2*).

The resulting surface is obtained by combining an adequate cursor-function with each one of the profiles and overlapping all resulting 3D-sinoids in the Cartesian space. Additional harmonics can be combined in order to describe more accurately yarn and filament profiles. The aim is always to relate the amplitudes and frequencies used with the textile elements and their classical parameters. To construct another

type of plain fabrics such as twill or Panama, an adequate selection and alternation of special cursor waves is necessary.

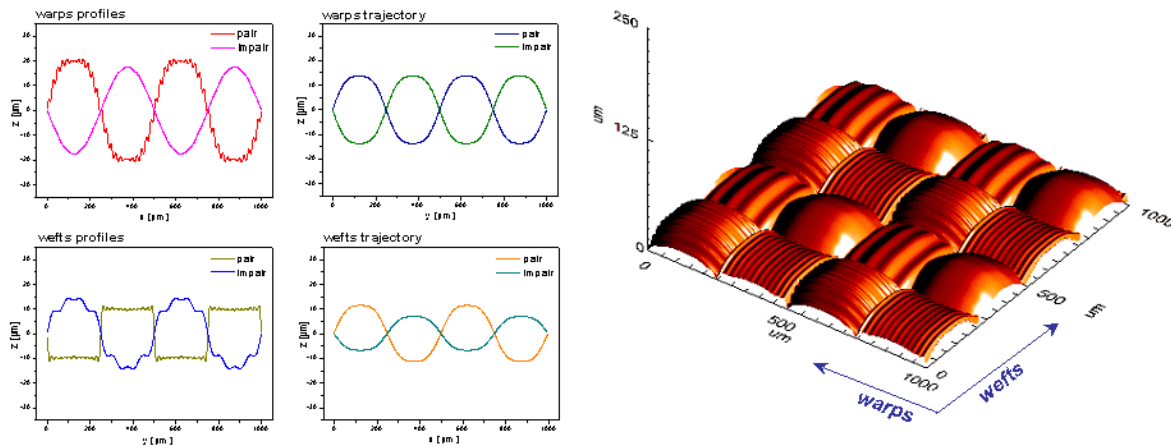


Figure 6.2 Cursor-functions and profiles (left). Result of combine cursor-functions with each one of the profiles and of the overlap of all resulting 3D-sinoids (right).

Fig. 6.3 shows a schematization of the analytical-synthetical process described above in order to construct a woven plain surface: measure and topographical characterization of a real surface (Fourier Analysis) followed by the generation of a virtual surface (Fourier Synthesis) by using the topographical parameters as an input of a system of equations similar to 6.1. In this case, 8 equations are needed: four for profile-waves and four for cursor-waves. A submicrometrical detail can be simulated by random or fractal texture generators.

Table 6.1 Topographic characterisation parameters of a real and simulated surface corresponding to a woven plain structure.

	whole topography						sub-area extractions			
	Max [μm]	Mean [μm]	W_z [μm]	R_{rl} -	R_z [μm]	R_a [μm]	R_z (warps) [μm]	R_z (wefts) [μm]	R_a (warps) [μm]	R_a (wefts) [μm]
cut-off length L_m [μm]	(1000)	(1000)	(1000)	(1000)	(1000)	(1000)	(135)	(65)	(135)	(65)
real surface	89.654	50.762	36.105	1.870	74.112	10.966	13.431	8.049	2.466	1.576
simulated surface	90.905	47.952	38.022	2.367	68.923	11.096	12.105	6.629	2.531	1.579

In Table 6.1 topographic parameters of a real surface measured by MicroGlider are presented in comparison to a simulated one. The topographical data measured have taken to generate a simulated surface using equations described above. New topographical parameters were obtained from the simulated surface, which slightly differs from the original. These differences are caused basically by obvious

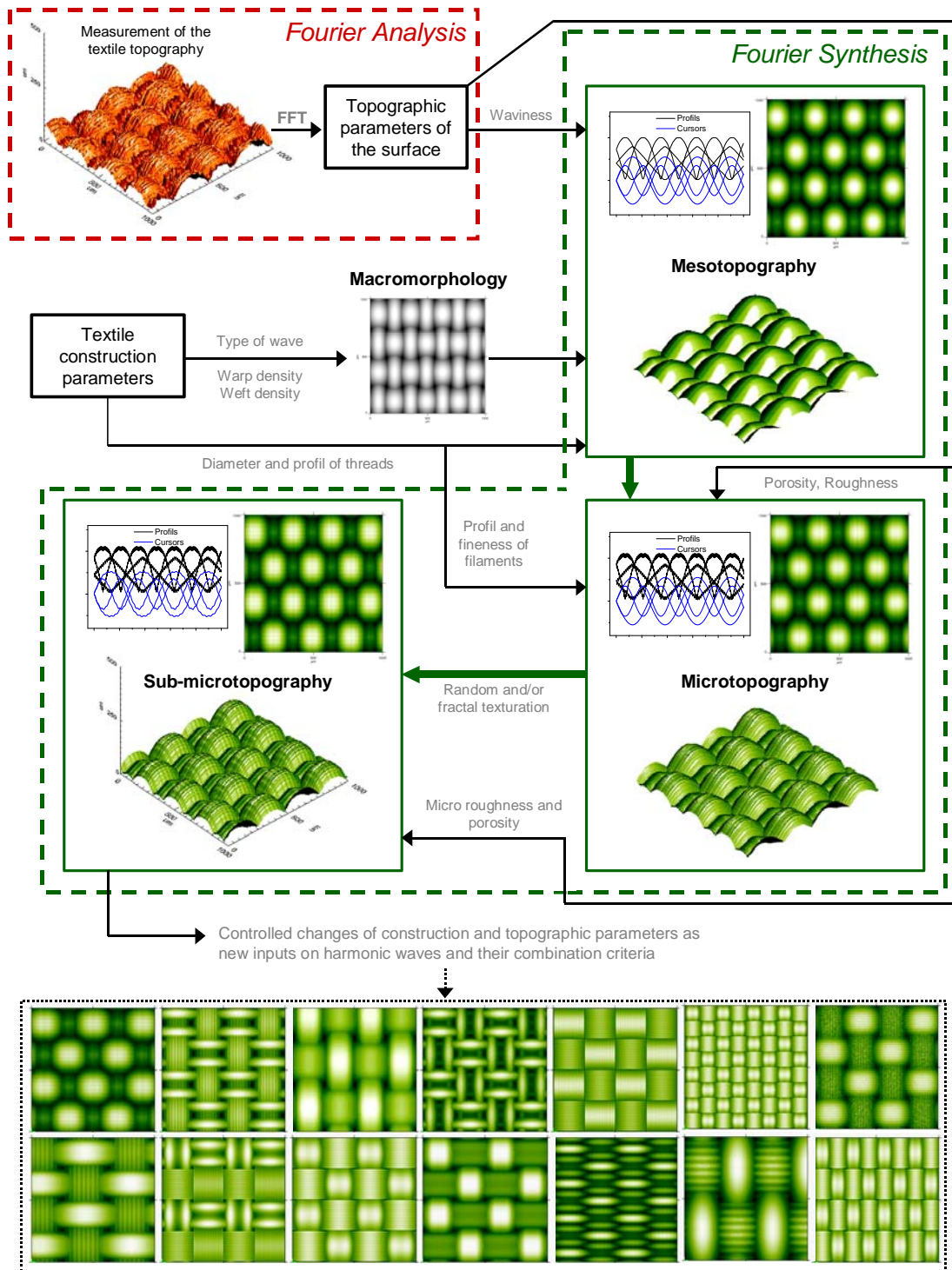


Figure 6.3 Schematization of the analytical-synthetic process.

inhomogeneities of a real surface, statistical character of the topographic parameters, mathematical efficiency of the FFT-algorithm used and by the number of harmonics used by the generation of each profile and cursor wave.

Simulated surface profile as illustrated in *Fig. 6.1* shows that the simulation process tends to produce wefts of lower height. This fact can be corrected by giving a new

amplitude to its cursor wave. A new run of the process could also include a new wavelength to reproduce more exactly the real warps density.

In order to study the porosity, both surfaces, the real and the simulated were characterised volumetrically, i.e. by calculation of debris volume of a material and the void volume enclosed by a flat surface and material debris. Void (filling) volumes were calculated at 30, 40, 50 and 60 μm height levels.

Fig. 6.4 shows that after the first run the simulated morphology by the 40 μm -level failed to reproduce the real one. Nevertheless, this deviation can be corrected by a new run, as suggested above.

Void volumes and their projected surfaces are shown in Fig. 6.5. A simulation of the projected surfaces is

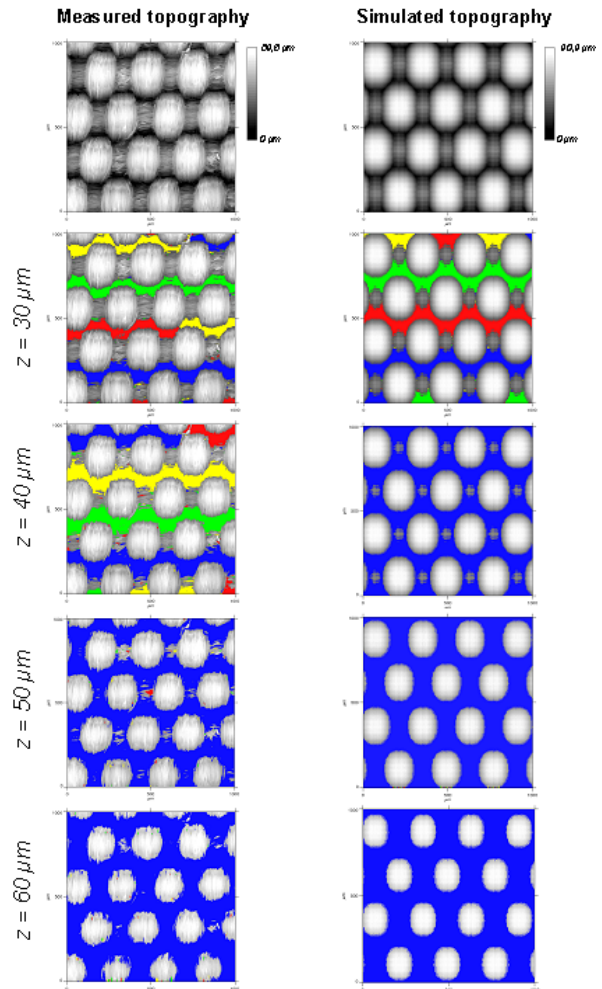
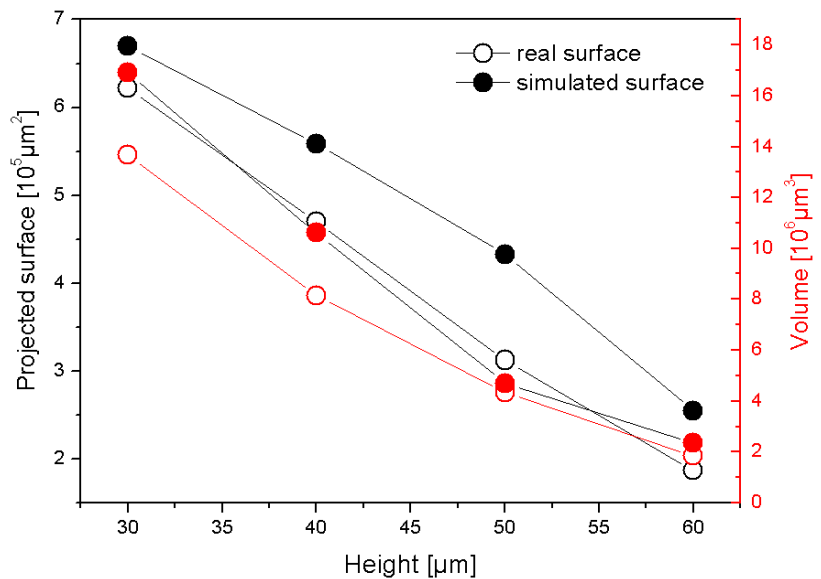


Figure 6.4
Projected surfaces of void (filling) volumes of a woven plain structure under different level-heights (z). Different colored areas represent unconnected cavities.

Figure 6.5
Void volumes and their projected surfaces for a woven plain structure measured at different heights.



much more difficult than to reproduce the void volumes. This fact is due basically to the natural surface inhomogeneities of the real surface.

In any case, the presented process conduces unequivocally to know a mathematical relationship between the textile and the topographical parameters. If topographical changes caused by modification are known, it is possible to use the model after reaching an optimal simulation in order to manipulate digitally the textile parameters and to obtain virtual modified surfaces.

6.3 Application of the model proposed to the studying polymer surfaces

The method presented above give possibilities to simulate controlled changes in the textile parameters and to study their effect on the resulting topography.

In this section three different applications of the method are described in order to predict and understand the effect of topographical changes on the wetting behaviour of textiles and the effect of moulding conditions on the surface quality of SMC.

6.3.1 Simulating surface modifications on polyester fabrics by thermofixing

In Section 5.2.1.2, the effect of thermo-mechanical changes (thermofixing) on topography and, as a consequence, on spreading, wetting and soiling of polyester fabrics were studied. For woven plain fabrics, five important changes in the topography were found:

- two-dimensional shrinkage,
- decrease of waviness,
- decrease of wefts micro-roughness,
- increase of warps micro-roughness and
- decrease of void volume (porosity).

These changes were justified (cf. *Fig. 5.23*) as responsible for the smaller spreading rates and extremely longer wetting times measured for thermofixed fabrics (cf. *Fig. 5.21*).

To study the effect of shrinkage and a decrease of waviness, eight different surfaces were generated using equations 6.1 and 6.2 by $a_m = 0$ as a first approach, applying the input values listed in Table 6.2.

Table 6.2 Input values to simulate thermofixing for polyester woven plain fabrics.

Surface	a_1 [μm]	waviness decrease [%]	a_k [μm]	k adim.	surface shrinkage [%]	$\lambda^{(1)}$ [μm]
Sim 1 (Reference)	78.208	0	0.3	12	0	326.1
Sim 2	71.855	-5	0.25	15	15.36	300.0
Sim 3	68.073	-10	0.25	15	15.36	300.0
Sim 4	64.291	-15	0.25	15	15.36	300.0
Sim 5	60.509	-20	0.25	15	15.36	300.0
Sim 6	56.728	-25	0.25	15	15.36	300.0
Sim 7	52.946	-30	0.25	15	15.36	300.0
Sim 8	49.164	-35	0.25	15	15.36	300.0

(1) distance between wefts or between warps

Fig. 6.6 demonstrates that the combination of surface shrinkage (5%) and a decrease of warps and wefts amplitude (waviness) is enough to produce a decrease of meso-porosity and wefts/warps micro-roughness. Meso-porosity controls spreading, and micro-roughness of yarns controls wetting time because of its proportionality with micro-porosity, as probed in Section 5.2.1.1. The closing of the spaces between yarns (meso-porosity) prevents spreading by making it shorter and slower. At the same time, less micro-porosity (spaces between filaments) prolongs

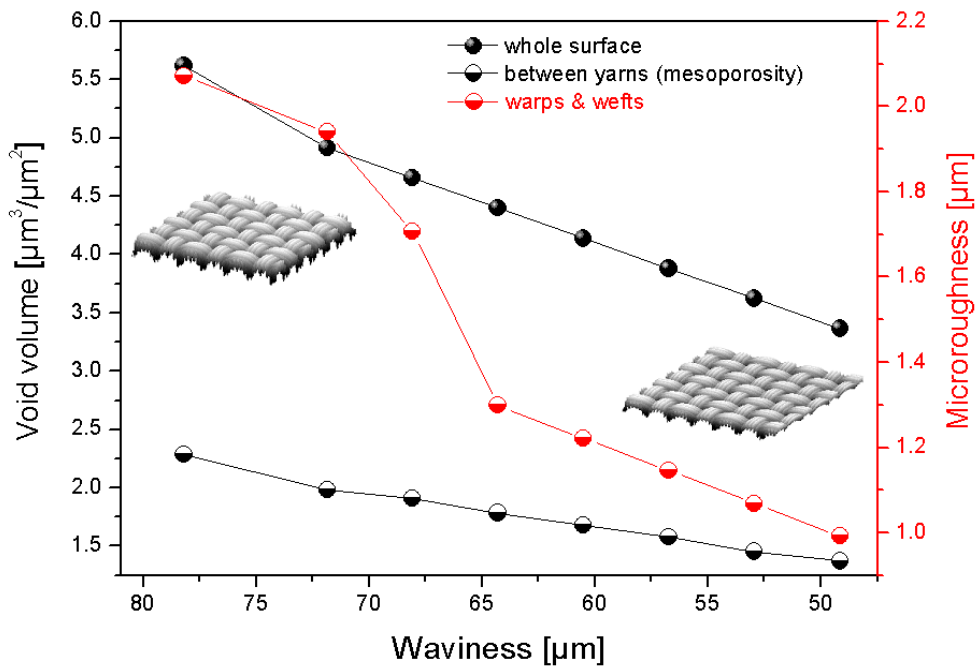


Figure 6.6 Simulation of thermofixing effect by shrinkage and decrease of warps/wefts amplitudes.

wetting in this case, which was experimentally demonstrated in Section 5.2.1.2 (cf. [Fig. 5.23](#)). The consequence is slower horizontal capillarity between filaments.

6.3.2 Simulating surface modifications on cotton fabrics by wash-dry cycles

In Section 5.2.2.1, the topographical effect of wash-dry cycles for cotton fabrics and their effect on soiling and cleanability was studied. According to the results, wash-dry cycles shrink the textile structure, but simultaneously increase spaces between yarns, because of an extraordinary closing of the spaces between cotton fibres. As a consequence, the new topography produces faster water spreading along the spaces between yarns (meso-porosity) but a slower penetration of water in shorter spaces between cotton fibres (micro-porosity). Under the new wetting conditions, a soil spot is larger but more superficial, resulting in better cleanability (cf. [Fig. 5.51](#)).

Topographical changes produced by wash-dry cycles for cotton woven plain fabric were simulated by generating virtual textile surfaces using the input data listed in [Table 6.3](#).

Table 6.3 *Input values to simulate washing and drying for a cotton woven plain fabric.*

Surface	a_1 [μm]	waviness increase [%]	a_k [μm]	k adim.	surface shrinkage [%]	$\lambda^{(1)}$ [μm]
Sim 1 (Reference)	78.208	0	0.300	12.000	0	326.1
Sim 2	85.012	8.70	0.270	13.333	15.36	300.0
Sim 3	91.816	17.39	0.243	14.815	27.43	277.8
Sim 4	98.612	26.09	0.219	16.461	37.10	258.6
Sim 5	105.424	34.78	0.197	18.290	44.95	241.9
Sim 6	112.228	43.48	0.177	20.322	51.42	227.3
Sim 7	119.032	52.17	0.159	22.580	56.82	214.3

(1) distance between wefts or between warps

According to [Fig. 6.7](#), surface shrinkage up to 20% and simultaneous expansion of wefts/warps amplitudes produce an increase of volume between yarns (meso-porosity) and a closing of the inter-fibres spaces, exactly that was found experimentally (cf. Section 5.2.2.1, [Fig. 5.42\(a\)](#) and [Fig. 5.42\(c\)](#)). The most important effect of these changes is the more rapid spreading because a fluid finds wider canals for its motion ([Fig. 5.48\(a\)](#)). At the same time, these spaces control the total wetting time of the liquid on a textile surface: more meso-porosity causes shorter wetting times ([Fig. 5.48\(b\)](#)).

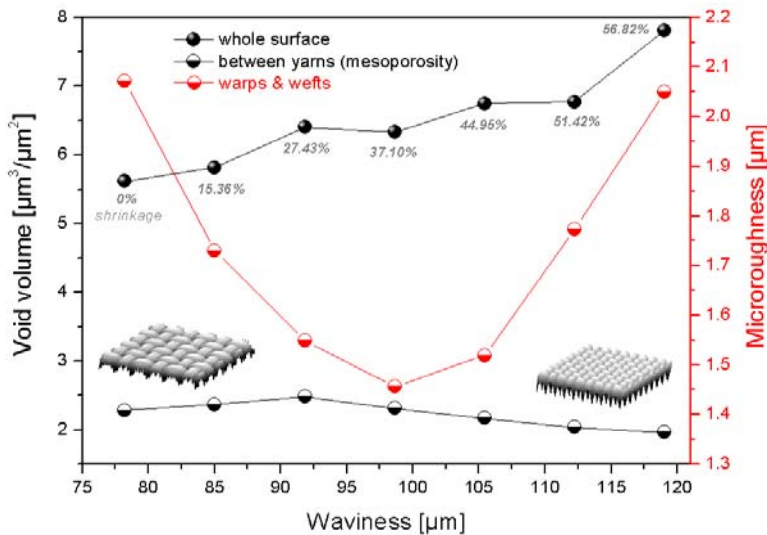


Figure 6.7 Simulation of wash-dry effect by sequential shrinkage and increase of warps/wefts amplitudes.

It is interesting to note, that by surface shrinkage (Fig. 6.7), the simulation predict a decrease of spaces between yarns and the existence of a minimal value of wefts/warps roughness. A subsequent shrinkage will produce an increase of wefts/warps roughness.

6.3.3 Simulating the effect of mould surface and mould/sheet separation on SMC topography

Special case of the model presented can be used to virtually recreate a SMC surface.

To construct the short waviness presented in Fig. 4.1(b), 2 surfaces having waving profiles (sinoidal as a first approach) in x- and y- direction respectively, have to be added in the Cartesian space. The amplitude of the resulting surface has to be adjusted to represent a desired surface waviness (W_z). Wave length has to be adjusted to reproduce empirical values, that in case of the studied SMC materials varies between 2 and 3 mm. Resulting surface is illustrated in Fig. 6.8(a).

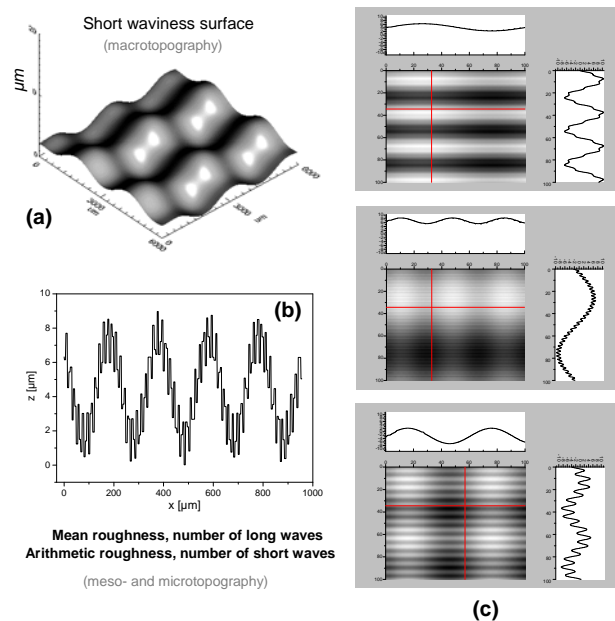


Figure 6.8 Simulated macrotopography (a), meso- and microtopography (b), and resulted SMC virtual surfaces (c).

Meso- and micro-morphology can be constructed by addition of two independent waves (*Fig. 6.8(b)*). The first of them has to be generated by using input values of R_z (mean roughness or amplitude of long waves) and N_z (number of long waves), and the second one by R_a (arithmetic roughness or amplitude of short waves) and N_a (number of short waves) according to what explained in Section 4.1.8.1.

30 surfaces ($L_m = 6 \text{ mm}$) have been reconstructed using input values listed in *Table 6.4*.

Table 6.4
Input values for the simulation of SMC surfaces.

Variable	Input values		
W_z [μm]	0.2	-	6
R_z [μm]	6	-	14
R_a [μm]	0.77		
N_z	35		
N_a	650		

Total area and total volume of cavities under defined threshold ($h = 6 \mu\text{m}$) were calculated for all the synthesized surfaces in order to qualify their coatability (cf. Section 4.1.8.2).

According to results (*Fig. 6.9*), the simulation makes possible to compare the impact of metallic mould surface and the influence of adhesion during mould-sheet separation, that according to Section 4.1.7, correlates with mean roughness and short waviness.

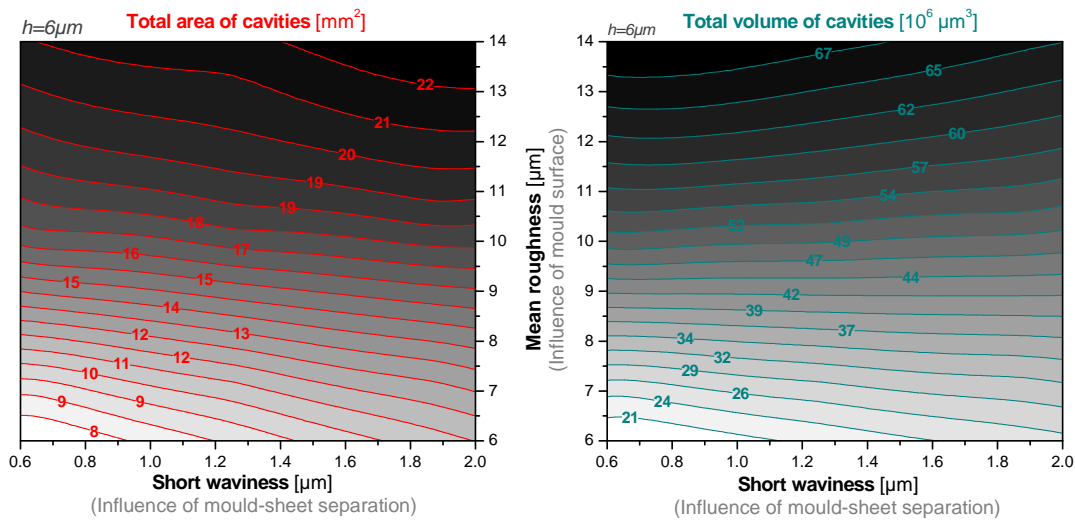


Figure 6.9 Impact of mould quality and mould sheet separation on resulting SMC surface quality in compare.

As a relevant conclusion, a mould surface influences stronger on the formation of cavities than adhesion between metallic mould and sheet during their separation.

7 Conclusions

In the study presented, non-contact chromatic confocal imaging was chosen and justified as the optimal measuring method for studying and correlating surface topography and surface properties of SMC materials as well as polyester and cotton fabrics. Before topographical characterisation, an adequate selection of optimal sampling conditions (cut-off length and resolution) were done by a systematic procedure proposed for periodic and non periodic surfaces.

Topographical characterisation of the surfaces was realized by an innovative method separately considering different length scales in dependence on the surface morphologies of materials under investigation.

For SMC materials, the influence of moulding conditions (pressure, moulding time, metallic mold topography, metallic mold form, prepregs placement procedure, glass fibres content and orientation) on resulting macro-, meso- and micro-topography was studied. After analysing the topographic characterisation parameters calculated on macro-, meso- and micro- length scales manufactured at constant temperature, it was possible to present a model to conceptualize the influence of each of the most important moulding conditions on topographic variables and, as a consequence, on the quality of the resulting surface. To quantify the effect of surface modification treatments, a new parameter (Surface Relative Smooth) was described, applied and probed, which can be used for the characterisation of surface modification of any solid material.

Wetting experiments results for SMC surfaces given by measuring static contact angles with water drops, indicate that measured contact angles correlate with the meso-topography if the surface morphology remains invariable due to influence of the same metallic mould surface. Independently of mould position, a linear relationship between wetting and meso-morphology was revealed. Larger pores

decrease the contact angle, that corresponds to the Wenzel regime of surface wetting.

A very important and innovative part of the present study is the development of new concepts of the topographic characterisation of textile materials using different length scales, that makes possible to consider and analyse separately their specific morphologies caused by weave, yarn and filament/fibres, and to investigate the influence of topography on wettability by modification processes, e.g. construction parameters, thermofixing, impregnation with SRP and wash-dry cycles.

The present study showed, how construction parameters of polyester textiles, such as fineness of filaments and yarn, warp and weft densities as well as the type of weave, control the surface topography - characterized as meso-porosity (spaces between yarns) and micro-porosity (spaces between filaments) - and as a consequence strongly influences capillarity. On the basis of experimental results, revealing differences in three basic types of woven fabrics - plain, twill and Panama – in respect to water penetration, the concept of an innovative novel wicking model was developed.

Thermofixing of polyester textiles was probed to modify the yarns amplitude and porosity, which leads to changes in the wetting behaviour according to the type of weave, morphology, topography and yarns characteristics. These changes influence strongly the soiling behaviour which results in larger but superficial spots due to modification in the capillarity capability of yarns. To characterise the soiling behaviour, an innovative 'spot analysis method' was presented, allowing the study of anisotropic wetting dynamic of fabrics. This method is applicable also to surfaces with anisotropic roughness and porous media.

The influence of impregnation with Soil Release Polymers (SRP) on topography, wetting and cleanability of three woven plain polyester fabrics having different wefts were as well studied. Topographical characterisation did not detect any film formation or SRP agglomeration in the spaces between filaments, but the impregnation leads to micro-topographical changes in the spaces between filaments, especially in wefts, whose micro-roughness controls wetting dynamics. Wetting characteristics, in turn, have been probed to control the penetration of soils and their release. According to results, a critical value of micro-roughness seems to allow a

maximum of cleanability and then the best effect of SRP impregnation on soil release.

The effect of wash-dry cycles on topography of woven plain and knitted cotton fabrics was in addition studied. Topographic characterization of textile surfaces shows that the relationship between macro-, meso- and micro-topography depends on type of weave. Mechanical effect of wash cycles also leads to surface tear and pilling that, combined with the relaxation-shrinkage effect, can produce additional changes not only in the meso- but also in micro-porosity (spaces between fibers) of the fabrics. As an important conclusion, more or less presence of free water inside the cotton fabrics does not control the water absorption capability by capillary. According to the results, for knitted structures a total amount of absorbed water does not depend on pilling. For woven plain, the fabric density especially controls the total water absorption capability. On the other hand, more intricate geometrical structure of knitted fabric makes difficult to interpret the optimal conditions for capillarity. The effect of wash-dry cycles on spreading, wetting and soiling was as well studied. In the case of woven plain structures, shrinkage is the result of a considerable decrease of spaces between fibres, but a simultaneous effect an increase of spaces between yarns. In other words, measured macro-morphological shrinkage is due to the contraction of yarns interior structure, that causes an increase of meso-porosity. These topographical changes are responsible for a higher spreading rate, and rapid and longer horizontal capillary penetration between yarns. As a consequence, a formation of larger, but superficial spots while soiling, that, in turns, leads to better soil release.

In all cases studied, the topographical characterisation and interpretation of results on different length scales contributed to a better understanding of the wetting phenomena.

Finally, a mathematical model to virtual construction and prediction of effects resulting from topographic changes on the behaviour of polymer and textiles surfaces was developed. Woven plain textiles and SMC surfaces were mathematically synthesized by a combination of various harmonic waves, i.e. Fourier synthesis. Topographic and technical construction parameters were taken into account to build their virtual topographies. In the case of textile surfaces, on the basis of the real topography of a given textile surface, it was possible to investigate the effect of wash-dry cycles for cotton fabrics and thermofixing for polyester fabrics on their meso- and

micro-morphology. The model allows to predict changes in the porosity of the resulting textile, its wetting and soiling behaviour. The use of additive Fourier series makes this method even simpler, faster and more topography-oriented than a numerical simulation of 3D-fabrics by an explicit Finite Element Method presented by other groups. Moreover, by using a directed random generation and/or fractal geometry, the way to a more realistic model of a given yarn or filament surface is open. The method presented also opens possibilities to simulate controlled changes in textile construction parameters and to study their effect on the resulting topography. For this reason, the model could be applied to design of functional textile surfaces. By applying the model to construct virtual SMC surfaces, it was possible to quantify and compare the influence of metallic mould surface and undesired adhesion during mould-sheet separation on the resulting SMC surface quality.

8 References

- [1] Wendt, U.; Stiebe-Lange, K.; Smid, M. (2002), "On the influence of imaging conditions and algorithms on the quantification of surface topography", *Journal of Microscopy* **207**: 169-179.
- [2] Stout, K.J.; Sullivan, P.J.; Dong, W.P.; Mainsah, E.; Luo, N.; Mathia, T.; Zahouani, H. (1993), *The development of methods for the characterisation of roughness in three dimensions*, Brussels-Luxemburg: Commission of the European Communities, Brussels-Luxembourg, ISBN 0 7044 1313 2
- [3] Beck, U. (2007), "Bestimmung der Topographie technischer Oberflächen und der Haftfestigkeit an beschichteten Bauteilen", *Galvanotechnik* **10**: 2377-2387.
- [4] Fries Research & Technology GmbH (October 2008), *Basis FoRT-Bildung 01, FRT Metrologie Seminar*, Bergisch-Gladbach.
- [5] Contet, Ph.; Ville, J-F. (1995), "Surfscan 3D – an industrial 3D surface texture characterisation instrument", *Int. J. Mach. Tools Manufact.* **35**: 151-156.
- [6] Garatt, J.D. (1982), "A new stylus instruments with a wide dynamic range for use in surface metrology", *Precision engineering* **3**: 145-151.
- [7] Liberman, A.G.; Vorburger, G.H.W.; Risko, D.G.; Resnick, T.; Rose, J. (1965), "Capacitance versus stylus measurement of surface roughness", cited by [2].
- [8] Blessing, G.V.; Eitzen, D.G. (1988), "Surface roughness sensed by ultrasound", *Proc. 4th Int. Conf. Metrology and Props. of Engineering Surfaces*, Washington.
- [9] Arechi, F.T.; Bertani, D.; Cileberto, S. (1979), "A fast versatile optical profilometer", *Optics communic.* **32-33**: 260-266.
- [10] Gorecki, C.H.; Tribillon, G.; Mignot, J. (1983), "Profilomètre optique en lumière blanche", *J. Optics* **14**(1): 19-23.
- [11] Sayles, R.S. ; Wayte, R.C. ; Twee Dale, P.J. ; Brissoc. B.J. (April 1988), "The design construction and commissioning of an inexpensive prototype laser optical profilometer", *Proc. 4th Int. Conf. on Metr. and Props. of Eng. Surf.*
- [12] Lee, C.S.; Kim, S.W.; Yim, D.Y. (1987), "An in-process measurement technique using laser for non-contact monitoring of surface roughness and form accuracy of ground surfaces", *Annals of the CIRP* **36**.
- [13] Beckmann, P.; Spizzichino, A. (1963), *The Scattering of Electromagnetic Waves from Rough Surfaces*, Pergamon Press, Oxford, ISBN-13: 9780080134888.
- [14] Biegen, J.F.; Smythe, R.A. (April 1988), "High resolution phase measuring laser interferometric microscopy for engineering surface metrology", *4th Int. Conf. on Metr. and Props. of Eng. Surf.*
- [15] Bhushan, B.; Wyaut, J.C.; Koliopoulos, C.L. (1985), "Measuring of surface topography of magnetic tapes by Mirau interferometer", *Applied Optics* **24** (10): 1489-1497.
- [16] Kalaidji, D. (1984), *Réalisation d'un interféromètres holographique hétérolyne. Application à la mesure des déformations*, Dissertation.
- [17] Wyant, J.C., *White Light Interferometry (PDF)*, Optical Sciences Center, University of Arizona, Tucson, (http://www.optics.arizona.edu/jcwyant/pdf/meeting_papers/whitelightinterferometry.pdf).
- [18] Hehl, K., Hertzsch, A., Kröger, K. (2003), "Topographiemessungen technischer Oberflächen mit einer Streulichtanordnung", *INNOVENT e.V. Technologieentwicklung Jena, Technisches Messen* **70**: 4-9.
- [19] Hertzsch, A.; Kröger, K.; Truckenbrodt, H. (2002), "Microtopographic analysis of turned surfaces by model-based scatterometry", *Precision Engineering* **26**: 306-313.
- [20] Hingle, H.T.; Rakels, J.H. (1983), "The practical application of diffraction techniques to assess surface finish of diamond turned parts", *Annals of the CIRP* **32**(1): 499-501.

- [21] Brodmann, R.; Rodenstock, R.; Gast, M.; Thurm, G. (1984), "An optical instrument for measuring the surfaces roughness in production control", *Annals of the CIRP* **33**(1): 403-406.
- [22] Stover, J.C. (1975), "Roughness characterisation of smooth machine surfaces by light scattering", *Applied optics* **14**(8): 1796-1802.
- [23] Fujii, H.; Asakura, T. (1977), "Roughness measurements of metal surfaces using laser Speckle", *Journal of the Optical Society of America* **67**(9): 117.
- [24] Leger, D.; Mathieu, E.; Perrin, J.C. (1975), "Optical surface roughness determination using speckle correlation technique", *Applied optics* **14** : 972-977.
- [25] Tribillon, G. (1974), "Corrélation entre deux speckles obtenus avec deux longueurs d'onde. Application à la mesure de rugosité", *Optics Communications* **11** : 172-174.
- [26] Parry, G. (1974), "Some effects of surface roughness on the appearance of speckle in polychromatic light", *Optics Communications* **12**: 75.
- [27] Müller, T.; Kumpe, R.; Gerber, H.A.; Schmolke, R.; Passek, F.; Wagner, P. (2001), "Techniques for analysing nanotopography on polished silicon wafers", *Microelectronic Engineering* **56**: 123-127.
- [28] Albrecht, P.; Michaelis, B. (August 1998), Stereo Photogrammetry with Improved Spatial Resolution, *Proceedings of Fourteenth International Conference on Pattern Recognition* **1**: 845-849.
- [29] A Practical Guide to SPM (2005), Veeco Instruments Inc. (<http://www.veeco.com/>)
- [30] Suganuma, T. (1985), "Measurement of Surface Topography Using SEM with Two Secondary Electron Detectors", *Journal of electron microscopy* **34**(4): 328-337.
- [31] Kodama, T.; Li, X.; Nakahira, K.; Ito, D. (2005), "Evolutionary Computation Applied to the Reconstruction of 3-D Surface Topography in the SEM", *Journal of electron microscopy* **54**(5): 429-435.
- [32] Shotton, D.M. (1989), "Confocal scanning optical microscopy and its applications for biological specimens", *Journal of Cell Science* **94**: 175-206.
- [33] Wilson, T. (1990), *Confocal Microscopy*, London: Academic Press, ISBN 0-12-757270-8.
- [34] FRT, Fries Research & Technology GmbH, Bergisch-Gladbach, Germany (<http://www.frt-gmbh.com/de/>).
- [35] Wiesendanger, F.; Körner, K.; Ruprecht, A.K.; Windecker, R.; Tiziani, H.J.; Osten, W. (2004), "Fast confocal point-sensor for in-process control of laser welding", *Proceedings of International Conference on Laser Applications and Optical metrology*, New Delhi, 336-339.
- [36] Wiesendanger, F.; Ruprecht, A.; Pedrini, G.; Körner, K.; Tiziani, H.J.; Osten, W.; Zaslansky, P.; Weiner, S. (2003/2004), "Full Field, Fast Confocal Laser Microscopy for Measuring the Mechanical Properties of Cortical Bone", *Annual Report, Institut für Technische Optik, Universität Stuttgart*.
- [37] Solarius Development Inc., Sunnyvale, California, USA (<http://www.solarius-inc.com>).
- [38] Breitmeier Messtechnik GmbH, Ettlingen, Germany (<http://www.breitmeier.com>).
- [39] Mugnier, L. (1995), "Conoscopic Holography: Toward Three-Dimensional Reconstructions of Opaque Objects", *Applied Optics* **34**(8): 1363-1371.
- [40] Optical Metrology Ltd., Jerusalem, Israel (<http://optimet.com>).
- [41] Depeursinge, Ch. ; Charrière, F.; Montfort, F. (2006), "Digital Holographic Microscopy for Comparative Metrology in Micro-Optics and MOEMs", *Technisches Messen* **73**(3): 172-179.
- [42] Kemper, B.; von Bally, G. (2007), "Digital holographic microscopy for live cell applications and technical inspection", *Applied Optics* **47**(4): A52-A61.
- [43] Baumbach, T.; Osten, W.; von Kopylow, C.; Jüptner, W. (2006), "Remote metrology by comparative digital holography", *Applied Optics* **45**: 925-934.

- [44] Kohler, C.; Schwab, X.; Proll, K.-P.; Osten, W. (2003/2004), "Evaluation and Characterization of Liquid Crystal SLMs for Digital Comparative Holography (DISCO)", *Annual Report, Institut für Technische Optik, Universität Stuttgart*.
- [45] Sciences et Techniques Industrielles de la Lumière, France (<http://www.stilsa.com/>).
- [46] Ruprecht, A.K.; Körner, K.; Wiesendanger, T.F.; Tiziani, H.J.; Osten, W.; Lücke, P. (September 2005), "Chromatic confocal sensors for micro-topography measurements", *50. Internationales Wissenschaftliches Kolloquium der TU Ilmenau: Maschinenbau von Mikro bis Nano*.
- [47] Ruprecht, A.K.; Körner, K.; Wiesendanger, T.F.; Tiziani, H.J.; Osten, W. (2004), "Chromatic confocal detection for high speed micro-topography measurements", *Proceedings of SPIE*, 5360-61
- [48] Micro-Epsilon Messtechnik GmbH & Co. KG, Ortenburg, Germany (<http://www.micro-epsilon.com>).
- [49] Pawley JB, editor (2006), *Handbook of Biological Confocal Microscopy*, Berlin: Springer, 3rd ed.; ISBN 038725921x
- [50] Leica Microsystems GmbH, Wetzlar, Germany (<http://www.leica-microsystems.com>).
- [51] Alicona Imaging GmbH, Grambach, Austria (<http://www.alicon.com/>).
- [52] NanoFocus AG, Oberhausen, Germany (<http://www.nanofocus.de>).
- [53] Droste, U.; Körner, K.; Goretzky, A.; Osten, W.; Lehmann, P. (2004/2004), "A new white light interferometer", *Annual Report, Institut für Technische Optik, Universität Stuttgart*.
- [54] Shabana, H.M.(2004), "Determination of film thickness and refractive index by interferometry", *Polymer Testing* **23**: 695-702.
- [55] Fogt, N.; King-Smith, P.E.; Tuell, G. (1998), "Interferometric measurement of tear film thickness by use of spectral oscillations", *J. Opt. Soc. Am.* **A15**: 268-275.
- [56] Marklund, O.; Gustafsson, L. (2001), "Interferometry-based measurements of oil-film thickness", *Proceedings of the I MECH E Part J, Journal of Engineering Tribology* **215** (3-17): 243-259.
- [57] King-Smith, P.E.; Fink, B.A.; Nichols, J.J.; Nichols, K.K.; Hill, R.M. (2006), "Interferometric imaging of the full thickness of the precorneal tear film", *J. Opt. Soc. Am.* **A23**: 2097-2104.
- [58] Kampffmeyer, G. (1977), "Self-Supporting Thin-Film Beam Splitter for Far-Infrared Interferometers", *Applied Physics* **14**: 313-317.
- [59] Lewandowski, J. ; Mongeau, B. ; Cormier, M.(1984), "Real-time interferometry using IR holography on oil films", *Applied Optics* **23**: pp. 242-244.
- [60] Lechthaler, M.; Bauer, W. (2006), „Rauigkeit und Topographie – ein Vergleich unterschiedlicher Messverfahren“, *Wochenblatt für Papierfabrikation* **21**: 1227-1234.
- [61] *Assessment of Surface Texture, Part 1. Methods and Instrumentation* (1988), British Standard BS 1134.
- [62] *Surface Texture: Surface Roughness, Waviness and Lay* (1985), American Standard ANSI B.46.1.
- [63] *Surface Roughness – Terminology, Part 1: Surface and its Parameters* (1984), International Standard ISO 4287/1.
- [64] Reason, R.E.(1961), "Report on reference lines for roughness and roundness", *CIRP Annalen*, **XI**(2): 95-104.
- [65] Whithesouse, D.J. (1972), "Surface of reference line in the assessment of surface texture", *Annals of the CIRP*, **21**(2): 267-273.
- [66] *British standard specification for surface plate* (1988), British Standards Institution, BS 817.
- [67] ISO/R110/I-1969
- [68] De Bruin, W. ; Meijer, J.; Nawijn, A. (1977), "Surface plate measurements", *Annals of the CIRP* **25**(1): 251-256.

- [69] Chetwynd, D.G. (1985), "Applications of linear programming to engineering metrology", *Proc. Inst. Mech. Engrs.* **199** B-2: 93-100.
- [70] Shunmugam, M.S. (1987), "Comparison of linear and normal deviations forms of engineering surfaces", *Precision Engineering*, **9**(2): 96-102.
- [71] *Assessment of surface texture: Part 1: Methods and Instrumentation* (1988), British Standard BS 1134.
- [72] *Surface Texture: Surface roughness, waviness and lay* (1985), American Standard ANSI B.46.1.
- [73] Christensen, R. (1984), *Data distributions - a statistical handbook*, Entropy Limited, ISBN-10: 0938876171.
- [74] Whitehouse, D.J.; Archard, J.F. (November 1969), "The properties of random surfaces in contact", *ASME Winter Annual Meeting*: 36-37.
- [75] King, T.G.; Spedding, T.A. (1983), "Towards a rational surface profile characterisation system", *Precision Engineering* **5**(4): 153-160.
- [76] Selvam, M.S.; Balakrishnan, K.(1977), "The study of machined surface roughness by random analysis", *Wear* **41**: 287-293.
- [77] Longuet-Higgins, M.S. (1957), "The statistical analysis of a random, moving surface", *Philosophical Transactions of the Royal Society* **249-A**: 321-384.
- [78] Longuet-Higgins, M.S. (1957), "Statistical properties of an isotropic random surface", *Philosophical Transactions of the Royal Society*, **250-A**: 157-174.
- [79] Nayak, P.R. (July 1971), "Random process model of rough surfaces", *Journal of Lubrication Technology, Transactions of the ASME*: 384-407.
- [80] Sayles, R.S.; Thomas T.R. (1979), "Measurements of the statistical microgeometry of engineering surfaces", *Journal of Lubrication Technology, Transactions of the ASME* **101**: 409-418.
- [81] DeVries, W.R. (1982), "A three-dimensional model of surface asperities developed using moment theory", *Journal of Engineering for Industry, Transactions of the ASME* **104**: 343-348.
- [82] Box, G.E.P.; Jenkins, G.M. (1994), *Time Series Analysis Forecasting and Control*, San Francisco: Prentice Hall, 3rd edition, ISBN-10: 0130607746.
- [83] Pandit, S.M.; Wu, S.M. (1983), *Time series and system analysis with applications*, Krieger Publishing Company, ISBN-10: 1575241692.
- [84] Watson, W.; King, T.G.; Spedding, T.A.; Stout, K.J. (1979), "The machined surface-time series modelling", *Wear* **57**: 195-205.
- [85] Watson, W. (1988), "The 3D representation of engineering surfaces", *Surface Topography* **1**: 165-182.
- [86] You, S.J.; Ehmenn, K.F. (1991), "Computer synthesis of three-dimensional surfaces", *Wear* **145**: 29-42.
- [87] Whitehouse, D.J. (1982), "The parameter rash – is there a cure?", *Wear* **83**: 75-78.
- [88] *DIN, Measurement of Surface Roughness: R_k , R_{pk} , R_{vk} , M_{r1} , M_{r2} for the Description of the Material Portion in the Roughness* (1990), German Standard, DIN 4776.
- [89] *E00.14.015.N – Aout: Etats geometriques de surface calcul des criteres de profil* (1983), C.N.O.M.O.
- [90] Davis, E.J. ; Sullivan, P.J. ; Stout, K.J. (1988), "The application of 3D topography to engine bore surfaces", *Surface Topography* **1-2**: 229-251.
- [91] Bodschwinn, S.U.; Mikro-Emo, S.U. (1987), "Funktionsgerechte rauheitskennwerte durch auswerten der Abbott-Kurve", *Antriebstechnik* **26**(9): 65-69..
- [92] Fahl, C.F. (1982), "Motif combination – a new approach to surface profile analysis", *Wear* **83**: 165.179.
- [93] Boulanger, J. (1992), "The 'motifs' method: an interesting complement do ISO parameters for some functional problems", *Int. J. Mach. Tools Manufact.*, **32** (1-2): 203-209.

- [94] Roques-Carnes, C. ; Wehbi, D. ; Quiniou, J.F. ; Tricot, C. (1988), "Modelling engineering surfaces and evaluating their non-integer dimension for application in material science", *Surface Topography* **1**: 435-443.
- [95] Wehbi, D. (1986), *Fractal approach to surface roughness and analytical implications*, PhD. Thesis, ENSMM Besancon.
- [96] Thomas, T.R.; Thomas A.P. (1988), "Fractals and engineering surface roughness", *Surface Topography* **1**(2): 143-152.
- [97] Gagnepain, J.J. ; Roches Carnes, C. (1986), "Fractal approach to two-dimensional and three-dimensional surface roughness", *Wear* **109**: 119-126.
- [98] Majumdar, A.; Bhushan, B. (1991), "Fractal model of elastic-plastic contact between rough surfaces", *Trans. of ASME, Journal of Tribology* **113**: 1-11.
- [99] Zhou, G.Y.; Leu, M.C.; Blackmore, D. (1995), "Fractal geometry modelling with applications in surface characterisation and wear prediction", *Int. J. Mach. Tools Manufact.* **33**(2): 203-209.
- [100] Brown, C.A.; Savary, G. (1991), "Describing ground surface texture using contact profilometry and fractal analysis", *Wear* **141**: 211-226.
- [101] Kirk, T.B.; Stachowiak, G.W.; Batchelor, A.W. (1991), "Fractal parameters and computer image analysis applied to wear particles isolated by ferrography", *Wear* **145**(2): 347-365.
- [102] Zhou, J.G.; Leu, M.B.; Blackmore, D. (1993) (1993), "Fractal Geometry Model for Wear Prediction", *International Journal of Wear* **170**(1): 1-14.
- [103] Mandelbrot, B.B. (1977), *The fractal geometry of nature*, San Francisco: Freeman, ISBN 0-7167-1186-9
- [104] Jordan, D.L.; Hollins, R.C.; Jakeman, E. (1986), "Measurement and characterisation of multiscale surfaces", *Wear* **109**: 127-134.
- [105] Ling F.F. (1990), "Fractals, engineering surfaces and tribology", *Wear* **136**: 141-156.
- [106] Wallach, J. (1969), Surface topography description and measurement, *Proceedings of ASME Symposium on Surface Mechanics* **1**: 23.
- [107] Sherrington, I.; Smith, E.H. (1990), "Areal Fourier analysis of surface topography - Part 1: Computational methods and sampling considerations", *Surface Topography* **3**(1): 43-68.
- [108] Bendat, J.S.; Piersol, A.G. (2000), *Random data : analysis and measurement procedures*, Wiley Series in Probability and Statistics, ISBN-10: 0-471-31733-0.
- [109] Kalil, R.C. (May 2004), *Evaluation of frictional characteristics of precision machined surfaces*, Ms.Sc. Thesis in Mechanical Engineering, Woodruff School of Mechanical Engineering, Georgia Institute of Technology: 39-49.
- [110] Pratt, W.K. (1991), Digital Image Processing, 2nd. ed., Wiley, New York, ISBN 0-471-37407-5.
- [111] Brigham, E.O. (1988), *The Fast Foutier Transform and its applications*, N.J.: Prentice Hall, ISBN 0-13-307505-2.
- [112] Raja, J.; Radhakrishnan, V. (1978), "Waviness separation in surface profiles using digital filters", *Eng. Prof. (New Delhi)* **2**: 139-144.
- [113] Raja, J.; Radhakrishnan, V. (1977), "Analysis and synthesis of surface profiles using Fourier series", *Int. J. Mach. Tool. Des. Res.* **17** : 245-251.
- [114] Raja, J.; Radhakrishnan, V. (1979), "Filtering of surface profiles using fast Fourier transform", *Int. J. Mach. Tool. Des. Res.* **19**: 133-141.
- [115] Raja, J.; Radhakrishnan, V. (1979), "Digital filtering of surface profiles", *Wear* **57**: 147-155.
- [116] Dong, W.P.; Luo, N.L.; Sullivan, P.J.; Stout, K.J. (1992), "A proposal of parameters for characterising 3D surface topography", A research report in circulation in European academy and industry.
- [117] Yim, D.Y.; Kim, S.W. (1991), "Optimum sampling interval for R_a roughness measurement", *Proc. Instrn. Mech. Engrs.* **205**: 139-142.

- [118] Lin, T.Y.; Stout, K.J.; Sullivan, P.J. (1991), "Determination of proper sampling spacing for 3D topography measurement of machined surfaces using power spectral analysis", *Proceedings of 7th America Society of Precision Engineering*: 324-327.
- [119] Tsukada, T.; Sasajima, K. (1982), "An optimum sampling interval for digitizing surface asperity profiles", *Wear* **83**: 119-128.
- [120] Thomas, T.R.; Rosén, B.G. (2000), "Determination of the optimum sampling interval for rough contact mechanics", *Tribology International* **33**: 601-610.
- [121] Wenzel, R. N. (1936), "Resistance of solid surfaces to wetting by water", *Ind. Eng. Chem.* **28**: 988-994.
- [122] Wenzel, R. N. (1949), "Surface roughness and Contact Angle", *J. Phys. Colloid Chem.* **53**: 1466.
- [123] Russ, J.C. (1994), *Fractal surfaces*, New York: Plenum Press, ISBN 0-306-44702-9.
- [124] Calvimontes, A.; Müller, A.; Grundke, K.; Bellmann, C.; Schäfer, N.; Riske, T. (June 2008), "Modern non-destructive analytical methods for the surface characterization of Sheet Moulding Compounds (SMC)", *The 29th FATIPEC CONGRESS*, Ghent-Belgium.
- [125] Calvimontes, A.; Grundke, K.; Müller, A.; Stamm, M. (2009), "Advances for the topographic characterisation of Sheet Moulding Compounds", *Materials*, under review.
- [126] Kim, Y.S.; Lee, H.H.; Hammond, P.T. (2003), "High density nanostructure transfer in soft molding using polyurethane acrylate molds and polyelectrolyte multilayers", *Nanotechnology* **14**: 1140.1144.
- [127] Calvimontes, A.; Grundke, K.; Müller, A.; Stamm, M. (2009), "Volumetrical characterisation of Sheet Moulding Compounds topography", *Materials*, under review.
- [128] Calvimontes, A.; Synytska, A.; Dutschk, V.; Bell, Ch.; Lehmann, B. (2006), "Einfluss der Struktur von Polyestergewebe auf ihre Benetzbarkeit", *Melliand Textilberichte*, **1**(2): 64-67, and *Melliand English*, **1**(2): E16- E18.
- [129] Dutschk, V.; Myat, S.; Martin, J.; Stolz, M.; Breitzke, B.; Cherif, Ch.; Heinrich, G. (2007), "A Comparative Analysis between Different Ether Carboxylic Acids with Respect to Wettability and Surface Topography of Abrasively Treated Polyester Fabrics", *Tenside Surf. Det.* **44**(6): 248-254.
- [130] Hasan, M.M.B.; Calvimontes, A.; Synytska, A.; Dutschk, V. (2008), "Effects of topographic structure on wettability of differently woven fabrics", *Textile Research Journal* **78**(11): 996-1003.
- [131] Calvimontes, A.; Dutschk, V.; Breitzke, B.; Offermann, P.; Voit, B. (2005), "Soiling Degree and Cleanability of Differently Treated Polyester Textile Materials", *Tenside Surf. Det.* **42**(1): 17-22.
- [132] Calvimontes A.; Dutschk, V.; Koch, H.; Voit, B. (2005), "New Detergency Aspects through Visualisation of Soil Release Polymer Films on Textile Surfaces", *Tenside Surf. Det.* **42**(4): 210-216.
- [133] Hasan, M.M.B.; Dutschk, V.; Calvimontes, A.; Hoffmann, G.; Heinrich, G.; Cherif, Ch. (2008), "Influence of the cross-sectional geometry on wettability and cleanability of polyester woven fabrics", *Tenside Surf. Det.* **45**(5): 274-279.
- [134] Hasan, M.M.B.; Calvimontes, A.; Dutschk, V. (2009), "Correlation between wettability and cleanability of polyester fabrics modified by soil release polymer and their topographic structure", *Journal of Surfactants and Detergents*, DOI 10.1007/s11743-009-1130x.
- [135] Schubel, P.J.; Warrior, N.A.; Kendall, K.N.; Rudd, C.D. (2006), "Characterisation of thermoset laminates for cosmetic automotive applications: Part I – Surface characterisation", *Composites: Part A* **37**: 1734-1746.
- [136] Le, T.H.; Dumont, P.J.J.; Orgéas, L.; Favier, D.; Salvo, L.; Boller, E. (2008), "X-ray contrast microtomography for the analysis of the fibrous microstructure of SMC composites", *Composites: Part A* **39**: 91-103.
- [137] Schubel, P.J.; Parsons, A.J.; Lester, E.H.; Warrior, N.A.; Rudd, C.D. (2006), "Characterisation of thermoset laminates for cosmetic automotive applications: Part II – Cure of residual volatile assessment", *Composites: Part A* **37**: 1747-1756.
- [138] Ruffier, M.; Merle, G.; Pascault, J.P.; Bouleçane Vincent, N. (1966), "The shrinkage compensation of unsaturated polyester resins – polyvinyl acetate blends polymerization proceeds through fractal morphologies: characterization and simulation", *Journal of Materials Science* **31**: 4679-4687.

- [139] Wenzel, R.N. (1936), "Resistance of solid surfaces to wetting by water", *Industrial and Engineering Chemistry* **28**: 988-994.
- [140] Drelich, J., Miller J.D. (1993), "Modification of the Cassie Equation", *Langmuir* **9**: 619-621.
- [141] Nakae, H.; Inui, R.; Hirata, Y.; Saito, H. (1998), "Effect of surface roughness on wettability", *Acta Mater* **46**: 2313-2318.
- [142] Nakae, H.; Yoshida, M.; Yokota, M. (2005), "Effects of roughness pitch of surfaces on their wettability", *Journal of Materials Science* **40**, 9(10): 2287-2293.
- [143] Cassie, A.B.D.; Baxter, S. (1944), "Wettability of porous surfaces", *Trans. Faraday Soc.* **40**: 546-551.
- [144] Sheng, Y.J.; Shaoyi, J.; Tsao, H.K. (2007), "Effects of geometrical characteristics of surface roughness on droplet wetting", *The Journal of Chemical Physics* **127**: 234704-7
- [145] Kissa, E. (1996), "Wetting and Wicking", *Textile Re. J.* **66**(10): 660-668.
- [146] Bell, Ch. (2004), *Herstellung und Evaluierung hochdichter PES-Mikrofilamentgewebe für OP-Textilien* Ms.Sc. Thesis in Textile and Clothing Engineering, Technischen Universität Dresden, Fakultät Maschinenwesen, Institut für Textil- und Bekleidungstechnik, Dresden, Germany.
- [147] Dutschk, V.; Sabbatovskiy, K.G.; Stolz, M.; Grundke, K.; Rudoy, V.M. (2003), "Unusual wetting dynamics of aqueous surfactant solutions on polymer surfaces", *J. Colloid Interf. Sci.* **267**: 456-462.
- [148] Lord, P.R. (1974), "A Comparison of the Performance of Open-End and Ring Spun Yarns in Terry Toweling", *Textile Res. J.* **44**: 516-522.
- [149] Calvimontes, A. (2004), *Schmutzabweisende Eigenschaften von Textil- und Polymermaterialien durch Imprägnierung mit Soil-Release-Polymeren*, Ms.Sc. Thesis in Textile and Clothing Engineering, Technischen Universität Dresden, Fakultät Maschinenwesen, Institut für Textil- und Bekleidungstechnik, Dresden, Germany.
- [150] Cartes, Machines for the textile industry (<http://www.cartes.it>).
- [151] Calvimontes, A.; Dutschk, V.; Breitzke, B.; Stamm, M. (August 2008), "Influence of changes in Topography of Textile Materials Caused by Different Modifications on their Cleanability: A New Concept", 17th *International Conference "Surfactants in Solution"*, Berlin, Germany.
- [152] Jacobasch H-J.; Grosse, I.(1978), "Möglichkeiten und Grenzen der Modifizierung von Synthesefaserstoffen zur Erzielung schmutzabweisender Eigenschaften", *Textiltechnik* **28**(2): 98-103.
- [153] Rees, W.H. (1954), "The Soiling of Textile Materials", *J. Textile Inst.* **45**: 612-631.
- [154] Flath, H-J. (1968), "Prüfmethoden für die Anschmutzung von Textilien", *Deutsche Textiltechnik* **18**: 97-105.
- [155] Magne, F. C.; Portas, H. J.; Wakeham H. (1947), "Calorimetric Investigation of Moisture in Textile Fibers", *J. Amer. Chem. Soc.* **69**: 1896-1902.
- [156] Goring, D. A. I. (1978), *The Effect of Cellulose on the Structure of Water: View 1*, Transactions of 6th Symposium of Paper Physics, Cambridge: 43-62.
- [157] Hatakeyama, H.; Hatakeyama, T. (1981), "Structural Change of Amorphous Cellulose by Water- and Heat-Treatment", *Macromol. Chem.* **182**: 1655-1668.
- [158] Nakamura, K.; Hatakeyama, T.; Hatakeyama, H. (1981), "Studies on Bound Water of Cellulose by Differential Scanning Calorimetry", *Textile Research Institute*: 607-613.
- [159] Froix, M. F.; Nelson, R. (1975), "The Interaction of Water with Cellulose from Nuclear Magnetic Resonance Relaxation Times", *Macromolecules* **8**: 726-730.
- [160] Wilhelmy, J. (1864), "Über die Abhängigkeit der Capillaritäts - Constante des Alkohols von Substanz und Gestalt des benetzten festen Körpers", *Ann. Physik* **119**: 177.
- [161] Washburn, E. W. (1921), "Dynamics of capillary flow", *Phys. Rev.* **17**: 374-375.

- [162] Calvimontes, A.; Dutschk, V.; Cherif, C.; Heinrich, G. (October 2007), "Ein neues Konzept zum besseren Verständnis der Penetration von Flüssigkeiten in textilen Oberflächenstrukturen", *Beschichtung und Modifizierung von Kunststoffoberflächen: NDVaK, 15. Neues Dresdner Vakuumtechnisches Kolloquium*, Dresdner Transferstelle für Vakuumtechnik e.V.: 48-52, ISBN 978-3-00-022604-5.
- [163] Çay, A.; Atav, R.; Duran, K. (2007), "Effects of Warp-Weft Density Variation and Fabric Porosity of the Cotton Fabrics on their Colour in Reactive Dyeing", *Fibres & Textiles in Eastern Europe* **15**(1): 91-94.
- [164] Nicoll, A.; Meseth, J.; Müller, G.; Klein, R. (2005), "Fractional Fourier Texture Masks: Guiding Near-Regular Texture Synthesis", *Computer Graphics Forum* **24**(3): 569-579.
- [165] Calvimontes, A.; Dutschk, V.; Cherif Ch.; Stamm, M.; Heinrich, G. (December 2008), "Modelling of Fabric Topography by Fourier Synthesis Techniques", *2nd International Textile Conference Aachen-Dresden, Dresden, Germany*.
- [166] Finckh, F. (2004), "Numerische Simulation der mechanischen Eigenschaften textiler Flächengebilde-Gewebeherstellung", *3. LS-DYNA Anwendenforum F-I*: 1-15.
- [167] Chwastiak, S. (1973), "A Wicking Method for Measuring Wetting Properties of Carbon Yarn", *J. Colloid Interface Sci.* **42**: 298-309.
- [168] Peltonen, J.; Järn, M.; Areva, S.; Linden, M.; Rosenholm, J. (2004), "Topographical Parameters for Specifying a Three-Dimensional Surface", *Langmuir* **20**: 9428-9431.
- [169] De Gennes, P.G. ; Brochard-Wyart, F.; Quéré, D. (2004), *Capillarity and Wetting Phenomena, Drops, Bubbles, Pearls, Waves*, Springer, New York, ISBN –13 978-0387005928.
- [170] Synytska, A.; Ionov, L.; Dutschk, V.; Stamm, M.; Grundke, K. (2008), "Wetting on Regularly Structured Surfaces from "Core-Shell" Particles: Theoretical predictions and Experimental Findings", *Langmuir* **24**: 11895-11901.
- [171] Grundke, K.; Nitschke, S.; Minko, S.; Froeck, C.; Simon, F.; Uhlmann, S.; Pöschel, K.; Motornov, M. (2003), "Merging two concepts: Ultrahydrophobic polymer surfaces and switchable wettability", *Contact Angle, Wettability and Adhesion*, **3**: 1-25.

Lebenslauf (curriculum vitae)

Alfredo Calvimontes Candia

Ausbildung

- 1985-1990: Universität La Salle, Mexiko-Stadt (Mexiko), Fakultät für Chemie; **Diplom in Chemieingenieurwesen**
- 1985-1988: Universität La Salle, Mexiko-Stadt, Mexiko, Fakultät für Chemie, **Diplom im Berufsethos**, 1989
- 1992: Stiftung Carl Duisberg Gesellschaft, Deutschland, und die Nationale Industrie- und Handelskammer, La Paz (Bolivien) **Aufbaustudium in Produktionsverwaltung**
- 1992-1994: Universität Mayor de San Andrés, La Paz, Bolivien, Fakultät für Naturwissenschaften, **Mathematikstudium** (vier erste Semester)
- 2002-2004: Technische Universität Dresden, Fakultät für Maschinenwesen, Institut für Institut für Textil- und Bekleidungstechnik; 2004: **Master of Science (M.Sc.) in Textil- and Bekleidungstechnik**

Berufserfahrung

- 1988-1989** **Mitarbeiter des Projekts: "Analyse von Polymer-Mischungen", Conductores Mexicanos S.A. (CONDUMEX) und die Nationale Autonome Universität Mexiko, Mexiko-Stadt, Mexiko**
Dieses Projekt wurde von dem mexikanischen Unternehmen CONDUMEX; Hersteller von elektrischen Leitern, und der internationalen Gruppe PIRELLI, der es gehört, finanziert.
Das Projektziel war die Entwicklung von Plastiküberzügen für Kabel hoher Umweltbeständigkeit.
- 1990** **Mitarbeiter des Projekts "Polymer-Membrane für die Gastrennung", Mexikanisches Institut für Erdöl (IMP) und die Nationale Autonome Universität Mexiko, Mexiko, Mexiko.**
Dieses Projekt hatte als Ziel die Entwicklung von sauerstoffangereicherten Membranen für Medizin Zwecke und ihre Anwendung im Bereich der Kraftfahrzeugindustrie (Erhöhung des Verbrennungsnutzungsgrades).
- 1991-1992** **Ingenieur auf Forschungsebene, Abteilung Hydrometallurgische Forschungen, Unternehmen Inti Raymi GmbH, Oruro, Bolivien**
Die Aufgaben umfassten die Kontrolle und Optimierung der chemischen Variablen innerhalb des Golderzlaugungsprozesses, die Entwicklung von Forschungsprojekten für das Unternehmen im Metall- und Hydrometallurgischen Bereich, sowie die Entwicklung von Forschungsprojekten für andere Bergbauunternehmen. Einige von diesen Projekten wurden in Zusammenarbeit mit der Firma Battle Mountain, Nevada, USA, durchgeführt.
- 1992-1993** **Leiter für Chemische Optimierung Bolivianische Gesellschaft für Zement, Viacha, Bolivien**
Die Aufgaben umfassten die Kontrolle der physikchemischen Variablen des Rohstoffes innerhalb eines Prozesses und im Fertigprodukt, die Auswertung der physikchemischen Abläufe in der Zementherstellung und die Computersimulation des chemischen Industrieprozesses.

- 1994** **Geschäftsleiter der Anlage, Fábrica de Aguas Gaseosas Oriental Ltda., La Paz, Bolivien**
 Volle Verantwortung über die Industrieanlage und ihre sechs Abteilungen: Verwaltung, Produktion, Wartung, Sicherheit, Labor und Qualitätskontrolle.
- 1995-1997** **Technischer Geschäftsführer, Magnetrón S.R.L., La Paz, Bolivien**
 Design, Bau und Wartung von Trocknungsöfen und Holzsanitierung durch Mikrowelle. Kontrolle der industriellen Holz Trocknungsprozesse.
- 1997-1998** **Leiter des Labors für Qualitätskontrolle von Textilfarben, Quimiza Ltda., La Paz, Bolivien**
 Planung und Durchführung von chemischen Proben für die Qualitätskontrolle der Textilfarben. Prüfung zum Farbton für Textilindustrievorgänge. Entwicklung von Formulierungen für das Färben von Baumwolle und Polyesterfasern.
- 1998-2001** **Universaltex Ltda., La Paz, Bolivien**
Stellvertretender Leiter für die Färberei:
 Analyse der Zeiten und Bewegungen; Optimierung der Einzelgänge und Prozesse. Inangsetzung von Optimierungsabläufen in Einzelgängen für die Textilfärberei. Bearbeitung der Information über die Fortschritte der Produktion im Bereich der Färberei.
Leiter der Strickerei:
 Analyse der Strukturen der Gestricke und Anpassung der Großrundstrickmaschinen. Bearbeitung und Systematisierung der Berichte in Realzeit über den Fortschritt der Produktion. Bearbeitung und Systematisierung der Information über die Wirksamkeit der Großrundstrickmaschinen. Programmierung von Strukturen in Minijacquard. Analyse und Bearbeitung von Layoutprogrammen für Muster von vier oder mehr Farben.
Stellvertretender Geschäftsführer für Produktionsplanung:
 Verantwortlich für die Planung, Programmierung und Produktionskontrolle der Anlagen für Gestricke, Färberei und Fertigbearbeitung.
- 2001- 2002** **Technischer Textilberater, Dimetex Ltda., La Paz, Bolivien**
 Technischer Dienst und industrielle Fachberatung und Optimierung der Vorgänge der Textilindustrien in La Paz, Cochabamba und Santa Cruz. Analyse der Strukturen von Gestricke, Programmierung von elektronischen Maschinen, Planung, Programmierung und Produktionskontrolle. Seminare für Mitarbeiter der erwähnten Betrieben zu verschiedenen Textilthemen. Bearbeitung von Diagnosen bezüglich der Prozesse für die Kunden von Dimetex Ltda.
- 2004- 2005** **Wissenschaftlicher Mitarbeiter am Leibniz-Institut für Polymerforschung Dresden e.V.**
 Bearbeitung des Industrieprojektes mit der Firma SASOL zu „Grundlagenuntersuchungen zur Benetzungskinetik von Tensiden auf Festkörperoberflächen“.
- 2007-** **Wissenschaftlicher Mitarbeiter am Leibniz-Institut für Polymerforschung Dresden e.V. und Doktorand an der Technischen Universität Dresden**
 Machbarkeitsstudie an verschiedenen Baumwoll- und Polyestertextilien zwecks identifizierung eines Soil-Release-Polymer-Films an deren Oberflächen mittels MicroGlider-Technik.
 Untersuchungen zur Topographie und Benetzbarkeit von Oberflächen. Grundlegende Untersuchungen von Zusammenhängen zwischen Substratdefekten und Beschichtungsfehlern bei SMC-Materialien.
 Anwendung von Methoden zur quantitativen Charakterisierung der Rauheit und Porosität der SMC-Oberflächenregion mittels Rasterkraftmikroskopie und MicroGlider, statistische Analyse der Porosität im SMC-Material.
 Mikroskopisch-topographische Charakterisierung von durch Nanoteilchen stabilisierten Emulsionen zwecks Klärung der Stabilisierungsmechanismen.

Akademische Tätigkeiten

- 1987 –1988** Assistent des Dozenten für Anorganische Chemie, Universität La Salle, Mexiko-Stadt, Mexiko.
- 1987 – 1988** Assistent im Computerlabor, Universität La Salle, Mexiko-Stadt, Mexiko.
- 1989 –1990** Beaufsichtigung des Labors für Chemieingenieurwesen, Universität La Salle, Mexiko-Stadt, Mexiko.
- 1989 –1990** Dozent für Allgemeine Chemie, Panamerikanische Universität, Mexiko-Stadt, Mexiko.
- 1992** Lehrer für den Kurs „Fraktale Geometrie“, Universität Mayor de San Andres, Fakultät für Naturwissenschaften, La Paz, Bolivien
- 2000** Lehrer für den Kurs „Einführung in die Analyse der Gestrigenstruktur“, Gruppe America Textil, S.A., La Paz, Bolivien
- 2005- 2006** Dozent für Physik, Nationale Universität Chile, Santiago (Chile)

Auszeichnungen

- Erfolgs- und Auszeichnungsurkunde, Schule La Salle, Jahrgang 1982.
- Erfolgsurkunde 1987, Nationale Autonome Universität Mexiko (Abt. Für angeschlossene Universitäten).
- Urkunde aufgrund des besten Durchschnitts der Fachrichtung innerhalb der der Nationalen Autonomen Universität Mexiko angeschlossenen Universitäten.
- Medaille „Tageszeitung von Mexiko“ für den besten Studenten der Fachrichtung Chemieingenieurwesen aller Universitäten in Mexiko-Stadt (ausgehändigt vom dem Präsidenten von Mexiko selbst, Mexiko-Stadt), 1990.
- Medaille „Hermano Miguel“ (Bruder Michael), gewährt von der Universität La Salle dem Studenten mit dem besten Durchschnitt zum Studiumsabschluss, 1990.
- SASOL-Diplomandpreis. Masterarbeit: „Schmutzabweisende Eigenschaften von Textil- und Polymermaterialien durch Imprägnierung mit Soil-Release-Polymeren“ wurde vom SASOL Germany GmbH mit großem Interesse aufgenommen.

Kurse, Seminare und Technische Veranstaltungen

- **Makromolekular Synthese** (Aufbaustudiengang), Fakultät für Chemie, Nationale Autonome Universität, Mexiko-Stadt, 1989.
- **Charakterisierung von Copolymeren** (Aufbaustudiengang), Fakultät für Chemie, Nationale Autonome Universität, Mexiko-Stadt, 1989.
- **Hydrodynamische Chromatographie** (Aufbaustudiengang), Fakultät für Chemie, Nationale Autonome Universität, Mexiko-Stadt, 1989.
- **Seminar für Produktionsleiter**, Inti Raymi, La Paz, 1992.
- **Kurs über Spektralphotometrie atomarer Absorption**, SOBOCE, 1994.
- **Kurs über Holz Trocknung mit warmer Luft**, INFOCAL, La Paz, 1998.

- **Kurs über Standardisierungstechniken und Qualitätskontrolle in Betrieben**, IBNORCA, La Paz, 1998.
- **Kurs über die Einführung in das Management des Qualitätssystems und ihre Dokumentation für ISO-Normen**, IBNORCA und das Uruguayische Institut von Technischen Normen, La Paz, 1999.
- **Kurs über die Analyse von Strickstrukturen**, Prof. Rogelio Casal, Universaltext Ltda., La Paz, 1999.
- **Trainingskurse: „Structure Analyse Single and Double Jersey, Technical Training Inter Rib 4 1.6 and Inter Rib 4 1.6 R, Mini-Jacquard Relanit SE and OV 2.4 SE, SEL Software Basics of PIC 3, Pattern Editor, Rapport Editor, Rapport Software for Inter Rib 4 1.6 R.“**, Mayer & Cie., Albstadt, Deutschland 2000.
- **Projektmanagement–Arbeitsvorbereitung–Montage/Demontage** (Aufbaustudiengang), Institut für Produktionstechnik, Fakultät Maschinenwesen, Technische Universität Dresden, 2003.
- **Verfahren und Maschinen der Textilveredlung** (Aufbaustudiengang), Institut für Makromolekulare Chemie und Textilchemie, Fakultät Mathematik und Naturwissenschaften, Technische Universität Dresden, 2003.
- **Textilrecycling** (Aufbaustudiengang), Sächsisches Textilforschungsinstitut e.V., Chemnitz und Dresden, 2003-2004.
- **Allgemeine Makromolekulare Chemie, Chemie der Faserstoffe**, Institut für Makromolekulare Chemie und Textilchemie, Fakultät Mathematik und Naturwissenschaften, Technische Universität Dresden, 2003-2004.
- **Physikalische Chemie der Oberflächen**, Vorlesung im Wintersemester 2007/08, Prof. Dr. M. Stamm, Technische Universität Dresden, Fakultät Mathematik und Naturwissenschaften.
- **Polymeroberflächen und -grenzflächen: Charakterisierung**, Funktionalisierung, Anwendungen, Kurs, Gesellschaft Deutscher Chemiker und Leibniz-Institut für Polymerforschung Dresden e.V., 8-10 Oktober 2007.
- **Streumethoden zur Strukturbestimmung von Polymeren**, Vorlesung im Sommersemester 2008, Prof. Dr. M. Stamm, Technische Universität Dresden, Fakultät Mathematik und Naturwissenschaften.

Arbeits- und Forschungsgebiet

- Topographische Charakterisierung polymerer Oberflächen; topographische Mikrodefekte und ihre Auswirkung auf die resultierende Qualität polymerer Oberflächen
- Physikalisch-chemische Charakterisierung von Baumwoll- und Polyestertextilien: Topographie, Morphologie und Benetzbarkeit
- Entwicklung von Konzepten und mathematischen Modellen zur Voraussage von Effekten resultierend aus den topographischen Änderungen auf das Verhalten von Polymer- und Textiloberflächen bei Waschen und Trocknen

Veröffentlichungen über Topographie und Benetzbarkeit von Polymeroberflächen (2004-2009)

Veröffentlichungen in Fachzeitschriften

Calvimontes, A.; Dutschk, V.; Breitzke, B.; Offermann, P.; Voit, B. (2005), "Soiling Degree and Cleanability of Differently Treated Polyester Textile Materials", *Tenside Surfactants Detergents* **42**: 17-22.

Calvimontes, A.; Dutschk, V.; Koch, H.; Voit, B. (2005), "New Detergency Aspects through Visualisation of Soil Release Polymer Films on Textile Surfaces", *Tenside Surfactants Detergents* **42**: 210-216.

Calvimontes, A.; Synytska, A.; Dutschk, V. (2006), "Einfluss der Struktur von Polyestergewebe auf ihre Benetzbarkeit", *Melliand Textilberichte* **1(2)**: S. 64-67, *Melliand English* **1(2)**: E16-E18.

Hasan, B.; Calvimontes, A.; Synytska, A.; Dutschk, V. (2008), "Effects of topographic structure on wettability of differently woven fabrics", *Textile Research Journal* **78(11)**: 996-1003.

Hasan, B.; Dutschk, V.; Calvimontes, A.; Hoffmann, G.; Heinrich, G.; Cherif, C. (2008), "Influence of the cross-sectional geometry on wettability and cleanability of polyester woven fabrics", *Tenside Surf. Det.* **45(5)**: 274-279.

Hasan, M.M.B.; Calvimontes, A.; Dutschk, V. (2009), "Correlation between wettability and cleanability of polyester fabrics modified by soil release polymer and their topographic structure", *Journal of Surfactants and Detergents*, DOI 10.1007/s11743-009-1130x.

Calvimontes, A.; Grundke, K.; Müller, A. (2009), "Advances for the topographic characterisation of Sheet Moulding Compounds", *Materials*, under review

Calvimontes, A.; Grundke, K.; Müller, A. (2009), "Volumetrical characterisation of Sheet Moulding Compounds topography", *Materials*, under review.

Calvimontes, A.; Dutschk, V.; Stamm, M. (2009), "Advances in topographic characterisation of textile materials", *Textile Research Journal*, accepted for publication.

Calvimontes, A.; Dutschk, V.; Stamm, M. (2009), "Effect of cellulase enzyme on cellulose nanotopography", *Tenside Surfactants Detergents*, under review.

Vorträge

Calvimontes, A.; Dutschk, V. (Oktober 2007), "Benetzungsdynamik an Polymerwerkstoffoberflächen", GDCH-Kurs, *Polymeroberflächen und –grenzflächen: Charakterisierung, Funktionalisierung, Anwendungen*, Dresden.

Calvimontes, A.; Dutschk, V.; Cherif, C.; Heinrich, G. (Oktober 2007), "Ein neues Konzept zum besseren Verständnis der Penetration von Flüssigkeiten in textilen Oberflächenstrukturen", *15. Neues Dresdner Vakuumtechnisches Kolloquium*, Dresden.

Calvimontes, A.; Dutschk, V.; Cherif, C.; Heinrich, G. (November 2007), "A new concept to understand the liquid penetration into polyester fabrics", *Aachen-Dresden International Textile Conference*, Aachen.

Calvimontes, A. (April 2008), "Fractal dimension as parameter for the surface characterization: theory, examples, applications", *Seminar "Computational Polymer Materials Science 2008, Leibniz-Institut für Polymerforschung Dresden e.V.*

Calvimontes, A.; Grundke, K.; Bellmann, C.; Schäfer, N.; Riske, T.; Eichhorn, J-K.; Müller, A. (June 2008), "Modern non-destructive analytical methods for the surface characterization of Sheet Moulding Compounds (SMC)", *The 29th FATIPEC CONGRESS, Ghent – Belgium*.

Calvimontes, A.; Dutschk, V.; Cherif, C.; Stamm, M.; Heinrich, G. (December 2008), "Modelling of Fabric Topography by Fourier Synthesis Techniques", *Aachen-Dresden International Textile Conference, Dresden*.

Calvimontes, A. (April 2009), "Surface Roughness Analysis, Case Study", *COST D43 SCHOOL "Interfacial engineering in nanotechnology", Leibniz-Institut für Polymerforschung Dresden e.V.*

Calvimontes, A.; Stamm, M.; Dutschk, V. (May 2009), "Effect of cellulose enzyme on cellulose nanotopography", *44th International Wfk Detergency Conference, Düsseldorf*.

Calvimontes, A.; Grundke, K.; Müller, A. (October 2009), "New advances for the topographic characterisation of Sheet Moulding Compounds", *V International Conference on Science and Technology of Composite Materials, COMATCOMP 2009, San Sebastian, Spain*.

Beiträge in Tagungsbänden mit ISBN

Calvimontes, A.; Dutschk, V.; Cherif, C.; Heinrich, G. (2007), "Ein neues Konzept zum besseren Verständnis der Penetration von Flüssigkeiten in textilen Oberflächenstrukturen", In *Beschichtung und Modifizierung von Kunststoffoberflächen, NDVaK, 15. Neues Dresdner Vakuumtechnisches Kolloquium*, Dresdner Transferstelle für Vakuumtechnik e.V.: 48-52, ISBN 978-3-00-022604-5

Beiträge in Tagungsbänden

Petong, N.; Calvimontes, A.; Breitzke, B.; Dutschk, B. (2005), "Surface properties of differently modified human hair", *XVIIth European Chemistry at Interfaces Conference (ECIC-XVII), Loughborough*.

Calvimontes, A.; Dutschk, V.; Cherif, C.; Heinrich, G. (2007), "A new concept to understand the liquid penetration into polyester fabrics", *Aachen-Dresden International Textile Conference, Aachen*: 137

Calvimontes, A.; Grundke, K.; Bellmann, C.; Schäfer, N.; Riske, T.; Eichhorn, J-K.; Müller, A. (2008), "Modern non-destructive analytical methods for the surface characterization of Sheet Moulding Compounds (SMC)", *The 29th FATIPEC CONGRESS.- Ghent – Belgium*.

Calvimontes, A.; Dutschk, V.; Cherif, C.; Stamm, M.; Heinrich, G. (2008), "Modelling of Fabric Topography by Fourier Synthesis Techniques", *Aachen-Dresden International Textile Conference, Dresden*.

Dutschk, V.; Hasan, M.M.B; Calvimontes, A.; Cherif, C.; Hoffmann, G.; Heinrich, G. (2008), "Manufacturing and characterising polyester yarns having different cross-sectional shaped filaments for woven fabric design", *Aachen-Dresden International Textile Conference, Dresden*.

Calvimontes, A.; Stamm, M.; Dutschk, V. (2009), "Effect of cellulose enzyme on cellulose nanotopography", *44th International wfk Detergency Conference, Düsseldorf*.

Posters

Calvimontes, A.; Dutschk, V.; Breitzke, B.; Offermann, P.; Voit, B. (2004), "Estimation of soiling degree and cleanability of differently treated polyester materials", *Dresdner Textiltagung, Institut für Textil- und Bekleidungsstechnik (ITB) an der TU Dresden.- Dresden*.

- Petong, N.; Calvimontes, A.; Breitzke, B.; Dutschk, B. (2005), "Influence of oil in a shampoo formulation on wettability of differently modified hair", *XVIIth European Chemistry at Interfaces Conference (ECIC-XVII), Loughborough*.
- Dutschk, V.; Calvimontes, A.; Haessler, R.; Breitzke, B. (2006), "The effect of microemulsions and conditioning agents on wettability of human hair", *EUFOAM 2006 (6th European Conference on Foams, Emulsions and Applications).- Postdam*.
- Calvimontes, A.; Dutschk, V.; Breitzke, B.; Cherif, C. (2007), "A novel wicking model for polyester fabrics applied to detergent technology", *SEPAWA Congress, Würzburg*.
- Calvimontes, A.; Dutschk, V.; Breitzke, B.; Cherif, C.; Heinrich, G. (2007), "Penetrationsverhalten von Flüssigkeiten an Polyestertextilien aus der Sicht der Waschmitteltechnologie", *15. Neues Dresdner Vakuumtechnisches Kolloquium, Dresden*.
- Dutschk, V.; Calvimontes, A.; Horst, T.; Cherif, C.; Stamm, M.; Heinrich, G. (2007), "Nutzung neuer naturwissenschaftlicher Konzepte zur Oberflächencharakterisierung für innovative Anwendungen in der Polymerwerkstofftechnologie", *Dresdner Innovationsforum, Dresden*.
- Salem, T.S.; Uhlmann, S.; Nitschke, M.; Calvimontes, A.; Hund, R.-D.; Simon, F. (2007), "Surface modification of PET fabrics to improve their printing behaviour", *Dresdner Innovationsforum, Dresden*.
- Calvimontes, A.; Dutschk, V.; Cherif, C.; Heinrich, G. (2007), "A new concept to understand the liquid penetration into polyester fabrics", *Aachen-Dresden International Textile Conference, Aachen*.
- Calvimontes, A.; Dutschk (2008), "Influence of impregnation of Soil Release Polymers on topography and cleanability of polyester fabrics", *17th International Symposium on Surfactants in Solution; Berlin*.
- Calvimontes, A.; Dutschk, V.; Cherif, C.; Stamm, M.; Heinrich, G. (2008), "Modelling of Fabric Topography by Fourier Synthesis Techniques", *Aachen-Dresden International Textile Conference, Dresden*.
- Dutschk, V.; Hasan, M.M.B.; Calvimontes, A.; Cherif, C.; Hoffmann, G.; Heinrich, G. (2008), "Manufacturing and characterising polyester yarns having different cross-sectional shaped filaments for woven fabric design", *Aachen-Dresden International Textile Conference, Dresden*.
- Salem, T.S.; Uhlmann, S.; Nitschke, M.; Calvimontes, A.; Hund, R.-D.; Simon, F. (2009), "PET Surface Properties Affected by Low Temperature Plasma Modification", *Workshop "Oberflächentechnologie mit Plasma- und Ionenstrahlprozessen", Leipzig*.
- Calvimontes, A.; Stamm, M.; Dutschk, V. (2009), "Simulating surface modification of polyester fabrics by thermofixing and its effect on soiling and soil release", *European Detergents Conference (EDC) 2009, Würzburg*.

Versicherung

Hiermit versichere ich, dass die vorliegende Arbeit ohne unzulässige Hilfe Dritter und ohne Benutzung anderer als der angegebenen Hilfsmittel angefertigt habe; die aus fremden Quellen direkt oder indirekt übernommenen Gedanken sind als solche kenntlich gemacht. Die Arbeit wurde bisher weder im Inland noch im Ausland in gleicher oder ähnlicher Form einer anderen Prüfungsbehörde vorgelegt. Der Autor hat in der Vergangenheit kein erfolgloses Promotionsverfahren durchgeführt.

Die vorliegende Arbeit wurde unter der wissenschaftlichen Betreuung von Prof. Dr. Manfred Stamm, Dr. Karina Grundke und Dr. Victoria Dutschk am Leibniz-Institut für Polymerforschung Dresden e.V. angefertigt.

Die Promotionsordnung der Technischen Universität Dresden der Fakultät Mathematik und Naturwissenschaften erkenne ich an.

Dresden, 10.08.2009

Alfredo Calvimontes